Anoles & Drones: revealing controls on anole abundance and mapping sub-canopy thermal habitat using remote sensing, on the island of Utila, Honduras

Thesis submitted to the University of Nottingham for the degree of Doctor of Philosophy

March 2022

Emma A. Higgins

Supervised by

Prof Doreen S. Boyd – University of Nottingham

Dr Geertje Van der Heijden – University of Nottingham

Dr Adam C. Algar – Lakehead University

Abstract

In these times of rapid environmental change and species extinction, understanding the drivers and mechanisms governing species' abundance is more important than ever. The goal of this thesis was to further our understanding of what drives variation in species' abundance and microhabitat use through space, particularly in the context of rapid land cover and climate change, using the little explored anole fauna of the Honduran island of Utila. The work uncovered that when considering structural habitat, prey availability and the thermal environment, for the endemic *Anolis bicaorum*, thermal habitat quality and prey biomass both had positive direct effects on anole abundance. However, thermal habitat quality also influenced prey biomass, leading to a strong indirect effect on abundance. Consequently, the later part of this thesis focuses on the thermal environment and the use of unoccupied aerial vehicles (UAVs) and satellite remote sensing platforms for mapping thermal habitat quality and availability at scales relevant to the species. Thermal habitat quality for *A. bicaorum* was primarily a function of canopy density, measured as leaf area index (LAI), therefore this work combined indices of canopy cover and heterogeneity derived from UAV and WorldView-2 satellite imagery to map sub canopy operative temperature (T_e). Results indicate that such methods as using remote sensing imagery, when coupled with air temperature measures, are a reasonable way of mapping T_e continuously across space, allowing us to quantify the availability and spatial structure of the thermal environment, at spatial scales experienced by the organism. Lastly, I used WorldView-2 imagery and the proposed methods for mapping T_e to quantify available thermal habitat for *A. bicaorum* on Utila across land cover and climate scenarios. This work indicates the need to determine controls and niche interactions on animal abundance and the importance quantifying these niche factors at relevant spatial scales to estimate species responses to land cover and climatic change.

Acknowledgements

Pancake), of which there are too many to name, for their support and great lab meetings throughout the years. I would like to thank my PhD cohort and now close friends, Vanessa Cutts, Henry Fell, Phillip Jagessar, Hazel Wilson, as well as so many others, for their friendship and support. Last but certainly not least, I would like to thank my partner Jordan Sieniawski for being my rock, and my family and pets, who have continuously supported me, long before I even started this PhD, and thank you for quite frankly for putting up with me over these past few years. I thank and appreciate everyone involved in my experience over the past few years, and to those little charismatic lizards on Utila; I can honestly say my life would not be the same without you.

Anolis bicaorum

Table of Contents

List of Tables

List of Figures

xi

Chapter 1 : Introduction

1.1 Overview of Thesis

Understanding what determines spatial variation in species' abundance holds the key to understanding the geography of life, from local ecological communities to global biodiversity. Given accelerated environmental change and species' extinctions, understanding the drivers and mechanisms governing species' abundance and distributions is now more important than ever (Ehrlén and Morris, 2015). As we continue to convert natural habitats for human use, identifying what habitat characteristics are most important for animal abundance, at a scale relevant to the organism, is crucial to conserving species in a human-dominated world. There is also a need to understand and model species responses to environmental change at a spatial scale relevant to the organism (Clusella-Trullas et al., 2021; Potter et al., 2013; Sears et al., 2011; Sears and Angilletta, 2015). However, current mechanistic models for predicting species distributions and responses to change do not consider the spatial heterogeneity of the landscape and consider the landscape to be homogenous (Potter et al., 2013; Sears et al., 2011), and therefore do not consider species' individual or population level responses to fine scale changes in their environment. This is due to the lack of high quality microclimate (Zellweger et al., 2019) data or input data for microclimate models at a spatially relevant scale.

This need for measuring species responses to environmental change at a scale relevant to them is important when considering anthropogenic land cover and climate change (Sears and Angilletta, 2015; Suggitt et al., 2018). Climate change is a key concern for future global biodiversity, however how we predict species' responses to climate change is currently based on broad homogenous landscapes, that do not accurately represent that experienced by the organisms (Sears and Angilletta, 2015; Suggitt et al., 2018). We know that the heterogeneity

of the landscape is important to consider when we look at species responses to climate change, by accounting for these microhabitats that may buffer impacts (Suggitt et al., 2018). Climate change and its influence on the thermal environment is particularly acute for forest dwelling ectotherms, the focus of this thesis, as it influences their ecological fitness. However, current methods for measuring climatic variables and responses to climate change are at a coarse spatial resolution, using compiled data from weather stations and mechanistic models (Kearney and Porter, 2017; Potter et al., 2013; Sears et al., 2011), which do not take into account these fine scale habitat characteristics relevant to the species themselves. Due to a current lack of relevant microclimate data. However, remote sensing data and methods have now been identified as a major emerging tool in monitoring this habitat heterogeneity and can provide relevant inputs for microclimate modelling at scales more relevant to species (Duffy et al., 2021; Zellweger et al., 2019).

Unoccupied aerial vehicles (UAVs) are one of said remote sensing platforms that can capture high spatial quality variables for microclimate modelling (Duffy et al., 2021; Kašpar et al., 2021; Milling et al., 2018; Zellweger et al., 2019), with the ability to capture highly detailed information on canopy structure from plot to landscape scales (Wallace et al.,2016; Ahmed et al., 2017). High spatial and spectral resolution satellites such as WorldView-2 (WV2) are also an exciting potential data source for microclimate and habitat heterogeneity modelling at fine spatial scales (30cm), with the addition of large spatial and temporal coverage. However, field tests of the capacity of remote sensing platforms to capture habitat characteristics relevant to animals living below the forest canopy are limited. This is particularly important as forest dwelling ectotherms have been highlighted as one of the most at risk from climate warming (Deutsch et al., 2008; Huey and Tewksbury, 2009; Kearney et al., 2009; Sinervo et al., 2010).

When considering the thermal environment, these microclimate data are important; however how we apply them to species has a major influence on our predictions of habitat use, abundances and response to future anthropogenic mediated habitat change. Microclimate influences the thermal environment of the landscape via multiple biophysical pathways (Gates, 1980; Kašpar et al., 2021). However, when we look to categorise the thermal suitability of an environment for an ectothermic species we use variables that relate to species' body temperature, such as a species critical thermal maximum (CT_{max}) based of thermal performance curves (TPCs). Measuring how the environment relates to these TPC ranges is usually done at fine spatial scales via morphologically accurate temperature models that represent operative temperature, the temperature of the animal at equilibrium with its environment (Bakken, 1992; Logan et al., 2013). Therefore, for microclimate data to be ecologically relevant for ectotherm species, we then need to predict the animals' body temperature from the microclimate data before then deciding on a reasonable measure of thermal habitat quality, introducing additional uncertainties to our predictions.

Another consideration of categorising the thermal suitability of an environment for a species, and the potential change of such conditions under anthropogenic mediated change, is what thermal indices are most important to consider. How we categorise the thermal landscape is important to consider for animal abundance, current methods look at the suitability of the environment compared to that of thermal ranges (for example CTMax) and thermal safety margins (Clusella-Trullas et al., 2021; Logan et al., 2013a) of a species. Although a reasonable indicator, the use of these indices as a sole indicator of ectotherm response to climate change has been called into question, as the impact of such indices on a population can vary depending on intrinsic and extrinsic factors (Clusella-Trullas et al., 2021; Sinclair et al., 2016). The spatial structure of the thermally suitable habitat at scales relevant to the organism, has also been highlighted as an important factor to consider when considering overall landscape suitability

(Sears and Angilletta, 2015), which currently cannot be considered with coarse measures of climate or operative temperature measures in the field.

In this thesis, I determine how multidimensional environments and niches, including measures of thermal habitat quality, interact to determine population abundance of an endemic anole lizard species along a habitat gradient in tropical forests and urban environments on the island of Utila, Honduras. I also test the ability of remote sensing techniques to predict variation in habitat characteristics, relevant to the anoles of Utila, at both a plot and at temporal landscape (island) level. Using thermal ecology and principles related to forest canopy, microclimate and lizard body temperature (Algar et al., 2018; Kašpar et al., 2021) I link canopy structure and species' abundance by integrating UAV and WorldView-2 Satellite data with field data on below-canopy lizard temperature and thermal habitat structure. This work will not only help reveal the secrets of this little understood fauna, and identify general principles underlying limits on animal abundance, but also proposes a step-towards new methods for mapping sub-canopy habitat characteristics, linked to the abundance of these species, across relevant spatial scales.

1.2 Background

1.2.1 Anoles (*Anolis spp*.)

The focus species of this thesis is a small endemic anole lizard (*Anolis bicaorum*) found on the island of Utila, Honduras. Anoles are a group of small arboreal Iguanid lizards belonging to the family *Dactyloidae,* native to the Caribbean, Central and South America (Losos, 2009); most scientists classify all species into a single genus, *Anolis*. With over 400 described species, anoles are one of the most species diverse lizard groups, occupying a range of ecological niches. Their high species diversity and diversity in form, physiology, behaviour, and ecology has led to them being a model system for evolutionary ecology. This has resulted in numerous studies of anole behaviour, physiology, neurobiology, community structure, and evolution

occurring, which has resulted in a considerable knowledge base of the relationships between anole species and their environments. However, no such work has been undertaken at considering how habitat characteristics mediate interactions between niche axes at spatial scales relevant to the animals, and how these interactions feed into the overall population size. The most characteristic structural features of anoles are their dewlaps and sub-digital toepads. The dewlap, a flap of skin beneath the chin, which can be extended by cartilaginous rods and combined with head and body movements (Nicholson et al., 2007) is primarily used for various signs and displays, mostly territorial and courtship displays. The expanded sub-digital toepads covered in lamellar scales with microscopic setae, aid in perching on substrates and climbing. Anoles have been divided into ecomorphs based on the structural microhabitat in which they are normally found (Losos, 2009). Each ecomorph is adapted in its ecology, behaviour and functional morphology to its specific microhabitat, for example longer legs confer an advantage for increased running speed on broad substrates, whereas shorter limbs provide greater manoeuvrability on narrow surfaces (Kolbe and Losos, 2005). There are six anole ecomorph designations, these are trunk, trunk-ground, trunk-crown, crown giant, grass-bush and twig anoles. These ecomorphs were first described by Williams (1983) and vary significantly in their morphology and behaviour with the two extremes of the scale being the crown-giants and the twig anoles.

Crown-giants as their name suggests are the largest of the ecomorphs and spend the majority of the time within the upper regions of the canopy, morphologically their limbs are moderately sized, their toepads large and their heads massive and casqued (Losos, 2009). In contrast, the twig anoles are the smallest of the ecomorph designations with slender bodies, long pointed snouts and short limbs and tails (Losos, 2009). The grass-bush anoles are always small; they are slender lizards with long hind limbs, short forelimbs, long narrow heads, poorly developed toepads and an extremely long tails. The different trunk ecomorphs again as their

name suggests spend their time living at different levels within the trunk of the tree, hunting and displaying in different areas. These ecomorph adaptations allow different species to adapt and co-occur within the same geographical space as an effective strategy for resource partitioning.

Quantifying anole habitat, preference therefore varies depending on the species and their ecomorphs. Although we have an idea of the factors that influence habitat suitability, what determines their relative abundance is largely unknown. Here, I focus on several different factors which are known to govern anole distribution, habitat preference, and therefore theoretically abundance. These are structural microhabitat, perch availability (Johnson et al., 2006), prey availability (Battles et al., 2013) and the thermal environment (Huey and Tewksbury, 2009; Sears et al., 2011; Sinervo et al., 2010). As ectotherms, anoles are dependent on the thermal conditions of their environment, as their body temperature (T_b) and therefore metabolic function is dependent on environmental conditions. Understanding these drivers is particularly important when considering endemic species and species of conservation concern, such as the focus species here *Anolis bicaorum* (Figure 1.1). Such endemic species, which are undergoing intense habitat alteration (personal observations) and potential invasive species threats (Brown et al., 2017b; Brown & Diotallevi, 2019), are under pressure from several fronts. We therefore need to understand the mechanisms underpinning their abundance and isolate important niche factors for monitoring and conservation planning implementation.

Figure 1.1: A male *Anolis bicaorum*, endemic to the island of Utila, Honduras extending its dewlap. Photo Credit – Tom Brown.

1.2.2 Study System

The research site for the work is Utila (16.0950° N, 86.9274° W), one of the Bay Islands of Honduras, which host a number of marine and terrestrial protected areas under SINAPH (Honduras National System of Protected Areas) that are of local and international significance. The island is small, with a total area of 41 km^2 (Figure 1.2).

Figure 1.2: Location of Utila, Isla de Bahia, Honduras

There is a single main elevation gradient located towards the north-east, Pumpkin Hill, with a maximum elevation of 74 metres above sea level. There is also a slight variation in elevation towards the northern regions of Utila town, which reaches up to 32 metres. The majority of the island varies from sea level to 8m in elevation (Figure 1.3).

Figure 1.3: Elevation map of Utila, Honduras using Shuttle Radar Topography Mission (SRTM) 1- arc second digital elevation model. Elevation in metres above sea level.

Utila features a mosaic of habitats, including red, white and black mangrove, neotropical dry forest, neotropical savannah, coastal palm and almond, urban areas, urban gardens and volcanic rock exposures (Schulte and Köhler, 2010; Fawcett et al., 2016), all of which contribute to the island's high biodiversity. The centre of the island is predominantly Neotropical savannah, Tique palm forest and areas of mangrove (personal observation), the central part of the island also hosts Turtle Harbour Marine Reserve and Wildlife Refuge, this refuge is managed by the Bay Islands Conservation Association (BICA). The remainder of the island is a mixture of different types of mangrove forest, coastal almond and scrub, neotropical dry forest and urban areas. To date, a total of 42 amphibian and reptile species have been recorded on the island (McCranie and Orellana, 2014), including the five species of anole: *Anolis sericeus, Anolis utilensis*, *Anolis. bicaorum*, *Anolis sagrei* and *Anolis allisoni*.

1.2.2.1 The Anoles of Utila

The *Anolis* lizards on the Honduran island of Utila provide an ecological laboratory to understand the links between habitat structure, ecological niches, and abundance in changing environments. Anoles are a classic evolutionary radiation that show repeated adaptation to specific microhabitats (Losos, 2009), a model system for thermal ecology (Kearney et al., 2009), and have diversified extensively on islands and the mainland (Algar and Losos, 2011). However, we still know little about what limits the abundance of these lizards (Losos, 2009), and are only beginning to understand how they respond to human disturbance (Winchell et al., 2016).

Within local ecological communities, anoles are thought to partition ecological space along three primary axes: structural microhabitat, thermal environment, and prey size (Schoener, 1974). Utila provides an opportunity to test the relative role of these different ecological axes in determining spatial variation in abundance across natural and anthropogenic habitats. It also allows us to look into the role of spatial availability of the thermal environment on the abundance of an endemic ectotherm species, across a series of habitat types and structure, Utila hosts a patchwork of land covers, (e.g. hardwood forest, palm savannah, mangrove) and expanding agricultural and urban land uses (Brown et al., 2017b). Five anole species inhabit the island, including two endemics (*Anolis bicaorum, Anolis utilensis*) and a recent invader, *Anolis sagrei* (Brown & Diotallevi, 2019; McCranie and Orellana, 2014). Previous observations suggest these anoles vary in habitat use but there has been no systematic study of their abundance-habitat relationships (Brown et al, 2017a). Given ongoing human land use expansion, the threat of climate change and *A. sagrei's* recent establishment, mapping and understanding Utila's endemic anole fauna is more urgent than ever. This needs conducting at a range of relevant scales – from the individual to the island landscape.

Of the five anole species found on Utila two are endemic (*Anolis bicaorum* and *Anolis utilensis*) and two are native to Central America (*Anolis sericeus, Anolis allisoni*). There is also the presence of an invasive anole, *Anolis sagrei*, which is a prolific invasive alien species, introduced to the island in 2014 (McCranie and Orellana, 2014). Although studies have been conducted on the anoles of Utila (Gutsche et al., 2004; McCranie and Orellana, 2014; Brown et al., 2017a, b), no systematic review of distribution and abundance has been undertaken to date.

For example, previously, *Anolis utilensis* was thought to be a mangrove specialist (Gutsche et al., 2004) and solely found in the mangrove areas of Utila at a maximum elevation of 8m. However, (Brown et al., 2017a) note that this species also occurs in the neotropical dry forest some 1.5km away from the nearest mangrove with a maximum elevation of 74 metres above sea level, the highest elevation of the island, Pumpkin Hill. As *A. utilensis* has only been encountered circa 40 times, no concrete morphological studies have been undertaken, but due to its preference to being higher up in the canopy and not being of crown-giant size, it can be suggested that *A. utilensis* likely conforms to the 'trunk-crown' ecomorph. However, more data on its distribution, morphology and microhabitat use is needed to determine its ecomorph status.

Anolis bicaorum, the focus species of this work, was first described by Köhler (1996). Males have an average snout-vent length (SVL) of approximately 64 mm SVL (McCranie & Köhler, 2015) and a bright orange-red dewlap. Despite initial reports (McCranie & Köhler, 2015), females are smaller than males (average SVL= 62 mm) with a smaller dewlap that varies from cream/grey to red (White *et al.,* 2019). *Anolis bicaorum* is thought to be a predominantly sit-and-wait predator that feeds primarily on arthropods (Brown et al. 2017b), and descends to the ground at times in pursuit of prey (personal observation). *A. bicaorum* is found predominantly in neotropical dry forest (Brown et al., 2017b) and its thermal ecology reflects

these relatively cool, thermally homogeneous environments (Logan et al., 2013). *A. bicaorum* is one of two anoles endemic to Utila. The other, *Anolis utilensis*, is the only potential congeneric competitor of *A. bicaorum* in forests. However, despite being found in similar habitats, *A. utilensis* is found at much lower abundances and perches substantially higher in the canopy than *A. bicaorum* (Brown et al., 2017b).

According to Brown *et al.* (2017b) *Anolis bicaorum* has been observed using various habitat types, ranging from preferred old growth broad-leaf/palm forest to secondary forest, coastal vegetation, White Mangrove (*Laguncularia racemosa*), and in more disturbed areas such as gardens, roadsides, and vegetated agricultural fringes. Their highest population density appears to be in old neotropical dry hardwood/broad-leaf palm forest (Brown, et al. 2017b), at a max elevation of 74m an increase in the previous 20m recorded by (McCranie and Orellana, 2014). Although most anoles can be grouped into a specific ecomorph, *A. bicaorum* does not tend to conform to its 'Trunk' ecomorph designation, which may be due to the lack of natural anole competitors constraining its movement and behaviour, as *A. utilensis* and *A. sericeus* may be too small morphologically to act as competitors (Brown et al., 2017a). The lack of competition and habitat restrictions results in, *A. bicaorum* found to inhabit almost every detectable layer from the ground up to a higher canopy layer, with individuals observed perched and sleeping on palm fronds and branches at a height above 5 m. However, due to lack of studies carried out on Utila's anoles, further evidence is required to draw conclusions that are more concrete. Other anoles on the island include native *A. sericeus*, which is found in open, grassy areas (McCranie & Orellana, 2014), the invasive species *A. sagrei* which is presently restricted to Utila Town (Brown & Diotallevi, 2019), and records of *A. allisoni,* also from Utila Town which likely reflects human introduction (Brown & Diotallevi, 2019).

Anolis sagrei, the Cuban brown anole, is a prolific invader (Edwards and Lailvaux, 2012) which has managed to invade several countries away from its native range including Honduras, Guatemala, Costa Rica, the USA and Taiwan. In regards to Utila, it is a recent invader, first recorded in 2014 (McCranie and Orellana, 2014). It is believed to have been introduced via ships and/or vegetation import into the island. *A. sagrei* is very adaptable in urban environments (Kolbe et al., 2016), and is believed to only be present within the urban areas towards the south-eastern regions of the island. However, anecdotally, the abundance and distribution of this species has increased drastically since its introduction, with individuals being recorded towards the eastern coastal areas in 2018. Losos (2009) notes *A. sagrei* as a trunk-ground ecomorph; however its ability to adapt in urban environments and the supposed lack of competition from the native anoles in these areas may lead to *A. sagrei* populations utilising the more available space within the suitable land cover types. It is therefore important to consider the current distribution and habitat use of this species on Utila, to be able to predict its possible effect on the native island species.

1.2.2.2 Conservation Threats to the Island of Utila

Like so many other natural areas worldwide, one of the main conservation threats to the island of Utila is that of human habitat conversion. The whole of the island is privately owned by individuals, and its increasing popularity as a destination for both tourists and expatriates has led to the development of many plots of land. This expanding tourism industry along with housing developments has led to ongoing habitat fragmentation and forest habitat degradation on the island (personal observation). Forest cover loss on the island can be seen using the Hansen et al. (2013) global forest change dataset, where Forest Loss is defined as 'a stand-replacement disturbance, or a change from a forest to non-forest state' (Figure 1.4)
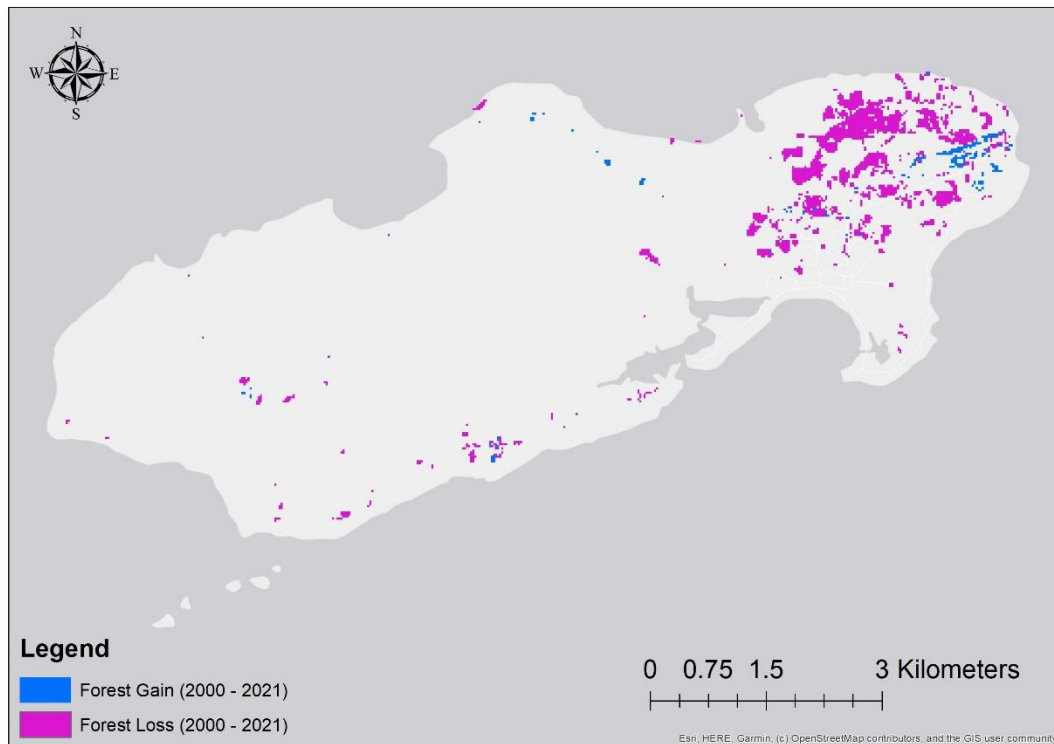
Figure 1.4: Forest cover change on Utila between 2000 and 2021, based on Hansen et al. (2013)

Initially, much of the development was concentrated along the south-east portions of the island. However, development of Pumpkin Hill Road, starting at the main airport road and leading to the north-east shore of the island, to accommodate larger vehicles, has increased the scale of the development in that locality. This is a significant conservation issue as much of the remaining hardwood forest is present around the area surrounding Pumpkin Hill (north-east corner of Utila) and the development of the road has already led to increased clearance of the forest (personal observation). This is also, where the highest density of both the endemic anoles (*A.bicaourm* and *A. utilensis*) are thought to be found (Brown et al., 2017a, b). It should be noted here that at present, much of this natural land cover (forest, mangrove etc.) clearance on Utila is for residential development. However, the current practice is to first clear the land (wholly or partially), and then to advertise the land for sale. In many cases, the land or house

is not sold and then goes into a state of disrepair. This has resulted in a lot of degraded forest and cleared/ disturbed areas on the island.

Along with the direct land conversion to presumably less favourable habitat for forest species, the increase in urbanised areas may lead to further spread of the invasive *Anolis sagrei,* which is comfortable in urban environments. At present, it is believed that the endemic anoles and the invasive *A. sagrei* are not within the same geographic range and therefore are not currently direct competitors. However as the island becomes more urban in its land cover, this may change resulting in direct competition between the invasive and endemic anoles. This is of particular concern as invasives tend to out-compete local species (Kolbe et al., 2016a; Winchell et al., 2016). In regards to agriculture, a growing island population has led to an increase in agricultural land, primarily in the form of cow pasture.

Another problem, similar to the remainder of the world is the presence of non-native and domestic predators such as feral dogs and cats and a recently noted racoon (*Procyon lotor*) population which has been introduced to the northern shores of the island. Utila has no native large mammalian predators; the presence of such introduced predators therefore is a significant threat to the local and endemic wildlife populations.

One of the major problems in regards to the anoles is that little is known about their distribution and what determines their abundance. Hence, conservation action planning and mitigating the effects of human habitat conversion for the anoles is difficult. Furthermore, as none of the endemic anole species of the island have been assessed by the IUCN, their conservation status remains unknown. However, Johnson *et al.* (2015) calculated the EVS (Environmental Vulnerability Score) of *A. bicaorum* as 17, placing it in the middle portion of the high vulnerability category. These combined conservation issues on the island of Utila is putting significant pressure on the island's wildlife as a whole. More research into the island

system is therefore urgently required in order to better understand the distribution of species and the favourable characteristics of habitats in order to better inform conservation action.

1.2.3 Thermal Ecology and Climate Change

Rising and more variable temperatures are a significant threat to biodiversity worldwide (Pereira et al., 2010; Thomas et al., 2004). In a warmer world, species' futures will depend on their ability to maintain favourable body temperatures, and thus maintain ecological function and evolutionary fitness (Kearney et al., 2009; Vasseur et al., 2014). The threat of warming is particularly acute for ectotherms, whose body temperature (T_b) depends on external environmental conditions. Many ectotherms are already operating close to their thermal limits, leaving little safety margin to behaviourally buffer higher temperatures (Bakken et al., 2014; Deutsch et al., 2008; Sunday et al., 2014). As organisms' thermal optima are surpassed, they will lose the ability to effectively obtain resources, avoid predation, withstand pathogens, and reproduce effectively, leading to population declines and, ultimately, extinction (Sinervo et al., 2010). Evidence is now mounting that tropical ectotherms will be the hardest hit from warming, and studies have warned that tropical forest lizards, in particular, are in danger of extinction (Huey and Tewksbury, 2009; Logan et al., 2013). Moreover, increased temperatures may lead to increased competition with species moving between different land cover types to areas, which are more favourable. For example, (Kearney et al., 2009) suggested that open-habitat lizards may invade the cooler forest habitats. One result of this 'invasion hypothesis' could be competitive exclusion of forest lizards, who are themselves already experiencing reduced performance due to warming alone (Logan et al., 2013). As ectotherms, anoles are dependent on the thermal conditions of their environment, as their body temperature and therefore metabolic function is dependent on environmental conditions. As a primarily tropical forest lizard, the endemic anoles of Utila are thought to have evolved in an environment that is

thermally homogeneous in both space and time and are therefore assumed to be 'thermal specialists' (De Frenne et al., 2019; Logan et al., 2013).

However, the way in which we categorise the thermal landscape and suitability for different species is important when considering the potential impacts of climate and land use change (Clusella-Trullas et al., 2021; Sears and Angilletta, 2015; Sinclair et al., 2016). Current methods look at the suitability of the environment compared to that of thermal ranges derived from thermal performance curves (for example CT_{max}) and thermal safety margins of a species (Clusella-Trullas et al., 2021; Logan et al., 2013; Sinclair et al., 2016). Although a reasonable indicator, the use of these indices as a sole indicator of ectotherm response to climate change has been called into question, as the impact of such indices on a population can vary depending on intrinsic and extrinsic factors (Clusella-Trullas et al., 2021; Sinclair et al., 2016). The spatial structure of the thermally suitable habitat at scales relevant to the organism, has also been highlighted as an important factor to consider when considering overall landscape suitability (Sears and Angilletta, 2015), due to its influence on behavioural thermoregulation. Therefore, in order to understand how the species of anoles found on Utila will fair in different climate scenarios we must first understand what thermal conditions are the most suitable to them and facilitate a healthier and more abundant population. Concerning available thermal performance and operative temperature data available for Utila's anoles, a single study was conducted in the Bay Islands of Honduras by Logan et al., in 2013 which included *Anolis bicaorum*. This thesis looks to determine what thermal indices have the greatest influence on anole abundance at fine spatial scales and how the thermal environment, prey availability and habitat structure interact and determine abundance over a habitat gradient across 20 x 20m plots. This will then feed into predictions on thermal habitat quality on the island of Utila under land use and climate change scenarios.

Understanding and predicting the effects of climate warming on organisms requires not only an understanding of the relevant thermal and habitat requirements of the species, but also accurate models of microhabitat and microclimate conditions on scales experienced by individual organisms (Duffy et al., 2021; Suggitt et al., 2018). Global climate datasets and projections of future climate change from mechanistic models capture broad-scale climatic conditions, rather than at the scales experienced by individual organisms. Microclimate conditions can differ greatly from climate averages and the weather stations in which they are based (Maclean and Klinges, 2021).Fine-scale variation in environmental conditions may provide micro-refugia to allow organisms to buffer the effects of rising global temperatures (Kearney et al. 2013; Lenoir et al. 2016). When considering current biophysical model limitations, direct interaction between organisms and their environment usually occurs at very small scales (Bakken and Angilletta, 2014), therefore current climatic data such as WorldClim (1 km^2 resolution) used within such models do not cover the scale experienced by individual organisms. Thus, models to predict microclimate heterogeneity through space and time are key to understanding how organisms currently function and the challenges they will face in a warmer and more thermally variable world. Remote sensing methods have been highlighted as a new tool for deriving inputs for such microclimate models that are at a spatial resolution relevant to what organisms experience (Duffy et al., 2021; Zellweger et al., 2019), which will lead to more accurate measures of microclimate. Which will in turn allow for better and more relevant predictions of the impact of climate and land use change on species distributions and persistence.

1.2.4 Remote Sensing

Emerging remote sensing technologies have the potential to transform our understanding of the link between species' abundances, habitat use, and environmental change (Boyd and Foody, 2011; Cavender-Bares et al., 2022; He et al., 2015). A variety of remote

sensing platforms have been highlighted as a potential source for microclimate model data (Duffy et al., 2021; Zellweger et al., 2019), which will allow microclimate to be modelled at scales more relevant to individual organisms and populations. Rapidly developing sensors and machine learning methods are allowing detailed environmental variables to be captured at unprecedented scales (Cavender-Bares et al., 2022).

Multispectral satellite sensors however have been a long running and essential resource within the field of remote sensing and land cover/habitat classification for over 50 years, ever since the launch of the LANDSAT missions in the 1970s. Technological advances within the last few years has seen the launch of higher resolution multispectral satellite imagery such as Sentinel-2 (13 band, 10m spatial resolution) launched in 2015 and WorldView-2 (8 band, 30cm spatial resolution) launched in 2009. These satellites have the capability of collecting multispectral data at a much finer spatial resolution, than that seen in the most recent LANDSAT missions (30m multispectral resolution). These satellite sensors provide valuable information of land cover spectral reflectance at high spatial and spectral resolutions, providing us with a valuable data resource.

This work utilises satellite sensors on two fronts, the first being to determine the land cover area of each habitat type of Utila, as no comprehensive land cover map had been undertaken for the island previously. One of the major advantages of satellite based remote sensing methods in Land Cover classification is that once a model with sufficient training data has been created, large areas can be classified and monitored with a limited amount of effort and resources (Rocchini et al., 2016). This means that large geographical areas at a time can be mapped with limited financial and time costs in comparison to physical surveys in the field. This is increasingly important in conservation due to the rapid change in land use as a result of anthropogenic and climatic change, especially in areas such as the tropics where field surveys are difficult and such practices as illegal logging are difficult to monitor.

Although satellite imagery does allow large areas to be monitored at a relatively fine scale, they do not tend to capture data at a fine enough resolution to represent what is experienced by individual organisms, especially species such as anoles who occupy a very small geographical home range and are extremely territorial. The coarser spatial resolution of such satellites as LANDSAT also encounters problems when the geographic area you are surveying is relatively small, for example the island of Utila, which has a total area of only 41km^2. This is where the recent development of unoccupied aerial vehicles (UAVs) with their high-resolution (sub 5cm pixel) and higher resolution commercial satellite data (WorldView-2) data has become imperative to the use of remote sensing methods to represent spatial scales that are more relevant to that experienced at individual organism levels.

Although a relevantly recent development, unoccupied aerial vehicles (UAVs) have quickly become established as a useful tool in remote sensing methods for a variety of ecological research purposes. This includes conservation (Koh and Wich, 2012), wildlife monitoring (Christiansen et al., 2016; Schiffman, 2014), vegetation mapping (Natesan et al., 2017; Nevalainen et al., n.d.; Waite et al., 2019), species level classification (Baena et al., 2017), wildlife classification and tracking (Chrétien et al., 2015; Stark et al., 2018) and agricultural expansion (Duffy et al., 2018). As UAV systems that produce high-resolution data can be relatively low cost, they can be used in long-term ecological monitoring. In addition, with techniques such as Structure from Motion (SfM) photogrammetry they can even be used as a reasonable alternative to Light Detection and Ranging (LiDAR) systems. This SfM approach, with a consumer-grade on board system camera, is becoming popular because it is cheaper and faster than traditional photogrammetric methods and UAV-light detecting and ranging systems UAV-LiDAR (Birdal et al., 2017; Kašpar et al., 2021).

The use of multispectral cameras deployed on unoccupied aerial vehicles (UAVs) in land cover and vegetation mapping applications continues to improve and receive increasing

recognition and adoption by resource management and forest survey practitioners (Ahmed et al., 2017) as well as in ecological and conservation monitoring. UAV-based flight and sensor data acquisition as well as in post-processing large numbers of individual aerial images into seamless orthomosaics have helped to introduce UAV systems as potentially convenient and effective aerial platforms for land cover and forest stand mapping, and vegetation species determination (Ahmed et al., 2017; Baena et al., 2017). UAVs offer an affordable alternative to satellites in obtaining both colour and near infrared imagery to meet the specific requirements of spatial and temporal resolution of a monitoring system. Combining this with their capacity to produce three-dimensional models of the environment provides an invaluable tool for species level monitoring (Baena et al., 2017)..

Currently available data for monitoring habitat conversion and climatic change is predominantly at large scales that fails to capture environmental variation at scales relevant to individual organisms. New technologies in remote sensing allow us to overcome such obstacles by measuring habitat variation at a fine scale. This thesis tests the mechanisms linking canopy structure and species' abundance by using high-resolution UAV aerial imagery (sub 1 cm spatial resolution) to map canopy structure and variation across a series of plots and link this with air temperature to predict sub-canopy lizard operative temperatures. Coupling this with information on what drives endemic lizard abundance will help determine these species' vulnerability to the rapidly changing landscape of their small island, which therefore contributes to the conservation of these endemic species. Along with this, the techniques developed and used during the project will provide new methods of incorporating remote sensing into species distribution modelling at a more appropriate scale relevant to such species as anoles.

1.3 Research Questions and Aims

There are two major aims to this work, the first is to further our understanding of what drives variation in species' abundance at fine spatial scales, particularly in the context of rapid land cover change and human habitat conversion. The second is to use high spatial resolution remote sensing platforms to predict sub canopy ectotherm operative temperatures, to map the thermally available environment at both ecologically and spatially relevant scales. I aim to improve our ability to predict species' ecological responses to habitat conversion and identify key ecological interactions between habitat structure, the thermal environment, prey availability and species' abundance. Lastly, I aim to improve public understanding and appreciation of Utila's little known *Anolis* fauna, promote its conservation and demonstrate how emerging technologies can help us understand and preserve the natural world.

Objectives:

1. Test how canopy structure, prey availability and thermal environment interact to determine lizard abundance and microhabitat use and how this is affected by land cover change and habitat conversion.

2. Test the availability of UAVs and WorldView-2 satellite data to determine sub-canopy lizard operative temperature.

3. Map operative temperature, a representative of thermal habitat for *Anolis bicaorum* at a plot (UAV) and landscape (WorldView-2) level spatial scales.

4. Determine the impact of habitat conversion and climate change on available thermal habitat for *A. bicaorum* across Utila using WorldView-2 data.

1.4 Thesis Chapter Structure

Table 1.1 below outlines the chapters of this thesis.

Table 1.1: Chapter numbers along with short chapter descriptions of the thesis

Chapter No.	Description
Chapter 1:	Introduction and background to the thesis.
Chapter 2:	Methods chapter detailing all primary data collection methods (field and desk based). Further data treatment and analyses are outlined in the methods section of each respective research chapter.
Chapter 3:	Research Chapter Titled: Disentangling controls on animal abundance. *(Published - Higgins, E. A., Boyd, D. S., Brown, T. W., Owen, S. C., & Algar, A. C. (2021). Disentangling controls on animal abundance: Prey availability, thermal habitat, and microhabitat structure. Ecology and Evolution, 11, 11414– 11424).*
Chapter 4:	Research Chapter Titled: Unoccupied Aerial Vehicles (UAVs) as a Tool to Map Operative Temperature in Tropical Environments
Chapter 5:	Research Chapter Titled: Quantifying available thermal habitat for *Anolis bicaorum* under anthropogenic land use and climate change using WorldView-2 imagery
Chapter 6:	Discussion and conclusions of the thesis

Chapter 2 : Materials and Methods

2.1 Chapter Overview

This chapter outlines all field data collection and imagery processing, along with preliminary results that aided in methods planning and data collection. Any relevant further processing and statistical analyses of the data outlined here, relevant to the specific research question, are outlined in the subsequent research chapters.

2.1.1 Research Permits and Ethics Statement

All work within this thesis was conducted in collaboration with Kanahau Utila Research and Conservation Facility (KURF), under appropriate research permits granted by Instituto Nacional De Conservacion y Desarrollo Forestal Areas Protegidas y Vida Silvestre (ICF), permit number DE-MP-054-2017 and DE-MP-006-2020. All methods and procedures underwent rigorous ethical review and were approved by the University of Nottingham's Animal Welfare & Ethical Review Body (AWERB; approval reference no. 014).

2.2 Research Study Area and Species

Research was conducted on the island of Utila, Honduras (16.0950° N, 86.9274° W). The primary study species was the endemic Bica anole (*Anolis bicaorum)*. For more detail on the study system and species, please see Chapter 1. Field data collection was conducted from April to June 2019.

2.2.1 Natural History

Whilst living and undergoing work on Utila between the years 2017 to 2019 (4 months in 2017, and 10 weeks each in 2018 and 2019), several personal observations of the Utila's natural history and the anole species present were noted, which are outlined in this section. As little is known on the species of interest (*Anolis bicaorum*), these personal observations, along with

literature on the species and general anole works, were used to help design data collection methods.

First, in regards to distribution on the island, personal observations noted that *A. bicaorum* is found predominantly in Neotropical dry forest, as first stated in Brown, et al. (2017b). Populations of *A. bicaorum* were found in all Neotropical dry forest areas visited, at different population densities, hence proposing the question of what determines abundance. *A. bicaorum* was found in forests across the island, which included the eastern portion of the island, and along the south, west and northern coasts. *A. bicaorum* were found across all elevation gradients, from sea level to the top of Pumpkin Hill (74 metres above sea level). No populations of *A. bicaorum* have been found to date in the central portion of the island, which is predominantly Neotropical savannah. Within Utila town, *A. bicaorum* was only in isolated fragments of forest, and was not found to be utilising gardens or more urbanised land cover types. Different land cover and habitat types on the island have been continuously surveyed as part of larger research and monitoring work by Kanahau (KURF). Table 2.1 below outlines information on the anole species of Utila and the habitats in which they have been found, based on these surveys by KURF and personal observations. Species presence (present/ not present) is stated here based solely on personal observations, therefore should be interpreted with the caveat that further comprehensive survey of the island would need to be undertaken to support these observations.

Table 2.1: Detail on land cover use of Utila's anoles from personal observations and KURF surveys.

Land Cover	Land Cover Description	Type of Observation	*Anolis bicaorum*	*Anolis sagrei*	*Anolis sericeus*	*Anolis utilensis*	*Anolis allisoni*
Agriculture	Cow pasture.	Not surveyed	Unknown	Unknown	Unknown	Unknown	Unknown
Coastal	Sandy beaches with volcanic rock exposures.	Observation only during beach cleans and turtle nesting patrols.	Not present	Present	Unknown	Unknown	Unknown
Coastal Scrub	Coastal plants such as Sea Grape (*Coccoloba uvifera*) found frequently in large patches along the coast.	Observed en-route to mangrove surveys. Surveyed during plot surveys.	Not present	Unknown	Present	Not present	Unknown
Coastal Forest	Coastal forest, with little to no understory, predominantly consisting of almond trees (*Terminalia catappa*).	Observed daily, surveyed during plot surveys.	Present	Present	Unknown	Unknown	Unknown
Rhizophora Mangrove	Areas of mangrove dominated by *Rhizophora spp.*	Surveyed extensively for *Ctenosaura bakeri* surveys.	Not present	Not present	Unknown	Not present	Unknown
Black Mangrove	Areas of mangrove dominated by *Avicennia germinans*.	Surveyed extensively for *C. bakeri* surveys.	Not present	Present	Unknown	Not present	Not present
White Mangrove	White mangrove (*Laguncularia racemose*) trees that grow sparsely around the coast.	Not Surveyed.	Unknown	Unknown	Unknown	Unknown	Unknown
Neotropical Forest	Old growth hardwood and palm forest.	Observed daily and surveyed for plots.	Present	Not present	Present	Present	Unknown
Neotropical Savannah	Neotropical savannah.	Observed on several occasions, not surveyed.	Unknown	Unknown	Unknown	Unknown	Unknown
Tique Palm Forest	Palm forest, bordering savannah.	Not surveyed	Unknown	Unknown	Unknown	Unknown	Unknown
Urban	Buildings, tarmac.	Observed and surveyed.	Not present	Present	Unknown	Unknown	Unknown
Urban gardens	Ornamental gardens in town.	Observed and surveyed.	Not present	Present	Present	Unknown	Present

In regards to microhabitat use of *A. bicaorum,* personal observations aligned with what is stated in Brown et al. (2017b). A. *bicaorum* individuals were found to perch primarily on tree trunks, but also utilised fallen logs, wooden fence posts and in one case a concrete outhouse. *A. bicaorum* were often observed sleeping on palm fronds or thin vines, sticking to the very tips of them to sleep, likely as a way to escape predators by sensing vibrations and jumping from the end (personal observation). Individuals were almost exclusively faithful to one particular perch and did not move horizontally in space often, choosing to stay on their perch and only moving vertically or around the trunk of the tree. From personal observations, no anole was seen to move out of the plot boundaries, sticking within a 20 x 20 m horizontal area, and mostly sticking to their own perch.

A. bicaorum are territorial and males especially would only tolerate females perching on the same perch as them. Territory size is unknown at present, however individuals would fight others who came within a metre of their perch, with the exception of males allowing females nearby. Males were also seen using their dewlaps as aggression displays to other males, as warnings to ourselves (as predators), and to females during courtship.

A.bicaorum were observed eating exclusively arthropods, although no diet analysis (stomach pumping, genetic faecal analysis) has been done. They would often eat whatever walked passed them on their perch or they would jump down to the forest floor to catch something in the leaf litter.

In regards to the invasive brown anole (*Anolis sagrei*), on Utila, a high abundance of the species was noted in urban areas, particularly in Utila town. They were primarily observed running along the ground in great numbers and occasionally using walls, trees and PVC piping as perches. They did not seem to conform to their trunk-ground ecomorph designation however, and were utilising all vertical levels of canopy and perches, preferring the ground overall. One

important note is that one anole seen in the forest, near Pumpkin Hill was identified as a potential *A. sagrei*. This was not confirmed as the individual escaped capture, and could not be concretely identified. This is important to note, as currently the species is restricted to the regions surrounding Utila town. However, urban expansion and the development of Pumpkin Hill Road means that more vehicles are moving back and forth the town which could lead to *A. sagrei* stowaways reaching Pumpkin Hill far more quickly than would happen via natural colonisation of the species.

2.3 Survey Plots

Field data collection was carried out across a series of sixteen 20 x 20m plots, which were set up across a habitat gradient, which covered several of the land cover classes of Utila. Plot level data collection was most suitable in order to measure habitat characteristics and animal abundance at a fine spatial scale. Transects were not considered a reasonable form of collection, as transects would likely cover a degree of habitat variation/ land cover change along their duration, as well as having a greater proportion of edge than plot level measures. As of late 2017 the land cover of Utila, had not been conclusively mapped. Therefore, a land cover map of Utila was produced prior to field data collection to determine the extent of the different land cover classes on Utila, which would aid in both plot selection and monitoring of land cover change on the island. Due to the inaccessibility of parts of the island, satellite remote sensing methods were used to create the map, which are outlined below.

2.3.1 Land Cover Map

Sentinel-2 Satellite data was used due to its suitably fine spatial resolution (bands at 10m pixel resolution) and its high spectral resolution (13 spectral bands). A cloud free Sentinel-2 Satellite image from July 2016 was used and all 13 image bands were combined into an image stack in ERDAS Imagine 2018 using the layer stack tool, and the stack was resampled to 10m using the resample tool in European Space Agency Sentinel Application Platform (SNAP). The resampled image was then subset to the island of Utila using ERDAS Imagine, an example of a RGB composite image from the processed Senitnel-2 satellite imagery can be seen in Figure 2.1.

Figure 2.1: Sentinel-2 RGB composite Image of Utila, Honduras - July 2016

This pre-processed Sentinel-2 imagery was classified using a polynomial Support Vector Machine (SVM) as this classification method tends to result in higher classification accuracies than of the standard Maximum Likelihood Classification methods (Ustuner et al.,

2015). A total of 443 ground GPS points, which noted the land cover, based on personal observation were collected using a Garmin e-trex handheld GPS unit in the field 2017, during a pre-PhD field season on the Utila. These were randomly subsampled using the Subset Features tool in ESRI ArcMap 10.4 software, where 50% (222 points) were used to train the SVM model, and the remainder used for independent test set model validation. The ArcMap generated training points were converted to regions of interest (ROIs) in ENVI. To ensure there was minimum of 100 training pixels per land cover class, additional training data ROIs were created manually in ENVI based on ground validated points, using pre-existing knowledge of the island (from the pre PhD 2017 field season) and Google Earth imagery, all 13 bands were included in the classification process. GPS training points were limited in spatial distribution due to access constraints during the 2017 field season, future work and mapping of the island would include more spatially distributed training classes to avoid bias in the classification model. A map of the GPS training points can be seen in Appendix 1. Eleven land cover classes were included in the classification, that were based on field observations of Kanahau Utila Research and Conservation Facility and previous ground validated GPS data. These classes, along with their descriptions can be seen in Table 2.2. These classes were chosen to highlight different land cover types of Utila, including areas of development and the potential extent of different natural habitats, as a land cover map of the island did not exist. This would aid the plot selection for this study but would also to feed into conservation objectives of Kanahau Utila (KURCF). Certain land cover classes were kept separate, for example, costal vegetation

was separated from mangrove to inform potential habitat distribution of the Utila spiny-tailed

iguana (*Ctenosaura bakeri*), another endemic and critically endangered species (Maryon *et al*.,

2021), which is found almost exclusively in mangrove (Gutsche, 2005).

Table 2.2: Land Cover Class Descriptions

Land Cover Class	Description
Agriculture	Agricultural areas, which includes cropland, pasture and plantations with sparse tree cover.
Coastal	Coastal areas, predominantly sandy beaches.
Coastal Vegetation	Coastal plants such as Sea Grape (*Coccoloba uvifera*) found frequently in large patches along the coast.
Dead-mangrove	Areas of dead and dried out mangrove.
Hard-surfaces	Tarmacked areas.
Hardwood Forest	Neotropical dry forest.
Coastal Volcanic Rock	Dark coastal volcanic rock, found along areas of the coast.
Neotropical Savannah	Neotropical savannah.
Tique Palm	Areas of mixed palm forest.
Urban	Urban areas, which includes tarmacked areas.
Water	Water.

A map of the final SVM classified land covers for Utila can be seen in Figure 2.2.
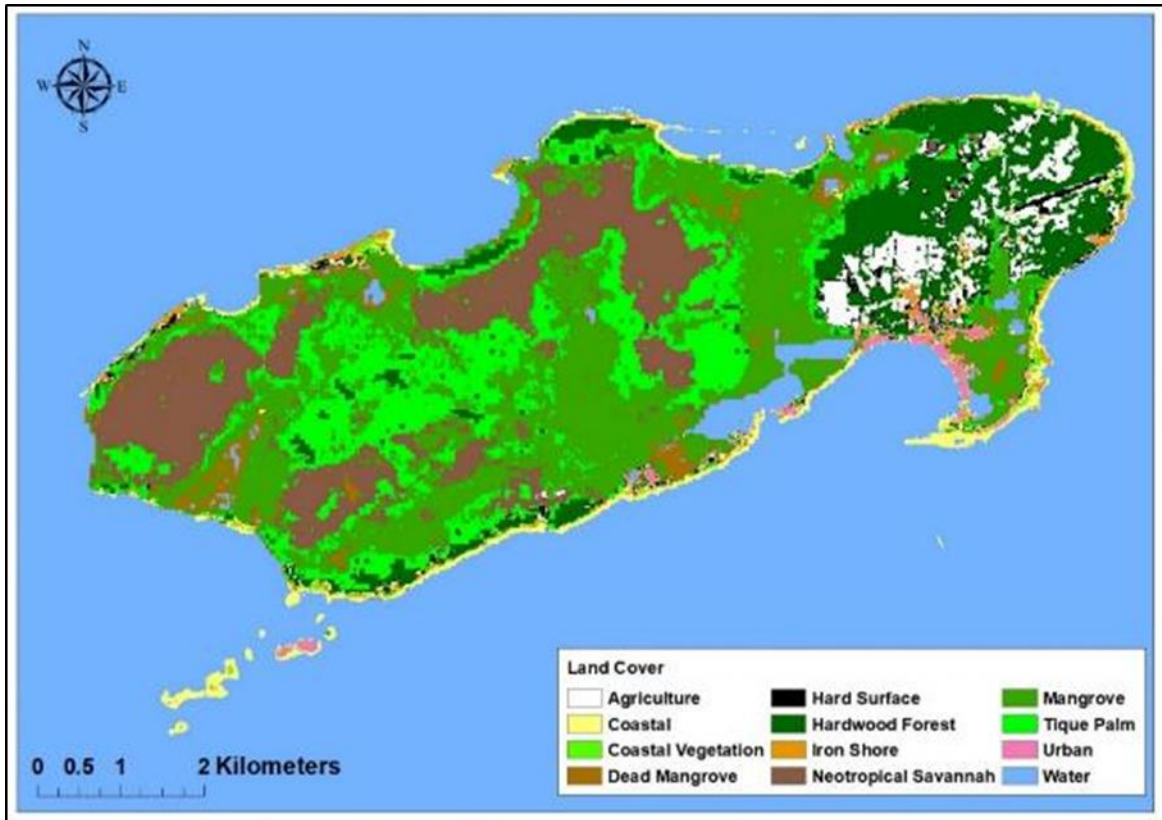
Figure 2.2: SVM Land Cover Classification Map of Utila, from Sentinel-2 Satellite Imagery
(Date: July 2016)

To test the accuracy of the land cover classification the remainder of the ground GPS points (222 points) were used to carry out a confusion matrix assessment. GPS shapefiles were again converted to ROIs and then used in the confusion matrix accuracy assessment carried out in ENVI software. All land cover types were included in the accuracy assessment. Overall accuracy was calculated at 87.86%, which was determined to be sufficient for selecting general regions for plot locations, as it was only to highlight regions where certain land cover classes could be present. This land cover map was then used to inform plot selection on the ground in Utila.

Using the land cover classification map produced from Sentinel-2 Data, sixteen 20 x 20 metre survey plots were set up across a series of land cover types, which included forest, mangrove and urban plots. Due to travel and accessibility constraints, reaching the western

portion of the island was not feasible for this study; all plots were therefore located towards the eastern portion of the island. However, the majority of the forest habitats where *A. bicaorum* is typically found is located towards the eastern portion of the island (Figure 2.2, Kanahau personal observations). Plots were set up within areas where accessibility and land access permissions were available, and were a minimum of 15 metres into the surveyed land cover type to minimise the impact of edge effects. Plots varied in their level of human disturbance (personal observation), including relatively intact forest, to heavily disturbed, sparsely treed areas, in Utila Town. A full description of plots can be seen in Appendix 2, a map showing the locations of each plot can be seen in Figure 2.3.
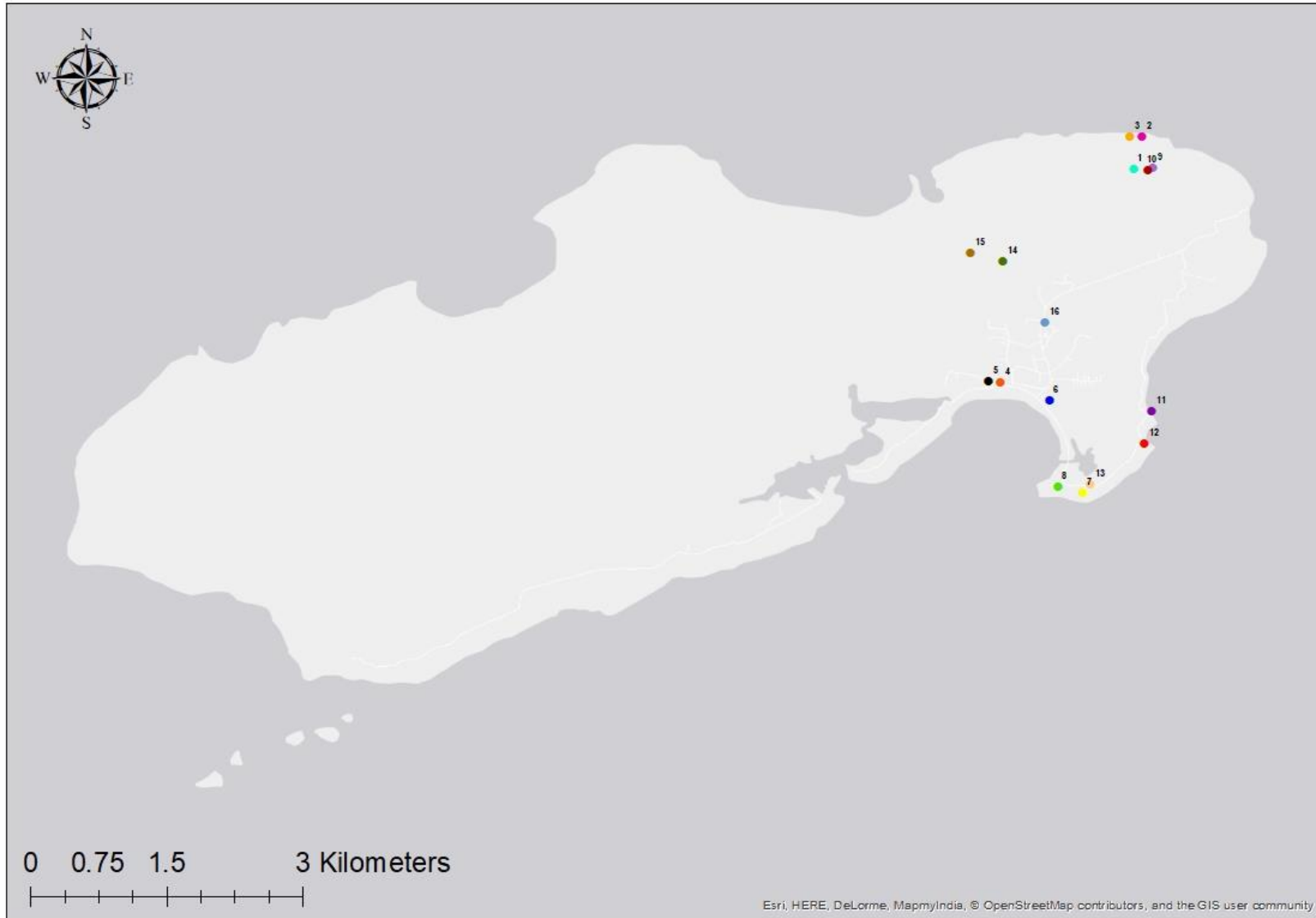
Figure 2.3: Plot locations, number refers to Plot ID number

2.4 Anole Abundance Surveys

Abundance surveys for *A. bicaorum* were carried out using standard mark-recapture methods, based on Heckel & Roughgarden (1979). In each plot, the same observers actively searched for anoles for 60 minutes on four occasions (09:00, 13:00, 17:00 and 09:00), over a twenty-five hour period. Each anole was marked with a visit-specific paint mark using an Indico Duz-all spray paint gun and non-toxic water-based paint (Figure 2.4), following (Frishkoff, et al., 2019, Heckel & Roughgarden, 1979). Plots were surveyed over a period of 10 weeks between April and June 2019. We avoided days with rain or high winds, which may influence detectability and recorded air temperature at 1.5m height using a shaded DS1921G-F5 iButton at each plot.

Figure 2.4: An adult female *A. bicaorum,* marked on four separate sampling occasions

2.5 Thermal Environment Surveys

To measure operative temperature in different microhabitats at each plot, and therefore map out the thermal environment available for *A. bicaorum*. Morphologically accurate 3D-printed replicas of an *Anolis* lizard with temperature DS1921G-F5 iButton data loggers inserted

were set up indifferent microhabitats within each plot. These replicas were created using the methods below.

An EinScan-S (Shining 3D) 3D Desktop Scanner was used to scan a male *Anolis sagrei* specimen provided by the Natural History Museum, London. Note that specimens of the primary focus species (*A. bicaorum*) were not present in the collection. The EinScan-S is a white light 3D scanner that uses white light interferometry to create high-resolution point clouds of a 3D surface. The *Anolis* specimen used for the scan (series no. 1938.10.4.8-79) was complete and in good condition, the collection location of the specimen was noted as Swan Island, Honduras (coordinates N17º 24' W83º 54') with a collection date of 14th November 1937. The specimen was placed on the turntable where the EinScan-S used white light scanning to generate a 3D point cloud of the specimen, turntable rotation steps was set at 30 to increase the level of detail captured. The morphometric measurements of the specimen used can be seen in Table 2.3; all measurements refer to the right side of the anole.

Table 2.3: Morphometric Measurements of *Anolis sagrei* Museum Specimen

Feature	Measurement (mm)
Snout to Right Femur Insertion	58.35
Feature	Measurement (mm)
Humerus Length	12.29
Ulna Length	11.28
Finger IV Length	9.81
Femur Length	16.41
Tibia Length	18.6
Metatarsus length	10.72
Toe IV Length	12.43

The snout to right femur insertion (Table 2.2) was used as a proxy for snout to vent length (SVL), as the vent was not visibly clear due to the nature of the specimen (preserved from 1938). It is noted that the male *A. sagrei* individual used for the model had a smaller SVL than the average male *A. bicaorum* (average 64mm). This may have influenced model

heating/cooling due to model size and surface area differences. However, the SVL of anole populations and individuals can vary and the difference in SVL is less than 10mm. In regards to their anatomy, *A .bicaorum* and *A. sagrei* are similar and they both conform to the same trunk-ground ecomorph designation (Brown et al. 2017; Losos, 2009), therefore 3D models printed at this resolution (Figure 2.5) would be similar for both species. The above coupled with the fact that models were calibrated against a live *A. bicaorum*, indicate that the temperature error from the models from using an *A. sagrei* specimen would be no more than that seen when comparing differences in individuals from across a population of *A. bicaorum.*

The three dimensional stereolithography (STL) point cloud file was imported into TinkerCAD editing software where a well was inserted to hold the iButtons. Note that due to limitations with the scanner not picking up areas of the feet and tail (due to them being smaller than 1mm), parts of the tail and the feet had to be manually reconstructed within the software. Replicas were prepared for printing in FlashPrint 3D slicing software and printed hollow in PLA plastic using a Flashforge Creator Pro 3D printer.
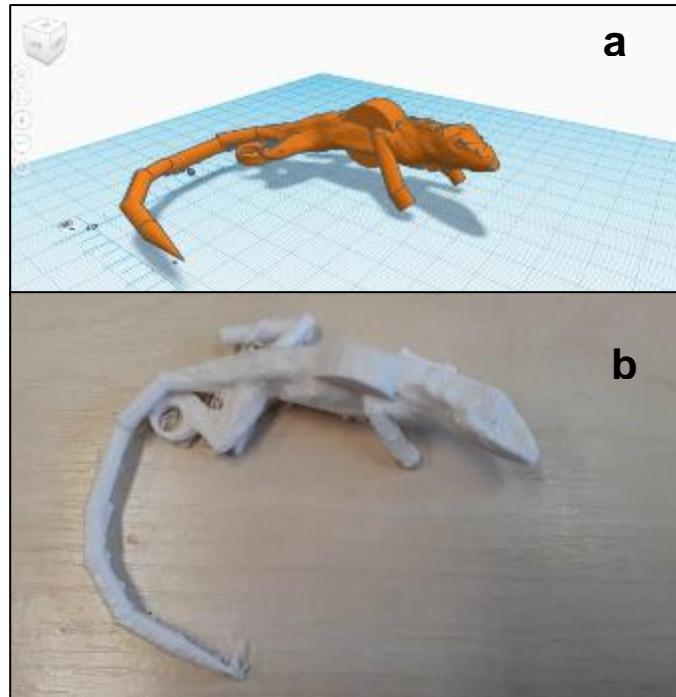
Figure 2.5: a) Replica preparation in TinkerCAD Software, b) 3D Replica Prior to Painting

Replicas were painted to match the solar-absorptivity of a live *Anolis sagrei*. To obtain the colour in the absence of live lizards, the mean RGB pixel value was calculated from a sample of 1000 random clips of 50 *A. sagrei* images. These RGB values were then compared to 27 different paint samples using an online colour-sampling tool and the most suitable paint chosen. Replicas were painted based on *A. sagrei* as neither live animals nor sample images for *A. bicaorum* were available in the UK prior to commencing fieldwork and suitable paint was not available on the island of Utila. However, models were thermally calibrated against A. *bicaorum*. The model colour was compared to a live *A. sagrei* following (Munoz et al., 2014 & Muñoz and Losos, 2017) by measuring reflectivity of the head, body, and tail using an Ocean Optics USB 2000 spectrometer. Reflectivity values were recorded as percent reflectance relative to a white standard using an Ocean Optics R400 ultraviolet visible (UV-VIS) reflectance probe in natural sunlight light conditions under the forest canopy. No additional light source was used, only natural daylight as would be experienced by the lizard. Results can be seen in Figure 2.6.
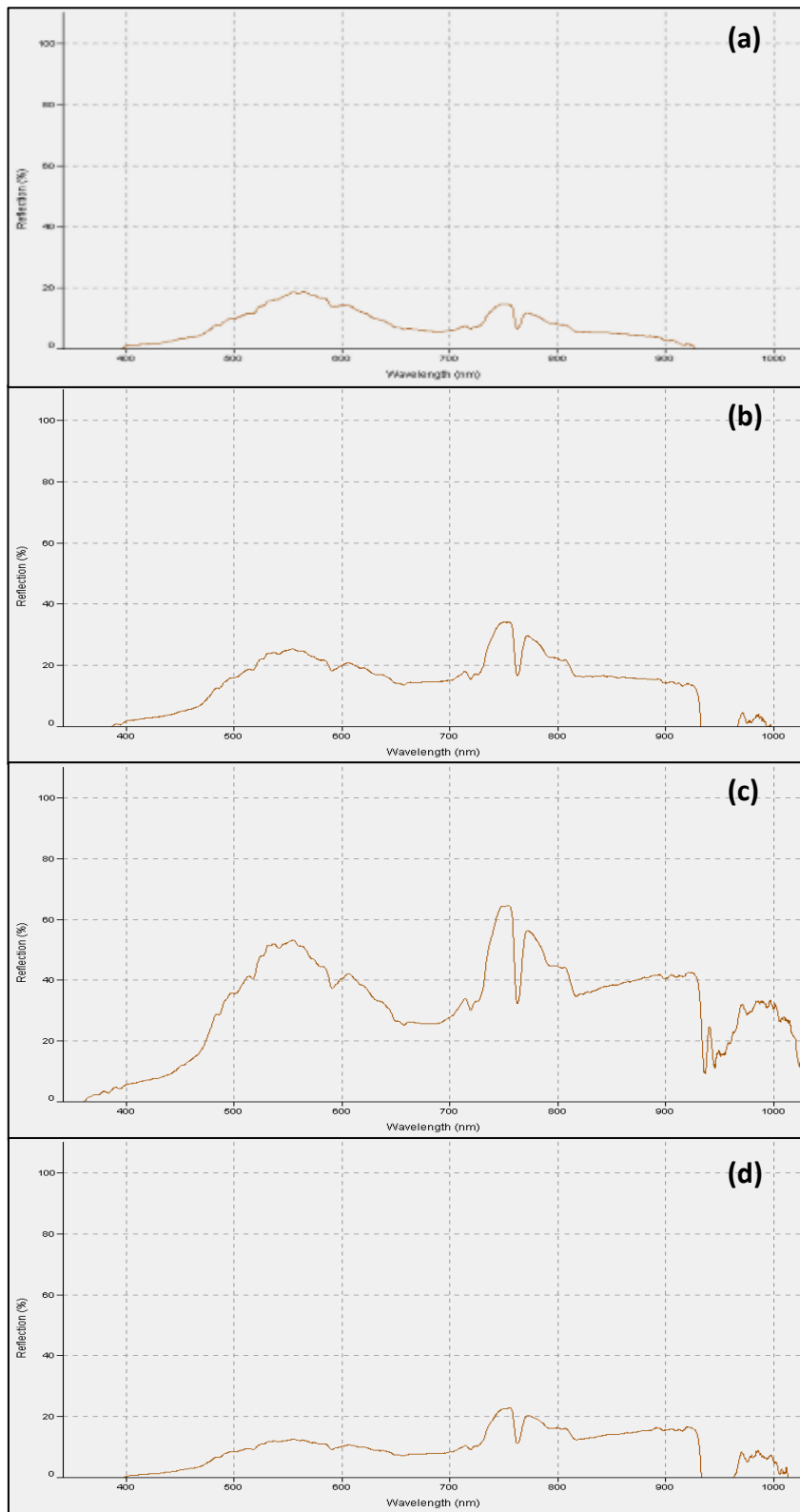
Figure 2.6: Reflectivity values as a percent reflectance relative to a white standard for the 3D lizard replicas and the live *A. sagrei.* Where; a) 3D replica, b) *A. sagrei* head, c) *A. sagrei* torso (dorsal measurement) and d) *A. sagrei* tail.

Reflectance measures indicated a relatively good colour match, however this varied depending on what part of the anole was measured. Where the replica was sometimes lighter or darker than the animal. The anoles themselves, both *A. sagrei* and *A. bicaorum* shift colour from dark to light depending on surrounding conditions, this was personally observed in the field and during the colour calibration measures. Live animals can also behaviorally thermoregulate, by such means as extending their dewlap and opening their mouths, as was noted in the *A. sagrei* during taking these measurements. The slight difference in replica colour, for example being slightly darker or lighter than the animal, may have an impact in replica warming and cooling due to reflectance of solar radiation. However, as animals shift their colour depending on the ambient conditions and behaviorally thermoregulate, such replicas can only be designed to be a best fit for all individuals in a population. Therefore, further model calibration took place in terms of thermal calibration against a live *A. bicaorum.*

Thermal replicas were calibrated against a live *Anolis bicaorum* following Muñoz *et al.* (2014). A thermocouple attached to an Omega /HH806AU Multilogger data logger was inserted into a live lizard (*A. bicaorum*) and a 3D model simultaneously; both were then exposed to different environmental conditions. Both the lizard and the model were first placed in a cool place (icebox) until their temperatures reached around 20°C (and model and animal were the same temperature). The lizard and model were then moved into the sun where their temperatures were logged for approximately 15 minutes at 15-second intervals, or until the animal's temperature reached 32°C. Model and lizard were then moved back into the original cool place (icebox) and their temperatures taken for a further 15 minutes. As models reached higher temperatures than the live animal, which could skew estimates of time spent within the preferred temperature range (Figure 2.7), a transfer function was generated to convert 3D model operative temperature (T_e) to lizard (T_e).

Change in lizard T_b (ΔT_b) per second was modelled as function of the change in 3D model T_e (ΔT_e) per second using linear regression through the origin (Figure 2.8), which had R^2=0.74, and was statistically significant (F=271.9, df=1,94, $P < 1 \times 10^{-15}$). I tested for curvilinearity using a quadratic regression, but the quadratic term was not significant ($P = 0.92$, R^2=0.74). The linear regression produced the following equation (slope $\pm$ s.e.):

$$\Delta Tb = 0.41 \pm 0.02 \times \Delta Te \text{ - \textbf{Equation 1}}$$

Equation 1 was used to model how lizard T_b would change in each time step, assuming that T_b and T_e were equal at 6am each day, which is realistic given the lack of direct solar radiation at this time. Comparing transformed T_e values (using Equation 1) to the anole T_b during the calibration experiment, I found that using equation 1 over-corrected T_e (Figure 2.7). Thus, the uncalibrated T_e measures and over-corrected T_e values represent an envelope in which the true T_e occurs. I thus present analyses using the average of the uncalibrated and over-corrected T_e values in the main text (calibrated T_e).
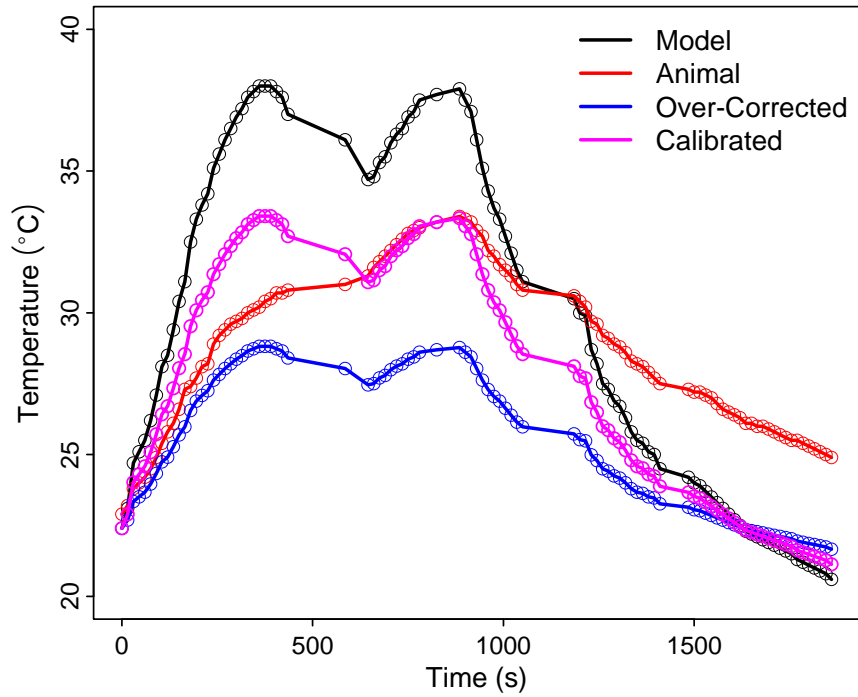
Figure 2.7: T_b of an adult male *Anolis bicaorum* (animal), uncalibrated, calibrated and over-corrected T_e over time during the calibration experiment. Hollow points on lines indicate data points.
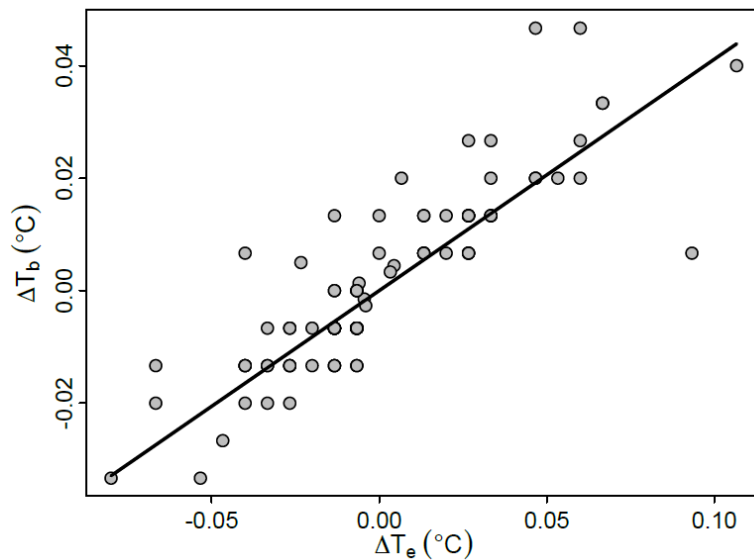
Figure 2.8: Change in lizard Tb (ΔT_b) per second as function of the change in 3D model T_e (ΔT_e) per second

2.5.1 Plot Operative Temperature

To measure the operative temperature (T_e) of lizards within different microhabitats in each survey plot. Twenty morphologically accurate 3D replicas, calibrated against a live lizard's body temperature and fitted with DS1921G-F5 iButtons, were set up in each plot for three days. iButtons were programmed to record temperatures at 1 hour intervals between the hours of 06:00 and 18:00, when anoles were active, giving a total sample period of 36 hours per plot. Replica position, substrate (trunk vs. ground), height (0–250 cm in 15-cm increments) and compass orientation (0–360° in 45° increments) were randomly chosen using a random number generator. Due to constraints on the number of iButtons and therefore *Anolis* replicas available, models were not always set out at the same time as lizard abundance surveys were undertaken. However, this is unlikely to have influenced results, as the mean air temperature recorded during lizard surveys was highly correlated with the mean air temperature of the dates models were in situ (r =0.85, P <0.001, Figure 2.9).
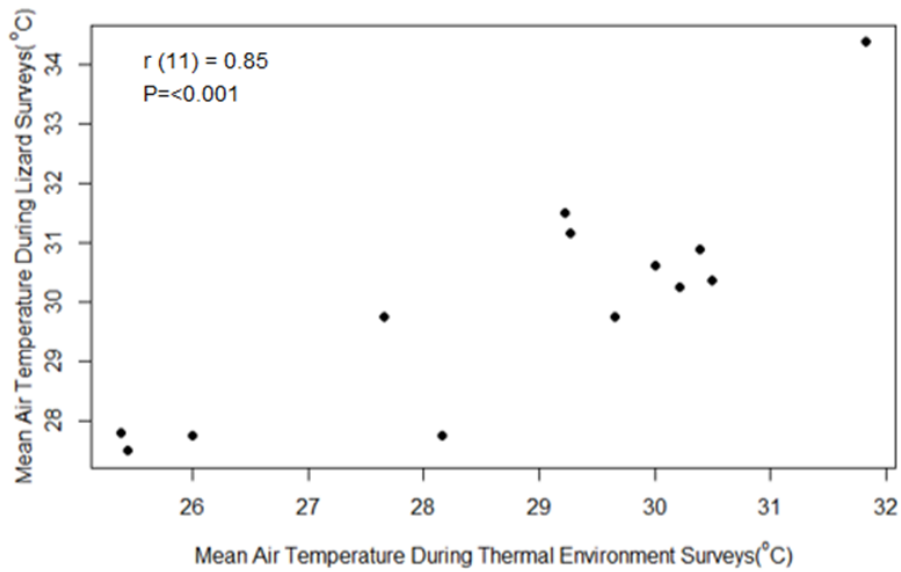
Figure 2.9: Comparison of mean air temperature recorded over all lizard surveys with the mean air temperature of the dates models were in-situ for the same times as lizard surveys (09:00, 13:00 and 17:00) across the 13 survey plots

Figure 2.10: 3D Replicas set up on different substrates and at different orientations within Hardwood Forest (left) and Mangrove (right).

Not all lizard 3D replicas were set up with the same aspect (vertical/ horizontal), as seen between in the images of Figure 2.10. This can influence the heating of the replica, for

example how much of the replica surface area is exposed to solar radiation throughout the day. However, this was to mimic some *A. bicaorum* individuals that were seen to perch horizontally (personal observation). The number of replicas set up horizontally was kept consistent across all plots, whilst positioning in the plot still being random. Four replicas in each plot were set up with a horizontal aspect; the remaining 16 in each plot were set up vertically to mimic the majority of the population who orientated themselves as such. The location of all tree trunks, palm stems and fence posts within each of the survey plots were recorded using a Spectra Pro Mark 120 differential GPS (DGPS) unit. Locations were imported into ArcMap 10.4.1 as a point shapefile and points of the locations with 3D anole replicas present were extracted to a new file using the Extract ArcMap function. Mean horizontal recording error of the DGPS measurements was calculated $\pm$ 0.86cm.

2.5.2 Thermal Preference

In order to determine the thermal preference (T_{pref}) range of *A. bicaorum*, thermal preference experiments were conducted on eight males and eight females of *A. bicaorum,* taken from different forest environments. Following Battles and Kolbe (2019), each individual was placed at the centre of a thermal gradient (150cm x 15cm x 25cm), heated by a heat lamp at one end and cooled by ice packs at the other, to obtain a gradient from approximately 10°C to 45°C. A thermocouple was inserted into the cloaca and secured with removable adhesive tape to the base of the tail. Animals were permitted to move freely within the gradient and select their preferred temperature. After a 10-minute adjustment period, internal temperatures were logged every 10 seconds by a data-logger attached to the thermocouple for a total of 60 minutes without disturbance by observers. Thermal preference range (T_{pref}) was calculated by finding the central 50% of body temperatures of each animal and averaging the 25th and 75th temperature quantiles across individuals. One individual, an adult male, was excluded from subsequent calculations because it behaved unusually by not moving from the cold end of the

gradient for the entire trial, despite a substantial drop in body temperature well below ambient. This individual was likely stressed, causing this unusual behaviour and was quickly removed from the experiment. It was placed in a cotton bag in a quiet area where its body temperature could warm back up. When the individual was warm and active it was quickly put back in the exact location it was found. The duration of the thermal gradient experiments was shorter than is common in the literature (e.g. Battles and Kolbe 2018) as a consistent temperature gradient could not be maintained for longer in field lab conditions and thus must be interpreted as indicative, but not definitive, measures of T_{pref}. I examined whether T_{pref} estimates were affected by sampling interval by re-computing the T_{pref} range using 1 minute and 5-minute sampling intervals. Measures of the mean T_{pref} range were consistent across different sampling intervals (Table 2.4).

Table 2.4: Tpref range of A. bicaorum measured at different sampling intervals of 10 seconds, 1 minute and 5 minutes.

Measurement Interval	Lower T_{pref} Range (± S.E)	Upper T_{pref} Range (± S.E)
10 Seconds	25.4 ± 1.56°C	28.0 ± 1.44°C
1 Minute	25.4 ± 1.53°C	28.0 ± 1.35°C
5 Minutes	25.5 ± 1.29°C	28.0 ± 1.27°C

2.5.3 Thermal Habitat Quality

Thermal habitat quality of each plot was calculated using two indices. The first was the percent of model hours that operative temperatures were within the T_{pref} range over the 36-hour study period for each plot. The second was the total number of degrees (°C) that the models deviated from the T_{pref} range across all models throughout the survey period for each plot. Unlike the former, the latter includes information on the extent to which temperatures deviated both above and below the T_{pref} range. In *A. bicaorum*'s sister species, *A. lemurinus*,

temperatures above preferred temperature range were found to have a greater impact on lizard performance than temperatures below the range (Logan et al., 2015). Therefore, along with the total deviation, the deviation above T_{pref} and the deviation below T_{pref} were calculated separately.

2.6 Structural Habitat Suitability

Perch availability, a measure of structural microhabitat quality, was calculated by counting the number of tree trunks and palm stems within each plot. Tree trunks and palm stems were focused on as *A. bicaorum* was observed almost exclusively on trunks and palm stems during microhabitat surveys, rather than on higher branches or on the ground. Where plots included fence posts, these were included in the measure of perch number. One plot had a small outbuilding, which was not included in the measure of perch availability. As an alternative measurement of structural habitat availability plot basal area, a measure of stand density was also calculated, by measuring each stem's diameter (including fence posts) at breast height (DBH) and using Equation 2, across all tree trunks, palm stems and fence posts in the plot.

$$\text{Basal Area} = \sum \pi \, (DBH/2)2 \quad \text{- } \textit{Equation 2}$$

2.7 Prey Availability

Prey availability was measured using arthropod biomass (g) from a combination of leaf litter sieving and sweep net samples taken in each plot. Sweep netting for arthropods was undertaken along two diagonal transects across each plot, sampling for five minutes along each transect. Leaf litter was sieved at five locations throughout each plot: the central point of the two diagonal transects and then halfway along each transect line from the centre of the plot out to the corners. All captured arthropods were placed whole in RNAlater solution for another study, then dried and weighed to determine plot arthropod biomass. No RNA extraction took

place before biomass calculation. As an alternative to biomass, all individuals were identified to family and both Simpson's and Shannon's diversity was then calculated for each plot. Sweep net and leaf litter samples were combined for plot level analyses.

2.8 Canopy Cover

I measured mean leaf area index (LAI) in each plot using an Accupar LP80 ceptometer. LAI is the one-sided area of leaves per unit ground area and is a measure of canopy density; it is expected to influence thermal environment via the interception of solar radiation (Campbell & Normal 1998; Algar et al 2018). Ten measurements for below canopy photosynthetically active radiation (PAR) were taken every two metres along two diagonal transects, running from each corner to the opposite diagonal corner, forming an 'X' across the plot. To measure LAI directly above each of the 3D thermal replicas measurements 10 measurements were also taken directly above each of the replicas. To obtain mean above canopy PAR, ten measurements were taken in full sunlight before and a further ten measurements were taken in full sunlight after sampling transects. LAI was calculated using a simplified version of the Norman-Jarvis model (1975), a full breakdown of this can be found in Appendix 3. All transect LAI values were then averaged to give a mean LAI for each plot.

2.9 Air Temperature

Air temperature of each plot was recorded at 1.5m height using a shaded DS1921G-F5 iButton. iButtons were set up as close to the centre of each plot as possible, depending on the nearest perch location where the iButton could be adhered to, and were set to record every hour over the survey period of ten weeks.

2.10 Unoccupied Aerial Vehicle (UAV) Imagery

Ultra high spatial resolution aerial imagery of each plot was acquired using a DJI Phantom 4 Advanced RTK quadcopter UAV equipped with an integrated RGB (red, blue,

green), 1-inch, 20-megapixel CMOS sensor mounted on a three-axis, gyro-stabilized gimbal. The UAV has an integrated GPS and GLONASS positioning system. The UAV was calibrated using the DJI Go application and flown using an automated flight system within the Maps Made Easy application; both apps were installed and operated using an iPad five. The flights were conducted during calm conditions to prevent wind effects on leaves, as per Whaite et al. (2019). The UAV was set to fly at a height of x 1.5 the height of the canopy, as to gather as higher spatial resolution pixels in the imagery as possible, whilst avoiding any potential obstructions to the UAV that may not have been seen through the canopy during flight planning. This resulted in a flight altitude of between 40 and 50 metres, a full list of flight altitudes per plot can be seen in Appendix 4. All flights were captured using the standard integrated RGB camera capturing images at a 90 by 90 % forward and side image overlap, in order to have adequate image overlap for creating orthomosaics of the canopy. UAV images were processed in Agisoft Metashape Professional V1.6.6, to create a 3-band RGB orthomosaic image for each plot, projected to WGS1984 UTM zone 16N. Results of each flight resulted in a mean pixel spatial resolution of 0.9 cm per pixel. Orthomosaics were validated for spatial accuracy by visually comparing known points (buildings, roads etc.) to base maps and also DGPS points taken in the field at each plot.

2.11 WorldView-2 Satellite Imagery

In order to gather very high spatial and spectral resolution imagery across the whole of Utila, WorldView-2 (WV-2) satellite imagery was acquired for the whole of the island for two years, 2018 and 2020, from Maxar (formerly Digital Globe). The WV-2 imagery acquired was a pre-processed orthorectified image with full radiometric and sensor calibration. The imagery had eight multispectral bands (red, blue, green, near-IR, red edge, coastal, yellow, near-IR2) at a spatial resolution of 2m and a panchromatic spatial resolution of 50cm. Further parameters

of the satellite data acquired, including the percentage of cloud cover, can be seen below in Table 2.5.

Table 2.5: WorldView-2 Imagery Details

Digital Globe Catalogue ID	Date Acquired (dd/mm/yyyy)	Cloud cover (%)	Area off Nadir
1030010083B5D300	01/08/2018	0.0	21.6
10300100A62C0900	09/05/2020	0.0	29.5

As high spatial resolution imagery was required, with the need to consider the multispectral bands. The imagery, for the years 2018 and 2020, was pan sharpened using the bilinear interpolation method in ERDAS Imagine using the HCS resolution merge function. Resulting in a 50cm pixel resolution multispectral image for each of the years (2018, 2020). The pan-sharpened images were used in subsequent analyses. Atmospheric correction was not carried out on the images due to insufficient calibration data in the field, leading to uncertainty on atmospheric correction efficiency. Steps taken to account for this and implications of no atmospheric correction are described in Chapter 5.

2.12 Imagery Canopy Metrics

In order to extract canopy metrics from both the UAV imagery (Section 2.9) and WorldView-2 imagery (Section 2.10), the following processing methods were conducted on both types of images separately. As a proxy for canopy presence and density, the proportion of green (greenness) of each pixel within the orthomosaic was calculated by using the Raster Calculator tool in ArcMap10.4.1. First, the Red, Green and Blue bands of the images were

extracted as individual raster layers, and then Equation 3 (Morris et al., 2013) was carried out in the raster calculator tool.

$$Greenness = \frac{Green}{(Red + Green + Blue)}$$ -   *Equation 3*

This resulted in a in a 'Greenness' raster layer with values between 0 (low greenness) and 1 (high greenness), for each image, at mean spatial resolution of 0.9cm per pixel. This greenness measure was deemed more appropriate than excess greenness as it gave a ratio of green within a pixel, and does not give a higher importance to green over the other bands (as is seen in excess greenness), as red/blue bands may be important in urban areas. However, other vegetation indices may be beneficial to pursue in future to compare their performances. An example of a processed UAV image can be seen in Figure 2.11.
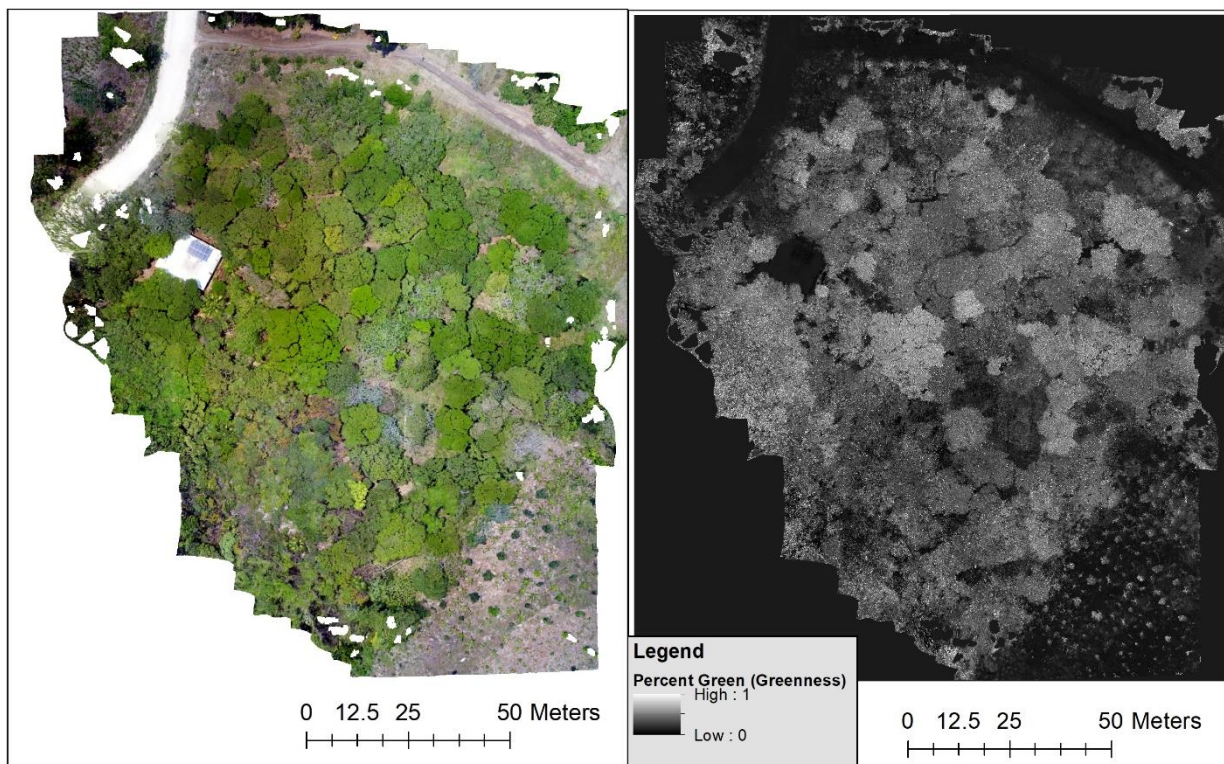
Figure 2.11 UAV RGB Orthomosaic (left), UAV Greenness raster following Equation 3 (right) where 1 = high greenness and 0 = low greenness values.

51

In order to capture measures of canopy heterogeneity and structure I carried out texture analysis on the Greenness raster layer. Grey level co-occurrence matrix texture analysis was undertaken using the glcm tool in the glcm package in R version 4.1.0. Whereby a 3 x 3 moving window was used, this size window was chosen as the smallest window possible for the function to retain as much information on canopy structure as possible at the smallest spatial scale. The output results in eight raster layers with per pixel an estimation of for the following texture metrics: Homogeneity, Contrast, Correlation, Dissimilarity, Entropy, Mean, Second-Moment and Variance. An example of each texture metric raster layer for the area surrounding Plot 1 can be found in Appendix 5. Please note that the Correlation texture layer was not considered in subsequent analysis as many pixels had no data and would therefore influence subsequent analyses.

Chapter 3 : Disentangling controls on animal abundance

3.1 Chapter Overview

The question of what controls animal abundance has always been fundamental to ecology, but given rapid environmental change, understanding the drivers and mechanisms governing abundance is more important than ever. Here, I determine how multidimensional environments and niches interact to determine population abundance along a tropical habitat gradient. Focusing on the endemic lizard *Anolis bicaorum* on the island of Utila (Honduras), I evaluate direct and indirect effects of three interacting niche axes on abundance: thermal habitat quality, structural habitat quality, and prey availability. I measured *A. bicaorum* abundance across a series of thirteen plots and used N-mixture models and path analysis to disentangle direct and indirect effects of these factors. Results showed that thermal habitat quality and prey biomass both had positive direct effects on anole abundance. However, thermal habitat quality also influenced prey biomass, leading to a strong indirect effect on abundance. Thermal habitat quality was primarily a function of canopy density, measured as leaf area index (LAI). Despite having little direct effect on abundance, LAI had a strong overall effect mediated by thermal quality and prey biomass. Results demonstrate the role of multidimensional environments and niche interactions in determining animal abundance and highlight the need to consider interactions between thermal niches and trophic interactions to understand variation in abundance, rather than focusing solely on changes in the physical environment.

3.2 Introduction

The question of what determines population size is fundamental to ecology, biogeography and conservation biology (Lack, 1954, Andrewartha and Birch, 1986, Brown, 1995). Complex intrinsic and extrinsic factors regulate population abundance (Pringle et al., 2019, Stapley et al., 2015), and classic and modern niche theory state that organisms are

affected by multiple abiotic and biotic factors along multiple niche axes. These limit their abundance and distribution either by limiting resource availability directly, or limiting species' ability to capture the resources that are available (Chase & Leibold, 2003). Identifying the factors responsible for population change along habitat gradients will improve our understanding of how multidimensional environments and niches interact to determine population abundance. Furthermore, conservation efforts and risk modelling can greatly benefit from isolating such mechanisms (Frishkoff et al., 2015).

While ecological niche theory is well developed, empirical evidence for which factors are most important, and how they interact, is still rare for many taxa. For example, *Anolis* lizards (anoles), my focus here, are a classic model system for evolutionary ecology and their behaviour, morphology, physiology, microhabitat use, and evolutionary history have been extensively studied (reviewed in Losos 2009). However, the question of what controls anole population size remains unanswered (Losos 2009). Research by Buckley and Roughgarden (2005) and more recently by Frishkoff et al. (2019) have begun to address this gap, focusing on anole abundance and community structure along elevational gradients. Their work has indicated a role for canopy loss, thermal environment, changes in food resources, and competitive interactions in influencing animal abundance, which varies depending on elevation. However, the relative importance of these factors, and how they interact to influence abundance, remains unknown.

Niche theory tells us that abundance can be limited by abiotic and biotic factors, acting either from the bottom-up or top-down (Elton, 1927, Leroux & Loreau, 2015). Potential limiting factors include microclimate, structural microhabitat, food resource (prey) availability, competitors, mutualists, predators, parasites and disease. For ectotherms, microclimate is expected to be especially important. Ectotherm body temperature (T_b), which affects metabolic and ecological function and evolutionary fitness, is determined by the interaction between

behaviour, biophysics, and microclimate (Gates 1980, Campbell & Norman 1998, Huey & Slatkin, 1976). Unfavourable microclimatic conditions, i.e. low thermal habitat quality, are predicted to restrict activity times, which in turn limits foraging, territory defence, and reproduction, leading to population declines (Sinervo et al., 2010). However, recent work has also suggested that anoles are often active in thermally sub optimal conditions, raising the possibility that thermal habitat quality may not exert as rigid controls on animal ecology, and thus population size, as traditionally thought (Gunderson & Leal, 2016, Méndez-Galeano et al., 2020) .

Changes in the suitability, extent, and complexity of structural microhabitat can potentially influence abundance. This may be especially true for semi-arboreal and arboreal species, including most anoles, which have specific adaptations to increase performance in particular arboreal microhabitats (reviewed in Losos, 2009). For example, longer legs confer an advantage for increased running speed on broad substrates, whereas shorter limbs provide greater manoeuvrability on narrow surfaces (Kolbe and Losos, 2005). Given these well-established microhabitat-ecology associations, perch availability is often used as an indicator of suitable habitat for anoles (e.g. Johnson et al., 2006). Changes in structural microhabitat, e.g. perch structure and availability, can alter anole abundance in species-specific ways (Frishkoff et al., 2019), and can select for phenotypic changes in urban anoles (Winchell et al., 2016). However, losses of suitable structural habitat do not occur in isolation and may be accompanied by altered prey communities and thermal conditions (Frishkoff et al., 2019), which in turn is mediated by changes in canopy cover (Algar et al., 2018).

Generally, predator biomass scales with prey biomass (Hatton et al., 2015). Loss of food resources, e.g. climate-induced declines in arthropod diversity and biomass, has been proposed to negatively affect the abundance of predators, including anoles (Lister & Garcia, 2018, but see Willig et al., 2019, Lister & Garcia 2019). As with climate, changes in prey

abundance may mediate impacts of other factors on abundance. For example, habitat alteration, such as urbanisation, can have a negative effect on terrestrial arthropod diversity and abundance (Fenoglio et al., 2020), and therefore has the potential to negatively impact insectivore populations. Similarly, competition for prey may reduce the amount of resources captured by a species, an effect that could be exacerbated by introduced or invasive species that can reach high abundances, especially in modified habitats. For example, *Anolis sagrei*, a successful invader of urban and human-modified environments (Kolbe et al., 2016) competes with native species, altering behaviour, microhabitat use, and inducing evolutionary change (Kamath et al., 2013, Stuart et al., 2014, Stroud et al., 2017),

Here, it is determined what factors influence the abundance of the endemic lizard, *Anolis bicaorum,* by considering multiple niche axes across gradients within tropical forest, on the island of Utila, Honduras. I focus on three niche axes potentially important for lizards: thermal habitat quality (Logan et al., 2013, Sears et al., 2016), structural habitat quality (Johnson et al. 2006) and prey availability (Battles et al., 2013) and use structural equation modelling disentangle direct and indirect effects of these factors on *A. bicaorum* abundance.

3.3 Material and Methods

3.3.1 Field Data Used

Field data used in this study included capture mark recapture (CMR) data for the anoles (*Anolis bicaorum*) across each plot to calculate abundance estimates and plot habitat characteristic measures that correspond to each of the niche factors considered (thermal, perch availability and prey availability). It also includes the measures for thermal preference (T_{pref}) in *A. bicaorum* from T_{pref} experiments. Table 3.1 below refers to the field data used in this study and the section within Chapter 2 (Materials and Methods chapter) that the full description of that data collection can be found. Subsequent method sections within this chapter outline chapter specific analyses.

Table 3.1: Outline of Field data used in this Chapter

Data	Description	Chapter & Section
Anole CMR data for abundance calculation	Anole count data from capture mark recapture surveys.	Chapter 2: 2.4
Plot operative temperature	Operative temperature data from 3D replicas fitted with iButtons in different microhabitats within a plot.	Chapter 2: 2.5.1
Thermal preference (T_{pref})	Thermal preference surveys of A. bicaorum.	Chapter 2: 2.5.2
Perch Number	Number of perches within each survey plot.	Chapter 2: 2.6
Basal Area	Basal area (m^2) of each plot.	Chapter 2: 2.6
Prey Biomass	Arthropod biomass	Chapter 2: 2.7
Prey Diversity	Arthropod diversity – Simpson and Shannon Indices.	Chapter 2: 2.7
Leaf Area Index (LAI)	Plot level LAI from ceptometer measurements.	Chapter 2: 2.8

Note that the operative temperature I use in the analyses is using the average of the uncalibrated and over-corrected T_e values in the main text (calibrated T_e – discussed in Chapter 2 section 2.5). Results of using the uncalibrated and over-corrected T_e for the work of this Chapter can be seen in Appendix 5. I found that the results were similar and led to the same conclusions regardless of whether calibrated, uncalibrated, or over-corrected T_e was used. Thus not that the results are not an artefact of imperfections in T_e models.

3.3.2 Habitat Variables

I used perch number and basal area for structural habitat suitability, arthropod (prey) biomass and diversity for prey availability, leaf area index as a measure of canopy cover and two indices of thermal habitat quality as habitat variables that were relevant to each of the three niche axis.

The first thermal habitat quality index was the percentage of 3D replica hours that operative temperatures were within the T_{pref} range over the 36-hour study period for each plot. The second index was the total number of degrees (°C) that the replicas deviated from the T_{pref} range across all replicas throughout the survey period for each plot. Unlike the former, the latter includes information on the extent to which temperatures deviated both above and below the T_{pref} range. In *A. bicaorum*'s sister species, *A. lemurinus*, temperatures above preferred temperature range were found to have a greater impact on lizard performance than temperatures below the range (Logan et al., 2015). Therefore, along with the total deviation, the deviation above T_{pref} and the deviation below T_{pref} were calculated separately.

3.3.3 Statistical Analyses

Anole abundance was estimated using multinomial N-mixture models. These flexible hierarchical models estimate abundance when captured individuals cannot be uniquely identified, can incorporate detection variability as well as covariates of abundance (Fiske & Chandler, 2011). This was relevant to this study, as the anoles could not be identified from afar (for example higher up on a tree trunk) with a unique identifier; hence, the anoles were only marked with a visit specific paint colour. Models were fit using the unmarked package (Fiske & Chandler, 2011) in R version 3.5.3 (R Development Core Team 2019). Specifically, using the multinomPois function, which fitted a multinomial-Poisson mixture model (Royle, 2004). Before estimating abundance and whether it covaried with individual habitat metrics, I evaluated the potential influence of differences in anole detection across plots by comparing

the AICc of models that held abundance and detection probability constant across plots, and that allowed one or both to vary. AICc values were determined using the modSel function within the unmarked package in R. As the model with varying abundance and constant detection rate had the lowest AICc (Table 3.2), detection rate was constrained to be equal across plots for subsequent models.

Table 3.2: AICc values for N-mixture models of abundance that allow abundance and or detectability of A. bicaorum to vary by site, or hold them constant

Model	Description	AICc
M0	Null model	399.87
Mboth	Model where abundance and detectability can vary by plot	252.64
Mdet	Model where only detectability can vary by plot	184.03
MSite	Model where only abundance can vary by plot	147.57

Univariate relationships between *A. bicaorum* abundance and each of the habitat variables (percent of time within T_{pref}, deviation from T_{pref}, perch number, basal area, arthropod biomass, arthropod diversity and LAI) were examined by including each predictor as a covariate in a multinomial-Poisson mixture model of abundance. These models were used to select a subset of variables (one representing habitat structure, one prey availability, and one thermal quality) for subsequent path analysis; LAI was included as the sole measure for canopy cover. Before fitting, all predictors were standardised to have a mean of zero and standard deviation of one to allow for comparison among variables with different units. Pseudo-R^2

values were calculated for each of the models using the *modSel* function within the unmarked package (Fiske & Chandler, 2011).

Path analysis was used to evaluate the relative strength of direct and indirect effects on abundance. As indirect paths within a single multinomial-Poisson mixture model could not be estimated, anole abundance for the path analysis was estimated from a multinomial Poisson mixture model that included no environmental covariates, held detection rate constant, and permitted abundance to vary by plot. The resulting abundance estimates, log-transformed to help meet linearity assumptions, were included as the response variable in the path analysis, which included all possible links between exogenous and endogenous variables. Path analysis was carried out using the lavaan (Rosseel, 2012) and semPlot (Epskamp, 2015) packages.

3.4 Results

3.4.1 Variation between plots

Abundance estimates for *A. bicaorum* varied from 1 to 20 individuals across plots, with a mean abundance of 7.07 ± 2.4. T_{pref} for *A. bicaorum* was (mean $\pm$ s.e) $25.4 \pm 1.56°C$ to $28.0 \pm 1.44°C$. Summaries for all niche measures are given in Table 3.3. Data for individual plots can be seen in Appendix 6.

Table 3.3: Summary of structural and thermal habitat, and prey availability across 13 forest plots on Utila, Honduras

Variable	Minimum	Maximum	Mean	SE
Time in T_{pref} (%)	6.34	47.91	30.29	4.15
Sum of Deviation from T_{pref} (^{o}C)	24.4	102.15	50.35	6.69
Deviation Above T_{pref} (^{o}C)	8.95	102.15	40.73	7.21
Deviation below T_{pref} (^{o}C)	0	40.00	9.62	4.03
Number of Perches	17	232	74.38	16.18
Basal Area (m^2)	0.40	6.35	1.90	0.43
Arthropod Diversity (Shannon)	0.91	1.91	1.68	0.08
Arthropod Biomass (g)	0.2	2.09	1.07	0.14
LAI	0.57	3.97	2.62	0.30

Abundance was not correlated with mean daily air temperature (measured in the shade 1.5m height; $r = -0.22$, $P = 0.46$, Figure 3.1), nor was it related to survey date ($r = -0.07$, $P = 0.82$, Figure 3.2), suggesting the results are not confounded by weather differences between days or as the field season progressed.
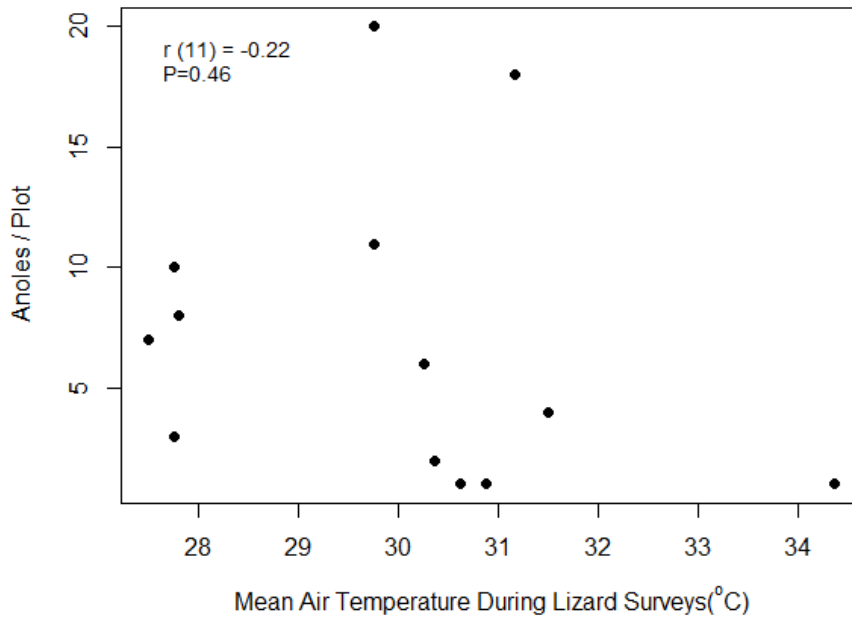
Figure 3.1: Comparison of anole abundance (Anoles/ Plot) with mean air temperature during lizard (abundance) surveys (°C)
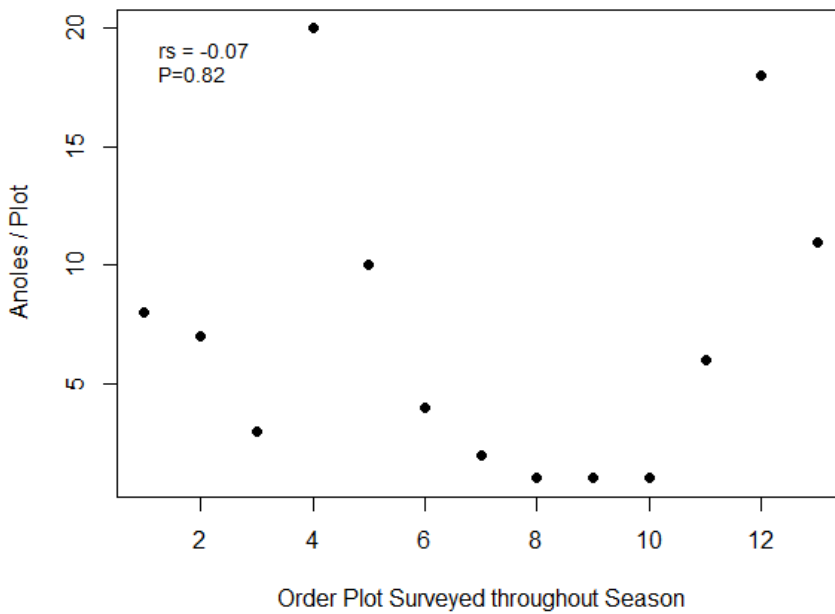
Figure 3.2: Comparison of anole abundance (Anoles/ Plot) with the order in which the plots were surveyed throughout the field season. Rank based on date order surveyed

3.4.2 Univariate Relationships

Abundance varied significantly with all measures of thermal habitat quality. The percentage of time each plot was within the T_{pref} range (Fig.3.3a, pseudo-r^2= 0.89, P= 1.88×10^{-6}) and the total sum of deviation of each plot (°C) from the T_{pref} range (pseudo-r^2= 0.79, P= 5.17×10^{-5}) were slightly more strongly related to abundance than the total sum of deviation above the T_{pref} range (pseudo-r^2= 0.68, P= 4.34×10^{-4}). The sum of deviation below the T_{pref} range was not significant (pseudo-r^2= 0.02, P= 0.58). For structural microhabitat quality, the number of perches was significantly related to abundance (Fig.3.3b, pseudo-r^2= 0.83, P= 1.92×10^{-7}), but plot basal area was not (pseudo-r^2= 0.03, P=0.52). LAI was significantly related to abundance (Fig.3.3d, pseudo-r^2= 0.40, P= 0.012). Arthropod diversity (Shannon index) was not significantly related to abundance (pseudo-r^2= 0.06, P= 0.38); using Simpson's index instead did not alter this result (pseudo-r^2= 0.01, P= 0.69). The relationship between abundance and arthropod biomass was significant (Fig.3.3c, pseudo-r^2 = 0.82, P=1.61×10^{-6}).
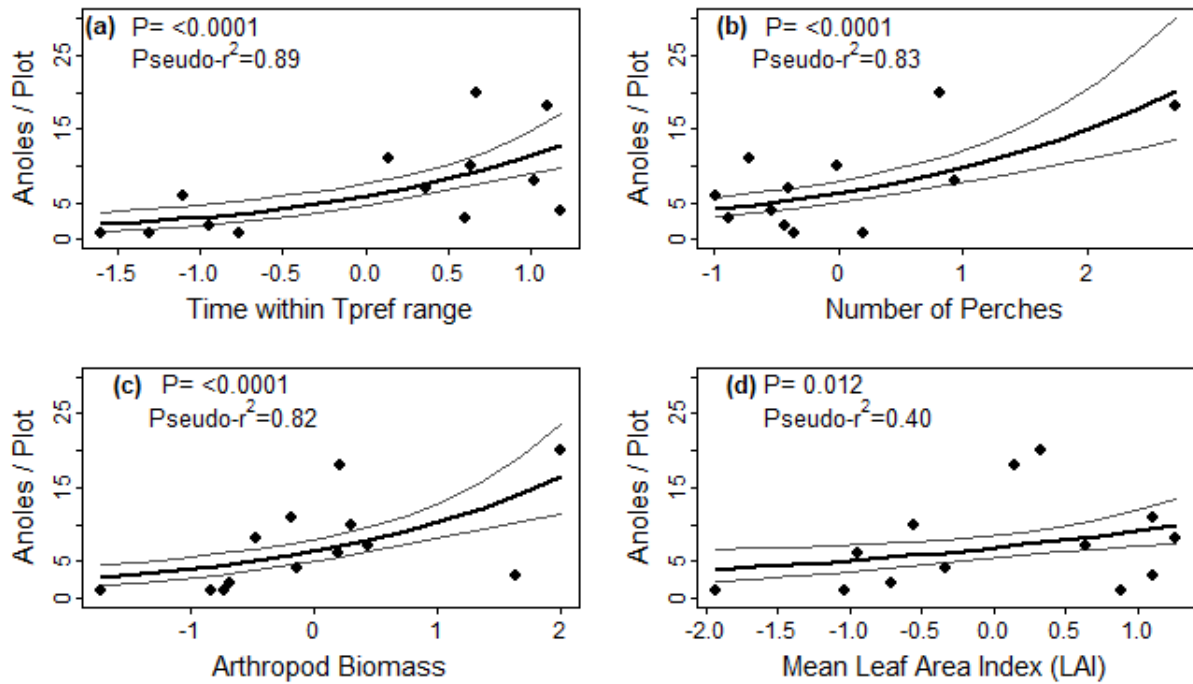
Figure 3.3: Relationships between *Anolis bicaorum* abundance and individual niche metrics in forest plots across Utila, Honduras. Relationships were estimated using multinomial Poisson mixture models with a constant detection rate across plots. All variables are scaled to a mean of zero and unit variance; (a) reflects thermal habitat quality, (b) reflects structural habitat quality, (c) reflects prey availability and (d) reflects canopy cover.

3.4.3 Path Analysis

Prey biomass and time within T_{pref} had the largest direct effects on *A. bicaorum* abundance (standardize coefficients: 0.40 and 0.47 respectively; Fig3.4a). The path coefficient between prey biomass and abundance was significant (*P*=0.049; Table 3.4), while the coefficient of the time within Tpref and abundance had a P of 0.055 (Table 3.4). LAI and number of perches had direct effects of smaller magnitude on abundance and neither were significant (Fig.3.4b, Table 3.4). Time-within Tpref also had a large effect on prey biomass (*P*= 0.074), leading to an additional, substantial indirect effect on *A. bicaorum* abundance (Fig 3.4b). While LAI had little direct effect on *A. bicaorum* abundance, or on prey biomass, it had strong indirect effects through its influence on time within Tpref. Number of perches had a substantial overall effect on *A. bicaorum* abundance, reflected by the large number of paths with relatively small effects, none of which were significant (Table 3.4, Figure 3.4a).
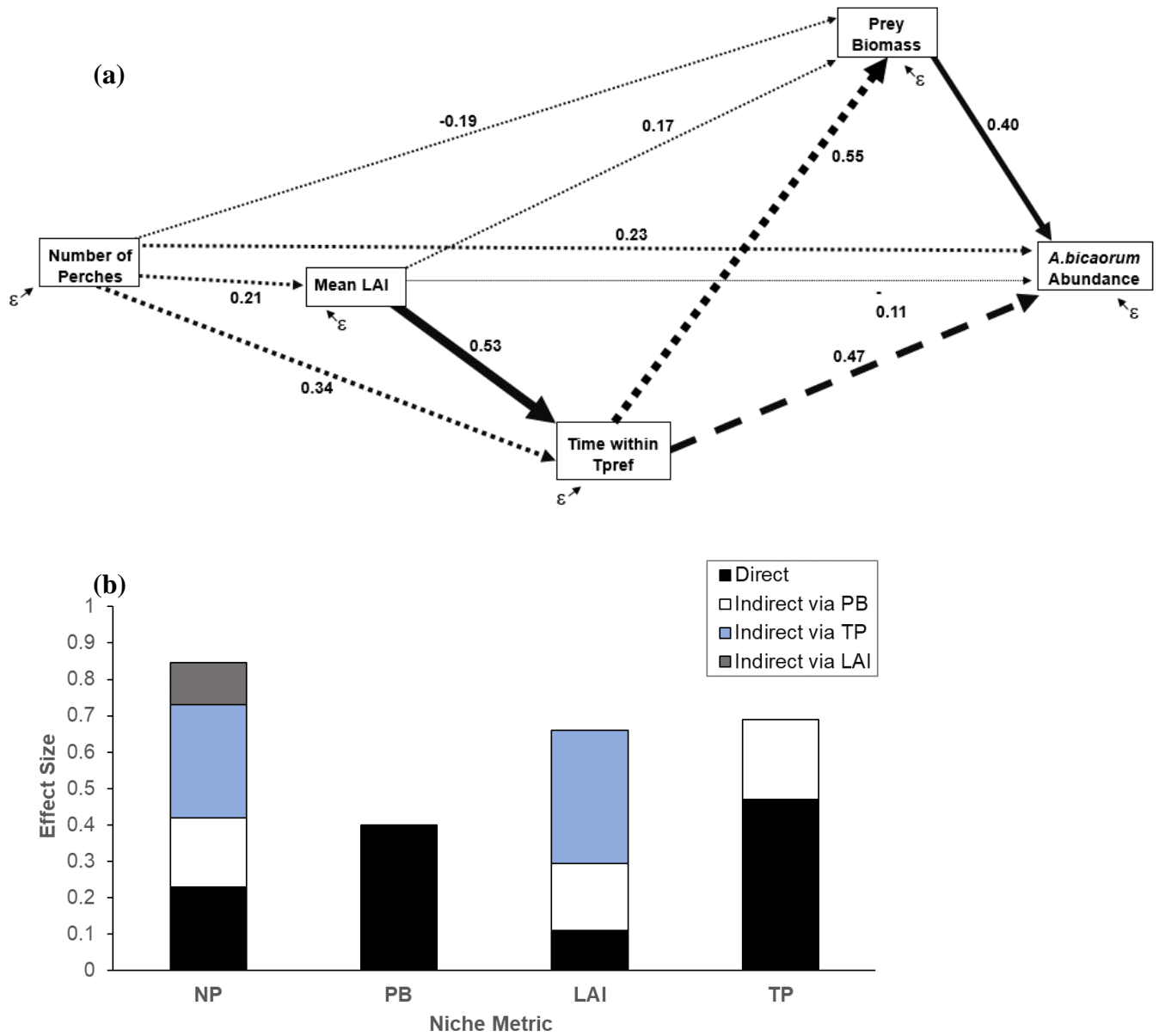
Figure 3.4: Direct and indirect effects of niche axes on *A. bicaorum* abundance. (a) Values are standardized path coefficients; line width is proportional to the strength of the effect, solid lines indicate statistically significant pathways. ε, unexplained variation. (b) The total effects of covariates on abundance. NP: number of perches; PB: prey biomass; LAI: mean leaf area index; TP: time within Tpref range.

Table 3.4: Results of the path analysis looking at indirect and direct effects, and relationships between, multiple niche axes on *A. bicaorum* abundance, in 13 forest plots on Utila, Honduras. Std.all, Standardised Coefficients.

Pathway	Estimate (± S.E)	*Z*	*P*-Value	Std.all
***A. bicaorum* Abundance ~**				
Number of Perches	0.25 ± 0.20	1.25	0.211	0.23
Prey Biomass	0.43 ± 0.22	1.97	0.049	0.40
Time within T_{pref}	0.51 ± 0.27	1.92	0.055	0.47
Mean LAI	-0.11 ± 0.22	-0.52	0.609	-0.11
Time within T_{pref} ~				
Mean LAI	0. 53 ± 0.21	2.58	0.010	0.53
Number of Perches	0.34 ± 0.21	1.66	0.097	0.34
Mean LAI ~				
Number of Perches	0.21 ± 0.27	0.76	0.449	0.21
Prey Biomass ~				
Time within T_{pref}	0.55 ± 0.30	1.79	0.074	0.55
Number of Perches	-0.19 ± 0.25	-0.74	0.457	-0.19
Mean LAI	0.17 ± 0.28	0.61	0.545	0.17

3.5 Discussion

Classic and modern niche theory states that organisms are affected by multiple abiotic and biotic factors along multiple niche axes (Chase & Leibold, 2003). Disentangling these effects is challenging because 1) environmental changes induce change in multiple factors at once, and 2) factors are interconnected and can mediate each other's effects. Thus, we still do not have a full understanding of which niche axis exerts most pressure on abundance and the extent to which these niche axes exert direct and indirect effects. Here I found that prey biomass and thermal habitat quality exerted the strongest direct control on the abundance of the endemic anole, *A. bicaorum*, on the island of Utila. However, thermal quality also had a strong indirect effect on anole abundance, mediated by prey biomass. Thermal habitat quality, in turn, was determined primarily by canopy density (LAI), which blocks incoming solar radiation, lowering operative temperatures (Algar et al. 2018) and creating heterogeneity for behavioural thermoregulation (Sears et al. 2016). Together, these results reveal the complex feedbacks among physical and biotic selection and highlight the importance of considering direct and indirect controls on abundance of species across habitat gradients.

The direct relationship between prey biomass and abundance is consistent with theory predicting that more food, i.e. higher biomass, supports higher numbers of individuals (Hatton et al., 2015, De Omena et al., 2019). Higher food availability may also affect population dynamics and intraspecific competition. For example, more food may lead to improved body condition and energy storage within individuals, allowing for greater investment in reproduction and increased fecundity (Orrell et al., 2004). The results also suggest that prey abundance, rather than prey diversity, is more important for maintaining population size. Many anoles are opportunistic predators (Losos, 2009) and natural history observations suggest that *A. bicaorum,* like many other anole species, is also an opportunistic predator and arthropod generalist (Köhler, 1996, Brown et al.*,* 2017), although there is a lack of quantitative diet data

for this species. Given its likely generalist diet, the diversity of prey taxa available should have little effect on the available resource base, which is consistent with the results. Although deforested tropical habitats often harbour reduced diversity, those species that do persist can often achieve high abundance (Foster et al., 2011), which could limit abundance declines of anoles and other generalist predators. However, no evidence for such compensatory dynamics was found here. Instead, more disturbed, built-up areas had lower prey biomass and reduced *A. bicaorum* abundance – likely because of the reduced tree cover degrading the thermal quality of these environments. This is consistent with findings from larger urban areas, where consistent declines in abundance of multiple insect taxa have been documented (Piano et al., 2020). Thus, at least on Utila, even if some arthropod taxa benefit from disturbance leading to a loss of canopy cover, these increases are insufficient to counter overall declines in arthropod biomass, which in turn limit abundance at higher trophic levels, effects which could be further intensified by climate change (Lister & Garcia, 2018, but see Willig et al. 2019 and Lister & Garcia 2019).

Thermal habitat quality has pervasive effects on ectotherms, including physiology and behaviour, which can scale to influence population dynamics (Diaz, 1997, Sinervo et al., 2010). As predicted, I found a positive association between the duration that operative temperature was within *A. bicaorum*'s T_{pref} and its abundance – although the *P*-value of this relationship in the path analysis was just above 0.05. Individuals within their preferred temperature range for longer benefit from an increase in activity time (Gunderson & Leal, 2016), which allows increased utilisation of available resources (Gvoždík 2002), and can increase anole persistence in natural and human-modified environments (Battles & Kolbe, 2019). Restriction of activity time, via thermal stress, can limit ectotherms' ability to effectively obtain resources, avoid predation, withstand pathogens, and reproduce effectively, leading to population declines and, ultimately, extinction (Huey et al., 2009, Sinervo et al., 2010). These results suggest that in

habitats of high thermal quality, *A. bicaorum* individuals are able to exploit longer activity times in thermally suitable plots and incur lower costs of thermoregulation. Explicitly testing this mechanism will require data on thermoregulatory efficiency of individuals across habitat types. A caveat to the results remains, however, as the estimates of T_{pref} in *A. bicaorum* were measured for a relatively short duration in field-lab conditions and improved measures of T_{pref} are needed, including increased understanding of plastic and adaptive variation among populations.

These results show that thermal and prey availability are not alternative controls on abundance. Rather, they are interconnected. In addition to its direct effect, thermal habitat quality had an indirect effect on *A. bicaorum* abundance, mediated by prey biomass. As arthropods are also ectotherms, they too will be affected by temperature, and their abundance is also vulnerable to warming (Lister & Garcia, 2018, but see Willig et al. 2019, Lister & Garcia 2019). While the measure of thermal quality was focused on *A. bicaorum*, it also captured variation in prey biomass, indicating alignment in thermal niches amongst predators and their prey. Thus, in areas of higher thermal quality, not only do anoles have more time for foraging, but there is also more food available, providing additional benefits of thermal habitat quality that extend beyond a species thermal performance. The corollary of this is that declines in thermal habitat quality will have greater negative effects than expected solely based on a species' thermal niche. Models to predict vulnerability of ectotherms to future warming tend to focus on direct effects on activity time, thermal safety margins, and thermoregulation (e.g. Sinervo et al., 2010, Sunday et al., 2014). Results suggest that such models may actually underestimate risks, and that warming impacts may actually be magnified due to thermally induced changes in food availability, highlighting the need for greater focus on direct and indirect effects of temperature change (Kearney et al. 2013,Duclos et al., 2019).

Thermal habitat quality was primarily controlled by canopy density. Canopy cover influences microclimate in multiple ways including reducing incoming solar radiation (Campbell & Norman 1998), which in turn lowers operative and body temperatures ectotherms (Kearney et al., 2009, Algar et al., 2018). This advantages cool-adapted species like *A. bicaorum* (Logan et al., 2013) and, as the results reveal, their food resources as well. When overall effects are considered, LAI had a strong effect on *A. bicaorum* abundance, despite having a small direct effect. Instead, it had strong indirect effects mediated by thermal quality and, subsequently prey biomass. While this study focused on mean LAI, canopy cover may have even stronger effects than measured here as canopy heterogeneity can generate patchy thermal environments that reduce the cost of behavioural thermoregulation (Sears et al. 2016). LAI, in turn, was mildly influenced by the number of perches (stems) in a plot. Perch number, essentially stem density, had relatively weaker overall effects on abundance than LAI and no individual paths were significant.

On Utila, personal observations suggest that human disturbance in proximity to Utila Town is the key driver of canopy variation, with clearing for housing projects ongoing, although other factors, such as variation in elevation and proximity to the coast may also play a role. The results of this study highlight the pervasiveness of canopy cover for mediating ecological dynamics at higher trophic levels, primarily through influencing the thermal landscape (*sensu* Nowakowski et al. 2018) but also indirectly through mediating trophic interactions. Lastly, these findings demonstrate the importance of maintaining canopy cover and structure to maximize thermal habitat quality for cool-adapted (Battles & Kolbe, 2019) and their prey (Lister & Garcia, 2018).

This study has identified a key role for resource availability in directly controlling anole abundance, alongside thermal environment, other biotic interactions, not examined here, may also play a role. Island anole populations are generally thought to be strongly influenced by

predators, with several experiments showing substantial predator effects on anole niche dynamics and density (Schoener et al., 2002, Pringle et al. 2019). As I was not able to measure predation pressure on *A. bicaorum,* the possibility that predators are exerting top-down effects on abundance cannot be discounted, in addition to the bottom-up effects of prey biomass. Nor can I determine the potential agonistic interactions of parasites on anole populations (Bonneaud et al., 2017). Competitive interactions could also limit abundance, although the only putative congeneric competitor, *Anolis utilensis,* is much rarer and perches much higher than *A. bicaorum* (Brown et al., 2017). The recently introduced brown anole, *A. sagrei*, could also have an effect on *A. bicaorum*'s abundance in the future, but currently it is restricted to Utila town, where *A. bicaorum* is not found (personal observations).

3.6 Chapter Conclusions

This work has demonstrated the interconnectedness of abiotic and biotic components that determine habitat quality and animal abundance. Rather than identify a single strong control on abundance, it was found that key abiotic factors (canopy cover and thermal environment) affect abundance through multiple pathways and have effects that are mediated by biotic interactions and the niche of the focal species. In particular, results suggest alignment of thermal niches across multiple trophic levels results in strong indirect effects of thermal environment on anole abundance. Losses of thermal habitat quality, particularly due to canopy loss, may thus have greater effects than appreciated when only direct effects are considered. Therefore, in subsequent chapters of this thesis, I focus on quantifying the thermal environment and mapping canopy heterogeneity on Utila, to consider its impact on *A. bicaorum* abundance.

Chapter 4 : Unoccupied Aerial Vehicles as a Tool to Map Lizard Operative Temperature in Tropical Forest Environments

4.1 Chapter Overview

As temperatures warm, many tropical ectotherms will need to increasingly seek out cooler microhabitats to avoid overheating; to fully understand how such ectotherms will be affected, we need information on thermal habitat quality at spatial scales relevant to the organism. However, how we measure thermal habitat suitability is either limited by spatial extent, such as with ground-based 3D operative temperature (T_e) replicas, or is based on microclimate derived from physical models that use land cover variables and downscale coarse climate data. These mechanistic microclimate models, although useful, do not provide direct ecologically relevant data on thermal habitat suitability of ectotherms such as *Anolis bicaorum*, which instead requires information on T_e measures and thermal performance estimates. Currently available microclimate models that can be applied across landscapes are also dependent on relatively coarse (from a small ectotherm's perspective) climate, and topography datasets, and rarely reflect the conditions experienced by individuals. However, although standard thermal ecological methods of measuring T_e using 3D replicas of the focal species provide ecologically relevant (T_e) data at relevant spatial scales, they are resource heavy and provide low spatial extent. In order to gather ecologically relevant T_e data for *A. bicaorum across* high spatial resolution and extent, I test the ability of unoccupied aerial vehicle (UAV) data to predict fine-scale heterogeneity in T_e in tropical environments. Results from random forest models indicate that a model incorporating solely air temperature and ground-based LAI from ceptometer measurements predicted T_e, well. However, a model with air temperature and UAV-derived canopy metrics performed slightly better with the added advantage of enabling the mapping of T_e with continuous spatial extent at high spatial resolutions. The work provides

a feasible workflow to map sub-canopy lizard T_e in tropical environments at spatial scales relevant to the organism, and across continuous areas, which will be imperative in risk modelling of such species to anthropogenic land cover and climate change.

4.2 Introduction

Thermal habitat quality has pervasive effects on ectotherms, including on physiology and behaviour, which can scale to influence population dynamics (Diaz, 1997, Sinervo et al., 2010). The thermal environment influences both performance and distribution of ectotherms by influencing metabolic and ecological function and evolutionary fitness, through the interaction between physiology, behaviour, biophysics, and microclimate (Gates 1980, Campbell & Norman 1998, Huey & Slatkin, 1976). Chapter 3 of this thesis demonstrated the role of the thermal environment, specifically a measure of thermal habitat quality based on operative temperature (T_e) and thermal preference, on the abundance of *Anolis bicaorum*, influencing it both directly and indirectly via prey availability.

Even though we know that thermal fluctuations influence all levels of biological organisation, from biochemical reactions to ecological interactions (Niehaus et al., 2012), the spatial scale at which we measure the thermal environment is often at scales that are not relevant to the organism (Logan et al., 2013; Sears et al., 2011; Sears and Angilletta, 2015). Mechanistic models such as NicheMapR, Microclima and Microclimic (Kearney and Porter, 2017; Maclean et al., 2018; Maclean and Klinges, 2021) have been developed to solve this spatial issue, using coarse resolution climate data to infer microclimate. These models for microclimate are a useful tool for ecologists and make important contributions to how we consider species responses to habitat and climate change. However, they are not without their limitations. Models such as NichemapR and Microclima downscale coarse resolution climate data from weather stations (Kearney and Porter, 2017; Maclean et al., 2018) using local topography to predict microclimate, meaning they are still dependent on coarse scale climate

data, and are limited by the spatial resolution of all input variables. They are therefore limited in terms of how accurately they represent the thermal heterogeneity in the landscape at organism relevant scales, i.e. the conditions experienced by many organisms (Sears et al., 2011; Sears and Angilletta, 2015; Suggitt et al., 2018).

Microclimate and thermal suitability for ectotherms do not refer to the same measures of the thermal environment. Microclimate influences the thermal environment of a landscape (Suggitt et al., 2018), however thermal suitability indices for ectotherms are based on ecologically relevant measures of species thermal performance using thermal performance curves (TCPs) and body temperature (Logan et al., 2013b; Sinclair et al., 2016). Thus, there is disconnect between measuring microclimate and then applying the measures in an ecologically relevant way for measuring thermal habitat suitability for ectotherm species. For example, to determine the thermal suitability of a study area, we need to first measure what the body temperatures of the species would be across the study area and then translate this into suitability using TCPs (or other measures). A key step to this translation is quantifying operative temperature (T_e), a measure of an animals body temperature at equilibrium with its environment (Logan et al., 2013), across the study area.

Measuring the thermal environment and thermal habitat quality at fine spatial scales relevant to the organism is a standard practice when it comes to thermal ecologists that use ground-based methods. Current ground-based methods for measuring the suitability of the thermal environment for a species is done by measuring T_e by deploying morphologically accurate 3D replicas of the focal species, fitted with temperature data loggers, in different microhabitats (Logan et al., 2013; Muñoz and Losos, 2018) . Such methods allow the T_e of the focal species to be measured in different microhabitats at very fine spatial scales, however as each replica measures a point estimate, they sample a very small amount of the thermal habitat. This means that they do not scale up to landscape level analyses well, as the spatial extent of

the methods is limited. This is partially due to cost and the resources required for such methods, including the materials used to create the replicas themselves, the costs of data loggers, and the deployment effort. These all factor in to the cost and effort of this method. The spatial data extent that can be obtained by this traditional method is limited by the availability of replicas, data loggers and often time constraints.

Another limitation of current methods of measuring thermal habitat quality is that due to spatial extent limitations of the ground-based methods and the spatial resolution limitations of the biophysical models, they cannot account for the spatial heterogeneity of the suitable thermal environment. The spatial structure and heterogeneity, i.e. patchiness of thermal environments, along with the mean temperature, influences thermoregulation, movement and energetics of ectotherms (Sears and Angilleta, 2015). For example, a spatially heterogeneous thermal environment of cool and warm patches confer advantages for behavioural thermoregulation, increasing thermoregulatory performance and lowering energy expenditure (Sears and Angilletta, 2015). However, current methods of measuring thermal habitat quality from both mechanistic models and on the ground T_e methods mostly consider the thermal environment to be homogenous over the study area and do not consider this spatial heterogeneity. There is, therefore, a need to measure ecologically relevant thermal measures of the environment at spatial scales relevant to the organism, across a spatial extent that will allow capture spatial heterogeneity of these thermal environment and the potential implications of future land cover and climate change across landscapes.

The use of remote sensing methods within the field of ecology is allowing such data to be captured. Remote sensing derived data products have been highlighted as a way to improve the spatial resolution of mechanistic microclimate model outputs by capturing fine scale measures of important data inputs such as topography and canopy metrics (Duffy et al., 2021; Milling et al., 2018; Zellweger et al., 2019). Canopy cover influences the thermal environment

in multiple ways including reducing incoming solar radiation (Campbell & Norman 1998). In tropical forests, the canopy acts as a thermal insulators, cooling the understory when ambient temperatures are hot, and warming the understory when they are cold (De Frenne et al., 2019). Such canopy metrics have been found to influence operative and body temperatures of ectotherms, specifically lizards (Kearney et al., 2009, Algar et al., 2018). Results of Chapter 3 corroborate this and have demonstrated that such measures such as leaf area index (LAI) influence the thermal environment (thermal habitat quality) which is linked to *A. bicaorum* abundance. Chapter 3 focused on plot level (20 x 20m) LAI (canopy cover), averaging LAI across the whole of the plot. However, the spatial configuration of canopy cover can generate patchy thermal environments that reduce the cost of behavioural thermoregulation (Sears et al. 2016). Emerging remote sensing technologies, such as unoccupied aerial vehicles (UAVs), can aid in capturing this canopy variation via optical sensors (most commonly RGB) and photogrammetry methods such as structure from motion (SfM) (Duffy et al., 2021; Milling et al., 2018; Zellweger et al., 2019). Their relative ease of use and now mainstream availability allow high spatial resolution data to be acquired without the need of excessive resources, time and costs. Although capturing specific canopy measures such as LAI from UAVs are still in their infancy (Duffy et al., 2021), we can capture other measures of vegetation structure such as greenness indices (Morris et al., 2013) and texture metrics as measures of heterogeneity, which can be used as proxies for canopy cover and heterogeneity.

This chapter uses high-resolution (<0.9cm) optical UAV RGB imagery captured across a series of survey plots on the island of Utila to test the ability of canopy pixel greenness and texture metrics to predict T_e *Anolis* lizards below the canopy. UAV-derived canopy metrics are coupled with ground-based measures of plot air temperature and the ability of UAV measures to predict T_e is compared to that of ground-based LAI measures taken using a ceptometer. The T_e outputs are related to *A. bicaorum* abundance for the survey plots. The work

highlights the ability of RGB UAV platforms to collect high spatial quality canopy data and the ability to consider the T_e of an animal below the canopy rather than solely considering microclimate. It provides a step forward in methods for estimating the thermal habitat suitability of a landscape at relevant spatial scales.

4.3 Material and Methods

4.3.1 Field Data Overview

Field data used in this chapter includes T_e measurements from 3D printed anole replicas (fitted with iButton data loggers), air temperature (recorded at 1.5m height with a shielded iButton data logger) at hourly intervals for the same three days as 3D replicas were *in situ*, and leaf area index (LAI) measurements above each 3D replica, taken using an Accupar-LP80 ceptometer. Imagery used in this chapter included post-processed UAV canopy metric layers, which included seven texture raster layers and one greenness layer for each of the 16 survey plots, and anole abundance estimates for each survey plot, derived from Chapter 3 analyses. Table 4.1 below outlines the field data used in this chapter and the section within this thesis where the full description of that data collection can be found. Subsequent method sections within this chapter outline chapter specific analyses.

Table 4.1: Outline of data used in this Chapter

Data	Description	Chapter and Section
Operative Temperature (T_e)	T_e data from 3D replicas fitted with iButtons in different microhabitats within a plot.	Chapter 2: 2.5.1
Locations of 3D replicas	DGPS spatial point locations of each 3D replica within each plot	Chapter 2: 2.5
Leaf Area Index (LAI)	LAI from ceptometer measurements.	Chapter 2: 2.8
Air Temperature	Air temperature at 1.5m height within each plot	Chapter 2: 2.9
UAV Greenness Layer	UAV Greenness raster layers for each plot, resulting from processing of RGB imagery	Chapter 2: 2.12
UAV Texture Layers	UAV derived raster layers for seven texture metrics (Homogeneity, Contrast, Dissimilarity, Entropy, Mean, Second-Moment and Variance) for each survey plot.	Chapter 2: 2.12
Anole abundance estimates for each survey plot	Anolis bicaorum abundance estimates for each survey plot, derived from Chapter 3	Chapter 3: Results

4.3.2 Operative and Air Temperatures

I used 3D replicas to measure sub-canopy T_e in different areas within each plot (Chapter 2: section 2.5). The iButtons within the replicas recorded T_e every 15 minutes. As I wanted to determine the influence of the canopy structure directly above the T_e replica, I extracted T_e at solar noon, where the majority (not including reflectance) of solar radiation would be coming from directly above the replica, therefore limiting the influence of variation in the angle of the sun. To account for the possibility of passing cloud or wind having an influence on the T_e at the one measurement closest to solar noon, two measurements either side of solar noon were taken (four measurements of T_e total) and the mean was taken to use in subsequent analysis. The T_e at solar noon for each individual replica over a period of three days, resulting in three measurements per replica, was used for subsequent statistical models.

The air temperature of each plot at solar noon was extracted for each day the models were *in situ*. Air temperature was measured at hourly intervals. Solar noon varied from day to day (i.e. sometimes being closer to 13:00 than 12:00). To account for the variation, the two hourly measurements, one on either side of solar noon were extracted and the mean taken for subsequent analyses. LAI measurements from a ceptometer taken directly above each of the 3D replicas were also included in the analyses.

4.3.3 Extracting UAV Canopy Metrics

Due to the spatial resolution of the UAV pixels (0.9cm), I placed a buffer around each of the 3D replica locations and extracted the UAV data for the pixels within the buffers, for each of the image layers, herein referred to as canopy metrics. This was to ensure encapsulation of canopy variation across a sufficient spatial area, rather than based on a single 0.9cm pixel. Considering the accuracy of the DGPS measurements (0.86cm), a 1m (0.5m radius) buffer was used to extract data around every DGPS point that held a 3D replica. The spatial point's data for the replica locations was first loaded into R version 4.1.0, and then the raster package (Hijmans, 2021) was used to extract the mean pixel values for each layer within the buffer area around the 3D replicas. This extraction process was carried out on the greenness raster layer and all seven texture raster layers (see Chapter 2: Section 2.12) for each survey plot.

4.3.4 Statistical Analyses

Random forest (RF) regression trees were used. Random forest algorithms are particularly useful in working with highly dimensional linear and non-linear relationships within the same model as well as provide estimates of variable importance plots (Breiman, 2001). They produce both classification and regression models based on building a specified number of random decision trees from bootstrapped samples of the data and using a random subset of the predictor variables at each split, then taking the mean of the outcome. Because of this, bootstrapping random forests are also slightly more attuned not to over fit a model, which

is useful when you have a low number of data points, as seen in this dataset. Due to the continuous nature of the response variables, the regression random forest model was used in the analyses. Random forest analysis was conducted using the ModelMap (Freeman *et al.*, 2009) package in R version 4.1.0. An outline of the variables included in each of the RF models can be seen in Figure 4.1.
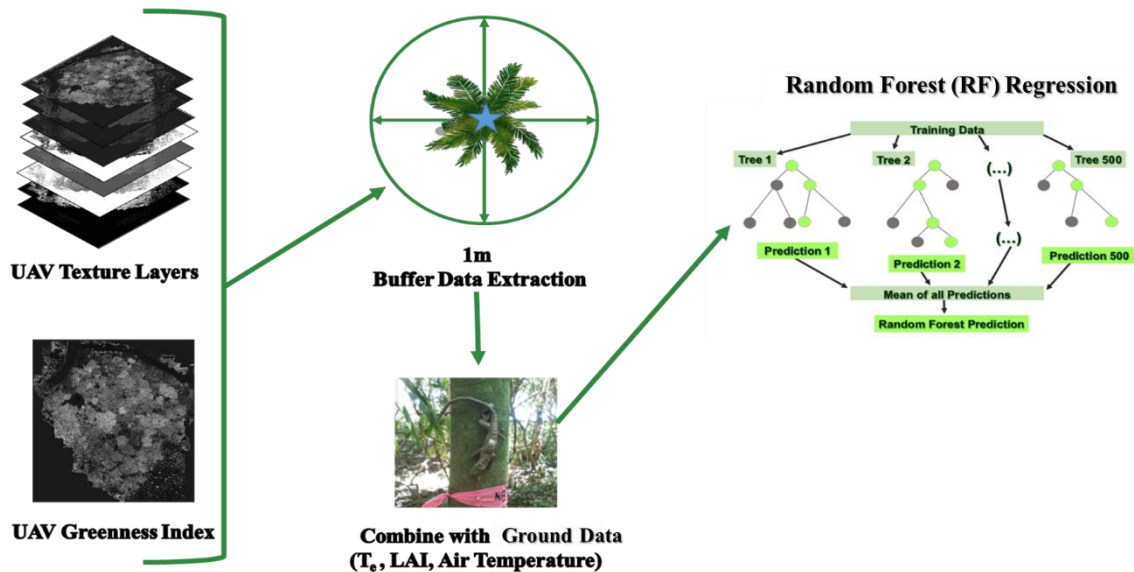
Figure 4.1: Simple workflow of data included in Random Forest Regression models

The complete dataset was first randomly subset into a training set (75% of data) and a test set (25 % of data) for independent model validation. I fit four random forest models to the T_e data, the first included plot air temperature and ground-based LAI measures from a ceptometer as predictors. The second model solely included UAV-based canopy measures (greenness and textures) as predictors of T_e. The third included the UAV-based canopy measures and plot air temperature as predictors of T_e. The final model incorporated all variables as predictors of T_e (ground-based LAI, plot air temperature, UAV canopy measures). Details and model parameters of all random forest models can be seen in Table 4.2.

Table 4.2: Details of all RF models conducted; Mtry = the number of variables randomly chosen at each split, Ntrees = number of trees grown within RF model

Model Name	Response Variable	Description/ Predictors
Te.Ground	T_e	Ground-based measurements only. Predictors = Plot Air Temperature and Ground-based LAI Mtry = 1 Ntrees = 500
Te.UAV	T_e	UAV measurements only. Predictors = UAV Greenness and UAV texture metrics Mtry = 3 Ntrees = 500
Te.Air.UAV	T_e	Air Temperature and UAV measures Predictors = Plot Air Temperature, UAV Greenness and UAV texture metrics Mtry = 3 Ntrees = 500
Te.All	T_e	Ground based and UAV measurements. Predictors = Plot Air Temperature, Ground based LAI, UAV Greenness and UAV texture Mtry = 3 Ntrees = 500

To validate all RF models seen in Table 4.2, the test data was input into the model.diagnostics function in ModelMap comparing observed and predicted T_e values for the test dataset. The model.diagnostics function also provides variable importance plots based on mean decrease accuracy (%IncMSE), which expresses how much accuracy the model loses by excluding each variable; the higher the value, the more important the variable is to the model. Lastly, random forest algorithms by nature are insensitive to multicollinearity of variables (Tang et al., 2020), but it is a factor when trying to disentangle the influence of two correlated variables. As only the texture variables in the models were correlated (Figure 4.2) and the aim was not to disentangle specific variables of import between the texture variables, multicollinearity was not an issue for the models used.
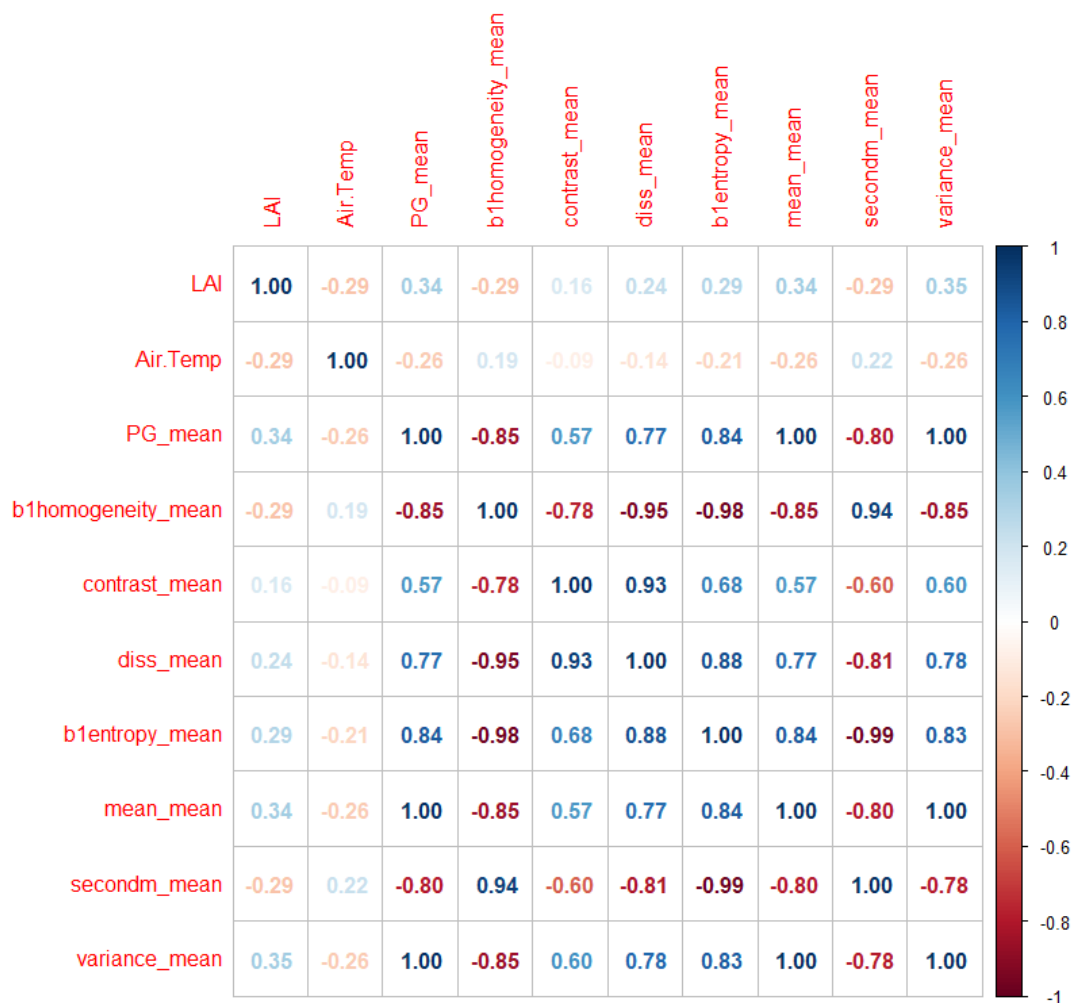
Figure 4.2: Correlation plot for all variables used in models

To evaluate predictive performance across different plots, a Jackknife approach was used where one plot was omitted from the training data and the data from the remainder of the plots were used to predict the omitted plot. This was then repeated omitting each plot separately and conducting the Te.Air.UAV model, as this was the model of most interest.

To evaluate whether RF modelling with UAV data improved the ability to predict T_e, I compared these models to a regression of T_e against air temperature. As simple biophysical models of T_e predict a linear relationship between air temperature and T_e (Algar et al., 2018), I first fitted a linear regression. However, as the T_e-T_a relationship exhibited curvilinearity, I also fitted a third-order polynomial relationship.

4.3.5 Mapping Thermal Habitat

In order to use the RF model to map T_e across the whole of a plot, the predict function in ModelMap was used to predict across the UAV orthomosaics for each plot. This function could only predict across the plot if data was present for every image pixel, therefore ground based LAI could not be included as it was only sampled in localised areas within the plot. As I assumed that air temperature was homogeneous across the plot, a uniform raster layer with the same spatial resolution and spatially matching pixel grid as the other input variables can be used to represent air temperature. Therefore, an air temperature raster layer for each plot was created using the conditional function in Raster Calculator in ArcMap 10.4.1. Mean air temperature from the two hours around solar noon for all T_e surveys across plots was 30.4°C, so I used this value for predicting T_e across plots

4.3.6 Thermal Habitat Structure

In order to quantify the spatial configuration of thermally suitable habitat for each plot, I calculated standard landscape metrics focused on the spatial distribution of areas below 33.2°C, the CT_{max} measure for *Anolis bicaorum* (Logan et al., 2013). CT_{max} was used as a

threshold as the T_e measures predicted in the random forest model across plots were for solar noon and at an air temperature of 30.4°C, therefore above the T_{pref} range calculated for *A. bicaorum* (25.4 – 28.0 °C). Therefore, I assume that areas with a solar noon T_e measure above 33.2°C are unsuitable thermal habitat at that time. UAV T_e raster layers for each plot were reclassified into two categories relating to CT_{Max} of *A. bicaorum,* as seen in Table 4.3.

Table 4.3: Temperature Categories relating to *A. bicaorum* habitat quality

Category	Temperature (°C)
Thermally Tolerable	< 33.2
Thermally Intolerable	≥ 33.2

Areas within the thermally tolerable category were extracted for each of the plot raster layers and. the number of patches, total area (m^2), mean patch size (m^2), Euclidean distance (m^2) and standard deviation of nearest neighbour Euclidean distance (m^2) were calculated using the landscapemetrics R package (Hesselbarth *et al*., 2019). In order to consider the impact of pixel speckle on calculating landscape thermal patches, the analysis was re-run after resampling the resolution of T_e pixels to 15cm as it approximates the size of one adult *A. bicaorum*.

4.3.7 Relating UAV derived T_e to Anole Abundance

A. bicaorum abundance for each plot (calculated in Chapter 3) was plotted against several measures derived from the UAV imagery and significance of the relationships was evaluated simple linear regressions. These UAV measures were the mean, maximum and standard deviation of plot T_e from the standard RF outputs (0.9 cm resolution) and landscape metrics for reclassified thermally tolerable category patches at both a 0.9cm resolution and 15cm resolution.

4.4 Results

4.4.1 Prediction of T_e

T_e increased with air temperature. The linear regression was significant ($F=1162$, d$f=793$, $P<0.001$; adjusted $r^2=0.59$). However, the relationship showed considerable heteroscedasiticity (Figure 4.3), with greater variance at warmer temperatures. This is due to 3D replica placement within and between survey plots having an influence on Te. For example, some replicas being placed where there is no shade, getting a considerably higher amount of solar radiation, therefore leading to much higher logged temperatures than that seen in replicas placed in the thermally buffered forest. Fitting a 3rd order polynomial did not substantially improve model fit (Figure 4.3; $F = 392.9$, $df=791$ $P<0.001$, adjusted $r^2 = 0.60$).
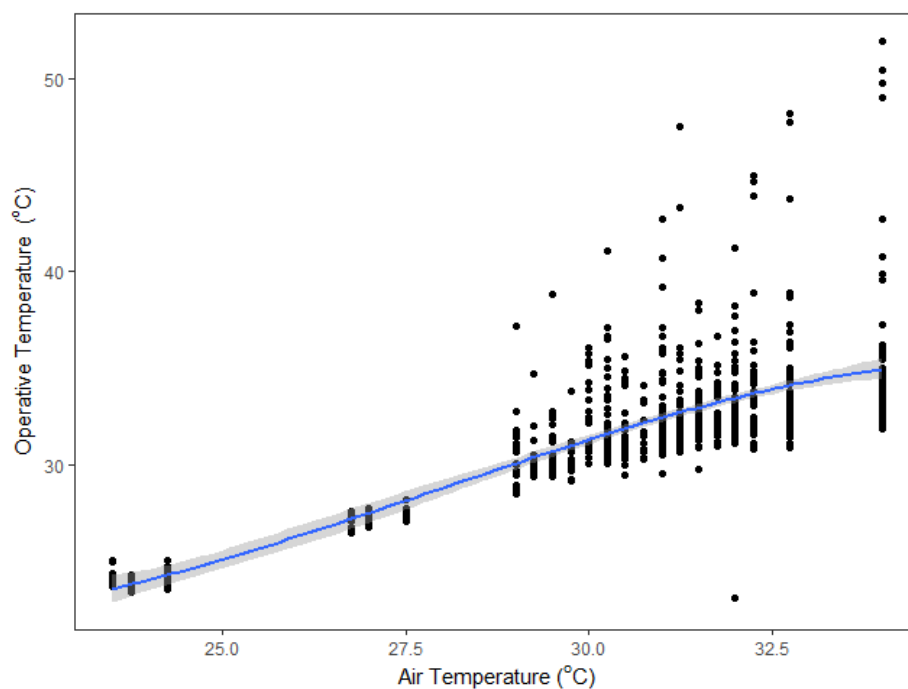
Figure 4.3: Air temperature vs T_e fitted with a third order polynomial curve. Each point is the T_e (°C) at solar noon of a 3D replica within a plot, plotted against the air temperature (°C) within the plot at solar noon. Shading around the curve = 95 % confidence intervals

Results of the random forest regression incorporating ground-based data alone (Model name = Te.ground), indicated that using only plot level air temperature and LAI within the

model accounts for 73.2% of the variation within T_e. Model validation revealed a strong relationship between observed and predicted values in the test data (Figure 4.4; $r^2 = 0.89$, P<0.001). The RMSE of this relationship was 1.07.
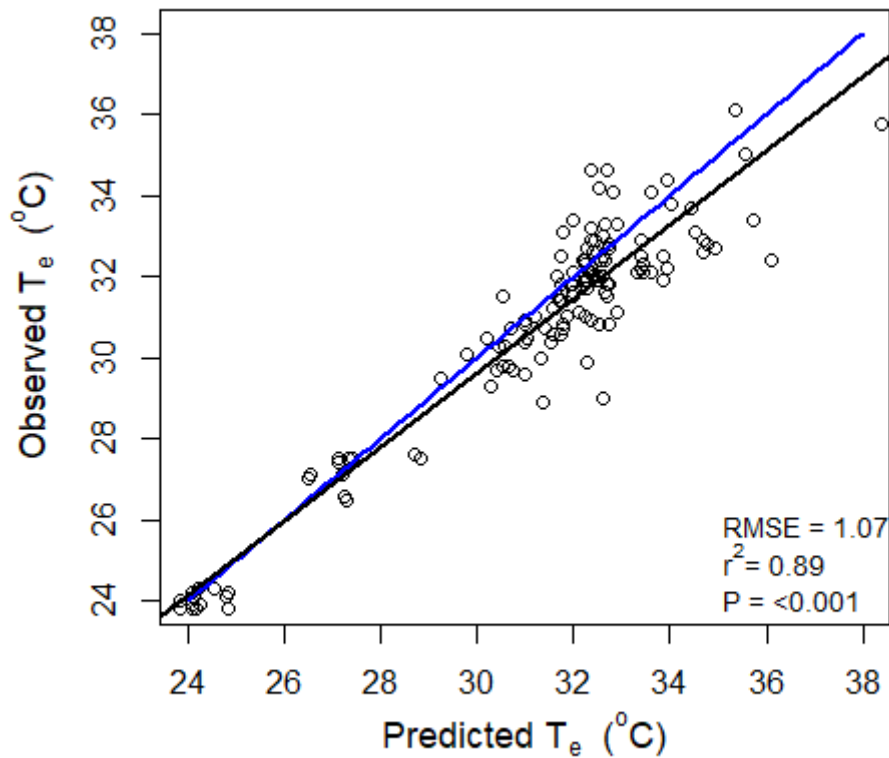
Figure 4.4: Scatterplot of observed T_e vs predicted T_e values for the test data for the Te.Ground random forest model, RMSE = Root Mean Square Error, r2 and associated P value derived from correlation of observed vs predicted T_e. Black line indicates linear regression line and the blue line indicates one-to-one line.

Variable importance estimates indicated that air temperature was more important than LAI (Figure 4.5).
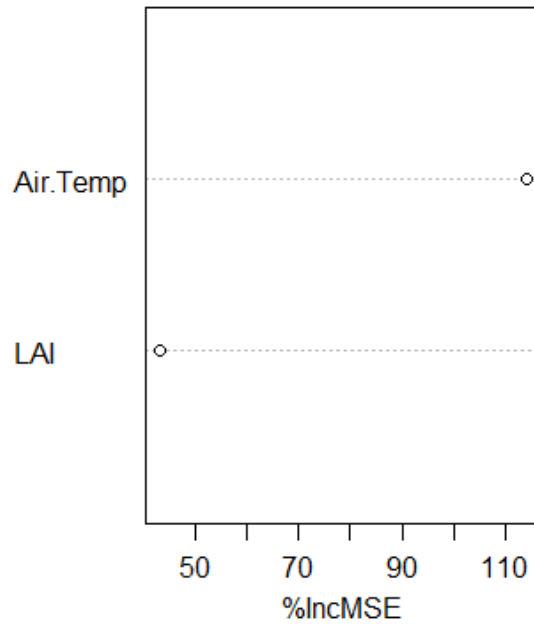
Figure 4.5: Variable importance plot derived from model validation function for model Te.Ground. Air.Temp = Air Temperature, LAI = leaf area index, %IncMSE = percent increase of mean squared error

The random forest (Model name = Te.UAV) model using only UAV-derived data accounted for 30.26% of the variation in T_e. Model validation revealed a negligible relationship between observed and predicted values in the test data (Figure 4.6; r^2 = 0.08 P<0.001). The RMSE of this relationship was 3.02.
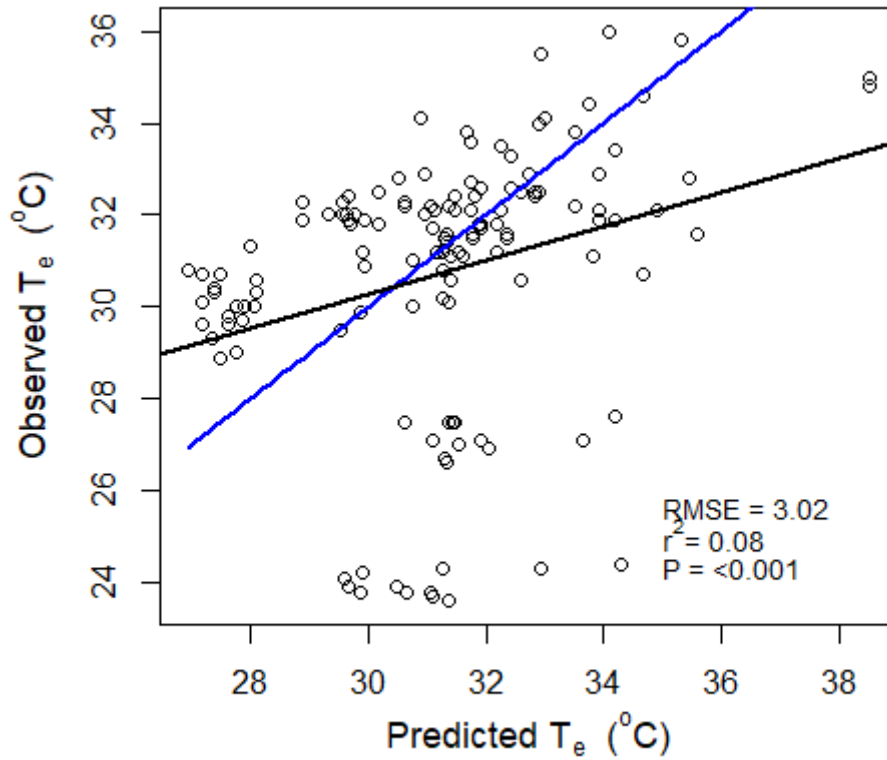
Figure 4.6: Scatterplot of observed T_e vs predicted T_e values for test data for the Te.UAV ramdom forest model, RMSE = Root Mean Square Error, r2 and associated P value derived from correlation of observed vs predicted T_e. Black line indicates linear model line and blue line indicates one to one line

Variable importance indicates that many of the texture metrics were on par with one and other, and the greenness index was of lower importance (Figure 4.7).
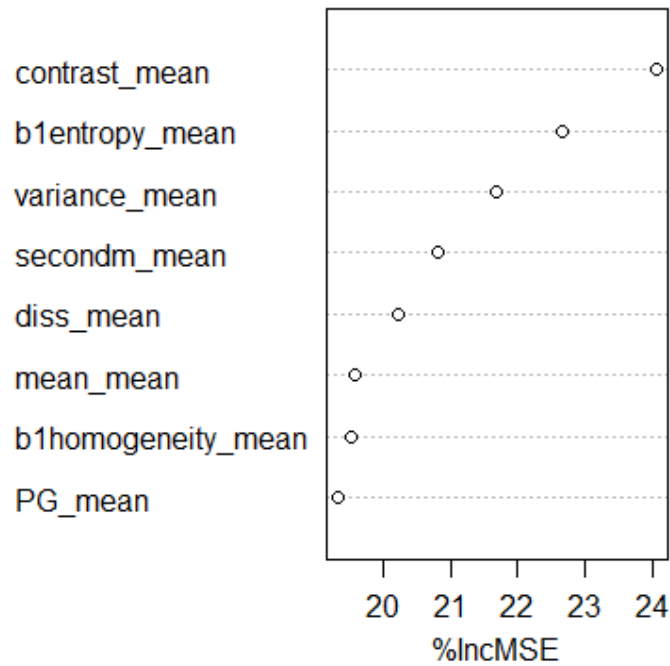
Figure 4.7: Variable importance plot for model Te.UAV. contrast_mean = Contrast texture layer, b1entropy_mean = Entropy texture layer, diss_mean = Dissimilarity texture layer, secondm_mean = Second Moment texture layer, b1homogeneity_mean = Homogeneity texture layer, PG_mean = Greenness layer, variance_mean = Variance texture layer, mean_mean = Mean texture layer, %IncMSE = percent increase of mean squared error

Including the influence of air temperature in the random forest along with the UAV metrics (Model name = Te.Air.UAV) accounted for 82.82% of the variation in T_e. Model validation revealed a strong relationship between observed and predicted values in the test data (Figure 4.8; $r^2 = 0.91$, *P*<0.001). The RMSE of this relationship was 1.03.
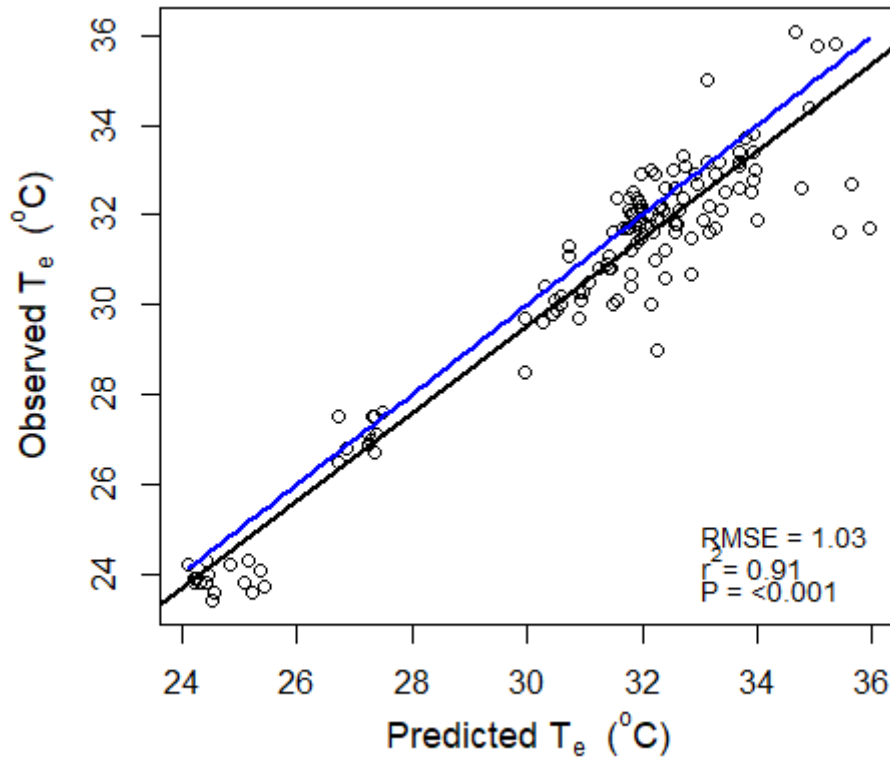
Figure 4.8: Scatterplot of observed T_e vs predicted T_e values for the test data for the Te.Air.UAV random forest model, RMSE = Root Mean Square Error, r2 and associated P value derived from correlation of observed vs predicted T_e. Black line indicates the linear regression line and blue line indicates the one-to-one line.

Variable importance estimates (Figure 4.9) show that plot air temperature is the most important variable in the model, followed by most of the texture metrics and then the greenness index, followed by the mean, dissimilarity and homogeneity texture variables.
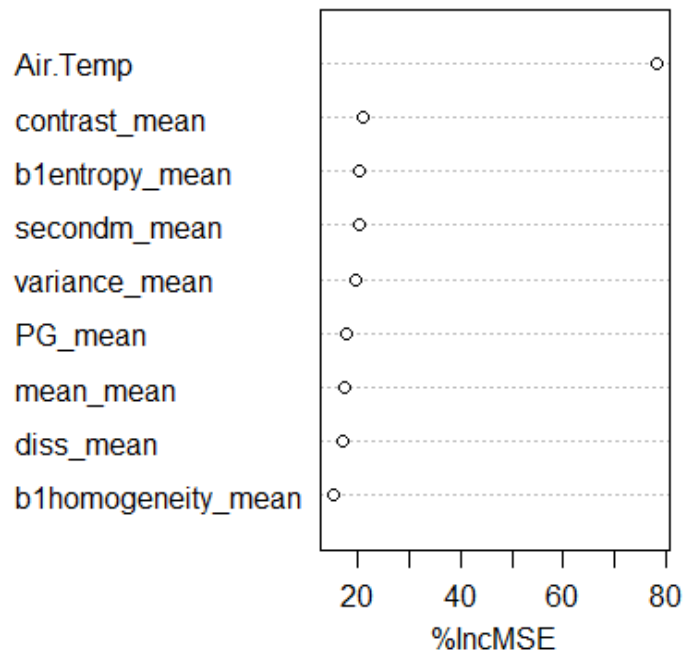
Figure 4.9: Variable importance plot for model Te.Air.UAV. Air.Temp = Air Temperature, contrast_mean = Contrast texture layer, b1entropy_mean = Entropy texture layer, diss_mean = Dissimilarity texture layer, secondm_mean = Second Moment texture layer, b1homogeneity_mean = Homogeneity texture layer, PG_mean = Greenness layer, variance_mean = Variance texture layer, mean_mean = Mean %IncMSE = percent increase of mean squared error

The RF model, which included ground and UAV-based variables (Model name = Te.All), explained the most (85.99%) variation within T_e. Model validation revealed a strong relationship between observed and predicted values in the test data (Figure 4.10; $r^2 = 0.91$, $P<0.001$). The RMSE of this relationship was 1.03.
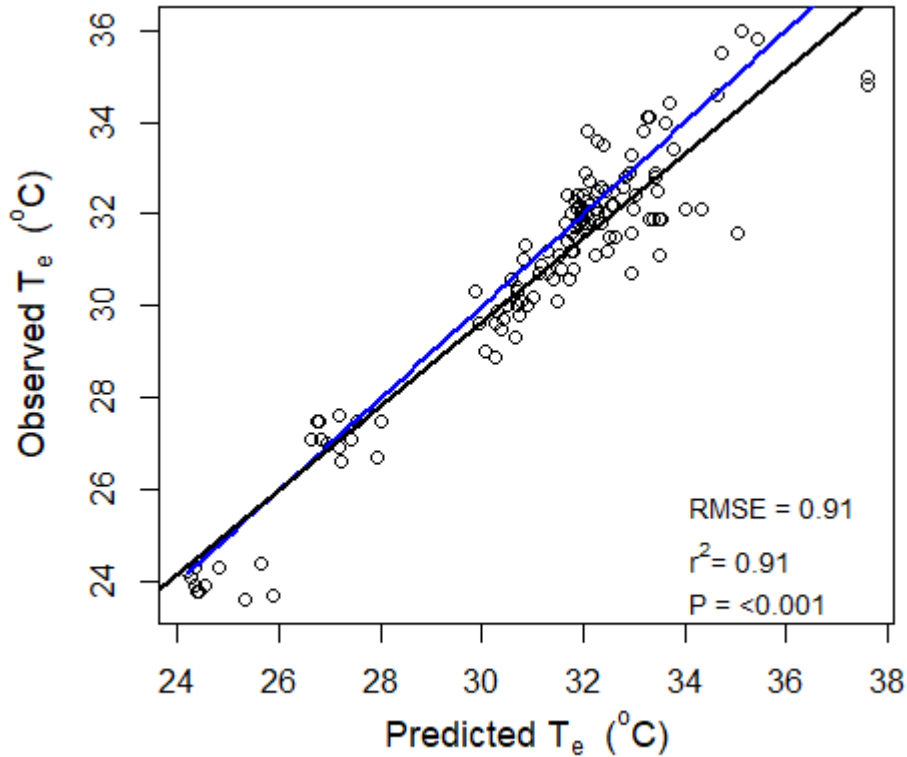
Figure 4.10: Scatterplot of observed T_e vs predicted T_e values for Te.All random forest model, RMSE = Root Mean Square Error, r^2 and associated P value derived from correlation of observed vs predicted T_e. Black line indicates linear regression line and blue line indicates one-to-one line.

Variable importance estimates for the Te.Air.UAV RF model (Figure 4.11) show that the ground-based data (plot air temperature and LAI) are the most important, with air temperature being the most important variable in the model, then LAI, and then the texture metrics and then the greenness index.
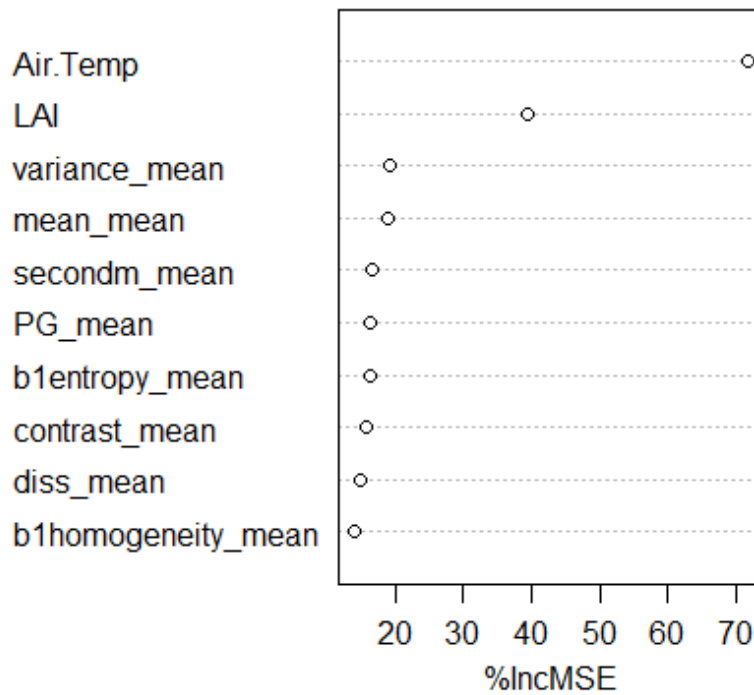
Figure 4.11: Variable importance plot derived from model validation function for model Te.Air.UAV. Air.Temp = Air Temperature, LAI = leaf area index, contrast_mean = Contrast texture layer, b1entropy_mean = Entropy texture layer, diss_mean = Dissimilarity texture layer, secondm_mean = Second Moment texture layer, b1homogeneity_mean = Homogeneity texture layer, PG_mean = Greenness layer, variance_mean = Variance texture layer, mean_mean = Mean texture layer, %IncMSE = percent increase of mean squared error.

The Jackknifing approach to model evaluation showed that predictions vary substantially between plots and land cover classes (Table 4.4; Figure 4.12),. Forested plots generally had higher r^2 values between the observed and predicted values for T_e (Table 4.4) than those found for urban forest and urban plots with little vegetation.

94

Table 4.4: Random forest validation outcome for each plot using the Te.Air.UAV random forest model with a Jackknifing approach, where the plot indicated in the Plot No. column was omitted from training data and then used as a validation set, r2 and the associated P-value derived from correlation of observed vs predicted T_e.

Plot No.	Land Cover Class	r^2	P-Value
1	Forest	0.72	< 0.001
2	Forest	0.83	< 0.001
3	Forest	0.92	< 0.001
4	Urban Forest	0.04	0.12
5	Urban Forest	0.01	< 0.001
6	Urban Forest	0.10	0.01
7	Urban	0.16	0.04
8	Urban	0.90	< 0.001
9	Forest	0.85	< 0.001
10	Forest	0.82	< 0.001
11	Forest	0.06	0.08
12	Urban Forest	0.00	< 0.001
13	Urban	0.02	< 0.001
14	Forest	0.85	< 0.001
15	Forest	0.94	< 0.001
16	Urban Forest	0.09	0.06

Figure 4.12 indicates a bimodal type structure in the majority of forest plots. This is likely due to the cluster of cooler temperatures being where 3D replicas are in areas where there is a more closed and shaded canopy, resulting in more stable and lower temperatures, and the higher temperatures indicating where replicas were exposed to more solar radiation, likely by being placed where there is less or no canopy. Figure 4.12 (k) is an exception to this bimodal structure, this plot is coastal forest located right on the beach at the south-eastern point of the island, with exposed winds. The canopy consists solely of Caribbean almond (*Terminalia catappa)* trees which form an a unique forest structure with no understory present. Canopy make up, coastal winds and proximity to volcanic rock exposures all may have influenced the thermal regime of this plot, and the ability for the RF model to predict temperatures within this plot , as the model is based solely on canopy structure. However, please note, Figure 4.12 (b and c) are also coastal almond forest, and still show this bimodal structure.
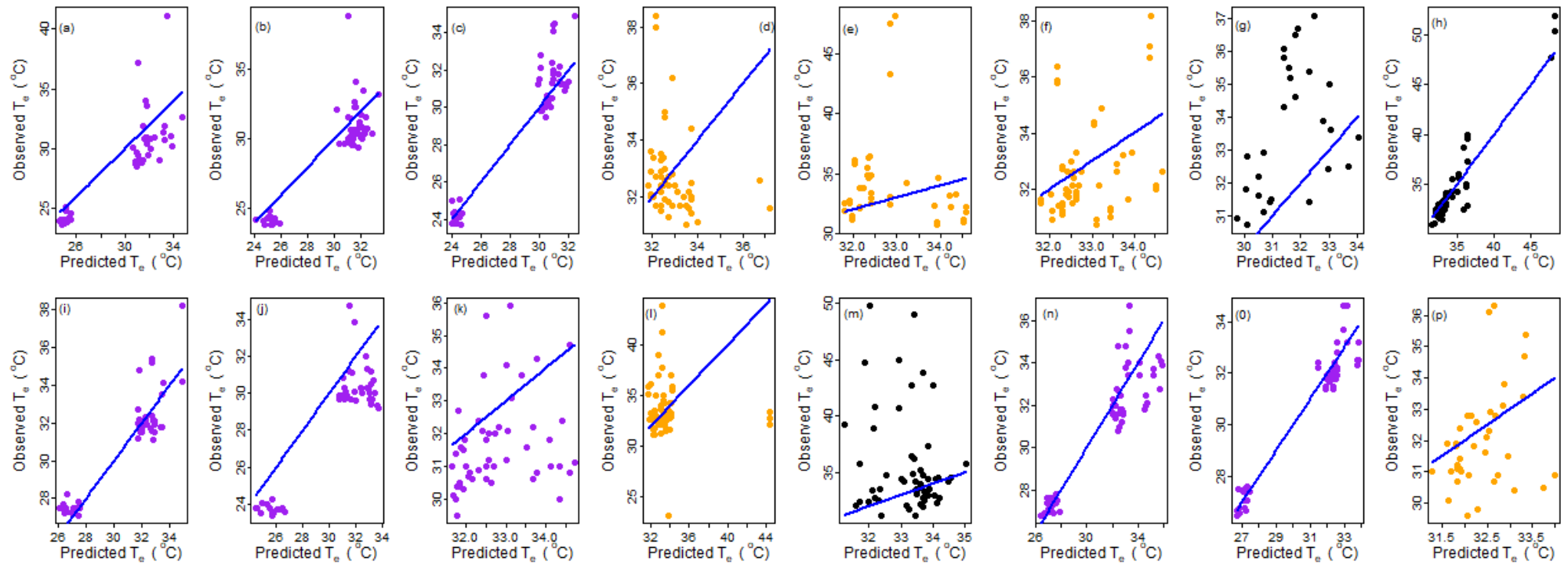
Figure 4.12: Observed vs Predicted T_e for each plot using the Te.Air.UAV random forest model with a Jacknifing approach. Labels a to p correspond to Plot number sequentially from 1 to 16. Point colours refer to land cover where purple = forested plots, orange = urban forest plots and black = urban plots. Blue lines indicate a one to one relationship.

4.4.2 Mapping T$_e$

The model Te.Air.UAV, which included air temperature and the UAV metrics (greenness and textures), was used to map T$_e$ across the whole of each plot. Figures 4.13 to 4.22 show example raster layers for areas surrounding survey plots including the original RGB imagery and the T$_e$ prediction raster based on the Te.Air.UAV Random Forest model. Figures 4.13 to 4.22 show RGB and T$_e$ raster maps for a subset of forest and more urbanised areas; similar figures for the remainder of the plots can be seen in Appendix 7. Maps highlight the whole of the orthomosaic as well as regions of interest to consider mapping performance. Examining Figures 4.13 to 4.22, the model has identified cooler areas where there are denser, or more homogenous, canopies and has also picked out warmer areas of canopy gaps well. It has also identified differences between tree species, whereby some species have more open canopies that allow more solar radiation to reach sub-canopy dwelling ectotherms. Examining plots within urban areas, the model has picked up that the areas are warmer, but there are some discrepancies when looking such areas, particularly relating to water and areas of agriculture. This corroborates results of the Jackknife approach for the model (Table 4.4; Figure 4.12), which showed that the model performed better in forested areas.
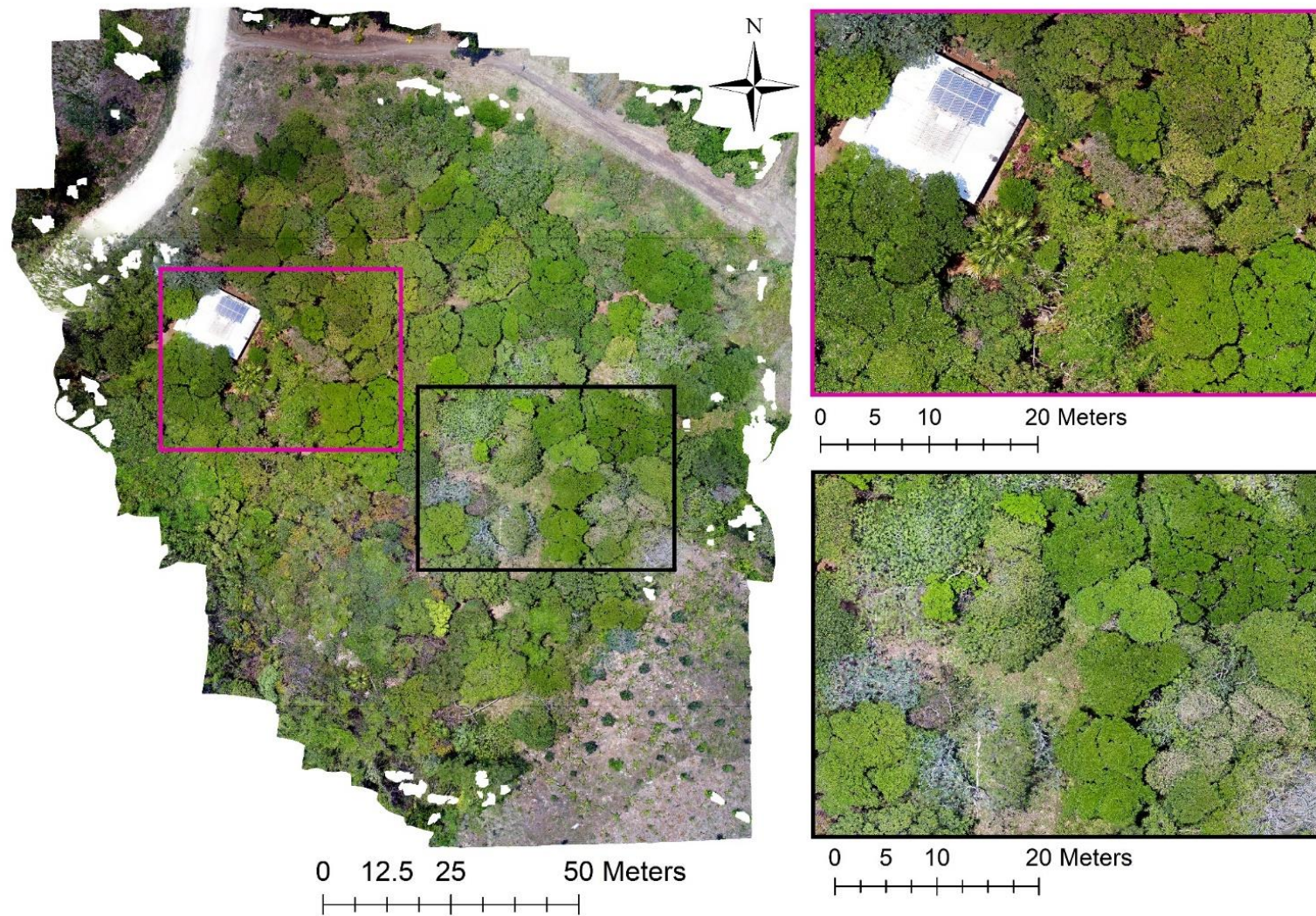
Figure 4.13: RGB raster layer of area surrounding Plot 1 with zoomed in and highlighted areas of interest (magenta and black insets)
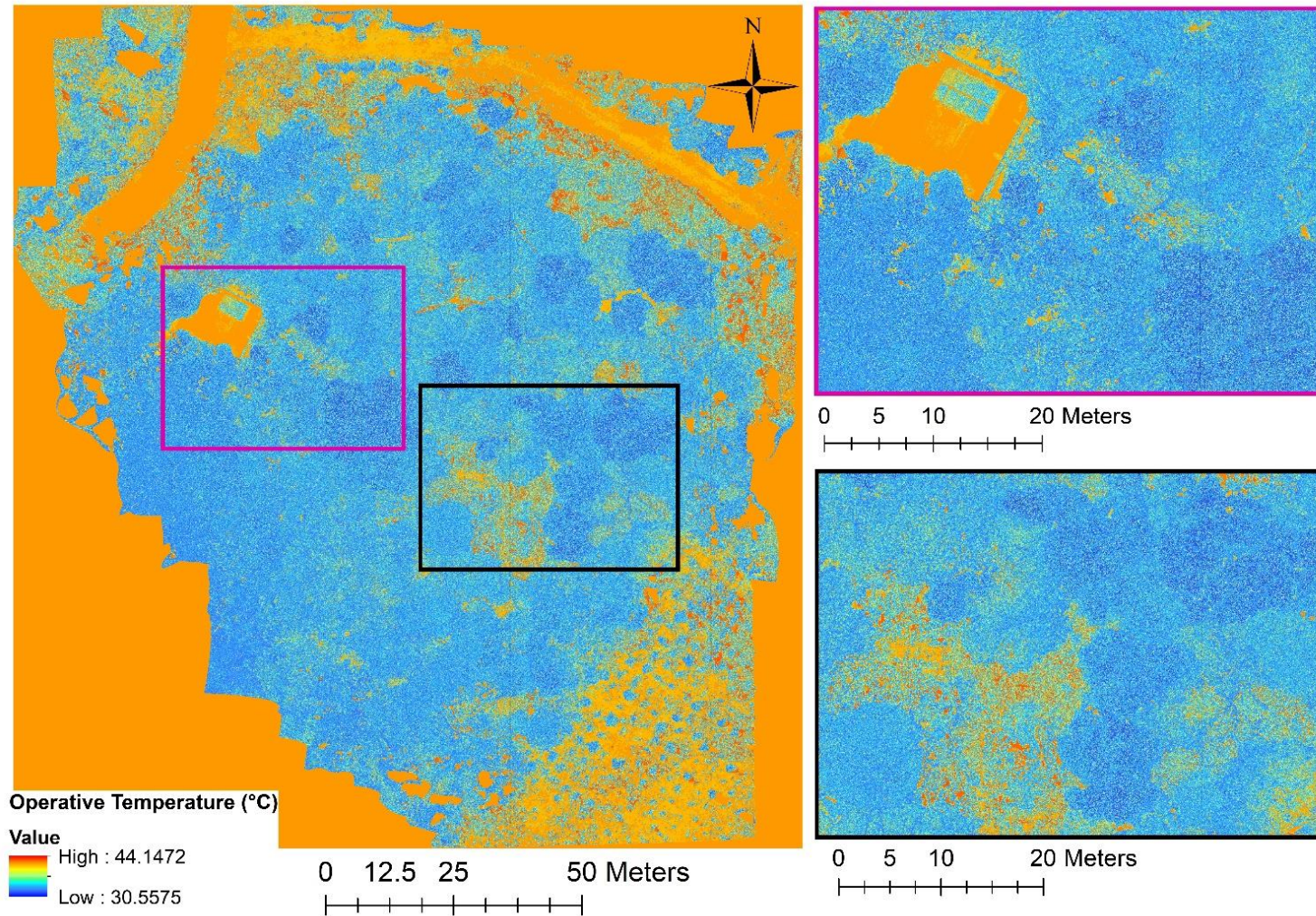
Figure 4.14: Operative Temperature (T_e) raster layer derived from predictions of Te.Air.UAV random forest model of area surrounding Plot 1 with zoomed in and highlighted areas of interest (magenta and black insets)
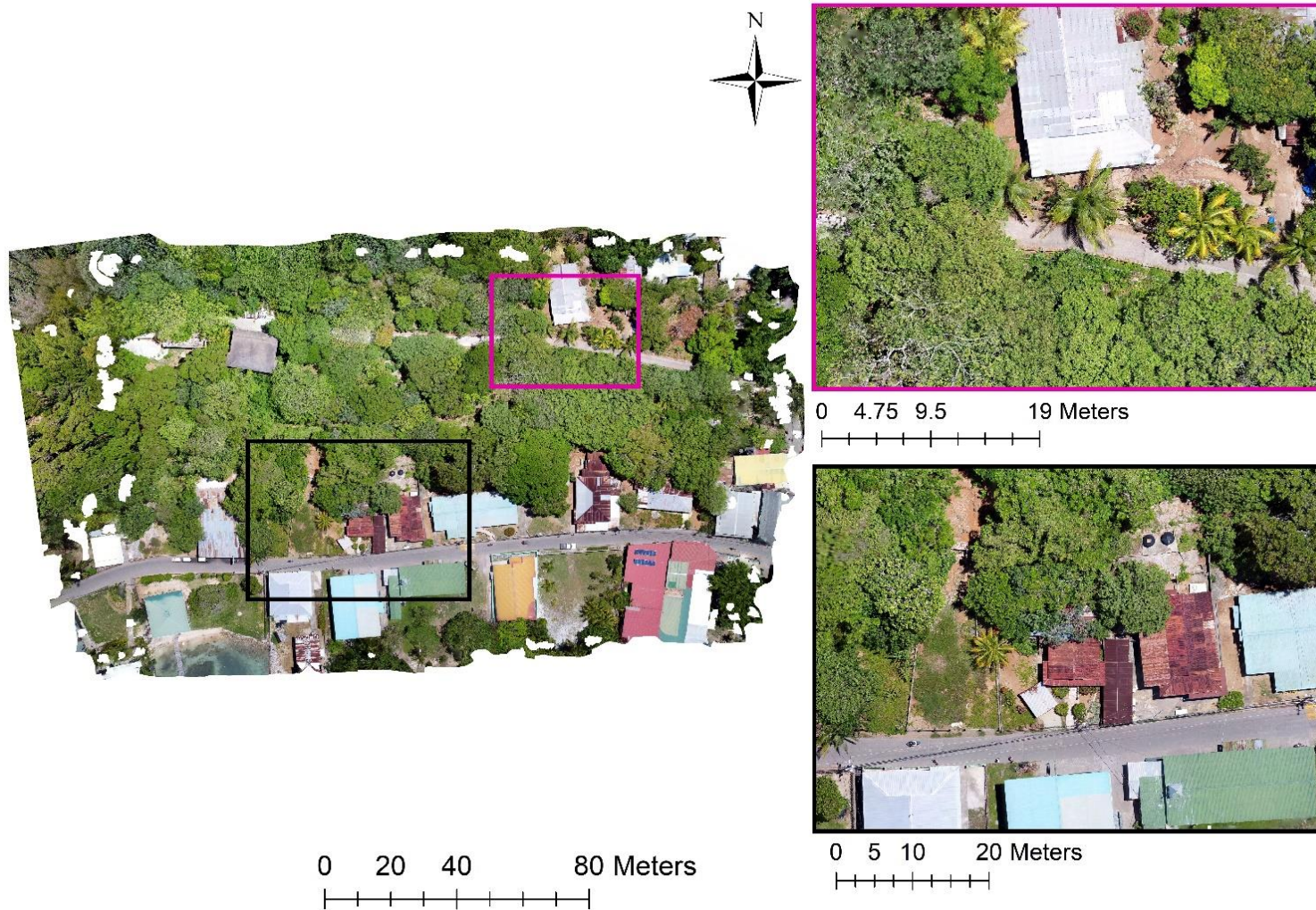
Figure 4.15: RGB raster layer of area surrounding Plot 4 with zoomed in and highlighted areas of interest (magenta and black insets)
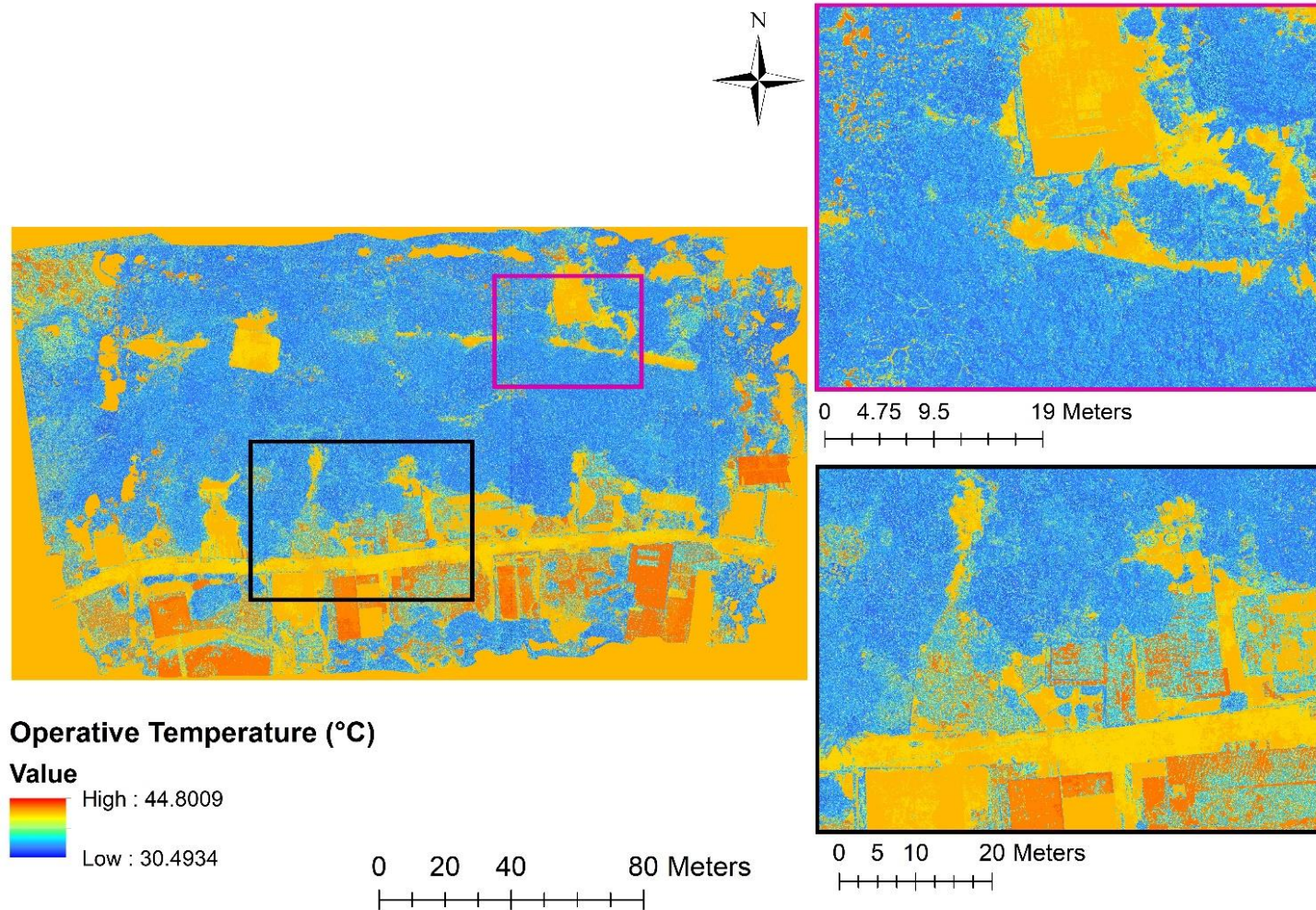
Figure 4.16: Operative Temperature (T_e) raster layer derived from predictions of Te.Air.UAV random forest model of area surrounding Plot 4 with zoomed in and highlighted areas of interest (magenta and black insets)
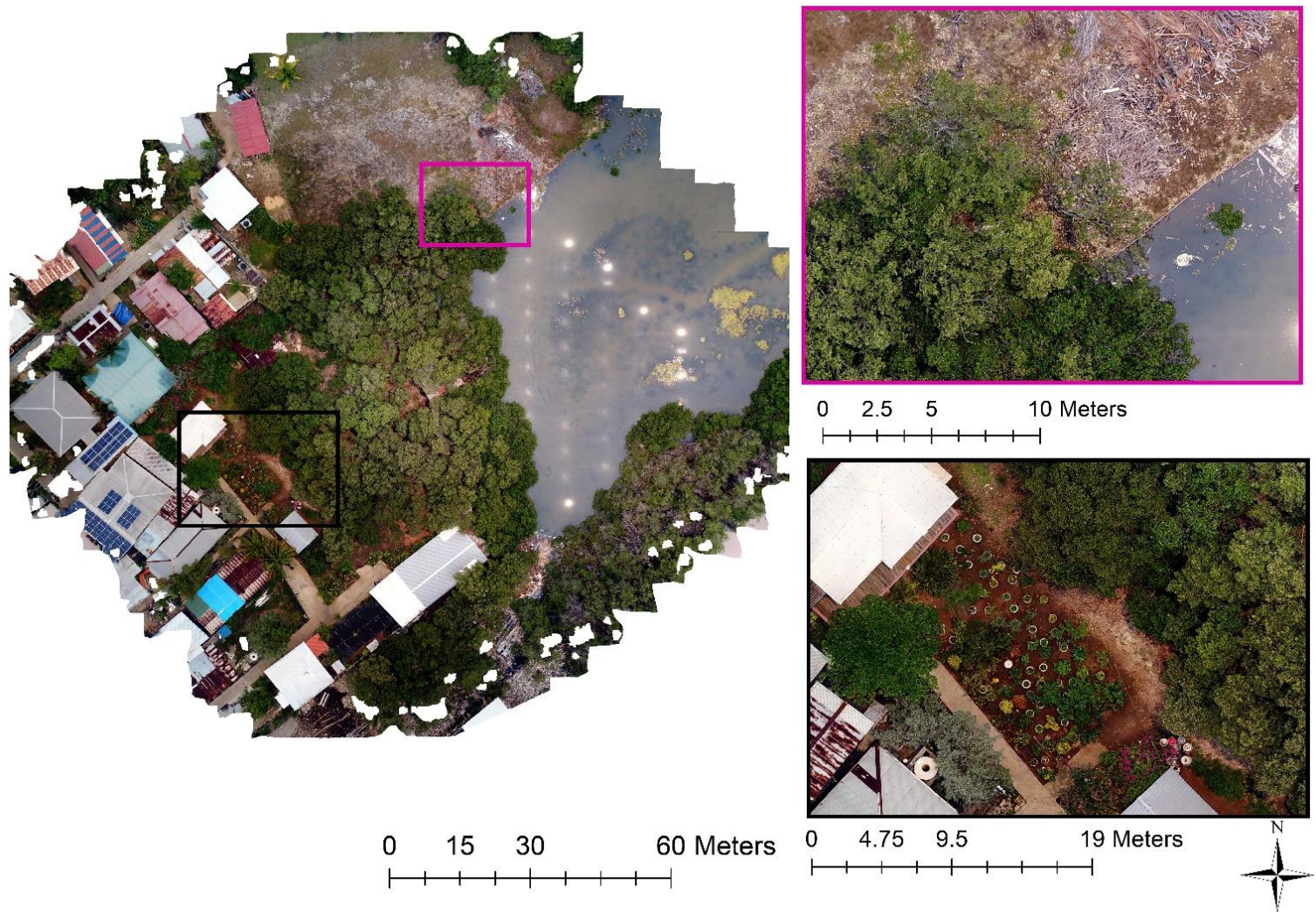
Figure 4.17: RGB raster layer of area surrounding Plot 6 with zoomed in and highlighted areas of interest (magenta and black insets)

103
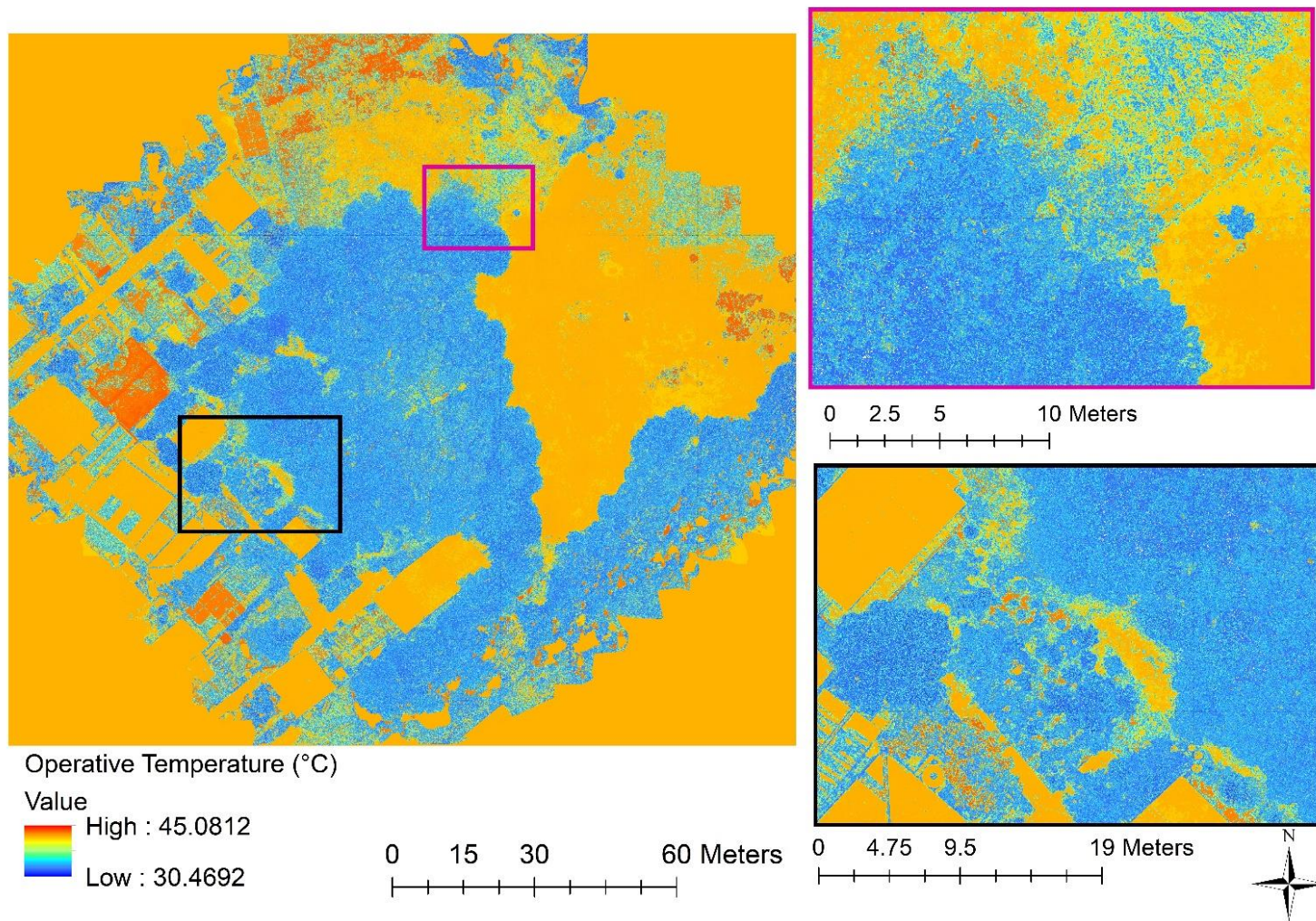
Figure 4.18: Operative Temperature (T$_e$) raster layer derived from predictions of Te.Air.UAV random forest model of area surrounding Plot 6 with zoomed in and highlighted areas of interest (magenta and black insets)
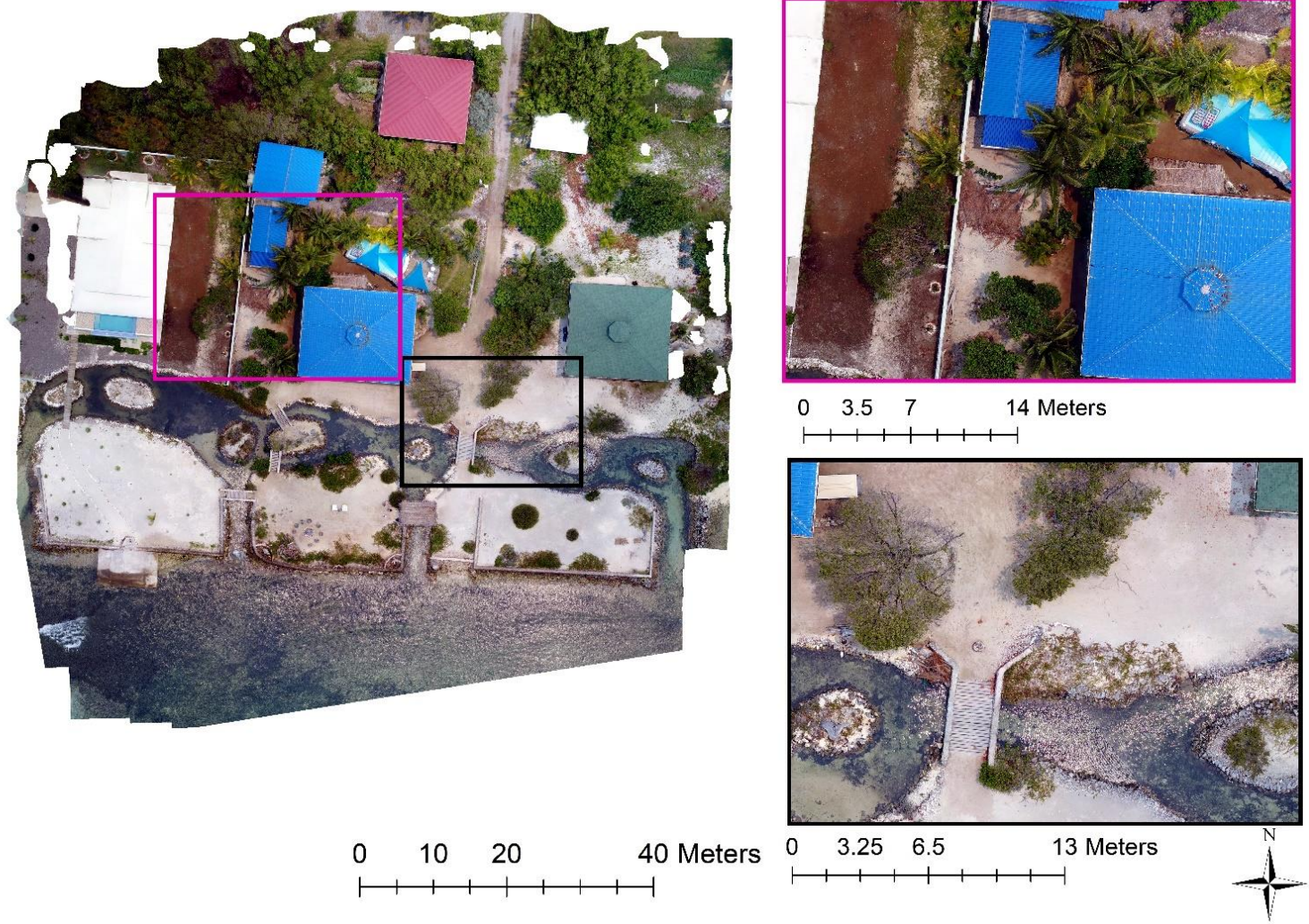
Figure 4.19: RGB raster layer of area surrounding Plot 7 with zoomed in and highlighted areas of interest (magenta and black insets)
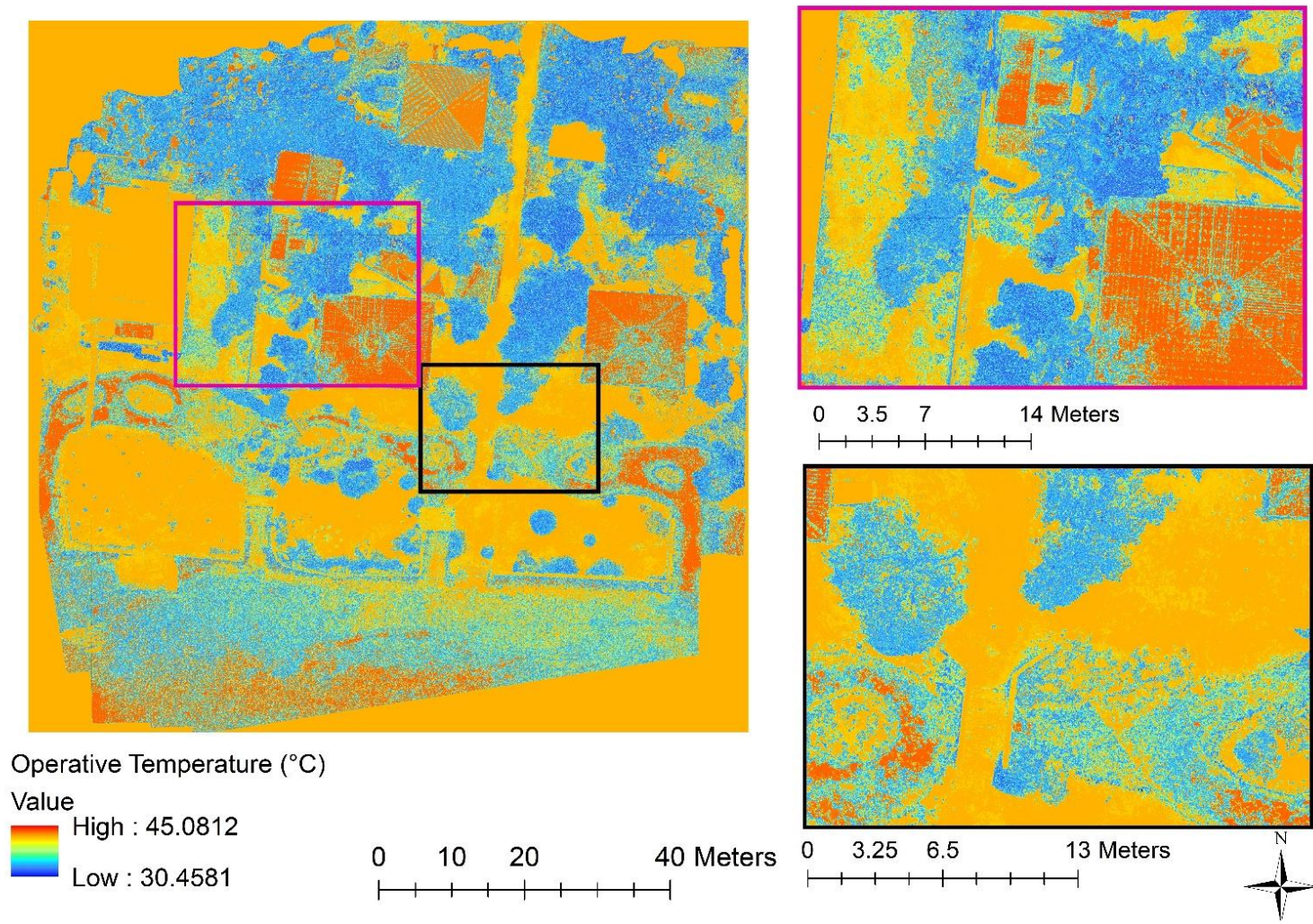
Figure 4.20: Operative Temperature (T$_e$) raster layer derived from predictions of Te.Air.UAV random forest model of area surrounding

Plot 7 with zoomed in and highlighted areas of interest (magenta and black insets)
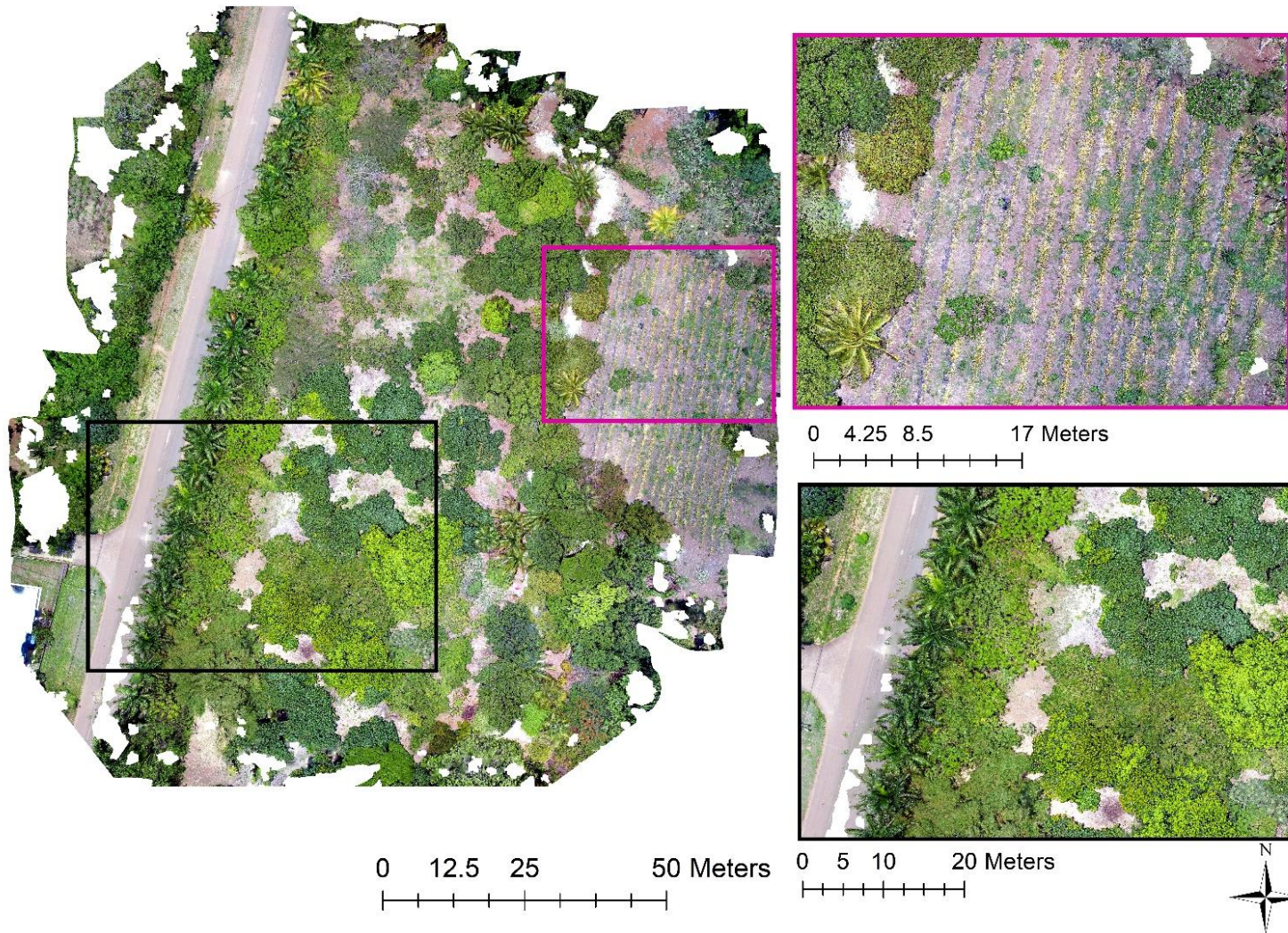
Figure 4.21: RGB raster layer of area surrounding Plot 16 with zoomed in and highlighted areas of interest (magenta and black insets)
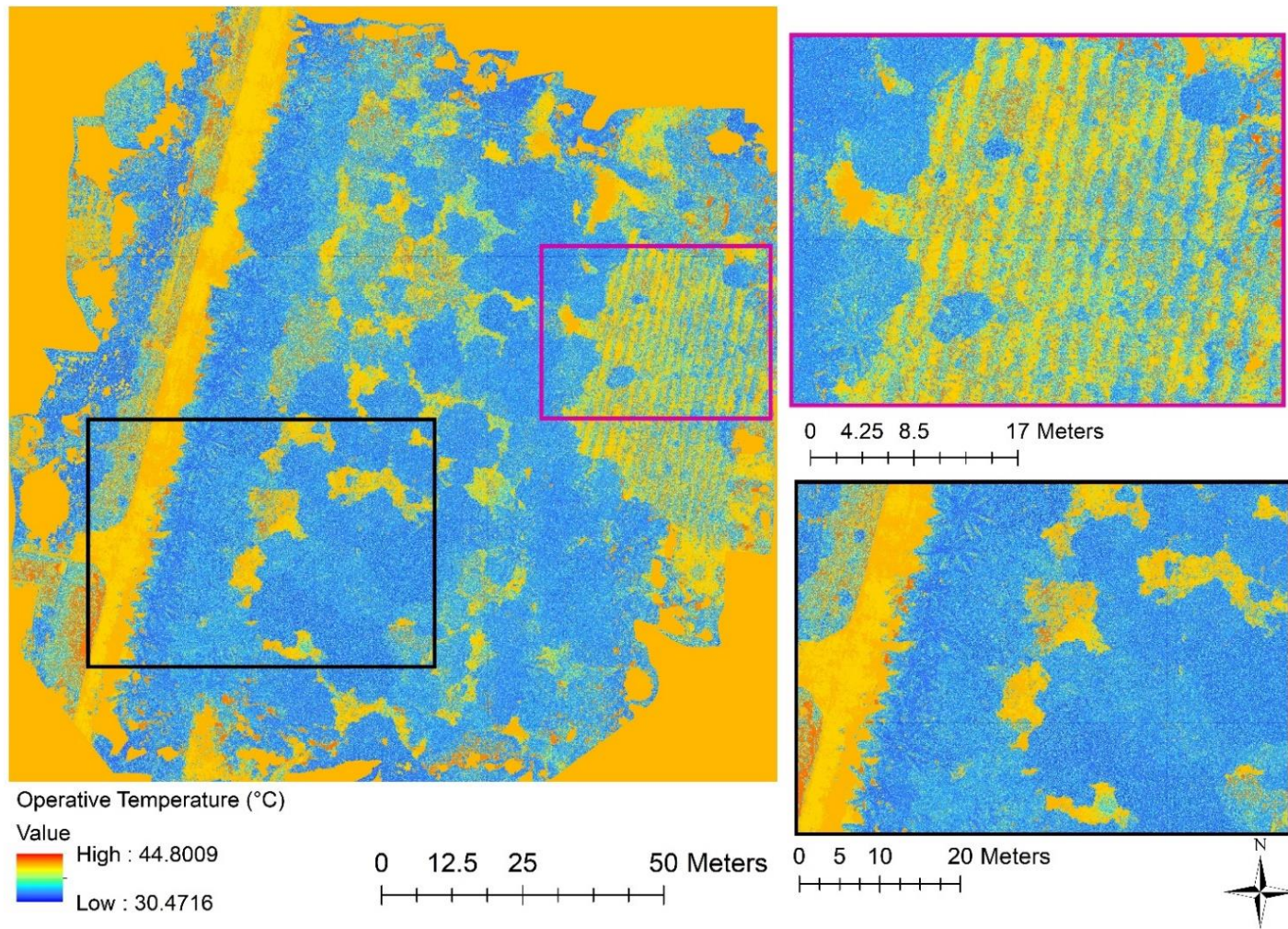
Figure 4.22: Operative Temperature (T_e) raster layer derived from predictions of Te.Air.UAV random forest model of area surrounding Plot 16 with zoomed in and highlighted areas of interest (magenta and black insets)

4.4.3 Anole Abundance and UAV Predicted T_e

Relating *Anolis bicaourm* abundance to the T_e metrics derived from the Te.Air.UAV random forest model found that none of the metrics derived across of the whole of the plot significantly related to anole abunndance (Figure 4.23). Neither SD of T_e (Figure 4.23; F = 1.34, df =11, P = 0.27, r^2 = 0.10), mean T_e of the plot (Figure 4.23; F =0.01, df =11, P = 0.93, r^2 = 0.00), or maximum T_e of the plot (Figure 4.23; F = 0.07, df =11, P = 0.80, r^2 = 0.00) were significantly related to anole abundance.
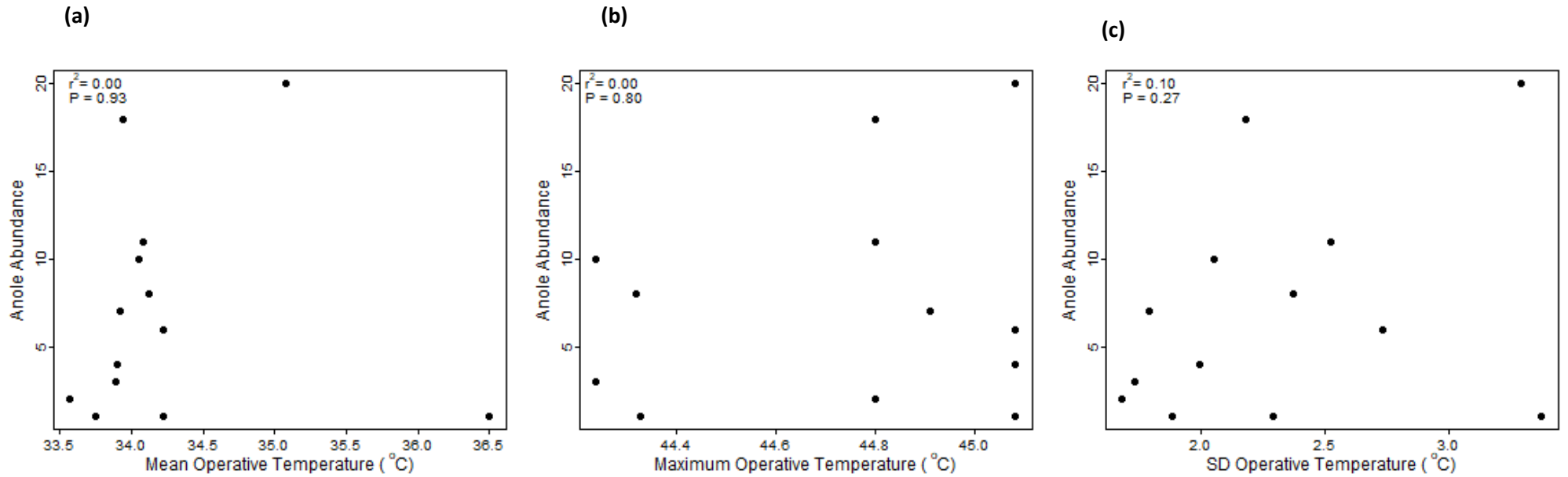
Figure 4.23: Te.Air.UAV Random Forest orthomosaic measures vs *Anolis bicaorum* (Anole) abundance across the whole of each survey plot.

a) Mean plot T_e, b) Maximum T_e and c) Standard deviation of T_e

Landscape metrics based on Thermally Tolerable areas (below CTmax) using 0.9cm resolution date were not significantly related to abundance (Figure 4.24). However results for total area (Figure 4.24.a, $r^2 = 0.25$, $P = 0.08$) and number of patches (Figure 4.24.c, $r^2 = 0.25$, $P = 0.08$), while not significant, warrant future investigation, with an increased sample size.

When looking at the same landscape metrics for the resampled imagery (15cm resolution), there is still no significant relationship with *A. bicaorum* abundance for the survey plots (Figure 4.25). However, all the metrics, the total area and number of patches have the higher r^2 values, but this could simply be due to chance.
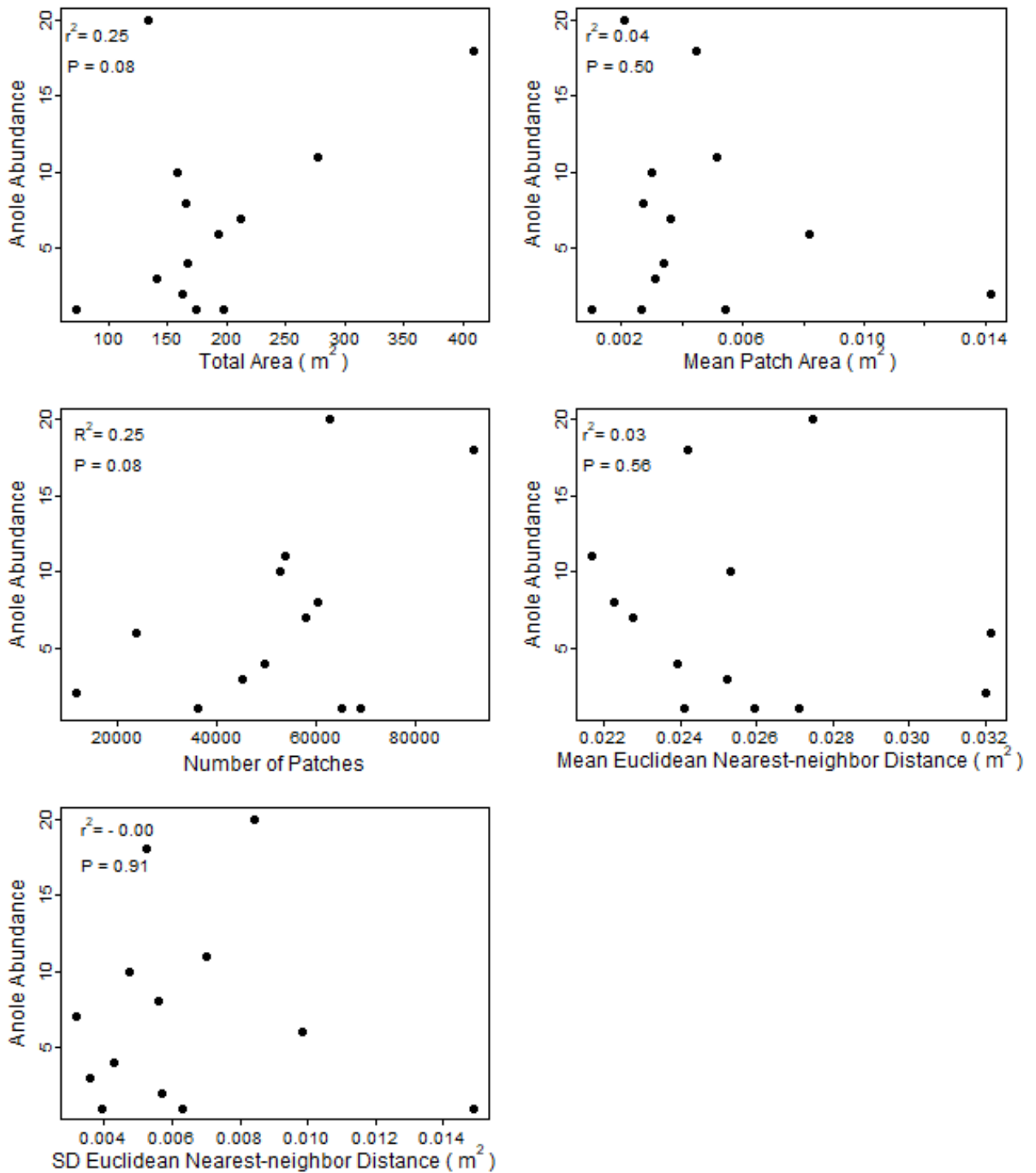
Figure 4.24: *Anolis bicaorum* (Anole) abundance vs Landscape measures for spatial structure of thermal Category 1 for plot raster layers at a spatial resolution of 0.9cm. a) Total Category Area, b) Mean Patch Area, c) Number of Patches, d) Mean Euclidean Nearest Neighbour Distance and e) Standard Deviation of Euclidean Nearest Neighbour distance

112
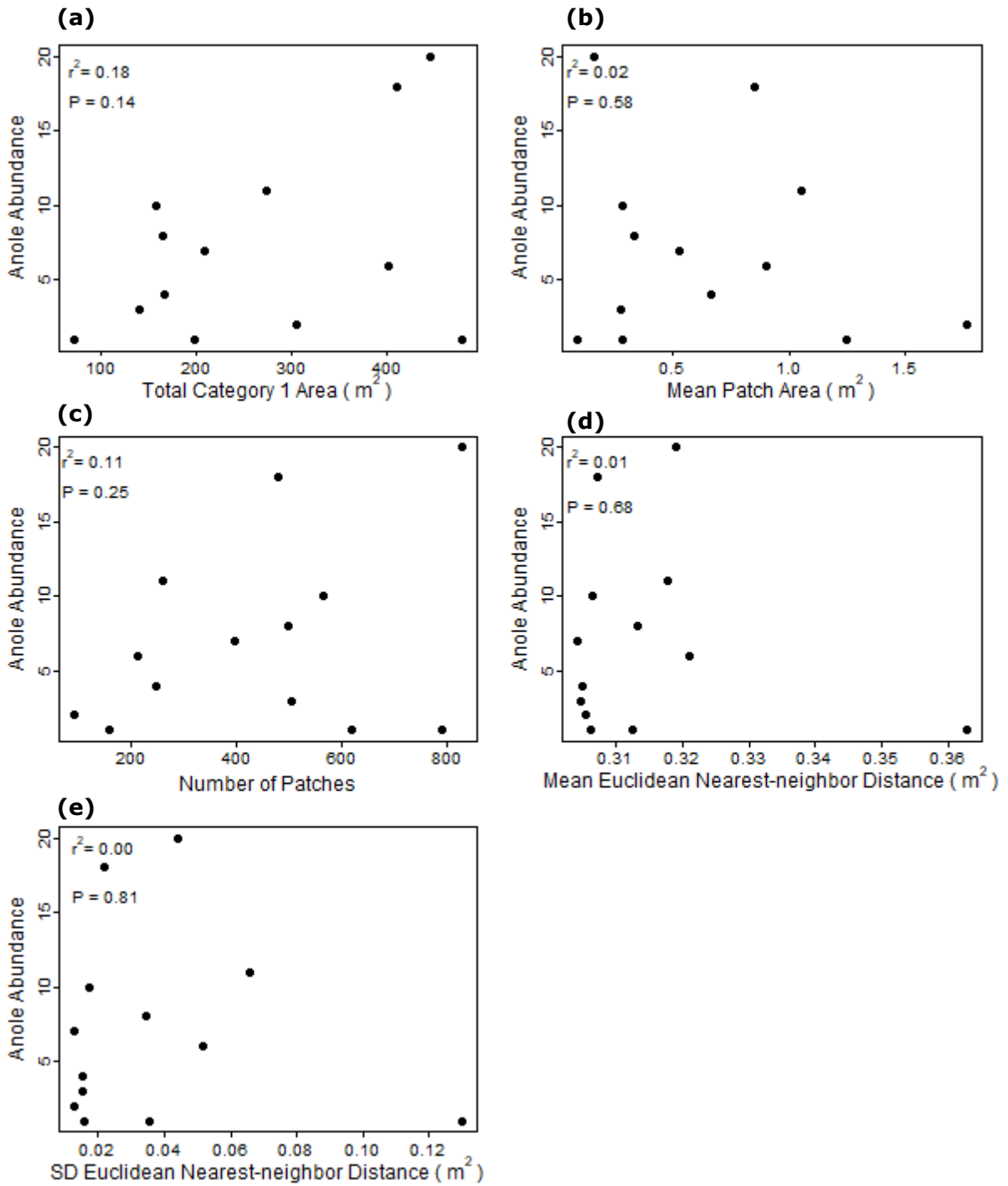
Figure 4.25: *Anolis bicaorum* (Anole) abundance vs Landscape measures for spatial structure of thermal Category 1 for plot raster layers at a spatial resolution of 15cm. a) Total Category Area, b) Mean Patch Area, c) Number of Patches, d) Mean Euclidean Nearest Neighbour Distance and e) Standard Deviation of Euclidean Nearest Neighbour distance

4.5 Discussion

Measurements of canopy structure from UAV imagery have the potential to provide fine-scale predictions of spatial heterogeneity of thermal habitat quality for animals at finer resolution than can currently be obtained from existing mechanistic models, or from ground-based methods traditionally used in thermal ecology. This chapter has proposed a workflow for mapping sub-canopy tropical lizard T_e at fine spatial scales using high-resolution optical UAV imagery coupled with air temperature data. This proposed workflow allows for high spatial resolution and spatial extent measures of T_e below the canopy, helping fulfil the need for data on T_e for forest lizard species at ecologically relevant spatial resolution and extent.

Results of the random forest regression models indicate that the model that included air temperature and the combined UAV data (greenness and texture) had higher predictive performance of T_e than models using just air temperature or coupling air temperature with ground based ceptometer LAI measurements. Plot air temperature accounted for the most variation in T_e, as a single variable, and in the models where it was included; it always was the most important variable within the model, highlighting the importance of having air temperature measures at relevant spatial resolutions, unlike those seen in broad climatic datasets. It was also to be expected that incorporating LAI into a model, which also included air temperature, would increase the model performance in predicting T_e, by incorporating a measure of canopy structure (Algar et al., 2018; Maclean and Klinges, 2021). However, my results indicate that including UAV-derived canopy measurements in the model with air temperature accounted for a higher percentage of variation within T_e than using air temperature and ground-based LAI. This suggests that greenness and texture captured biophysically relevant aspects of the canopy that influence incident solar radiation beyond that captured by LAI measurements from the ground. Nonetheless, the ground-based LAI, as only one variable, does well in the model when coupled with plot air temperature, and was more important, based

on variable importance plots, than the UAV derived data. However, when considering the applications of the models, the UAV-derived data allows T_e to be mapped across a larger spatial extent at higher spatial resolutions, with relatively simple data acquisition methods. It, therefore, confers an advantage to models including UAV data, rather than ground-based LAI measures.

The Te.Air.UAV model performed best within forested areas and less well in other land covers, including highly urban plots. This is seen in the example maps of areas surrounding the plots. For example, areas of open agriculture being classified as cooler and roofs of some urban buildings being classified as cooler areas. This highlights the need to train the model further across different land covers, and in the case of urban areas, consider that the modelling approach may not be suitable due to a general lack of canopy. In such cases, the UAV imagery is capturing variation in the ground, rather than the influence of shade. In forests, however, where the model performed best, the findings are consistent with that found in Algar et al., (2018). They found that measures of canopy density (LAI) improved microclimate-only models of lizard body temperature in closed canopy environments, but had little influence in environments that were more open.

UAVs have been highlighted as a method for capturing high resolution spatial data for microclimate modelling (Duffy et al., 2021; Kašpar et al., 2021; Milling et al., 2018; Zellweger et al., 2019) and canopy structure, which can be captured with UAVs, can produce significant differences in microclimate (Kašpar et al., 2021; Maclean and Klinges, 2021). My work extends this to map an ecologically relevant measure for ectotherms (T_e). This can then be used to determine thermal niche based suitability measures of the landscape at spatial resolutions relevant to the organism and across spatial extents relevant for use in species distribution modelling and to predict responses to environmental change (Sears et al., 2011; Sears and Angilletta, 2015). We can now set out air temperature loggers and T_e 3D replicas for model

training, and can then fly a standard easily accessible RGB UAV platform, to map T_e across the whole of the study area at a high spatial resolution, which will only be dependent on UAV flight area and image configuration.

The benefits to this proposed workflow is that it captures relevant landscape level and ecologically relevant data for ectotherms at a spatial resolution that is relevant to the organism. This information can inform species distributions, risk and persistence models that are not based solely on microclimate or coarse resolution environmental data, but go beyond this to ecologically relevant measures for ectotherms (T_e). The ability to map Te is especially important when considering thermal habitat suitability of *A. bicaorum*. In Chapter 3 it was demonstrated that even at a plot (20 x 20m) scale, variation in thermal habitat quality, which we measured as the percent of time the 3D T_e replicas were within the T_{pref} range (25.4 - 28°C) had an influence on anole abundance, as well as an influence on its prey abundance. The workflow proposed also now allows us to categorise the spatial structure of thermally preferable patches across the whole of the plot, which is important to consider for lizard behavioural thermoregulation and energetics, which influences population fitness (Sears and Angilletta, 2015). However, when comparing the T_e measures derived from the Te.Air.UAV models for the plots with *A. bicaorum* abundance, no significant relationships were found with coarse measures (Mean T_e, Maximum T_e and SD of T_e) or for the spatial arrangement of areas below 33.2°C (CT$_{Max}$ for *A. bicaorum*). This could be due to the model focusing on solar noon, and not considering the time budget of thermally favourable conditions which influence distribution and fitness (Caetano et al., 2020; Logan et al., 2015, 2013c). This is corroborated by findings of Chapter 3, where the percentage of time within T_{pref}, was found to be significantly related to *A. bicaorum* abundance. My approach could be extended to consider changes in T_e throughout the day. However, the ability to model T_e, even at a single point in

time but across a complete landscape, including fine-scale heterogeneity, is step forward in measuring thermal habitat quality for ectotherms.

Building on this foundation, future work toward improving model predictions could incorporate additional UAV data, such as canopy volumetric data from structure from motion (SfM) photogrammetry (Duffy et al., 2021; Zellweger et al., 2019). In addition UAV-derived tree and canopy height, which was found to be significantly related to microclimate by (Kašpar et al., 2021), could also improve my models. Such additional measures are relatively simple to obtain methodologically from UAV derived data, only requiring the UAV images to have a sufficient amount of overlap for photogrammetry derived SfM methods. However, implementation and extraction of relevant measures, such as LAI, from SfM are in their infancy and would require additional work, which was not feasible within the timeframe of this work. Additional measures such as these, would feed into further training the model to potentially consider T_e at other points in the day to incorporate the time budget element of thermal suitability modelling for tropical lizards.

4.6 Chapter Conclusions

My work has provided a step forward in mapping ectotherm T_e at fine spatial resolution using optical UAV data coupled with air temperature. This workflow and model will allow us to map ecologically relevant measures of the thermal environment across larger areas at scales relevant to the individual animals and populations, something that until now was not feasible with standard ground-based methods or with mechanistic niche modelling. This now allows for us to consider the impact of anthropogenic and climate change on such species that are dependent on suitable thermal environments, such as *A. bicaorum*, and how the thermal microhabitat may alter with such phenomena. In the next Chapter, I will apply the methods covered here across high spatial resolution satellite imagery data (WorldView -2) across Utila. In addition, I will determine the potential change in thermal environment under anthropogenic

habitat conversion and climate warming across the island to determine the potential impact on

A. bicaorum, and the conservation implications for this endemic species.

Chapter 5 : Quantifying available thermal habitat for *Anolis bicaorum* under anthropogenic land use and climate change using WorldView-2 imagery

5.1 Chapter Overview

Forest dwelling ectotherms, such as *Anolis bicaorum,* experience narrower fundamental thermal niches and are therefore may be more sensitive to a change in their thermal environment than species in more open habitats. Anthropogenic land use and climate change can both alter thermal habitats, where loss of forest canopy insulation and increased air temperatures are thought to degrade thermal conditions for forest thermal specialists. The island of Utila has undergone significant anthropogenic habitat conversion in recent years, leading to forest loss, and therefore a potential decrease in available thermal habitat for *A. bicaorum.* Here I use very high-resolution (VHR - 50cm spatial resolution) multispectral WorldView-2 (WV2) imagery to identify forest loss on Utila and map operative temperature (T_e) across the island of Utila for 2018 and 2020. Coupling these results with known critical thermal maximum (CT_{max}) estimates for *A. bicaorum*, I calculate the available area of forest on the island of Utila that is within the thermal range for *A. bicaorum* under different land use, air temperature, and climate change scenarios. Results indicate a 14.08% loss of forest area between 2018 and 2020, but only a slight loss of suitable thermal habitat, due to the concentration of forest loss in areas where T_e was already high. However, a scenario of 1.5°C warming in air temperature demonstrated a restructuring of the available thermal habitat, with a loss in the thermally suitable habitat and an increase in the warmer unsuitable classes. Results of this work demonstrate the potential use of this approach in considering thermal refuges for the survival of ectotherms under climate change and land use change, whilst also highlighting the caveats of this approach and suggests alterations for future work.

5.2 Introduction

Rising and more variable temperatures resulting from climate change are a significant threat to biodiversity worldwide (Thomas *et al*., 2004; Pereira et al., 2010). In a warmer world, species' futures will depend on their ability to maintain favourable body temperatures, and thus maintain ecological function and evolutionary fitness (Kearney et al., 2009; Vasseur et al., 2014). Many ectotherms are already operating close to their thermal limits, leaving little safety margin to behaviourally buffer higher temperatures (Deutsch *et al.,* 2008; Munoz *et al.,* 2014; Sunday *et al.,* 2014). Evidence is now mounting that tropical ectotherms will be the hardest hit from warming, and studies have warned that tropical forest lizards, in particular, are in danger of extinction (Huey et al., 2009; Logan et al., 2013b).

From previous chapters of this thesis, we know that thermal controls are important for *Anolis bicaorum* abundance. Results of Chapter 3 indicated that both leaf area index (LAI) and thermal habitat quality, specifically the time that each plot was within the T_{pref} range of *A. bicaorum*, are linked to *A. bicaorum* abundance by influencing their abundance both directly and indirectly, through multiple niche interaction pathways. Chapter 4 of this thesis highlighted the potential positive relationship between the amount of available habitat below the critical thermal maxima (CT_{max}) for *A. bicaorum* (determined from landscape metrics of total patch area and number of patches), and *A. bicaorum* abundance. While these relationships were not significant ($P = 0.08$), this could be due to sampling design (low plot sample size) or that simply considering areas below CT_{max} does not directly relate to abundance. As it does not relate to activity time budgets, as was found to be a significant variable when considering abundance in Chapter 3 (percent of time within T_{pref}). Chapter 4 also highlighted the role of canopy structure in regulating sub-canopy operative temperatures of the anoles. Canopy cover and its role in maintaining stable sub-canopy microclimate conditions is also predicted to play a key role in allowing specialist forest species time to adapt to future climate by providing stable conditions

and influencing lizard body temperature (Algar et al., 2018a; De Frenne et al., 2019; Lenoir, 2020) .

In Chapter 4 of this thesis, I demonstrated a workflow to map sub-canopy operative temperature (T_e) of lizards using unoccupied aerial vehicle (UAV) imagery. Standard RGB UAV imagery with a spatial resolution of 0.9cm was used to effectively map T_e continuously across the extent of the UAV imagery, when coupled with air temperature layers. The model within the workflow was found to work well and best in forest environments where canopy heterogeneity plays a role in sub-canopy microclimates and thermal environments (Algar et al., 2018a; Kašpar et al., 2021; Maclean and Klinges, 2021). Such workflows using UAV data are extremely useful for looking at T_e at resolutions relative to the organism. However, UAVs have a limited flight time and spatial extent per flight, relying on battery power and UAV platform specifications. Therefore, to cover large spatial extents, several flights would be required, and in many cases, constraints imposed by flight location, weather and field season duration, make large numbers of flights infeasible. UAV imagery can also be limited by temporal extent, as repeated survey flights would have to be undertaken to achieve measurements over time, which may be limited by the need for repeated access to field sites and costs of multiple field seasons. Thus, the UAV-based workflow is especially useful when high-resolution data over a small area at a single point in time is required, but is less feasible when it is necessary to scale it up to cover broader spatial extents and longer time periods. This is where satellite imagery products can be of use.

Satellites, such as WorldView-2 (WV2), which has eight multispectral bands, and up to 30cm spatial resolution, have the capability of collecting multispectral data at high spatial resolutions across a broader spatial extent than that achieved from UAVs. Satellites such as WordlView-2 also have a high temporal resolution as they continuously collect data of the earth surface. WV2 has a revisit time of no longer than two days, meaning they can collect high

121

temporal and spatial resolution data, providing data that cannot be easily, or feasibly, obtained through other approaches, such as UAVs. In this chapter, I apply the workflow developed in Chapter 4, developed for UAV data, toWV2 imagery to determine if this approach can also perform well using satellite imagery.

There were three main aims for this chapter; the first was to test the ability of WV2 imagery, with a spatial resolution of 50cm, to predict sub-canopy ectotherm operative temperatures, using the workflow developed for UAV data (Chapter 4). Aim 2 was to use WV2 satellite imagery to map land use change on Utila between the years 2018 and 2020 to determine forest loss on the island. Finally, the third aim was to map the sub-canopy operative temperature of Utila's forest in 2018 and 2020 to determine how tolerable thermal habitat structure and availability for *A. bicaorum* has been affected by land cover change, and how it will be altered by warming air temperature. The T_e RF models were predicted across the 2018 and 2020 WV2 images at a consistent air temperature to determine the difference in T_e of the forests solely due to changes in the canopy, which includes anthropogenic alteration and complete clearing of the forest. The RF models then were run on the 2018 and 2020 images with a rise in air temperature of 1.5°C to simulate a climate-warming scenario. Using these model outputs for T_e I quantified the available area and landscape configuration of tolerable thermal habitat for *A. bicaorum* under different scenarios.

5.3 Material and Methods

5.3.1 Data

Land cover change was calculated using the WV2 8-band pansharpened imagery for years 2018 and 2020. For the operative temperature (T_e) mapping, the ground-based data used in this chapter included operative temperature measurements for around solar noon for each 3D replica over three days, the leaf area index (LAI measure) above each 3D replica, the locations of each replica, and the air temperature around solar noon for each plot over the three

days. Imagery data for the T_e mapping was the WV2 texture metric raster layers and the WV2 greenness layer, for both 2018 and 2020. Table 5.1 below refers to the field data used in this study and the section within previous chapter(s) that the full description of that data can be found. Subsequent method sections within this chapter outline Chapter 5-specific analyses.

Table 5.1: Outline of data used in this Chapter (Chapter 5)

Data	Description	Chapter & Section
Operative Temperature (T_e) data at Solar Noon	Mean operative temperature of two measurements either side of solar noon (four measurements of Te total), for each 3D replica	Chapter 4: 4.3.2
Air Temperature	Mean air temperature for two measures, one each side of solar noon for each plot	Chapter 4:4.3.2
Locations of 3D replicas	DGPS spatial point locations of each 3D replica within each plot	Chapter 2: 2.5.1
WV2 imagery	Eight layer orthorectified and radiometrically calibrated WV2 images for the years 2018 and 2020	Chapter 2: 2.11
WV2 Greenness Layer	WV2 Greenness raster layers for 2018 and 2020, resulting from processing of RGB layers	Chapter 2: 2.12
WV2 Texture Layers	UAV derived raster layers for seven texture metrics (Homogeneity, Contrast, Dissimilarity, Entropy, Mean, Second-Moment and Variance) for 2018 and 2020.	Chapter 2: 2.12

5.3.2 Land Cover Change

To quantify land cover change on the island, particularly forest loss, I carried out a land cover classification on each WV2 image and then calculated change as the difference between the resultant land cover maps. A random forest (RF) classifier was used as for the land cover classification as RF algorithms are particularly useful in working with linear and non-linear relationships within the same model as well as providing estimates of variable importance (Breiman, 2001). They are also are insensitive to multicollinearity of variables (Tang et al.,

2020), and have been demonstrated to perform well with land cover classification (Adugna et al., 2022). The RF land cover classification was carried out using the ModelMap package (Freeman *et al*., 2009) in R version 4.1.2. Land cover training polygons were created in ArcMap 10.4 based on direct observation of land cover and GPS data gathered in 2017, 2018 and 2019 on the island, as well as personal observations and Google Earth imagery. Note that ground-based land cover training data was not present for 2020. Therefore, to account for the fact that some areas of the GPS training data may have altered between years, and to avoid training the model with inaccurate training data, the training polygons were checked against the WV2 imagery and only training data for land cover areas consistent between the years were used for training. Land cover training points were also biased towards the eastern portion of the island due to logistical difficulties in accessing the western regions of the island. Eight land cover classes were considered: Agriculture, Forest, Mangrove, Dead Mangrove, Neotropical Savannah, Urban, Coast and Water (for details of each land cover see Chapter 2: Section 2.3). As a step to obtain a minimum of 100 training pixels per class, a random stratified subsample of 900 training pixels was used for model training. Classification accuracy assessment took the form of confusion matrices generated from both the random forest out-of-bag (OOB) estimate and an independent test set of 300 pixels. Overall accuracy, user's accuracy and producer's accuracy were then calculated as a measure of classification accuracy. As forest loss was the focus here and forest cannot establish itself in the span of two years, I constrained the 2020 forest class output first by the forest in 2018. This also accounted for the fact that the 2018 WV2 image had a section of island masked by cloud in 2018, (and therefore areas of what was potentially forest masked) that was not masked in and would count as forest in 2020. Meaning that potential forest loss would not be underestimated due to cloud cover influences.

5.3.3 Mapping Operative Temperature under land cover change

Operative temperature (T_e) was mapped across the whole of the island for 2018 using random forest regression models, following the same steps as in Chapter 4 (Sections 4.3.2 – 4.3.5) and applying them to the WV2 image layers. Pixel values for the WV2 texture and greenness raster layers were extracted and incorporated into RF regression models along with the T_e at solar noon for each of the 3D lizard replicas and air temperature within the plot at solar noon. Unfortunately, suitable WV2 imagery for 2019 (when the ground T_e data was collected) were not available, due to either cloud cover or incomplete images. Modelling 2019 T_e data using 2018 imagery assumes that substantial canopy changes have not occurred. I thus manually examined the 2018 imagery at all 3D replica locations to determine if there were any observable canopy changes relative to on the ground observations made in 2019. While unable to detect slight canopy changes, this approach identified recent deforestation in the region surrounding plot 14 that occurred after the WV2 images from 2018 but prior to collection of 2019 T_e data. Thus, this plot was removed from the data used to train and validate the RF model (Te.WV2018 in Table 5.2). This model was then used to map T_e across the forested areas of Utila assuming an air temperature of 30.4 °C, the mean air temperature measured across all plots (WV2018 scenario in Table 5.3).

To determine how recent land cover change has affected thermally tolerable habitat on Utila, I mapped T_e in 2020 by projecting the Te.WV2018 into 2020 using the WV2 imagery from that year, assuming a constant air temperature of 30.4 °C (WV20.RF18 in Table 5.3). However, there was a lack of atmospheric correction between the satellite imagery for the two years (see Chapter 2, Section 2.11). Thus, changes in pixel data may be driven by atmospheric variation between image scenes, rather than actual canopy change. However, my RF model relied on percent greenness, and it will therefore, be less sensitive to atmospheric differences than if they used absolute values. Nonetheless, to account for potential confounding effects of

atmospheric differences, I trained a second RF model using the T_e data from 2019 and WV2 imagery from 2020 (model Te.WV2020 in Table 5.2). Before training the model, I checked that there had been no deforestation in any of the plots since T_e data were collected in 2019; no such changes were identified so no additional plots were removed from this analysis. I then used this model to create a second map of T_e across Utila in 2020, again assuming an air temperature of 30.4 °C (WV20 in Table 5.3). The Te.WV2018 assumes that all changes in T_e between 2018 and 2020 are due to canopy changes, with no component resulting from atmospheric differences. In contrast, the Te.WV2020 model assumes that any changes in the canopy of the plots is due to atmospheric differences, rather than actual change. They therefore represent two ends of a continuum with the real values falling somewhere in between.

Table 5.2: Details of WV2 T_e Random Forest Regression Models

Model Name	Response Variable	WV2 Image Pixel Values Extracted From	Description/ Predictors
Te.WV2018	Operative Temperature (T_e)	All greenness and texture measures derived and extracted from 2018 WV2 Image	Air Temperature of Plot and WV2 greenness and texture measures based on the 2018 WV2 image pixel values. Predictors = Plot Air Temperature, WV2Greenness and WV2 texture metrics Mtry = 3 Ntrees = 500
Te.WV2020	Operative Temperature (T_e)	All greenness and texture measures derived and extracted from 2020 WV2 Image	Air Temperature of Plot and WV2 greenness and texture measures based on the 2020 WV2 image pixel values. Predictors = Plot Air Temperature, WV2Greenness and WV2 texture metrics Mtry = 3 Ntrees = 500

5.3.4 Mapping T_e under a climate warming scenario

To consider the possible impact of climate change, in this case air temperature warming, on the available area and distribution of suitable thermal habitat for *A. bicaorum*, I created new maps of T_e across Utila that assumed an air temperature of 31.9 °C, i.e. warming of 1.5 °C compared to the original analysis. Using this elevated air temperature, I remapped T_e in 2018 using the Te.WV2018 model (WV18.WARM in Table 5.3), and in 2020 by projecting Te.WV2018 model (WV20.WARM.RF18 in Table 5.3) and the Te.WV2020 model (WV20.WARM in Table 5.3). A warming of 1.5°C was chosen to highlight the impact of subtle

changes in air temperature on the thermal environment. Logan et al. (2013), whose work was based on Utila, in similar locations/ land cover types covered in this work, categorised changes to *Anolis bicaorum* fitness and activity time via a 3°C warming, based on IPCC (2007), therefore I decided to halve that prediction to be more conservative with respect to the magnitude of future change. However, this is an arbitrary number and the model could be run under several air temperature scenarios.

Table 5.3: Name of each scenario, the year of the image used, the random forest (RF) model used for prediction of T_e, the air temperature scenario and a short description for each of the six scenarios

Scenario	Year	RF Model	Air Temp (°C)	Description
WV18	2018	Te.WV2018	30.4	T_e at solar noon for all land cover classes in 2018 based on an air temperature of 30.4°C. Random forest prediction model is based on training the data on WV2 2018 image pixel values. Air temperature of 30.4°C is based on mean air temperature of plots during 2019 survey season.
WV18.WARM	2018	Te.WV2018	31.9	T_e at solar noon for all land cover classes in 2018 based on an air temperature of 31.9°C – representing a warming in air temperature of 1.5°C to that seen in WV18 model. Random forest prediction model is based on training the data on WV2 2018 image pixel values.
WV20	2020	Te.WV2020	30.4	T_e at solar noon for all land cover classes in 2020 based on an air temperature of 30.4°C. Air temperature of 30.4°C is based on mean air temperature of plots during 2019 survey season. Random forest prediction model is based on training the data on WV2 2020 image pixel values.
WV20.WARM	2020	Te.WV2020	31.9	T_e at solar noon for all land cover classes in 2020 based on an air temperature of 31.9°C – representing a warming in air temperature of 1.5°C to that seen in WV18 model. Random forest prediction model is based on training the data on WV2 2020 image pixel values.
WV20.RF18	2020	Te.WV2018	30.4	T_e in 2020 based on an air temperature of 30.4°C. Air temperature of 30.4°C is based on mean air temperature of plots during 2019 survey season. Random forest prediction model is based on training the data on WV2 2018 image pixel values.
WV20.WARM.RF18	2020	Te.WV2018	31.9	T_e at solar noon for all land cover classes in 2020 based on an air temperature of 31.9°C – representing a warming in air temperature of 1.5°C to that seen in WV18 model. Random forest prediction model is based on training the data on WV2 2018 image pixel values.

5.3.5 Quantifying change in Thermally Tolerable habitat

Because air temperatures at solar noon were outside of the T_{pref} range for *A. bicaorum*, I considered a more liberal measure of thermally suitable habitat based on the critical thermal maximum (CT_{max}). Work by Logan *et al.* (2013), found that *A. bicaorum* had a CT_{max} of 33.2°C. The use of such measures to predict responses to climate change have been called into question (Clusella-Trullas et al., 2021). But currently, there are no reasonable alternative measures to replace these metrics to determine responses for many ectotherms (Clusella-Trullas et al., 2021). Work from Chapter 3 of this thesis indicated the importance of time budgets of *A. bicaorum,* specifically the percent of time each plot had 3D replicas within *A. bicaorum* T_{pref} range, and abundance. Due to the nature of the models used in this chapter and in Chapter 4, I cannot estimate time budget as the models only consider the T_e at solar noon. In the absence of being to calculate thermal suitability metrics such as time in T_{pref} using these models I calculated the area of forest that sits below and above CT_{max} for *A. bicaorum* at solar noon as a measure of thermally suitable forest habitat.

As *A. bicaorum* is a forest dwelling species (Brown *et al.,* 2018; Chapter 3 Results), I first extracted the forested areas of Utila for both 2018 and 2020 from the land cover mapping (Chapter 5: section 5.3.2). I then clipped the T_e image for each of the predictions (Table 5.3) by the extent of the forest for the corresponding year (2018/2020). The resulting clipped T_e image was then reclassified into two categories (Table 5.4), based on CT_{max} for *A. bicaorum*. The thermally tolerable category included all areas with temperatures below 33.2°C within the clipped image, and the thermally intolerable category included any temperature 33.2°C and above. The thermally intolerable category depicts areas that would not be thermally suitable for *A. bicaorum,* as their T_e would rise above their CT_{max} if they remained in that area. In order to determine the available thermal habitat for *A. bicaorum*, the available area of forest that had

a T_e below their CT_{max} range (thermally tolerable category) was calculated for each of the scenarios outlined in Table 5.3.

Table 5.4: Temperature Categories relating to *A. bicaorum* thermal habitat quality

Category	Temperature (°C)
Thermally Tolerable	< 33.2
Thermally Intolerable	≥ 33.2

To determine the effect of land cover conversion and climate change on the spatial distribution of thermally favourable forest habitat for *A. bicaorum*, I quantified standard landscape metrics focusing on the spatial distribution of the thermally tolerable category (< 33.2°C). Forested areas within this category were extracted for each of the image scenarios outlined in Table 5.3 and loaded into the landscapemetrics (Hesselbarth *et al*., 2019) R package, whereby the number of patches, total area (m^2) and mean patch size (m^2) were calculated. Due to insufficient computing capacity the mean nearest neighbour Euclidean distance (m^2), and standard deviation of nearest neighbour Euclidean distance (m^2) could not be calculated.

5.4 Results

5.4.1 Land Cover Change

Random Forest land cover classifications had varying levels of overall accuracy, based on the OOB validation and independent test set (Table 5.5).

Table 5.5: Overall Accuracy for 2018 and 2020 land cover classifications as calculated from Out of Bag (OOB) and independent test data accuracy assessment

Year	OOB Overall Accuracy (%)	Test Data Overall Accuracy (%)
2018	83.03	76.36
2020	84.12	83.59

Forest class classification accuracy from 2018 and 2020 WV2 images varied depending on the year and validation type (OOB and Independent test set). The Users and Producers accuracies for these are shown in in Table 5.6. With regard to the lower accuracies for the forest class, the confusion matrices identified that the forest was often misclassified as mangrove and agricultural areas. Confusion matrices for the land cover maps derived for both 2018 and 2020, using the OOB validations and test validation sets can be seen in Appendix 8.

Table 5.6: Users and Producers Accuracy of the Random Forest classifications for the years 2018 and 2020 using the OOB Validation and Independent Test Dataset for the Forest Land Cover Class

Year	OOB Users Accuracy (%)	OOB Producers Accuracy (%)	Test Data Users Accuracy (%)	Test Data Producers Accuracy (%)
2018	79.83	75.40	64.10	62.50
2020	84.50	80.15	75.92	83.67

Due to forest being misclassified as mangrove and agriculture, and considering my aim of quantifying forest loss on the island (which is happening when looking at direct observation of the WV2 imagery between the years), I constrained the classified forest pixels in 2020 by what was classified as forest in 2018. This is to account for pixels classified as mangrove in 2018 being classified as forest in 2020 and underestimating forest loss. I also grouped any pixels classified as mangrove in 2020 that were within the original area of forest classified in 2018, to be considered as forest in 2020. Forest would not change to mangrove or vice versa in two years, therefore this change is likely due to differences in the classification and splitting between these classes, rather than physical changes on the ground. Note that these measures described above are used to account for land cover classification inaccuracies, and the selection of this area of forest is only used to constrain the T_e map for the whole of the island to ecological relevant land cover types for *A. bicaorum*, and comparing T_e within this defined area over the different scenarios.

Results of the RF land cover classification identified 10.86 km^2 of forest in 2018 and 9.33 km^2 in 2020, a loss of forest area of 1.53 km^2, a 14.08% loss in forest cover. Land cover maps for both 2018 and 2020 can be seen in Figure 5.1.
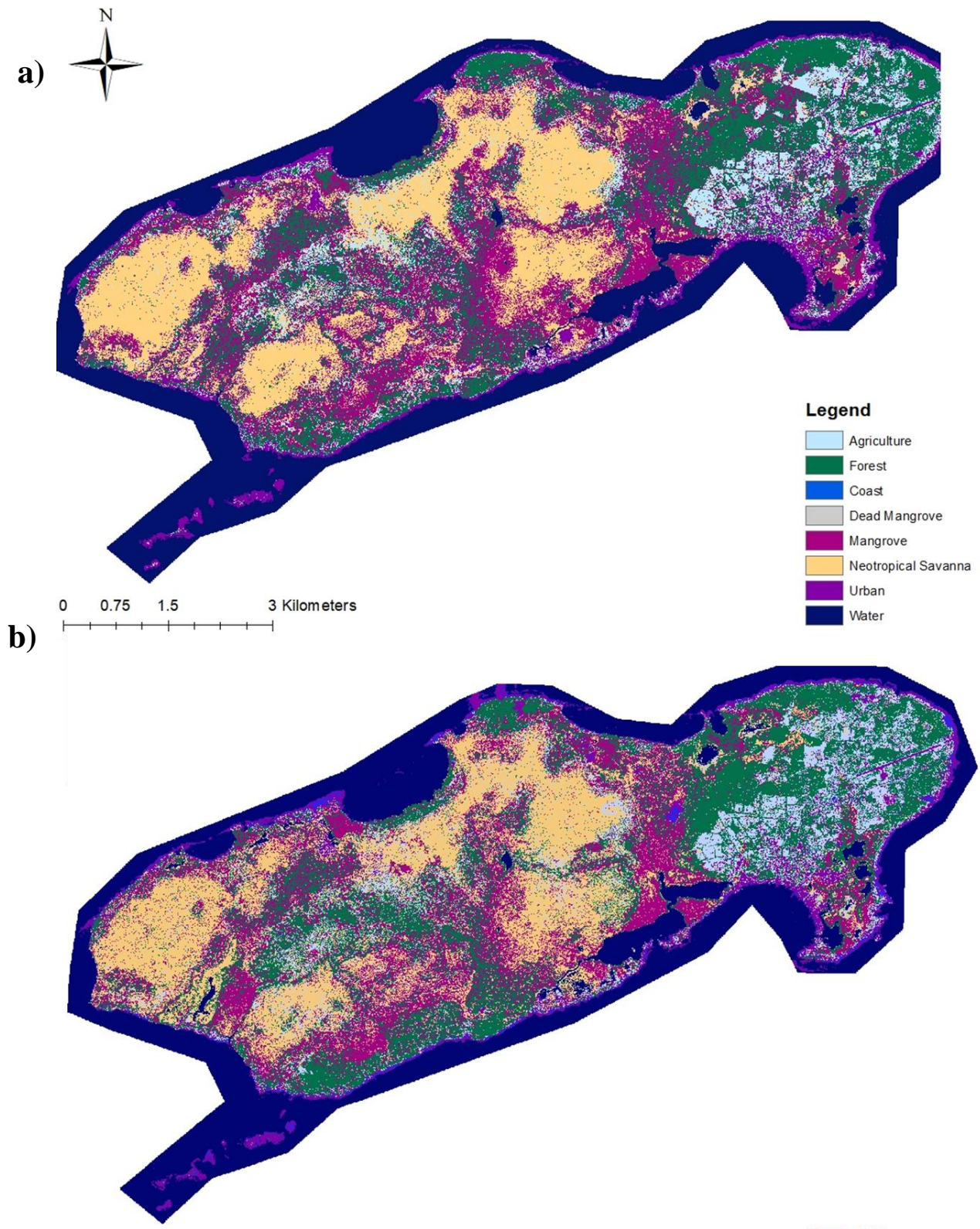
Figure 5.1: Land Cover on the island of Utila, Honduras derived from random forest classification of WorldView-2 (50cm spatial resolution) multispectral imagery, in the years a) 2018 and b) 2020

5.4.2 Mapping T$_e$

Results of the RF regression models to predict T$_e$ at solar noon indicated that WV2 imagery metrics (greenness and texture) coupled with air temperature reasonably predicted T$_e$ at solar noon (Figure 5.2). Both the RF models (Te.WV2018 and Te.WV2020) performed well when validating with an independent test dataset (Figure 5.2).
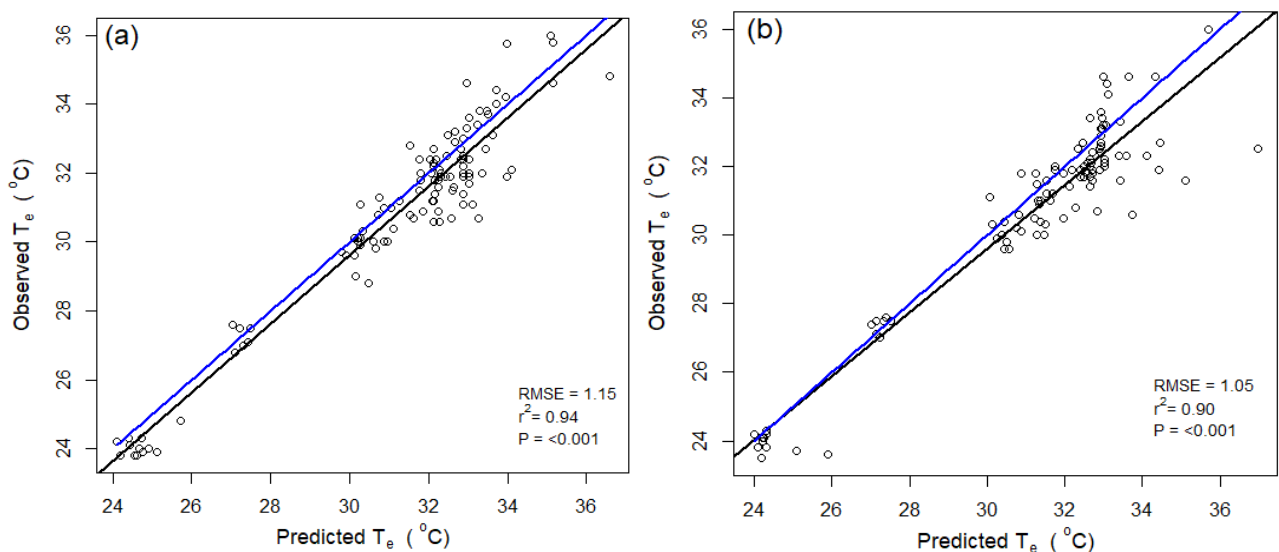
Figure 5.2: Observed vs predicted T$_e$ for test data for random forest models a) Te.WV2018 and b) Te.WV2020. Blue line indicates one to one line, black line indicates simple linear model between values

The variable importance plots differed between the two RF models (2018 and 2020; Figure 5.3). In the RF model based on 2018 pixel data (Te.WV2018 - Figure 5.3a), the percent green value was of higher importance that the texture variables. However, for the Te.WV2020 (Figure 5.3b) some of the texture variables had greater importance than percent green values. This could reflect real differences in the canopy components most influencing T$_e$, but also could be due to the OOB validation shuffling of variables. Air temperature is the most important variable in both models, which concurs with the results of Chapter 4.
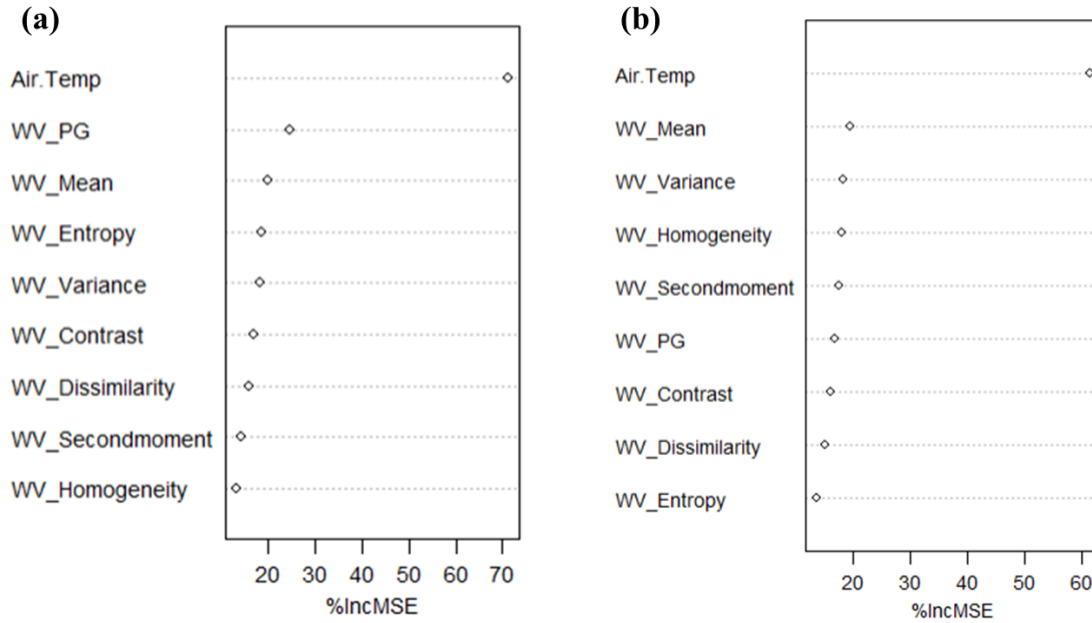
Figure 5.3: Variable importance plots for the Te RF models a) Te.WV2018 and b) Te.WV2020. WV_Contrast = Contrast texture layer, WV_Entropy = Entropy texture layer, WV_Dissimilarity = Dissimilarity texture layer, WV_Secondmoment = Second Moment texture layer, WV_Homogeneity = Homogeneity texture layer, WV_PG = Greenness layer, WV_Variance = Variance texture layer, WV_Mean = Mean texture layer, %IncMSE = percent increase of mean squared error

5.4.3 Mapping Change in Thermally Tolerable Habitat over Different Scenarios

Considering first the comparison between 2018 and 2020 using the RF model trained in 2018 at an air temperature of 30.4 °C (WV20.RF18 vs WV18), I found that the area of thermally tolerable habitat hardly declined, changing from 9.22 km^2 to 9.20 km. However, considering the model trained in 2020 (to account for atmospheric differences, WV20), the amount of thermally tolerable habitat declined to 8.87 km^2 (a decline of 3.8%). These losses in thermally tolerable areas likely reflect physical loss of forest area between 2018 and 2020. However, much of the forest that was already in the Thermally Intolerable category in 2018 (Figure 5.4, Table 5.7).

Based on 2018 conditions, a warming of air temperature by 1.5 °C (WV18.WARM) would result in a decline of thermally tolerable habitat from 9.22 km^2 (WV18) to 8.18 km^2, a decline of 11.3% (Table 5.7; Figure 5.4). In 2020, using the model trained in 2018, a warming of 1.5 °C (WV20.WARM.RF18) would reduce thermally tolerable habitat from 9.20 km^2 (WV20.RF18) to 7.90 km^2, a reduction of 14% (Table 5.7; Figure 5.4). Using the WV20.WARM model resulted in a much greater predicted loss of thermally tolerable habitat under warming, from 8.87 km^2 (WV20) to 5.42 km^2 (38.9%; Table 5.7, Figure 5.4).

Table 5.7: Area of forest within each thermal category for different scenarios on Utila. Scenarios as outlined in Table 5.3

Scenario	Year	RF Model Used	Air Temperature (°C)	Thermally Tolerable Area (km^2)	Thermally Intolerable Area (km^2)
WV18	2018	Te.WV2018	30.4	9.22	1.64
WV18.WARM	2018	Te.WV2018	31.9	8.18	2.68
WV20	2020	Te.WV2020	30.4	8.87	0.47
WV20.WARM	2020	Te.WV2020	31.9	5.42	3.91
WV20. RF18	2020	Te.WV2018	30.4	9.20	0.13
WV20.WARM.RF18	2020	Te.WV2018	31.9	7.90	1.40
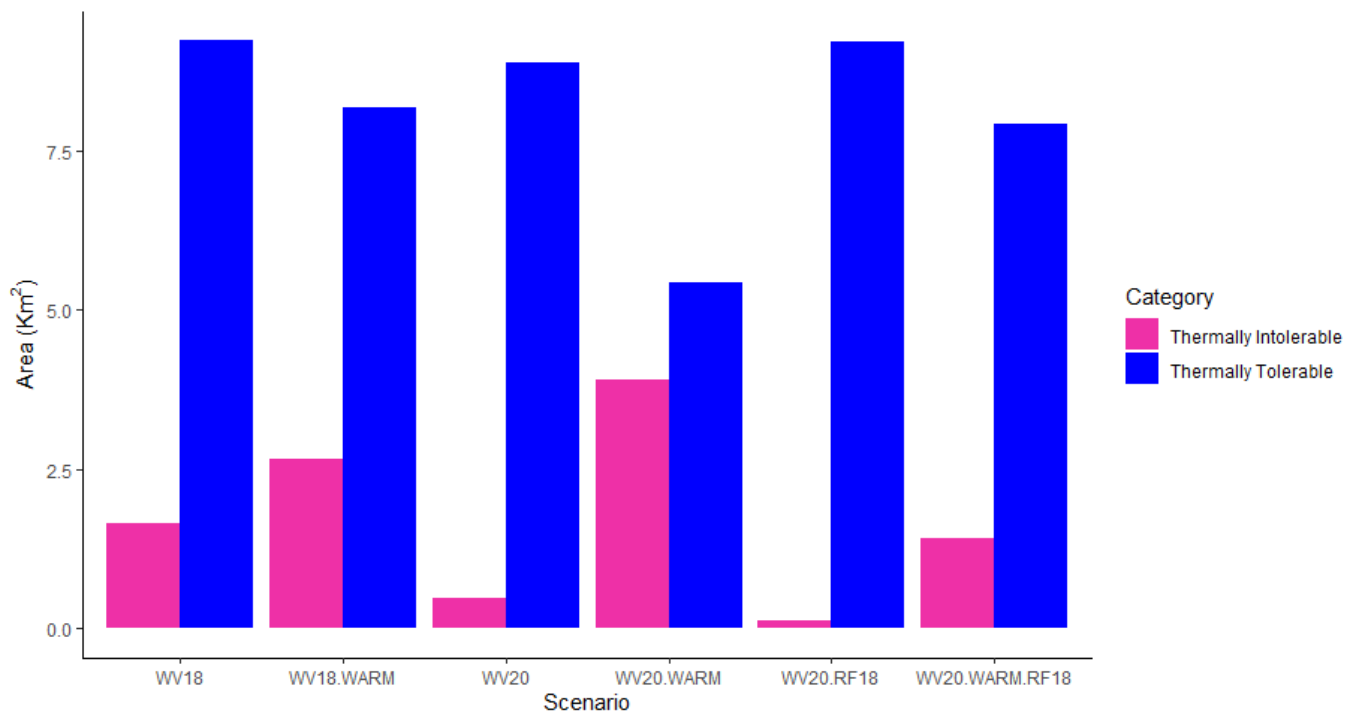
Figure 5.4: Area of Forest (km^2) within each thermal category on Utila, under different model scenarios, descriptions as seen in Table 5.3

Figures 5.5 to 5.7 depict the map of the spatial configuration of the thermal categories (Thermally Tolerable and Intolerable) across the entire island of Utila under all six model scenarios.
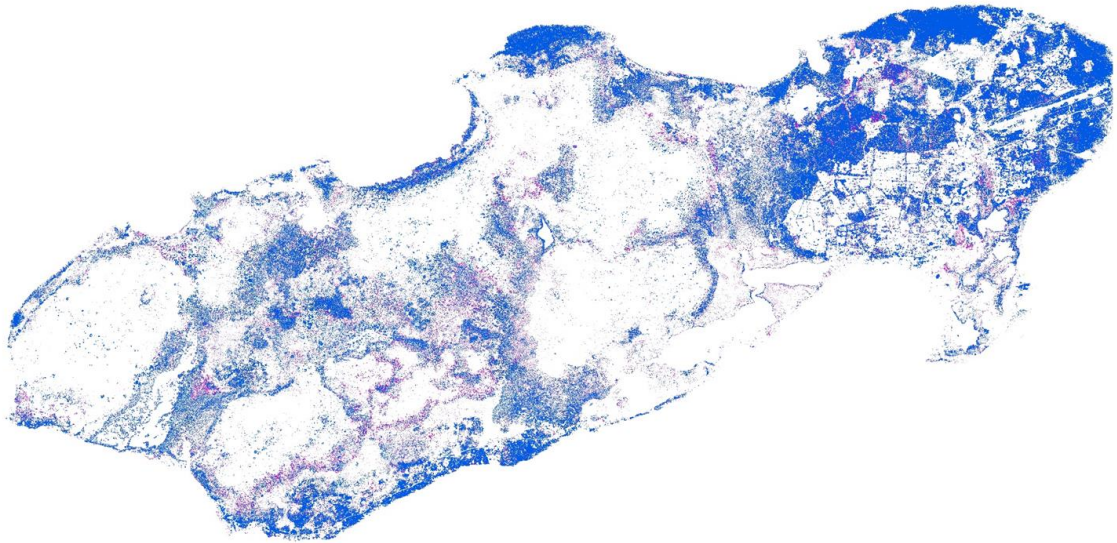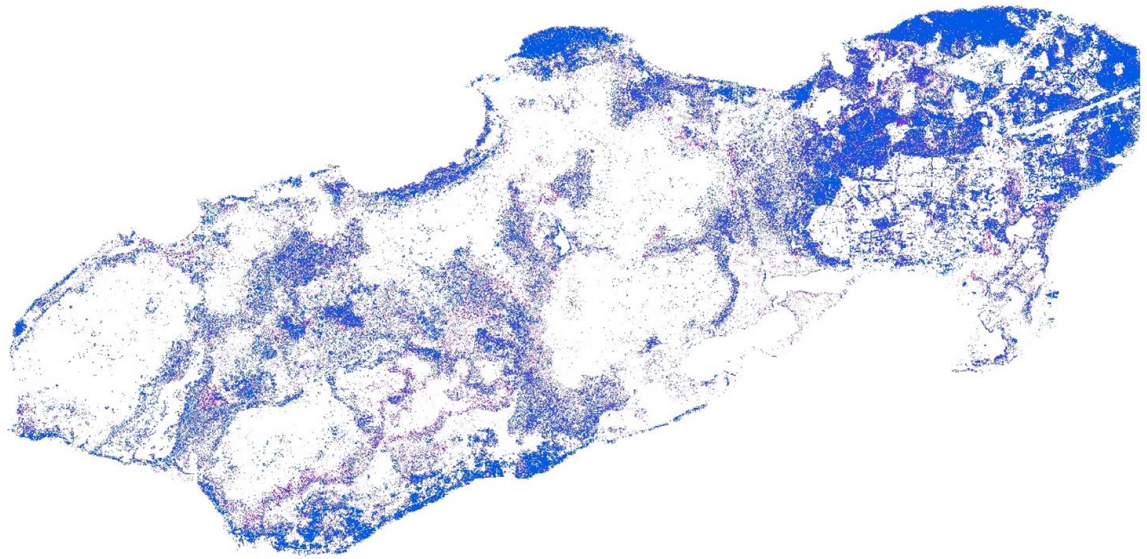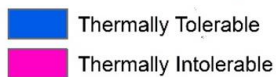
Figure 5.5: Map of operative temperature (T_e) within forest on Utila in 2018 (from predictions of the Te.WV2018 RF model), that are within the Thermally Tolerable ($<33.2°C$) and Thermally Intolerable ($\geq33.2°C$) categories, a) Scenario WV.18 and b) Scenario WV18.WARM.
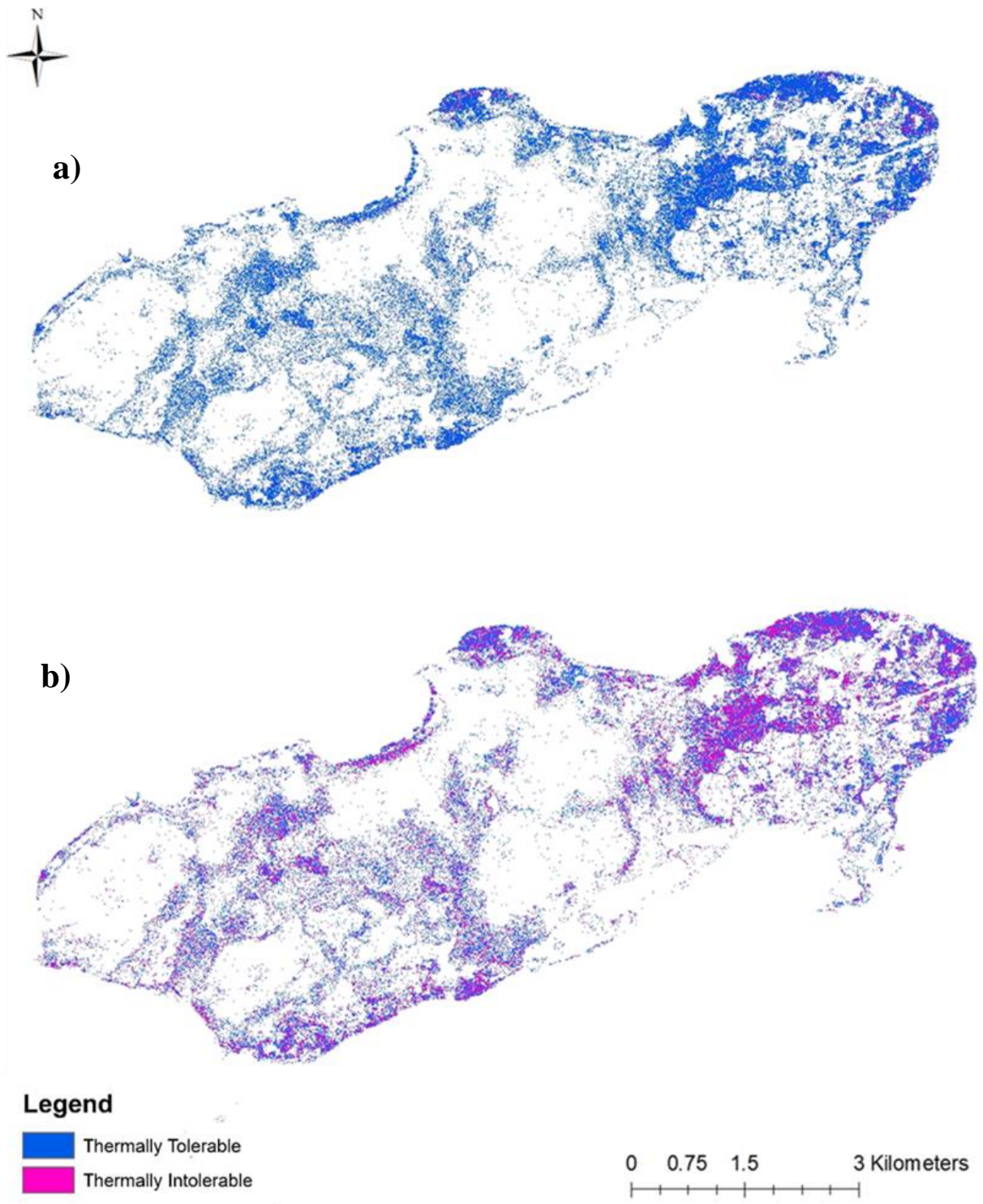
Figure 5.6: Map of operative temperature (T_e) within forest on Utila in 2020 (from predictions of the Te.WV2020 RF model) that are within the Thermally Tolerable (<33.2°C) and Thermally Intolerable (≥33.2°C) categories, a) Scenario WV.20 and b) ScenarioWV20.WARM.
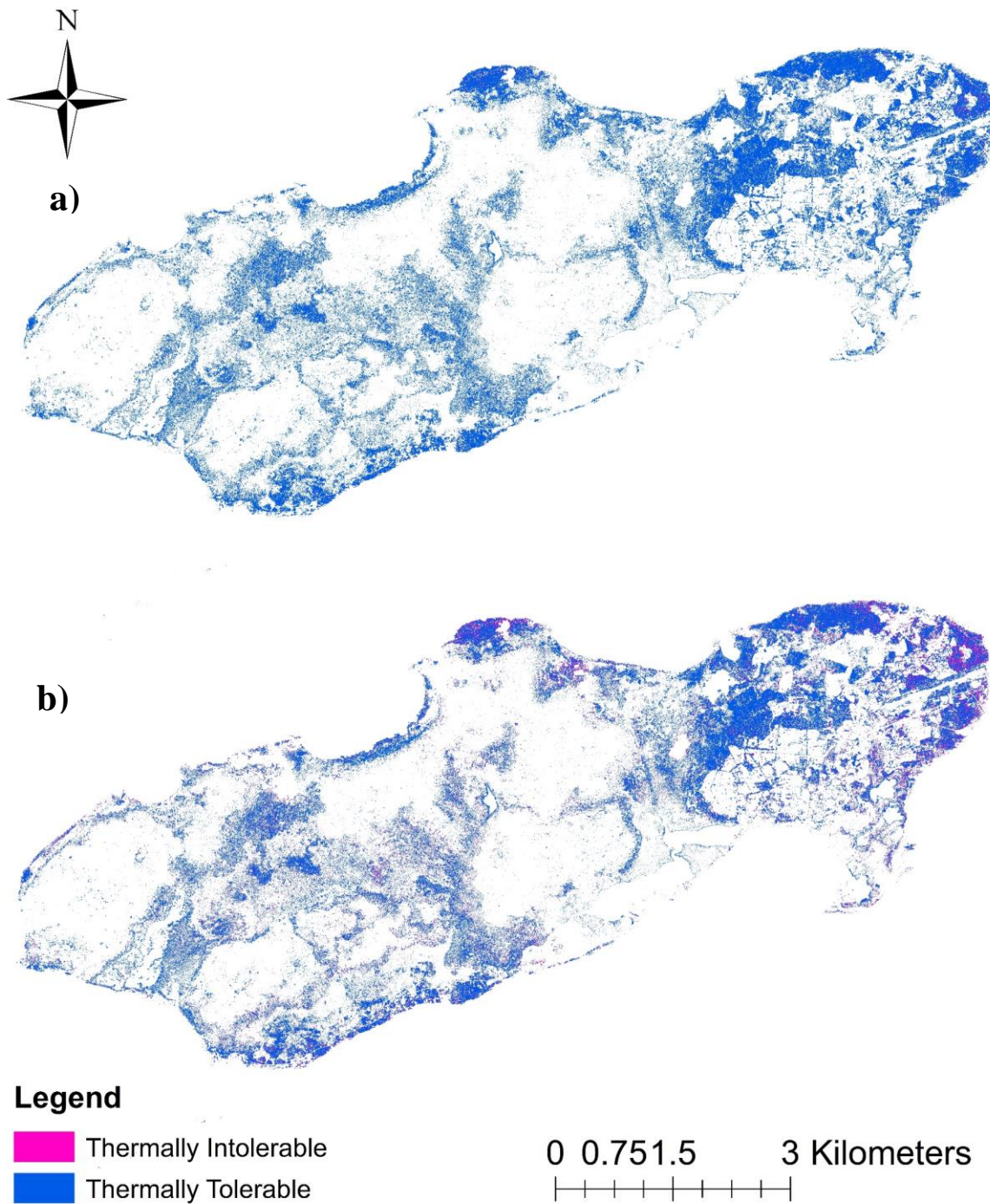
Figure 5.7: Map of operative temperature (T_e) within forest on Utila in 2020 (from predictions of the Te.WV2018 RF model) that are within the Thermally Tolerable (<33.2°C) and Thermally Intolerable (≥33.2°C) categories, a) Scenario WV20.RF18 and b) scenario WV20.WARM.RF18

141

Land cover change from 2018 to 2020 (air temperature = 30.4 °C) fragmented thermally tolerable habitat, resulting in more patches of smaller size, regardless of which model was used for 2020 (Table 5.8). As expected, based on total area calculations, projecting the 2018 model (WV18) into 2020 (WV20.RF18) resulted in small changes to patch number and area (approximately 1%), while comparing the WV20 model to WV18 identified greater changes of +3.2% and -6.8% for patch number and mean area, respectively (Table 5.8). Warming scenarios of 1.5 °C had greater effects on patch number and mean patch area. Warming under the WV20.RF18 model (WV20.WARM.RF18 – WV20.RF18) found large potential changes in patch number and mean patch area of +26.4% and -32.0%, respectively. Comparing WV20.WARM and WV20 revealed a smaller change in the decrease in patches, where the number of patches decreased by 2.6%, however patch area decreased by 57%.

Table 5.8: Landscape metrics derived from each of the image scenarios for Thermally Tolerable habitat

Scenario	Year	Air Temperature (°C)	Number of Patches	Mean Patch Size (m²)
WV18	2018	30.4	640535	14.38
WV18.WARM	2018	31.9	880442	9.30
WV20	2020	30.4	644440	21.04
WV20.WARM	2020	31.9	661499	13.40
WV20. RF18	2020	30.4	647266	14.23
WV20. WARM.RF18	2020	31.9	818268	9.68

5.5 Discussion

The results of this work demonstrate that WV2 satellite data at 50cm spatial resolution can be effectively used within the same workflow that was developed with UAV data in Chapter 4. This now allows T_e to be mapped at broad spatial extents with high temporal repeatability (e.g. up to every two days). These are far greater than could be feasibly achieved with a UAV, yet still maintain a relatively high spatial resolution. Theoretically, with appropriate training data, these methods could be used not just to map T_e across entire landscapes (as here), but also across whole continents or even globally. Secondly, the work has outlined the value of using such methods to quantify thermal habitat change and loss of thermally tolerable habitat for species on tropical islands under land cover and climate change scenarios, but has also highlighted the significant challenges that still remain in using satellite time series to achieve this goal.

Although the RF prediction models performed well in terms of predicting the test data, applying the workflow and RF models correctly across different images comes with limitations. For example, there is a need to gather ground data at the same time as the satellite image to train the model sufficiently. Due to considerations such as cloud cover, timing of the satellite passing over and image completeness, it is impossible to predict whether imagery during T_e replica deployment will be available. Such problems are common across many applications of satellite imagery (Dubovik et al., 2021; Xie et al., 2008). Another key consideration is that is crucial to collect sufficient ground spectral calibration data to allow for the images to be effectively atmospherically corrected, so that the correctly trained models can be predicted across images without the influence of potential differences in pixel values based solely on atmospheric variation between image scenes. This need for ground spectral data is highlighted by the fact that there are many atmospheric correction models, however very little comparative studies have been done to evaluate their performance on WV2 images (Marcello et al., 2016).

Differences between the outcomes from the two RF prediction models (Te.WV2018 and Tw.WV2020) had substantial consequences on the calculated area of thermally tolerable habitat between scenarios. Therefore, future work must consider these implications and look to develop best practice guidelines for those using this workflow.

Another limitation that must be considered when evaluating how deforestation has influenced T_e across Utila is the potential for errors in land cover classification. In my land cover classification, the initial land cover accuracy for the forest class was not as high as could be achieved using remote sensing methods which can be well over 90% overall accuracy (Xie et al., 2019). This is due to misclassification between mangrove, forest and agriculture, which are common misclassifications (Richards and Friess, 2016). Another likely limitation is the size and spatial distribution of on the ground training data. The majority of the training data acquired was for the eastern portion of the island due to logistical considerations, and ideally for random forest classification we would have more spatially independent training data and a higher volume of training points (Millard and Richardson, 2015). To account for pixel speckling influences on the classification, object-based image classification may also be a way forward for categorising forest area on the island. These limitations to the work, both in terms of training the T_e model and the relatively low land cover classification accuracy for forests, highlight that satellite remote sensing imagery, although a valuable resource, carry with them considerable challenges in implementing them to answer ecological questions. As remote sensing data and methods have become increasingly popular with ecologists, over the past several decades, and more recently with thermal ecologists (Kašpar et al., 2021; Milling et al., 2018; Still et al., 2019; Webster et al., 2018). And have been highlighted as key inputs for many avenues of biodiversity research (Cavender-Bares et al., 2022), highlighting such caveats when it comes to data application and workflows is important to limit incorrect use and over expectation of such data for their work.

Although my findings come with caveats, the results indicate the usefulness of considering thermal habitat change due to anthropogenic land-use and climate change on a scale relevant to individual organisms across the entire range of a species. Species such as *Anolis bicaorum* are limited in their dispersal potential by their isolation on a single island an are therefore unable to undergo large scale geographic range shifting as a mechanism to respond to climate change, as many (but not all) mainland species can (Algar et al., 2009; Chen et al., 2011; Kharouba et al., 2009; Parmesan et al., 1999). In addition, coarse scale climate data are not as useful for such dispersal limited species as they do not capture trends at the microhabitat scale (Lembrechts et al., 2019). Here, I have shown that VHR satellite imagery (WorldView-2), represents a viable alternative to broad-scale macroclimate data and coarser remote sensing datasets than have bene used previously (e.g. Algar et al. 2018) has been used to quantify the impacts and potential future risks of land cover and climate warming on species thermal environments .

Results of the random forest model for both the years 2018 and 2020 indicated similar results to that seen in Chapter 4 in that when coupled with air temperature, measures of greenness and texture derived from the WV2 imagery were a reasonable way to predict sub-canopy operative temperatures of anoles at a scale relevant to them. This work corroborates suggestions made by (Zellweger et al., 2019) in that remote sensing platforms can be used as inputs for species relevant measures of microclimate across spatial coverages. My work, however, goes beyond microclimate to predict the temperatures actually experienced by organisms, i.e. the operative temperature (Te; Bakken et al. 1985). My machine learning approach was also explained far higher amounts of variance in operative temperature than previous applications that considered coarser remote sensing data and biophysical models (Algar et al., 2018), and at resolutions that make quantifying thermal habitat variability for highly range-restricted species like *A. bicaorum* feasible.

On Utila, between 2018 and 2020, I identified a loss of forest of around 14%. Such losses are important, considering that *A. bicaorum* is a primarily a forest dwelling species (Brown et al., 2017) and is endemic to the island of Utila. Although not all forested areas on Utila are of equal quality for *A. bicaorum* (Chapter 3), any forest loss is a conservation concern given its restricted distribution and is also likely to negatively effect other species that use these habitats, especially if their niches are thermally aligned with *A. bicaorum's*, as is the case for forest arthropods (Chapter 3).

My analysis of changes in the amount of thermally tolerable habitat from 2018 to 2020 demonstrated that although forest loss had occurred on the island, there was limited change in thermally tolerable habitat. Thus, the forest loss was primarily from areas where the forest sat in the Thermally Intolerable temperature range. Practices such as thinning of the forest are commonly seen in Utila, to raise the aesthetic appearance of the area and consequently sell forest plots for development, this results in an alteration in canopy structure. These results of primarily loss of forest from Thermally Intolerable category may indicate a phased approach to forest loss on the island, where alteration in canopy structure from this thinning for aesthetic purposes would result in a hotter environment, before the plot is cleared altogether for development.

These results for the land cover change scenario highlight several key considerations for conservation, the first being the need to monitor the quality of forest for the species and whether all forest is thermally suitable (which I have also highlighted in the results of Chapter 3). The second is the need to monitor alterations to the environment at small scales, such as forest degradation at a plot level (and how this influences niche factors such as the thermal environment at small scales). Thirdly the need to monitor change within a habitat at relevant spatial scales to pick out these fine scale areas of degradation. The work of this chapter and

Chapter 4 has also proposed a workflow and model in which to do this at relevant spatial scales across large geographic spatial extents via remote sensing methods.

I found that climate warming of 1.5 °C would have far greater effects on the amount of thermally tolerable habitat than the observed land cover change. This is in apparent contrast to recent work which has suggested thermal changes due to land cover alteration will greatly outstrip those from climate change (De Frenne et al., 2021). However, my analysis considered land cover change over a limited time (2 years) and compounding changes over the time taken for temperatures to warm 1.5 °C would likely produce different results. I found that WV20.WWARM scenario has far less areas of favourable habitat than that seen in WV18.WARM scenario. However, a less dramatic restructuring is seen when comparing the WV18.WARM and WV20.WARM.RF18 scenarios. This increase in the effect of warming in 2020 compared to 2018 suggests that while land cover changes alone, may not have tipped thermal habitat over the tolerable/intolerable threshold, it did result in warmer habitats which render *A. bicaorum* more vulnerable to warming. This highlights the importance of considering how land cover change and climate warming are going to influence species on two fronts, and the importance of considering the spatial scale of these measures. This is also a key consideration when modelling the persistence of such species as tropical forest ectotherms who are adapted to a thermally homogenous environment and are already operating close to their thermal limits (Huey et al., 2009; Logan et al., 2013; Sunday et al., 2014). This potential shift in availability of thermal habitat is of import to *A. bicaorum* as, outlined in Chapter 3, the thermal environment is important for abundance both directly and indirectly, with prey biomass also being influenced by the thermal environment. This potential coupling of thermal niches between prey and *A. bicaorum*, and consequently loss of thermal habitat will lower fitness levels and abundances by influencing two important niche axes for of a species already at threat from direct habitat conversion on an island with a growing human population.

The spatial configuration of the thermal environment is also a key consideration for ectotherms, the efficiency of behavioural thermoregulation (Bakken et al., 2014; Sears et al., 2011; Sears and Angilletta, 2015) and individuals' ability to gather sufficient resources (Sears et al., 2011; Sears and Angilletta, 2015). My work has demonstrated that land cover change and potential climate change will alter the number of thermally tolerable patches of forest as well as mean patch size by further fragmenting available thermally suitable habitat and reducing the size of thermal refuges. The ability to quantify these metrics across whole landscapes is a methodological step forward. Fragmentation of thermal environments will not only influence thermoregulation opportunities, but may also result in edge effects and edge warming which could influence species persistence. For example fragmentation of forest and thermal habitats would lead to an increase in edge area; edges experience , hotter and more variable conditions than forest interiors (Ewers and Banks-Leite, 2013; Magano et al., 2015). These warmer edges and areas of thermally intolerable habitat interlacing between the thermally tolerable areas may also lead to other potential ecological implications, such as invasion pathways for warmer adapted species. On Utila, one such warm-adapted species is *Anolis sagrei* (Battles and Kolbe, 2019)*,* which is invasive on Utila (Brown & Diotallevi, 2019) and a potential invasive competitor for *A. bicaorum* should it be able to expand its range out of the warmer urban environments of Utila town. The approach I have introduced here advances our ability to quantify fine scale change in the spatial configuration of thermal habitats across large spatial extents.

5.6 Chapter Conclusions

This chapter has outlined and demonstrated how VHR satellite imagery can be used to monitor and predict changes in not just suitable land cover classes, but also in thermal suitability of these classes, which is important for our predictions for species persistence under climate and land use change, which can inform conservation and management practices.

However, my work has also highlighted the need for proper planning when it comes to remote sensing imagery training and considerations that must be made when applying such data. The work also has larger implications for how we can use such data in large-scale assessments of the thermal habitat across a landscape and as potential inputs for mechanistic models to model how species persists in an ever-changing world.

Chapter 6 : Thesis Summary and Conclusions

The motivation behind this thesis is that current measures of thermal environments and landscapes do not sufficiently capture what is experienced by individuals on the ground, and therefore our understanding of individual responses to the thermal environment, which scales to population level dynamics, is limited. Within this broader motivation, there were two aims. The first was to further our understanding of what drives variation in species' abundance, specifically the endemic *Anolis bicaorum* on the island of Utila, at fine spatial scales, particularly in the context of rapid land cover change and human habitat conversion,. The second was to evaluate different remote sensing systems for predicting sub canopy ectotherm operative temperature (T_e) in order to map the thermally available environments for *A. bicaorum*, at both ecologically and spatially relevant scales.

To meet the first aim (Chapter 3), I tested which niche axes influenced the abundance of the focal species (*A. bicaorum*). The work focused on how thermal habitat suitability, prey availability and structural habitat suitability, all of which are relevant to anoles (Battles et al., 2013a; M.A. Johnson et al., 2006; Logan et al., 2013b; Sears et al., 2016), interacted and influenced anole abundance. The research revealed that prey availability had the greatest direct effect on *A. bicaorum* abundance, but it also highlighted the interconnectedness of abiotic and biotic components that determine habitat quality and animal abundance. Rather than identify a single strong control on abundance, it was established that key abiotic factors (canopy cover and thermal environment) affect abundance through multiple pathways and have effects that are mediated by biotic interactions and the thermal niche of the focal species. Specifically, the results obtained indicated that the main thermal control on *A. bicaorum* abundance was the percentage of time each plot was within the thermal preference (T_{pref}) range. These findings further our understanding of the importance of activity time, not just for individuals, but also for populations. Individuals that can spend more time within their preferred temperature range

benefit from an increase in activity time (Gunderson & Leal, 2016), which allows increased utilisation of available resources (Battles and Kolbe, 2019; Gvoždík 2002; Huey et al., 2009; Logan et al., 2013; Sinervo et al., 2010). My work demonstrates that these effects scale to determine population abundance, and how it varies at fine spatial scales across a habitat gradient. It also informs current discussions as to how we should quantify the thermal quality of an environment, and therefore how best to model species responses to environmental change (Clusella-Trullas et al., 2021; Gunderson and Leal, 2016). Such understanding is especially important for forest dwelling ectotherms such as *A. bicaorum,* which have narrow fundamental thermal niches and are therefore are more sensitive to a change in their thermal environment (Huey et al., 2009; Logan et al., 2013b).

My results also highlight the pervasiveness of canopy cover for mediating ecological dynamics at higher trophic levels, primarily through influencing the thermal landscape (*sensu* Nowakowski et al. 2018) but also indirectly through mediating trophic interactions. These findings demonstrate the importance of maintaining canopy cover and structure to maximize thermal habitat quality for cool-adapted species (Battles & Kolbe, 2018) and their prey (Lister & Garcia, 2018). Therefore, losses of thermal habitat quality, particularly due to canopy loss, may thus have greater effects than appreciated when only direct effects are considered. This is important to consider as models to predict vulnerability of ectotherms to future warming tend to focus on direct effects on activity time, thermal safety margins, and thermoregulation (e.g. Sinervo et al., 2010, Sunday et al., 2014). Results presented in this thesis therefore suggest that such models may actually underestimate risks, and that warming impacts may actually be magnified due to thermally induced changes in food availability, highlighting the need for greater focus on direct and indirect effects of temperature change (Kearney et al. 2013,Duclos et al., 2019) on species abundances. It also highlights the need to incorporate canopy measures at an organism-relevant spatial scale to meaningfully characterise the heterogeneity within

broader scale mechanistic models. I therefore focused on mapping lizard operative temperature on Utila using remote sensing methods (the second aim of this thesis), implementing current understanding of the link between canopy structure and lizards' body temperatures (Algar et al., 2018b), to infer potential impacts of environmental change on *A. bicaorum* abundance.

The use of remote sensing afforded the mapping of operative temperatures of species below the canopy. This is important as measuring species distributions and responses to environmental change currently rely on coarse scale landscape and climatic data at around 1km^2; however, species experience their environment at a much finer spatial scales (Sears et al., 2011). The need to measure species responses to their environment, specifically with such phenomena as climate change has been highlighted by many (Kearney and Porter, 2017; Maclean and Klinges, 2021; Sears et al., 2011; Sears and Angilletta, 2015; Suggitt et al., 2018). Mechanistic microclimate models have been developed, e.g. NichemapR (Kearney and Porter, 2017) and Microclimc (Maclean and Klinges, 2021), to allow ecologists to consider microclimatic scales in their analyses. However, these mechanistic models downgrade the spatial resolution of coarse spatial data from weather stations, which often do not accurately represent the heterogeneity in the landscape and therefore conditions experienced by many organisms (Potter et al., 2013; Sears et al., 2011; Sears and Angilletta, 2015; Suggitt et al., 2018). Remote sensing methods and data have been highlighted as a way in which we can gather sufficient spatial scale data to input into such mechanistic models (Duffy et al., 2021; Zellweger et al., 2019). The final two research chapters of this thesis (Chapters 4 and 5) were therefore geared towards how we can utilise such data and apply it to mapping ecologically relevant operative temperature data for ectotherms, at spatial scales relevant to the organism.

Vegetation and canopy structure are often used in microclimate modelling (Duffy et al., 2021; Maclean and Klinges, 2021; Milling et al., 2018), have been linked to lizard body temperature (Algar et al., 2018), and were found to be an important regulator of the thermal

environment within Chapter 3 of this thesis. The use of UAVs to gather sufficient microclimate input data has been highlighted previously (Duffy et al., 2021; Milling et al., 2018; Zellweger et al., 2019), however, studies actually using UAVs to acquire such data are limited, and there has been no attempt to extend beyond microclimate to directly predict animal operative temperatures. Results indicated that UAV-derived texture and greenness measures accurately modelled operative temperature when coupled with air temperature, and that the UAV measures performed slightly better than measures of canopy taken from the ground (i.e., with a ceptometer). However, there is a significant additional benefit to using a UAV rather than ground-based ceptometer measurements – the higher spatial resolution and coverage that are obtained compared to ground-based measures, and therefore the ability to map the operative temperature, across spatial extents that are only limited by your UAV flight area. This work will not only allow us to continuously map operative temperatures across continuous flight areas at high spatial resolutions, but will also allow us to consider the spatial heterogeneity of the thermal environment across entire landscapes, and how this influences behavioural thermoregulation and individuals ability to gather sufficient resources (Bakken et al., 2014; Sears et al., 2011; Sears and Angilletta, 2015).

I did not find any significant relationships between the amount or configuration of thermally suitable habitat and *A. bicaorum* abundance, using operative temperatures from the UAV-model and CT_{max} (Logan et al., 2013) to determine thermal suitability. These results highlight that simply measuring operative temperature is not enough to quantify thermal habitat suitability and that we also need to know which niche limits are most important for the study species. There is currently debate on which niche metrics are most suitable for determining the thermal suitability for a species (Clusella-Trullas et al., 2021). In Chapter 3, I found that *A. bicaorum* abundance was most strongly related to the percent of time the operative temperature of a plot was within the T_{pref} range for the species. The lack of a relationship with

abundance and a CT_{max} based measure of suitability (Chapter 4) suggest that Tpref, and not critical limits are more appropriate for measuring thermal quality. However, other factors may also have influenced the lack of association between abundance and UAV-derived thermal suitability. In particular, my model was only for solar noon and thus activity time budgets and thermally favourable habitat time budgets (such as the time within T_{pref}) could not be extracted from the UAV model data. Future work will look at the potential for the model to predict operative temperature across the time of day, and therefore incorporate these time budgets for species. A proposed avenue for this is to exploit the structure from motion (SfM) photogrammetry capabilities of UAVs to incorporate canopy point clouds into the model, as proposed by Duffy et al., (2021). These UAV SfM methods could also be combined with data on from a mobile terrestrial laser scanner (e.g. Geoslam Zeb-Revo), which would provide high-resolution point cloud data for the whole of the plot to extract relevant measures such as canopy depth, canopy height (Kašpar et al., 2021), as well as understory measures.

The UAV-based model of operative temperature appears to be better suited to forests, and predicts less well in other land covers, especially urban areas. This is not particularly an issue when looking at thermal suitability metrics for *A. bicaorum*, which is found in forested land covers. But it does highlight the need to train the model further across different land covers, and in the case of urban areas, consider that the model at present is not overly suited due to a general lack of canopy (Algar et al., 2018). Future work will look to train and apply the model across different land covers and geographical regions, as well as for different ectotherm species, to test its validity.

The UAV-based approach can map thermal environments on a fine spatial scale, but is currently limited in its ability to cover large spatial extents, and requires repeated field visits to collect changes through time. An alternative approach is to use high-resolution satellite based imagery that can cover broader spatial extents and document changes through time.

Documenting such changes is important as anthropogenic land use and climate change are two drivers of thermal habitat alteration, where loss of forest canopy insulation, and increased air temperatures are thought to lead to a decrease in suitable thermal conditions for forest thermal specialists (Algar et al., 2018; De Frenne et al., 2021, 2019; Huey et al., 2009; Logan et al., 2013c; Sinervo et al., 2010). The island of Utila has undergone significant anthropogenic habitat conversion in recent years, leading to forest loss, and therefore a potential decrease in available thermal habitat for *A. bicaorum.* The final research chapter (Chapter 5) of this thesis applied the model proposed in Chapter 4 to high-resolution (50cm spatial resolution) multispectral WorldView-2 satellite imagery over two periods (2018 and 2020) and across different air temperature scenarios.

Results of the Worldview-2-based operative temperature model indicated similar performance as that seen in the UAV-based model; therefore, I propose that this workflow and model can be applied to high-resolution satellite imagery. This is important as now we can determine landscape-level influences on the thermal environment, measuring ecologically relevant (operative temperature) metrics at a spatial scale that is relevant to the species. These canopy heterogeneity outputs can also be used within mechanistic modelling as a source of higher resolution data as suggested by Zellweger et al. (2019). Remote sensing satellite platforms are becoming more sophisticated in both spatial and spectral resolutions (Cavender-Bares et al., 2022; Heijden et al., 2022), this development of new sensors can provide exciting new data, at higher spatial and spectral resolutions that can potentially to be incorporated into future models. However, the work of this thesis also highlighted the significant challenges that remain in using satellite time series data, and the need for best practice when using these data.

Land cover change on the island on Utila led to a loss of thermally tolerable habitat (Chapter 5). This was proposed to likely be due to forest thinning activities taking place on the island and a phased approach to habitat clearance. This indicates the potential for such methods

to monitor habitat degradation, and its influence on the thermal environment, rather than solely focusing on complete forest loss. This work also corroborates what was found in Chapter 3 of this thesis, in that not all forest habitats are thermally optimal environments for *A. bicaorum.* This then in turn, highlights the actual need to map such habitat characteristics at these fine spatial scales, relevant to species niche requirements.

Although land cover change had an impact on the thermal environment, results indicated that a 1.5^oC warming in air temperature might lead to a complete restructuring of the available thermal habitat, with a loss in the thermally tolerable habitat. It was also found that the impact of this warming is far greater when also considering land cover change between 2018 and 2020. This highlights the importance of considering how land cover change and climate warming are going to influence species on two fronts, and the importance of considering the spatial scale of these measures (Nowakowski et al., 2018; Tuff et al., 2016). My approach takes a major step toward in quantifying the spatial configuration of thermally suitable habitat under different land cover and climate change scenarios across entire landscapes at organism relevant scales. It is also highlights the potential of temporal monitoring of land cover and operative temperature change across large spatial scales at fine resolutions, using satellite imagery such as WorldView-2 satellite missions that have an average revisit time of less than two days.

The workflow developed in Chapters 4 and 5 allows for temporal monitoring of operative temperatures to be carried out by either continuous UAV flights or high temporal and spatial resolution satellite imagery, in conjunction with animal replicas and air temperature loggers. However, it is important to consider that while the models developed with this workflow worked well for the data within this thesis, tests were restricted to a single island. Utila is a relatively flat island with only one area of slightly higher elevation (approximately 75 m.a.s.l). Therefore, recommendations for future research would be to test the model across

156

different geographic areas. For example, the neighbouring island of Roatan has dramatically different topographical features; therefore the model could theoretically be tested there to determine its validity across different more topographically complex landscapes. Another avenue of research would be to test the workflows and models proposed in this thesis against well-established mechanistic models such as NichemapR and Microclimc, or even to combine the two approaches, gathering additional data from mechanistic microclimate modelling to add to the model proposed here. Some research has been conducted on differences in performance of mechanistic and empirical models, e.g. Kearney et al. (2014), where both modelling avenues were found to perform similarly, but with different limitations. Future research on this topic would greatly benefit how we use such models to map species responses to climate and land use change.

Advances and developments of remote sensing technologies are changing how we measure the natural world, and feed into several research avenues for biodiversity and conservation, as discussed in Cavender-Bares et al., (2022). In regards to the motivations behind this thesis, measuring the thermal environment at organism relevant scales, the development of thermal cameras, especially those fitted on UAVs, are exciting new avenues for research. These high-resolution thermal images could be integrated into the workflow developed in this thesis, which could potentially enhance the workflow proposed, especially over land covers that lack a canopy, areas where the current workflow and model did not perform as well. These high-resolution thermal imagery are not limited to those fitted to UAVs, there are now plans to launch high spatial resolution (3 to 4m) thermal satellites, allowing such data to be incorporated into the satellite workflow outlined in chapter 5. These thermal data products, as well as multi-system UAVs such as NASA's G-LiHT, that capture thermal, multispectral and LiDAR data simultaneously (Cook et al., 2013), allow multidimensional remote sensing data to be collected and integrated into ecology based workflows, such as

developed in this thesis. Future research on the uses of these new data, and how they may increase the performance of such workflows, would be beneficial, especially when considering applying these workflows across different landscapes.

Endemic species such as *A. bicaorum* are under significant threat from anthropogenic land use and climate change. As forest species, they likely have narrower fundamental thermal niches and therefore are more sensitive to a change in their thermal environment. They are endemic to a single island, the island of Utila, and are limited in their dispersal and range shifting capacity; they are therefore reliant on suitable habitat and thermal buffers to anthropogenic mediated habitat change. Results of this thesis have contributed to the ecological understanding of one of Utila's endemic anole species, which will inform its monitoring and conservation. Specifically, my work has highlighted the importance of thermal suitability and activity time on *A. bicaorum*'s abundance, as well as the importance of trophic interactions, which are themselves not independent of thermal environment. Such relevant information can be applied to habitat management and efforts to conserve this endemic and threatened species. My work also quantifies the combined risk to thermal habitat quality from land cover and climate change and has proposed a method to monitor this thermal quality using ecologically relevant data at scales relevant to the organisms that experience them. Such methods are becoming increasingly important for monitoring species under the ever present threat of climate change and land use change, and are crucial to conserving species in a human-dominated world.

In conclusion, this thesis has demonstrated the need to consider species niche requirements at organism relevant spatial scales, as well as considering the interactions between abiotic and biotic mechanisms for regulating animal abundance. For ectotherms such as *A. bicaorum,* it has highlighted the need to determine which of these thermal niche measurements are most important for regulating species abundances, which in turn will be key

for determining species and community responses to habitat alteration. High spatial resolution remote sensing platforms have been utilised to create a workflow for measuring sub-canopy operative temperature, which performs well in forests. This approach is a step forward in how we measure these thermal environments at organism relevant spatial scales, continuously over a landscape, and will feed into how we determine species responses to anthropogenic land use and climate change.

References

Adugna, T., Xu, W., Fan, J., 2022. Comparison of Random Forest and Support Vector Machine Classifiers for Regional Land Cover Mapping Using Coarse Resolution FY-3C Images. Remote Sens. 14, 574. https://doi.org/10.3390/rs14030574

Ahmed, O. S. et al. 2017. 'Hierarchical land cover and vegetation classification using multispectral data acquired from an unmanned aerial vehicle', International Journal of Remote Sensing. Taylor & Francis, 38(8–10), pp. 2037–2052. doi: 10.1080/01431161.2017.1294781.

Algar, A.C., Kharouba, H.M., Young, E.R. and Kerr, J.T. (2009), Predicting the future of species diversity: macroecological theory, climate change, and direct tests of alternative forecasting methods. Ecography, 32: 22-33. https://doi-org.nottingham.idm.oclc.org/10.1111/j.1600-0587.2009.05832.x

Algar, A. C. and Losos, J. B. 2011. 'Evolutionary assembly of island faunas reverses the classic island-mainland richness difference in Anolis lizards', Journal of Biogeography, 38(6), pp. 1125–1137. doi: 10.1111/j.1365-2699.2010.02466.x.

Algar, A.C., Morley, K., Boyd, D.S., 2018. Remote sensing restores predictability of ectotherm body temperature in the world's forests: XXXX. Glob. Ecol. Biogeogr. 27, 1412–1425. https://doi.org/10.1111/geb.12811

Andrewartha, H.G., Birch, L.C., 1986. The Ecological Web: More on the Distribution and Abundance of Animals. University of Chicago Press.

Baena S, Moat J, Whaley O, Boyd DS .2017. Identifying species from the air: UAVs and the very high resolution challenge for plant conservation. PLOS ONE 12(11): e0188714. https://doi.org/10.1371/journal.pone.0188714

Bakken, G. S., W. R. Santee, and D. J. Erskine. 1985. Operative and standard operative temperature: Tools for thermal energetics studies. Integrative and Comparative Biology 25:933–943.

Bakken, G.S., 1992. Measurement and Application of Operative and Standard Operative Temperatures in Ecology. Am. Zool. 32, 194–216. https://doi.org/10.1093/icb/32.2.194

Bakken, G.S. and Angilletta, M.J., Jr (2014), How to avoid errors when quantifying thermal environments. Funct Ecol, 28: 96-107. https://doi.org/10.1111/1365-2435.12149

Battles, A.C., Kolbe, J.J., 2019. Miami heat: Urban heat islands influence the thermal suitability of habitats for ectotherms. Glob. Change Biol. 25, 562–576. https://doi.org/10.1111/gcb.14509

Battles, A.C., Whittle, T.K., Stehle, C.M., Johnson, M.A., 2013. Effects Of Human Land Use On Prey Availability And Body Condition In The Green Anole Lizard, Anolis carolinensis.- Herpetol. Conserv. Biol. 8(1): 16-26.

Birdal, A. C., Avdan, U. and Türk, T. 2017. 'Estimating tree heights with images from an unmanned aerial vehicle'. Taylor & Francis, 5705. doi: 10.1080/19475705.2017.1300608.

Bonneaud, C., Sepil, I., Wilfert, L., Calsbeek, R., 2017. Plasmodium Infections in Natural Populations of Anolis sagrei Reflect Tolerance Rather Than Susceptibility. Integr. Comp. Biol. 57, 352–361. https://doi.org/10.1093/icb/icx044

Boyd, D.S., Foody, G.M., 2011. An overview of recent remote sensing and GIS based research in ecological informatics. Ecol. Inform. 6, 25–36. https://doi.org/10.1016/j.ecoinf.2010.07.007

Breiman, L., 2001, Random Forests. Machine Learning 45, 5–32. https://doi.org/10.1023/A:1010933404324

Brown, J.H., 1995. Macroecology. The University of Chicago Press, USA.

Brown, T.W. et al. 2017a. Habitat diversification and natural history observations in Norops utilensis (Squamata; Dactyloidae) on Isla de Utila, Honduras. - Mesoam Herpetol 4 (4): 974-979.

Brown, T, Maryon.D, Vanderburg.T, Lonsdale.G. 2017b. Distribution and natural history notes on Norops bicaorum (Squamata : Dactyloidae) endemic to Isla de Utila, Hondruas. Mesoamerican Herpetology 4(2). pp. 493-497.

Brown, T.W. and Diotallevi, F. 2019. Confirmation of the Mourning Gecko, Lepidodactylus lugubris (Duméril and Bibron 1836), on Isla de Utila, with Remarks on the Island's Invasive Reptiles. - IRCF Reptiles Amphib 26 (2): 151-154.

Buckley, L.B., Roughgarden, J., 2006. Climate, competition, and the coexistence of island lizards. Funct. Ecol. 20, 315–322. https://doi.org/10.1111/j.1365-2435.2006.01095.x

Campbell, G. S., and J. M. Norman. 1998. An introduction to environmental biophysics. 2nd edition. - Springer-Verlag, New York.

Cavender-Bares, J., Schneider, F.D., Santos, M.J., Armstrong, A., Carnaval, A., Dahlin, K.M., Fatoyinbo, L., Hurtt, G.C., Schimel, D., Townsend, P.A., Ustin, S.L., Wang, Z., Wilson, A.M., 2022. Integrating remote sensing with ecology and evolution to advance biodiversity conservation. Nat. Ecol. Evol. https://doi.org/10.1038/s41559-022-01702-5

Chase, J.M., Leibold, M.A., 2003. Ecological Niches: Linking Classical and Contemporary Approaches. University of Chicago Press.

Chrétien, L., Théau, J. and Ménard, P. 2015. 'Wildlife Multispecies Remote Sensing Using Visible And Thermal Infrared Imagery Acquired From An Unmanned Aerial Vehicle (UAV)', XL(figure 2), pp. 241–248. doi: 10.5194/isprsarchives-XL-1-W4-241-2015.

Christiansen, F. et al. 2016. 'Noninvasive unmanned aerial vehicle provides estimates of the energetic cost of reproduction in humpback whales', Ecosphere, 7(10), pp. 1–18. doi: 10.1002/ecs2.1468.

Clusella-Trullas, S., Garcia, R.A., Terblanche, J.S., Hoffmann, A.A., 2021. How useful are thermal vulnerability indices? Trends Ecol. Evol. 36, 1000–1010. https://doi.org/10.1016/j.tree.2021.07.001

Cook, B. D., L. W. Corp, R. F. Nelson, E. M. Middleton, D. C. Morton, J. T. McCorkel, J. G. Masek, K. J. Ranson, V. Ly, and P. M. Montesano. 2013. NASA Goddard's Lidar, Hyperspectral and Thermal (G-LiHT) airborne imager. Remote Sensing 5:4045-4066, doi:10.3390/rs5084045.

De Frenne, P., Lenoir, J., Luoto, M., Scheffers, B.R., Zellweger, F., Aalto, J., Ashcroft, M.B., Christiansen, D.M., Decocq, G., De Pauw, K., Govaert, S., Greiser, C., Gril, E., Hampe, A., Jucker, T., Klinges, D.H., Koelemeijer, I.A., Lembrechts, J.J., Marrec, R., Meeussen, C., Ogée, J., Tyystjärvi, V., Vangansbeke, P., Hylander, K., 2021. Forest microclimates and climate change: Importance, drivers and future research agenda. Glob. Change Biol. 27, 2279–2297. https://doi.org/10.1111/gcb.15569

De Frenne, P., Zellweger, F., Rodríguez-Sánchez, F., Scheffers, B.R., Hylander, K., Luoto, M., Vellend, M., Verheyen, K., Lenoir, J., 2019. Global buffering of temperatures under forest canopies. Nat. Ecol. Evol. 3, 744–749. https://doi.org/10.1038/s41559-019-0842-1

De Omena, P.M., Srivastava, D.S., Romero, G.Q., 2019. Consumptive effects and mismatch in predator–prey turnover rates cause inversion of biomass pyramids. Oecologia 190, 159–168. https://doi.org/10.1007/s00442-019-04394-0

Deutsch, C.A., Tewksbury, J.J., Huey, R.B., Sheldon, K.S., Ghalambor, C.K., Haak, D.C., Martin, P.R., 2008. Impacts of climate warming on terrestrial ectotherms across latitude. Proc. Natl. Acad. Sci. 105, 6668–6672. https://doi.org/10.1073/pnas.0709472105

Diaz, J.A., 1997. Ecological correlates of the thermal quality of an ectotherm's habitat: a comparison between two temperate lizard populations. Funct. Ecol. 11, 79–89. https://doi.org/10.1046/j.1365-2435.1997.00058.x

Dubovik, O., Schuster, G.L., Xu, F., Hu, Y., Bösch, H., Landgraf, J., Li, Z., 2021. Grand Challenges in Satellite Remote Sensing. Front. Remote Sens. 2, 619818. https://doi.org/10.3389/frsen.2021.619818

Duclos, T.R., DeLuca, W.V., King, D.I., 2019. Direct and indirect effects of climate on bird abundance along elevation gradients in the Northern Appalachian mountains. Divers. Distrib. 25, 1670–1683. https://doi.org/10.1111/ddi.12968

Duffy, J. P. et al. 2018. Location, location, location: considerations when using lightweight drones in challenging environments', Remote Sensing in Ecology and Conservation, 4(1), pp. 7–19. doi: 10.1002/rse2.58.

Duffy, J.P., Anderson, K., Fawcett, D., Curtis, R.J., Maclean, I.M.D., 2021. Drones provide spatial and volumetric data to deliver new insights into microclimate modelling. Landsc. Ecol. 36, 685–702. https://doi.org/10.1007/s10980-020-01180-9

Dufour, C.M.S. et al. 2018. Ecological character displacement between a native and an introduced species: the invasion of Anolis cristatellus in Dominica. - Biol. J. Linn. Soc. 123: 43–54. https://doi.org/10.1093/biolinnean/blx116

Edwards, J. R. and Lailvaux, S. P. 2012. Display Behavior and Habitat Use in Single and Mixed Populations of Anolis carolinensis and Anolis sagrei Lizards', 118, pp. 494–502. doi: 10.1111/j.1439-0310.2012.02037.x.

Ehrlén, J. and Morris, W. F. 2015. Predicting changes in the distribution and abundance of species under environmental change', Ecology Letters, 18(3), pp. 303–314. doi: 10.1111/ele.12410.

Elton, C.S., 1927. Animal ecology. Sidgwick & Jackson, London.

Ewers, R.M., Banks-Leite, C., 2013. Fragmentation Impairs the Microclimate Buffering Effect of Tropical Forests. PLOS ONE 8, 7.

Epskamp, S. (2015). semPlot: Unified visualizations of structural equation models. - Struct Equ Modeling, 22(3): 474–483.

Fawcett, S., Phillips, T., Strand, M., Rebertus, A., 2016. Flora and ecology of a neotropical savanna, Utila, Bay Islands, Honduras. Folia Geobot. 51, 77–91. https://doi.org/10.1007/s12224-016-9245-0

Fenoglio, M.S., Rossetti, M.R., Videla, M., 2020. Negative effects of urbanization on terrestrial arthropod communities: A meta-analysis. Glob. Ecol. Biogeogr. geb.13107. https://doi.org/10.1111/geb.13107

Fiske, I., Chandler, R., 2011. unmarked : An *R* Package for Fitting Hierarchical Models of Wildlife Occurrence and Abundance. J. Stat. Softw. 43. https://doi.org/10.18637/jss.v043.i10

Foster, W.A., Snaddon, J.L., Turner, E.C., Fayle, T.M., Cockerill, T.D., Ellwood, M.D.F., Broad, G.R., Chung, A.Y.C., Eggleton, P., Khen, C.V., Yusah, K.M., 2011. Establishing the evidence base for maintaining biodiversity and ecosystem function in the oil palm landscapes of South East Asia. Philos. Trans. R. Soc. B Biol. Sci. 366, 3277–3291. https://doi.org/10.1098/rstb.2011.0041

Freeman, E., Frescino.T., 2009, ModelMap: Modeling and Map production using Random Forest and Stochastic Gradient Boosting. USDA Forest Service, Rocky Mountain Research Station, 507 25th street, Ogden, UT, USA

Frishkoff, L.O., Gabot, E., Sandler, G., Marte, C., Mahler, D.L., 2019. Elevation shapes the reassembly of Anthropocene lizard communities. Nat. Ecol. Evol. 3, 638–646. https://doi.org/10.1038/s41559-019-0819-0

Frishkoff, L.O., Hadly, E.A., Daily, G.C., 2015. Thermal niche predicts tolerance to habitat conversion in tropical amphibians and reptiles. Glob. Change Biol. 21, 3901–3916. https://doi.org/10.1111/gcb.13016

Gates, 1980. Biophysical Ecology. Springer-Verlag, New York.

Gunderson, A.R., Leal, M., 2016. A conceptual framework for understanding thermal constraints on ectotherm activity with implications for predicting responses to global change. Ecol. Lett. 19, 111–120. https://doi.org/10.1111/ele.12552

Gutsche,Alexander, McCraine,James.R, N. K. E. 2004. Field observations on a nesting site of Norops utilensis K ÖHLER , 1996 (Reptilia , Squamata), 1996, pp. 297–302.

Gutsche, A. (2005). 'Distribution and habitat utilization of Ctenosaura bakeri on Utila'. Iguana: Conservation, Natural History, and Husbandry of Reptiles 12(3):142–151.

Gvoždík, L., 2002. To heat or to save time? Thermoregulation in the lizard Zootoca vivipara (Squamata: Lacertidae) in different thermal environments along an altitudinal gradient. Can. J. Zool. 80, 479–492. https://doi.org/10.1139/z02-015

Hansen, M. C., P. V. Potapov, R. Moore, M. Hancher, S. A. Turubanova, A. Tyukavina, D. Thau, S. V. Stehman, S. J. Goetz, T. R. Loveland, A. Kommareddy, A. Egorov, L. Chini, C. O. Justice, and J. R. G. Townshend. 2013. "High-Resolution Global Maps of 21st-Century Forest Cover Change." Science 342 (15 November): 850-53. Data available on-line at: https://glad.earthengine.app/view/global-forest-change.

Hatton, I.A., McCann, K.S., Fryxell, J.M., Davies, T.J., Smerlak, M., Sinclair, A.R.E., Loreau, M., 2015. The predator-prey power law: Biomass scaling across terrestrial and aquatic biomes. Science 349, aac6284–aac6284. https://doi.org/10.1126/science.aac6284

He, K.S., Bradley, B.A., Cord, A.F., Rocchini, D., Tuanmu, M.-N., Schmidtlein, S., Turner, W., Wegmann, M. and Pettorelli, N. (2015), Will remote sensing shape the next

generation of species distribution models?. Remote Sens Ecol Conserv, 1: 4-18. https://doi.org/10.1002/rse2.7

Hesselbarth, M.H.K., Sciaini, M., With, K.A., Wiegand, K. and Nowosad, J. ,2019, landscapemetrics: an open-source R tool to calculate landscape metrics. Ecography, 42: 1648-1657. https://doi-org.nottingham.idm.oclc.org/10.1111/ecog.04617

Heckel, D.G. and Roughgarden, J., 1979. A Technique For estimating the Size of Lizard Populations .Published by : Wiley on behalf of the Ecological Society of America Stable URL : http://www.jstor.org/stable/1936865 References Linked refere 60, 966–975.

Heijden, G.M.F., Proctor, A.D.C., Calders, K., Chandler, C.J., Field, R., Foody, G.M., Krishna Moorthy, S.M., Schnitzer, S.A., Waite, C.E., Boyd, D.S., 2022. Making (remote) sense of lianas. J. Ecol. 110, 498–513. https://doi.org/10.1111/1365-2745.13844

Hijmans, R.J, 2022, raster: Geographic Data Analysis and Modeling. R package version 3.5-15. https://CRAN.R-project.org/package=raster

Huey, R.B., Deutsch, C.A., Tewksbury, J.J., Vitt, L.J., Hertz, P.E., Álvarez Pérez, H.J., Garland, T., 2009. Why tropical forest lizards are vulnerable to climate warming. Proc. R. Soc. B Biol. Sci. 276, 1939–1948. https://doi.org/10.1098/rspb.2008.1957

Huey, R.B., Slatkin, M., 1976. Cost and Benefits of Lizard Thermoregulation. Q. Rev. Biol. 51, 363–384. https://doi.org/10.1086/409470

Huey, R.B., Tewksbury, J.J., 2009. Can behavior douse the fire of climate warming? Proc. Natl. Acad. Sci. 106, 3647–3648. https://doi.org/10.1073/pnas.0900934106

Johnson, M.A., Kirby, R., Wang, S., Losos, J.B., 2006. What drives variation in habitat use by *Anolis* lizards: habitat availability or selectivity? Can. J. Zool. 84, 877–886. https://doi.org/10.1139/z06-068

Johnson, J. D., V. Mata-Silva, and L. D. Wilson. 2015. A conservation reassessment of the Central American herpetofauna based on the EVS measure. Amphibian & Reptile Conservation 9(2) [General Section] 1:94 (e100).

Kamath, A., Stuart, Y.E., Campbell, T.S., 2013. Behavioral Partitioning by the Native Lizard Anolis carolinensis in the Presence and Absence of the Invasive Anolis sagrei in Florida. Breviora 535, 1–10. https://doi.org/10.3099/MCZ8.1

Kašpar, V., Hederová, L., Macek, M., Müllerová, J., Prošek, J., Surový, P., Wild, J., Kopecký, M., 2021. Temperature buffering in temperate forests: Comparing microclimate models based on ground measurements with active and passive remote sensing. Remote Sens. Environ. 263, 112522. https://doi.org/10.1016/j.rse.2021.112522

Kearney, M., Shine, R., Porter, W.P., 2009. The potential for behavioral thermoregulation to buffer "cold-blooded" animals against climate warming. Proc. Natl. Acad. Sci. 106, 3835–3840. https://doi.org/10.1073/pnas.0808913106

Kearney, R. M. 2013. Activity restriction and the mechanistic basis for extinctions under climate warming. - Ecol. Lett 16:1470–1479.

Kearney, M.R., Shamakhy, A., Tingley, R., Karoly, D.J., Hoffmann, A.A., Briggs, P.R. and Porter, W.P., 2014, Microclimate modelling at macro scales: a test of a general microclimate model integrated with gridded continental-scale soil and weather data. Methods Ecol Evol, 5: 273-286. https://doi.org/10.1111/2041-210X.12148

Kearney, M.R., Porter, W.P., 2017. NicheMapR – an R package for biophysical modelling: the microclimate model. Ecography 40, 664–674. https://doi.org/10.1111/ecog.02360

Kharouba HM, Algar AC, Kerr JT. Historically calibrated predictions of butterfly species' range shift using global change as a pseudo-experiment. Ecology. 2009 Aug;90(8):2213-22. doi: 10.1890/08-1304.1. PMID: 19739383.

Koh, L. P. and Wich, S. A.,2012, Dawn of drone ecology : low- cost autonomous aerial vehicles for conservation, Tropical Conservation Science, 5(2), pp. 121–132.

Köhler, G. 1996. Additions to the known herpetofauna of the Isla de Utila (Islas de la Bahia, Honduras) with description of a new species of the genus Norops (Reptilia: Iguanidae).-Senck biol 76: 19–28.

Kolbe, J.J., Losos, J.B., 2005. Hind-Limb Length Plasticity in Anolis carolinensis. J. Herpetol. 39, 674–678. https://doi.org/10.1670/87-05N.1

Kolbe, J.J., VanMiddlesworth, P., Battles, A.C., Stroud, J.T., Buffum, B., Forman, R.T.T., Losos, J.B., 2016. Determinants of spread in an urban landscape by an introduced lizard. Landsc. Ecol. 31, 1795–1813. https://doi.org/10.1007/s10980-016-0362-1

Lack, D.L., 1954. The natural regulation of animal numbers. Clarendon Press.

Lembrechts, J.J., Nijs, I., Lenoir, J., 2019. Incorporating microclimate into species distribution models. Ecography 42, 1267–1279. https://doi.org/10.1111/ecog.03947

Leroux, S.J., Loreau, M., 2015. Theoretical perspectives on bottom-up and top-down interactions across ecosystems, in: Hanley, T.C., La Pierre, K.J. (Eds.), Trophic Ecology. Cambridge University Press, Cambridge, pp. 3–28. https://doi.org/10.1017/CBO9781139924856.002

Lister, B.C., Garcia, A., 2018. Climate-driven declines in arthropod abundance restructure a rainforest food web. Proc. Natl. Acad. Sci. 115, E10397–E10406. https://doi.org/10.1073/pnas.1722477115

Lister, B.C. and Garcia, A. 2019. Reply to Willig et al.: Long-term population trends in the Luquillo Rainforest. Proceedings of the National Academy of Sciences 116:12145–12146.

Logan, M.L., Fernandez, S.G., Calsbeek, R., 2015. Abiotic constraints on the activity of tropical lizards. Funct. Ecol. 7.

Logan, M.L., Huynh, R.K., Precious, R.A., Calsbeek, R.G., 2013. The impact of climate change measured at relevant spatial scales: new hope for tropical lizards. Glob. Change Biol. 19, 3093–3102. https://doi.org/10.1111/gcb.12253

Losos, J.B., 2009. Lizards in an Evolutionary Tree: Ecology and Adaptive Radiation of Anoles. University of California Press, Oakland, California.

Maclean, IMD, Mosedale, JR, Bennie, JJ., 2018, Microclima: An r package for modelling meso- and microclimate. Methods Ecol Evol. ; 10: 280– 290. https://doi.org/10.1111/2041-210X.13093

Maclean, I.M.D., Klinges, D.H., 2021. Microclimc: A mechanistic model of above, below and within-canopy microclimate. Ecol. Model. 451, 109567. https://doi.org/10.1016/j.ecolmodel.2021.109567

Magnago, L.F.S., n.d. Microclimatic conditions at forest edges have significant impacts on vegetation structure in large Atlantic forest fragments. Biodivers Conserv 15.

Marcello, J., Eugenio, F., Perdomo, U., Medina, A., 2016. Assessment of Atmospheric Algorithms to Retrieve Vegetation in Natural Protected Areas Using Multispectral High Resolution Imagery. Sensors 16, 1624. https://doi.org/10.3390/s16101624

Maryon, D., Pasachnik, S.A., Knapp, C.R., Brown, T.W. and Grant, T.D. (eds.) (2021). Útila spiny-tailed iguana (Ctenosaura bakeri): Conservation action plan 2020—2025. Gland, Switzerland: IUCN.

McCranie, J.R. and Köhler, G. 2015. The Anoles (Reptilia: Squamata: Dactyloidae: Anolis : Norops) of Honduras. Systematics, Distribution, and Conservation. - Bull. Mus. Comp. Zool. 161: 1–280. https://doi.org/10.3099/0027-4100-14.1.1

McCranie, J.R. and L.V. Orellana. 2014 New island records and updated nomenclature of amphibians and reptiles from the Islas de la Bahía, Honduras. - Herpetol. Notes 7: 41–49

Méndez-Galeano, M.A. et al. 2020. The highest kingdom of Anolis: Thermal biology of the Andean lizard Anolis heterodermus (Squamata: Dactyloidae) over an elevational gradient in the Eastern Cordillera of Colombia. - J. Therm. Biol. 89: 102498. https://doi.org/10.1016/j.jtherbio.2019.102498

Millard, K., Richardson, M., 2015. On the Importance of Training Data Sample Selection in Random Forest Image Classification: A Case Study in Peatland Ecosystem Mapping. Remote Sens. 7, 8489–8515. https://doi.org/10.3390/rs70708489

Milling, C.R., Rachlow, J.L., Olsoy, P.J., Chappell, M.A., Johnson, T.R., Forbey, J.S., Shipley, L.A., Thornton, D.H., 2018. Habitat structure modifies microclimate: An approach for mapping fine-scale thermal refuge. Methods Ecol. Evol. 9, 1648–1657. https://doi.org/10.1111/2041-210X.13008

Morris, D., Boyd, D., Crowe, J., Johnson, C., Smith, K., 2013. Exploring the Potential for Automatic Extraction of Vegetation Phenological Metrics from Traffic Webcams. Remote Sens. 5, 2200–2218. https://doi.org/10.3390/rs5052200

Munoz, M. M. et al. (2014) 'Evolutionary stasis and lability in thermal physiology in a group of tropical lizards', Proceedings of the Royal Society B: Biological Sciences, 281(1778), pp. 20132433–20132433. doi: 10.1098/rspb.2013.2433.

Muñoz, M. M. and Losos, J. B. (2017) 'Thermoregulatory Behavior Simultaneously Promotes and Forestalls Evolution in a Tropical Lizard', The American Naturalist, (January), pp. E000–E000. doi: 10.1086/694779.

Natesan, S., Benari, G., Armenakis, C., Lee, R., 2017. LAND COVER CLASSIFICATION USING A UAV-BORNE SPECTROMETER. Int. Arch. Photogramm. Remote Sens. Spat. Inf. Sci. XLII-2/W6, 269–273. https://doi.org/10.5194/isprs-archives-XLII-2-W6-269-2017

Nevalainen, O., Honkavaara, E., Tuominen, S., Viljanen, N., Hakala, T., Yu, X., Hyyppä, J., Saari, H., Pölönen, I., Imai, N., Tommaselli, A., 2017. Individual Tree Detection and Classification with UAV-Based Photogrammetric Point Clouds and Hyperspectral Imaging. Remote Sens. 9, 185. https://doi.org/10.3390/rs9030185

Niehaus, A.C., Angilletta, M.J., Sears, M.W., Franklin, C.E., Wilson, R.S., 2012. Predicting the physiological performance of ectotherms in fluctuating thermal environments. J. Exp. Biol. 215, 694–701. https://doi.org/10.1242/jeb.058032

Nicholson, K. E., Harmon, L. J. and Losos, J. B. (2007) 'Evolution of Anolis lizard dewlap diversity', PLoS ONE, 2(3), pp. 1–12. doi: 10.1371/journal.pone.0000274.

Nowakowski, A.J., Watling, J.I., Thompson, M.E., Brusch, G.A., Catenazzi, A., Whitfield, S.M., Kurz, D.J., Suárez-Mayorga, Á., Aponte-Gutiérrez, A., Donnelly, M.A., Todd, B.D., 2018. Thermal biology mediates responses of amphibians and reptiles to habitat modification. Ecol. Lett. 21, 345–355. https://doi.org/10.1111/ele.12901

Orrell, K.S., Congdon, J.D., Jenssen, T.A., Michener, R.H., Kunz, T.H., 2004. Intersexual Differences in Energy Expenditure of *Anolis carolinensis* Lizards during Breeding and Postbreeding Seasons. Physiol. Biochem. Zool. 77, 50–64. https://doi.org/10.1086/383497

Pereira, H. M. et al. ,2010, Scenarios for Global Biodiversity in the 21st Century, Science, 330(6010), pp. 1496–1501. doi: 10.1126/science.1196624.

Piano, E., Souffreau, C., Merckx, T., Baardsen, L.F., Backeljau, T., Bonte, D., Brans, K.I., Cours, M., Dahirel, M., Debortoli, N., Decaestecker, E., De Wolf, K., Engelen, J.M.T., Fontaneto, D., Gianuca, A.T., Govaert, L., Hanashiro, F.T.T., Higuti, J., Lens, L., Martens, K., Matheve, H., Matthysen, E., Pinseel, E., Sablon, R., Schön, I., Stoks, R., Van Doninck, K., Van Dyck, H., Vanormelingen, P., Van Wichelen, J., Vyverman, W., De Meester, L., Hendrickx, F., 2020. Urbanization drives cross-taxon declines in

abundance and diversity at multiple spatial scales. Glob. Change Biol. 26, 1196–1211. https://doi.org/10.1111/gcb.14934

Potter, K.A., Arthur Woods, H., Pincebourde, S., 2013. Microclimatic challenges in global change biology. Glob. Change Biol. 19, 2932–2939. https://doi.org/10.1111/gcb.12257

Pringle, R.M., Kartzinel, T.R., Palmer, T.M., Thurman, T.J., Fox-Dobbs, K., Xu, C.C.Y., Hutchinson, M.C., Coverdale, T.C., Daskin, J.H., Evangelista, D.A., Gotanda, K.M., A. Man in 't Veld, N., Wegener, J.E., Kolbe, J.J., Schoener, T.W., Spiller, D.A., Losos, J.B., Barrett, R.D.H., 2019. Predator-induced collapse of niche structure and species coexistence. Nature 570, 58–64. https://doi.org/10.1038/s41586-019-1264-6

Richards, D.R., Friess, D.A., 2016. Rates and drivers of mangrove deforestation in Southeast Asia, 2000–2012. Proc. Natl. Acad. Sci. 113, 344–349. https://doi.org/10.1073/pnas.1510272113

Rocchini, D., Boyd, D.S., Féret, J., Foody, G.M., He, K.S., Lausch, A., Nagendra, H., Wegmann, M., Pettorelli, N., 2016. Satellite remote sensing to monitor species diversity: potential and pitfalls. Remote Sens. Ecol. Conserv. 2, 25–36. https://doi.org/10.1002/rse2.9

Rosseel, Y. (2012). "lavaan: An R Package for Structural Equation Modeling." - J. Stat. Softw, 48(2): 1–36.

Royle, J.A., 2004. N-Mixture Models for Estimating Population Size from Spatially Replicated Counts. Biometrics 60, 108–115. https://doi.org/10.1111/j.0006-341X.2004.00142.x

Schiffman, R. (2014) 'Wildlife conservation: Drones flying high as new tool for field biologists', Science, 344(6183), p. 459. doi: 10.1126/science.344.6183.459.

Schoener, T. W. (1974) 'Resource Partitioning in Ecological Communities', Science, 185(4145), pp. 27–39. doi: 10.1126/science.185.4145.27.

Schoener, T.W.,et al., 2002. Predation on a Common Anolis Lizard: Can the Food-Web Effects
of a Devastating Predator be Reversed?. Ecological Monographs, 72: 383-407.
https://doi.org/10.1890/0012-9615(2002)072[0383:POACAL]2.0.CO;2

Schulte, U., Köhler, G., 2010. Microhabitat selection in the spiny-tailed iguana Ctenosaura
bakeri on Utila Island, Honduras 6.

Sears, M.W., Angilletta, M.J., 2015. Costs and Benefits of Thermoregulation Revisited: Both
the Heterogeneity and Spatial Structure of Temperature Drive Energetic Costs. Am.
Nat. 185, E94–E102. https://doi.org/10.1086/680008

Sears, M.W., Angilletta, M.J., Schuler, M.S., Borchert, J., Dilliplane, K.F., Stegman, M.,
Rusch, T.W., Mitchell, W.A., 2016. Configuration of the thermal landscape determines
thermoregulatory performance of ectotherms. Proc. Natl. Acad. Sci. 113, 10595–10600.
https://doi.org/10.1073/pnas.1604824113

Sears, M.W., Raskin, E., Angilletta, M.J., 2011. The World Is not Flat: Defining Relevant
Thermal Landscapes in the Context of Climate Change. Integr. Comp. Biol. 51, 666–
675. https://doi.org/10.1093/icb/icr111

Sinclair, B.J., Marshall, K.E., Sewell, M.A., Levesque, D.L., Willett, C.S., Slotsbo, S., Dong,
Y., Harley, C.D.G., Marshall, D.J., Helmuth, B.S., Huey, R.B., 2016. Can we predict
ectotherm responses to climate change using thermal performance curves and body
temperatures? Ecol. Lett. 19, 1372–1385. https://doi.org/10.1111/ele.12686

Sinervo, B., Mendez-de-la-Cruz, F., Miles, D.B., Heulin, B., Bastiaans, E., Villagran-Santa
Cruz, M., Lara-Resendiz, R., Martinez-Mendez, N., Calderon-Espinosa, M.L., Meza-
Lazaro, R.N., Gadsden, H., Avila, L.J., Morando, M., De la Riva, I.J., Sepulveda, P.V.,
Rocha, C.F.D., Ibarguengoytia, N., Puntriano, C.A., Massot, M., Lepetz, V., Oksanen,
T.A., Chapple, D.G., Bauer, A.M., Branch, W.R., Clobert, J., Sites, J.W., 2010. Erosion

of Lizard Diversity by Climate Change and Altered Thermal Niches. Science 328, 894–899. https://doi.org/10.1126/science.1184695

Stapley, J., Garcia, M., Andrews, R.M., 2015. Long-Term Data Reveal a Population Decline of the Tropical Lizard Anolis apletophallus, and a Negative Affect of El Nino Years on Population Growth Rate. PLOS ONE 10, e0115450. https://doi.org/10.1371/journal.pone.0115450

Stark, D. J. et al. ,2018, Combining drones and satellite tracking as an effective tool for informing policy change in riparian habitats: a proboscis monkey case study', Remote Sensing in Ecology and Conservation, 4(1), pp. 44–52. doi: 10.1002/rse2.51.

Still, C., Powell, R., Aubrecht, D., Kim, Y., Helliker, B., Roberts, D., Richardson, A.D., Goulden, M., 2019. Thermal imaging in plant and ecosystem ecology: applications and challenges. Ecosphere 10. https://doi.org/10.1002/ecs2.2768

Stroud, J.T., Giery, S.T., Outerbridge, M.E., 2017. Establishment of Anolis sagrei on Bermuda represents a novel ecological threat to Critically Endangered Bermuda skinks (Plestiodon longirostris). Biol. Invasions 19, 1723–1731. https://doi.org/10.1007/s10530-017-1389-1

Stuart, Y.E., Campbell, T.S., Hohenlohe, P.A., Reynolds, R.G., Revell, L.J., Losos, J.B., 2014. Rapid evolution of a native species following invasion by a congener. Science 346, 463–466. https://doi.org/10.1126/science.1257008

Suggitt, A.J., Wilson, R.J., Isaac, N.J.B., Beale, C.M., Auffret, A.G., August, T., Bennie, J.J., Crick, H.Q.P., Duffield, S., Fox, R., Hopkins, J.J., Macgregor, N.A., Morecroft, M.D., Walker, K.J., Maclean, I.M.D., 2018. Extinction risk from climate change is reduced by microclimatic buffering. Nat. Clim. Change 8, 713–717. https://doi.org/10.1038/s41558-018-0231-9

Sunday, J.M., Bates, A.E., Kearney, M.R., Colwell, R.K., Dulvy, N.K., Longino, J.T., Huey, R.B., 2014. Thermal-safety margins and the necessity of thermoregulatory behavior across latitude and elevation. Proc. Natl. Acad. Sci. 111, 5610–5615. https://doi.org/10.1073/pnas.1316145111

Tang, Z., Mei, Z., Liu, W., Xia, Y., 2020. Identification of the key factors affecting Chinese carbon intensity and their historical trends using random forest algorithm. J. Geogr. Sci. 30, 743–756. https://doi.org/10.1007/s11442-020-1753-4

Thomas, C. D. and Et, A. 2004, Extinction risk from climate change', Nature, 427, pp. 145–148. doi: 10.1038/427589a.

Tuff, K.T., Tuff, T. and Davies, K.F., 2016, A framework for integrating thermal biology into fragmentation research. Ecol Lett, 19: 361-374. https://doi-org.nottingham.idm.oclc.org/10.1111/ele.12579

Ustuner, M., Sanli, F. B. and Dixon, B., 2015, Application of Support Vector Machines for Landuse Classification Using High-Resolution RapidEye Images : A Sensitivity Analysis, pp. 403–422. doi: 10.5721/EuJRS20154823.

Vasseur, D. A. et al. , 2014, Increased temperature variation poses a greater risk to species than climate warming', Proceedings of the Royal Society B: Biological Sciences, 281(1779), p. 20132612. doi: 10.1098/rspb.2013.2612.

Wallace, L. et al., 2016, Assessment of Forest Structure Using Two UAV Techniques : A Comparison of Airborne Laser Scanning and Structure from Motion (SfM) Point Clouds, pp. 1–16. doi: 10.3390/f7030062.

Waite, C.E., Heijden, G.M.F., Field, R., Boyd, D.S., 2019. A view from above: Unmanned aerial vehicles (UAV s) provide a new tool for assessing liana infestation in tropical forest canopies. J. Appl. Ecol. 56, 902–912. https://doi.org/10.1111/1365-2664.13318

Webster, C., Westoby, M., Rutter, N., Jonas, T., 2018. Three-dimensional thermal characterization of forest canopies using UAV photogrammetry. Remote Sens. Environ. 209, 835–847. https://doi.org/10.1016/j.rse.2017.09.033

White, B.A., Prado-Irwin, S.R., Gray, L.N., 2019. FEMALE SIGNAL VARIATION IN THE ANOLIS LEMURINUS GROUP. Breviora 564, 1. https://doi.org/10.3099/0006-9698-564.1.1

Williams.E, 1983, Ecomorphs, faunas, island size, and diverse end points in island radiations of Anolis. Pp. 326–370 In R. B. Huey, E. R. Pianka, and T. W. Schoener (Eds.), Lizard Ecology: Studies of a Model Organism. Harvard University Press, Cambridge, Massachusetts, United States.

Willig, M.R., Woolbright, L., Presley, S.J., Schowalter, T.D., Waide, R.B., Heartsill Scalley, T., Zimmerman, J.K., González, G., Lugo, A.E., 2019. Populations are not declining and food webs are not collapsing at the Luquillo Experimental Forest. Proc. Natl. Acad. Sci. 116, 12143–12144. https://doi.org/10.1073/pnas.1820456116

Winchell, K.M., Reynolds, R.G., Prado-Irwin, S.R., Puente-Rolón, A.R., Revell, L.J., 2016. Phenotypic shifts in urban areas in the tropical lizard *Anolis cristatellus*: PHENOTYPIC DIVERGENCE IN URBAN ANOLES. Evolution 70, 1009–1022. https://doi.org/10.1111/evo.12925

Xie, Y., Sha, Z., Yu, M., 2008. Remote sensing imagery in vegetation mapping: a review. J. Plant Ecol. 1, 9–23. https://doi.org/10.1093/jpe/rtm005

Xie, Z.; Chen, Y.; Lu, D.; Li, G.; Chen, E. Classification of Land Cover, Forest, and Tree Species Classes with ZiYuan-3 Multispectral and Stereo Data. Remote Sens. 2019, 11, 164. https://doi.org/10.3390/rs11020164

Zellweger, F., Coomes, D., Lenoir, J., Depauw, L., Maes, S.L., Wulf, M., Kirby, K.J., Brunet, J., Kopecký, M., Máliš, F., Schmidt, W., Heinrichs, S., den Ouden, J., Jaroszewicz, B.,

Buyse, G., Spicher, F., Verheyen, K., De Frenne, P., 2019. Seasonal drivers of understorey temperature buffering in temperate deciduous forests across Europe. Glob. Ecol. Biogeogr. 28, 1774–1786. https://doi.org/10.1111/geb.12991

Figure A1.1: Map of land cover training points collected with a GPS in 2017 by Emma Higgins, used to inform the plot selection land cover classification.

Appendix 2 - Plot Locations

Table A2.1: Plot Location and descriptions for survey plots on Utila, Isla de bahia, Honduras.

Plot No.	Land Cover Type	Coordinates	Description
1	Forest	16.119337°N, 86.884782°W	Forest plot
2	Forest	16.122757°N ,86.883927°W	Forest plot
3	Forest	16.122662°N ,86.885067°W	Forest plot
4	Urban Forest	16.098153°N ,86.897892°W	Degraded forest within Utila town
5	Urban Forest	16.098343°N ,86.899317°W	Degraded forest within Utila town
6	Urban Forest	16.096538°N ,86.893332°W	Black mangrove forest within Utila town
7	Urban	16.087229°N ,86.889817°W	Urban garden plot
8	Urban	16.087989°N ,86.892382°W	Urban residential plot with house and garden
9	Forest	16.119527°N ,86.882598°W	Forest plot
10	Forest	16.119052°N ,86.883452°W	Forest plot
11	Forest	16.095303°N ,86.883168°W	Forest plot
12	Urban	16.091978°N ,86.883642°W	Urban clearing
13	Urban	16.087894°N ,86.888962°W	Urban clearing
14	Forest	16.110312°N ,86.897892°W	Forest plot
15	Forest	16.111072°N ,86.901026°W	Forest plot
16	Urban Forest	16.104080°N ,86.893527°W	Urban garden plot

Appendix 3 - Leaf area index (LAI) calculation

A general introduction to leaf area index (LAI) and radiation transmission through plant canopies can be found in Chapter 15 of Campbell and Norman (1998). We calculated LAI using a simplified version of the Norman-Jarvis model, as presented in Decagon Devices Inc (2013):

$$\text{LAI} = \frac{[\,1 - 1\,2K\ fb - 1]ln\tau}{A(1 - 0.47fb)} \qquad - \textbf{\textit{Equation A1}}$$

Where τ is the ratio of transmitted to incident photosynthetically active radiation (PAR), measured with the ceptometer. K is the extinction coefficient for the canopy, Fb is the fraction of incident PAR which is beam and is estimated by the ceptometer from incident radiation and the solar constant (Decagon Devices Inc (2013). In Equation A2, A is a function of leaf absorptivity in the PAR band (a, see below). K was modelled as a function of zenith angle (Θ), assuming a leaf angle distribution of 1.0, the default value for the AccuPAR LP-80 ceptometer. Calculations of LAI are not strongly affected by the leaf angle distribution (Decagon Devices Inc 2013).

$$K = \frac{1}{2Cos\Theta} \textbf{ - \textit{Equation A2}}$$

In Equation A2, A was calculated as:

$$A = 0.283 + 0.785a - 0.159\ a^2 \textbf{ – \textit{Equation A3}}$$

Where a is the leaf absorptivity in the PAR band. The AccuPAR LP-80 ceptometer assumes 0.9 in LAI sampling routines (see user manual – Decagon Devices, 2013).

Appendix 4 – UAV Plot Flight Heights 2019

Table A4.1: Flight altitude of the UAV flight for each plot.

Plot Number	UAV Flight Altitude (metres above ground)
1	48/50
2	45
3	45
4	45
5	45
6	45
7	40
8	40
9	50
10	50
11	45
12	45
13	40
14	55
15	55
16	42

Appendix 5 – Texture Metric Example
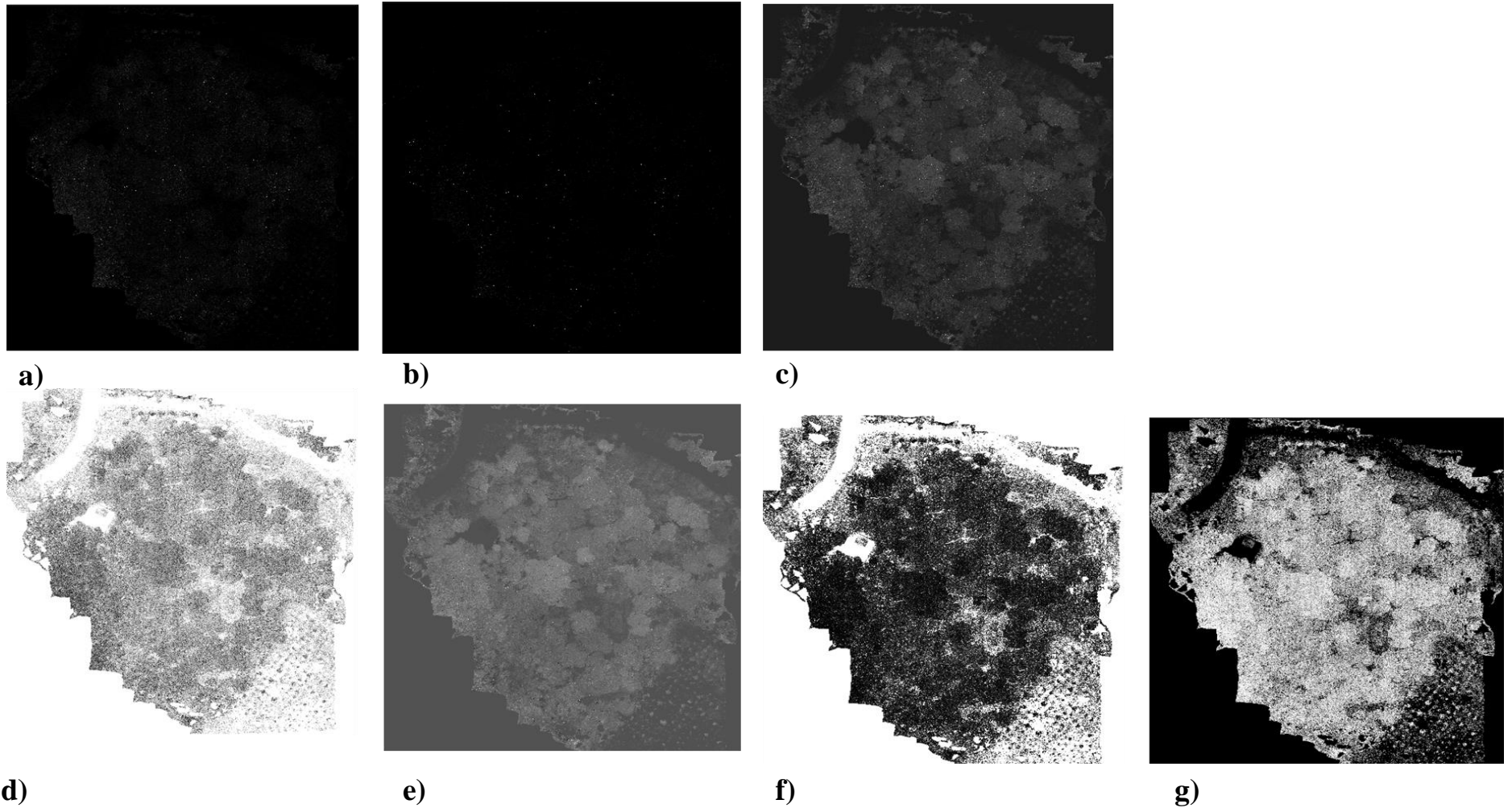
Figure A5.1: Example of all texture layers for area surrounding Plot 1, a) Dissimilarity, b) Contrast, c) Variance, d) Homogeneity, e) Mean, f) Second Moment and g) Entropy.

Appendix 6 – Chapter 3 Additional Information

Table A6.1: Summaries of thermal and structural habitat, prey availability across all plot surveyed for Chapter 3

| Plot No.	Time within T_{pref} (%)	Sum of Deviation from T_{pref} (ºC)	Deviation above T_{pref} (ºC)	Deviation below T_{pref} (ºC)	No. Perches	Basal Area (m²)	Mean Leaf Area Index across Transects	Arthropod Diversity (Shannon)	Arthropod Biomass (g)
1	55.47	15.05	3.12	11.94	129	2.27	3.97	-1.91	0.84
2	57.18	12.27	2.97	9.30	23	0.67	3.82	-1.91	1.90
3	53.85	13.76	3.21	10.55	51	1.08	3.30	-1.79	1.30
4	28.88	29.98	29.98	0	49	1.05	1.87	-1.63	0.73
5	19.74	42.57	42.58	0	17	1.34	1.62	-1.89	1.18
6	8.23	46.52	46.52	0	54	1.05	1.53	-0.91	0.70
9	51.28	19.54	19.53	0	74	1.71	2.04	-1.68	1.23
10	53.97	17.50	0.58	16.93	122	1.86	2.97	-1.86	2.09
11	35.49	17.78	17.78	0	86	3.10	3.58	-1.86	0.65
13	10.77	62.30	62.30	0	54	0.40	0.57	-1.57	0.20
14	66.40	8.96	8.96	0	232	2.76	2.79	-1.33	1.18
15	68.29	6.46	6.42	0.05	43	6.35	2.27	-1.70	1.01
16	55.64	14.35	14.40	0	33	1.18	3.81	-1.73	0.98
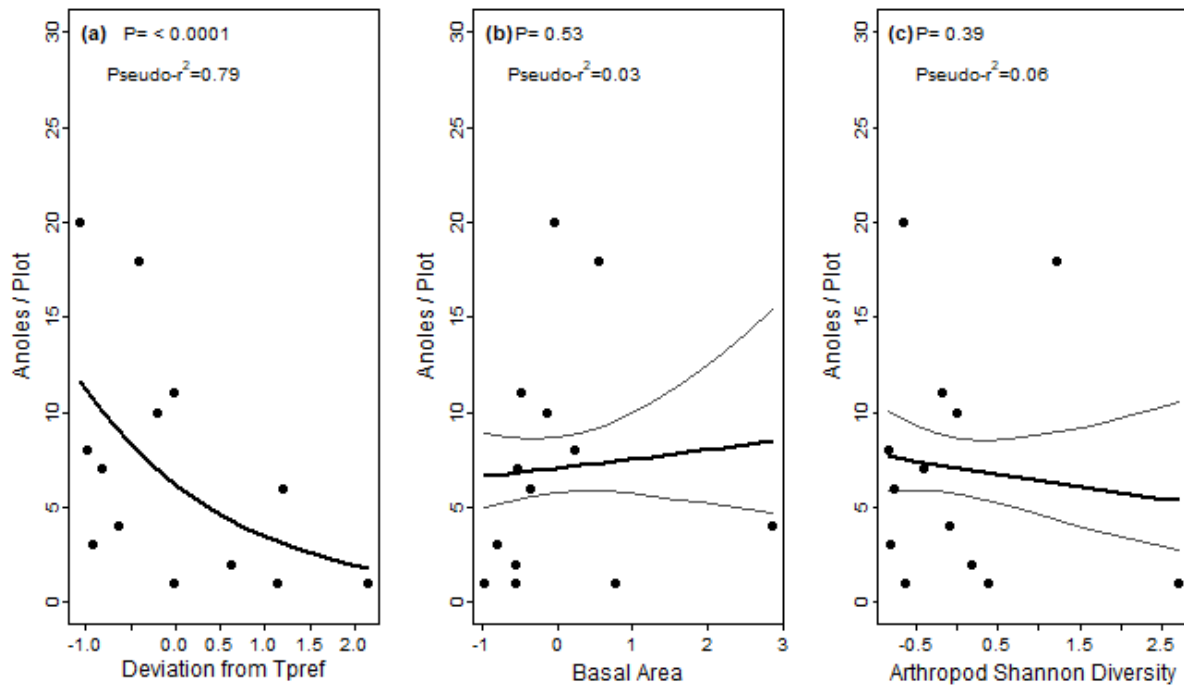
Figure A6.1: Relationships between *Anolis bicaorum* abundance and individual niche metrics in forest plots across Utila, Honduras, that were not included in the final analysis. Relationships were estimated using multinomial Poisson mixture models with a constant detection rate across plots. All variables are scaled to a mean of zero and unit variance, (a) deviation from T_{pref} range, (b) basal area and (e) prey diversity.
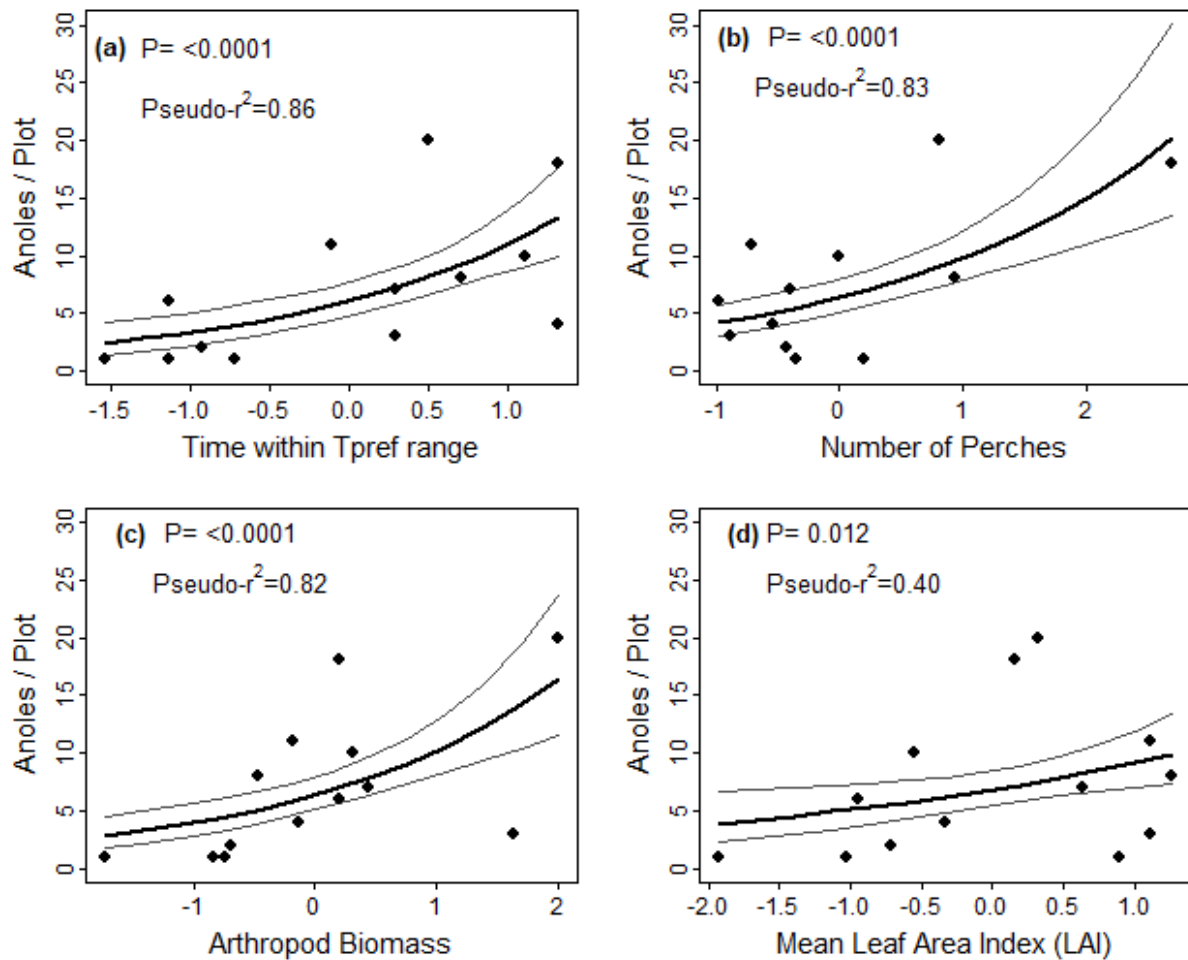
Figure A6.2: Relationships between *Anolis bicaorum* abundance and individual niche metrics in forest plots across Utila, Honduras, using the original uncalibrated thermal model data. Relationships were estimated using multinomial Poisson mixture models with a constant detection rate across plots. All variables are scaled to a mean of zero and unit variance, (a) reflects thermal habitat quality, (b) reflects structural habitat quality, (c) reflects prey availability and (d) canopy cover.
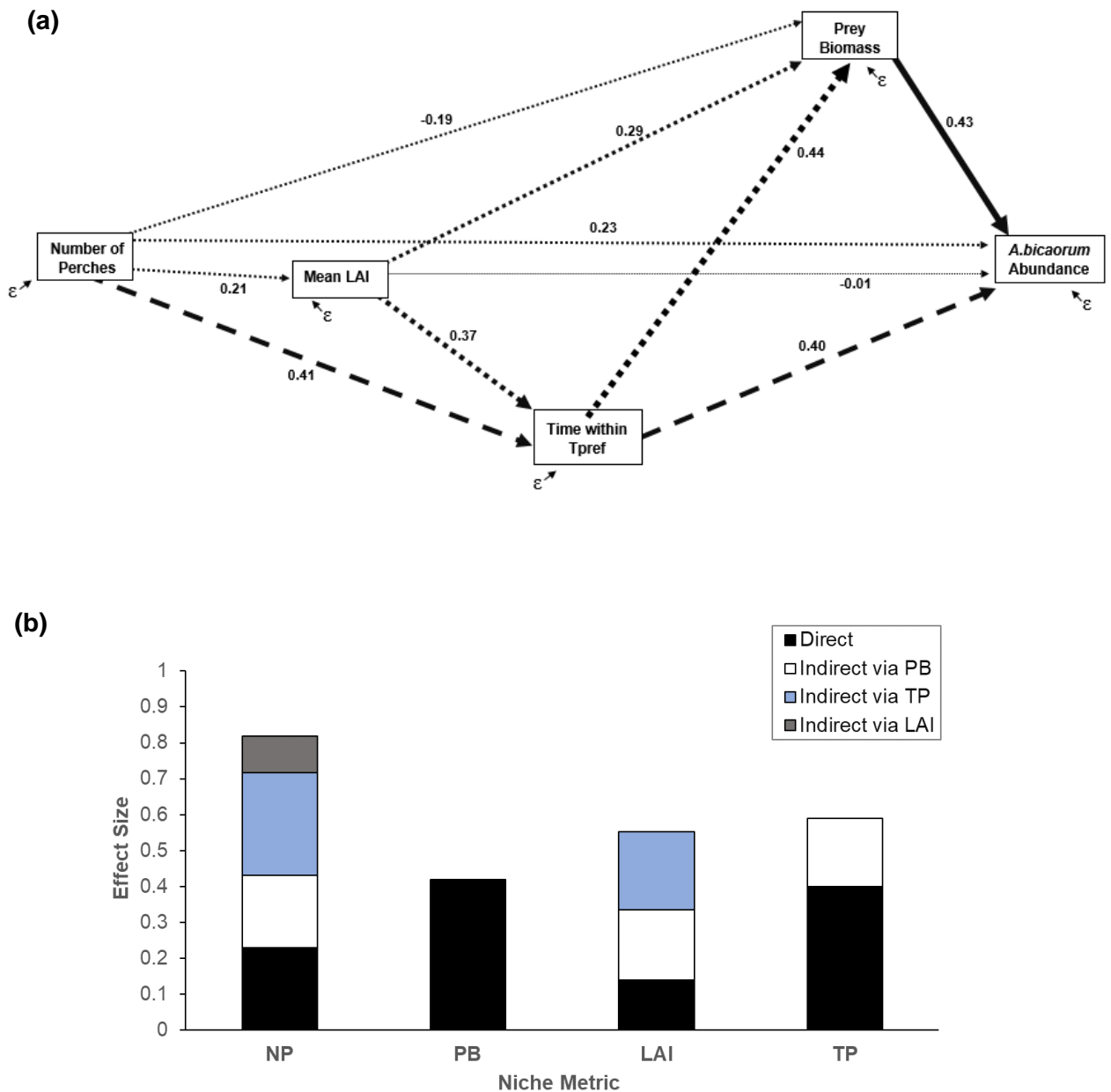
Figure A6.3: Direct and indirect effects of niche axes on *A. bicaorum* abundance using the original uncalibrated thermal model data. (a) Values are standardized path coefficients; line width is proportional to the strength of the effect, solid lines indicate P<0.05, dashed lines 0.05≥P<0.10, and dotted lines P≥0.10, and ε is unexplained variation. (b) The total effects of covariates on abundance. NP: number of perches; PB: prey biomass; LAI: mean leaf area index; TP: time within Tpref range.

Table A6.1: Results of the path analysis on the original uncalibrated thermal model data looking at indirect and direct effects, and relationships between, multiple niche axes on *A. bicaorum* abundance, in 13 forest plots on Utila, Honduras. Std.all, Standardised Coefficients.

Pathway	Estimate (± S.E)	*Z*	*P*-Value	Std.all
***A. bicaorum* Abundance ~**				
Number of Perches	0.24 ± 0.21	1.12	0.238	0.23
Prey Biomass	0.46 ± 0.21	2.14	0.032	0.43
Time within T_{pref}	0.43 ± 0.24	1.78	0.076	0.40
Mean LAI	-0.15 ± 0.21	-0.75	0.94	-0.01
Time within T_{pref} ~				
Mean LAI	0.37 ± 0.22	1.64	0.100	0.37
Number of Perches	0.42 ± 0.22	1.86	0.063	0.42
Mean LAI ~				
Number of Perches	0.21 ± 0.27	0.76	0.449	0.21
Prey Biomass ~				
Time within T_{pref}	0.45 ± 0.27	1.56	0.119	0.45
Number of Perches	-0.19 ± 0.26	-0.71	0.476	-0.18
Mean LAI	0. 29 ± 0.26	1.15	0.249	0.29
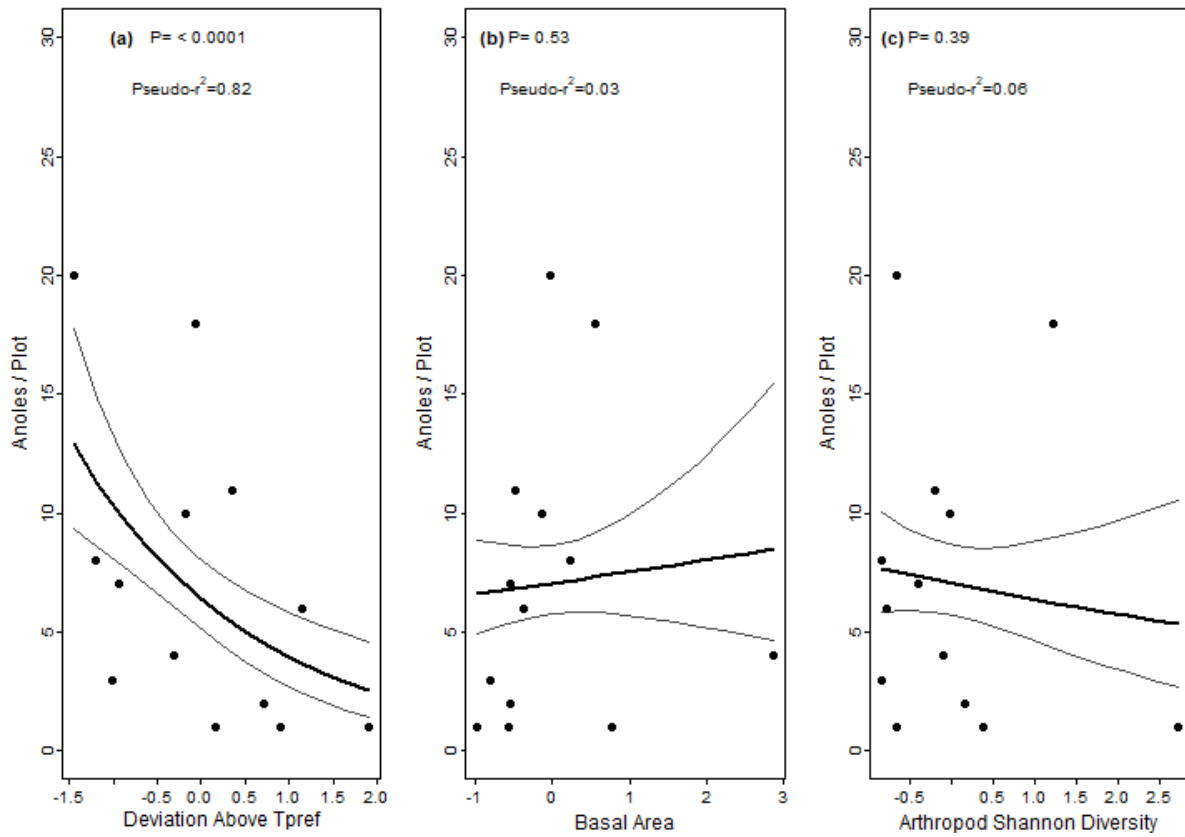
Figure A6.4: Relationships between *Anolis bicaorum* abundance and individual niche metrics excluded from the final analysis, using the original uncalibrated thermal model data. Relationships were estimated using multinomial Poisson mixture models with a constant detection rate across plots. All variables were scaled to a mean of zero and unit variance, (a) deviation from T_{pref} range, (b) basal area, (c) prey diversity.
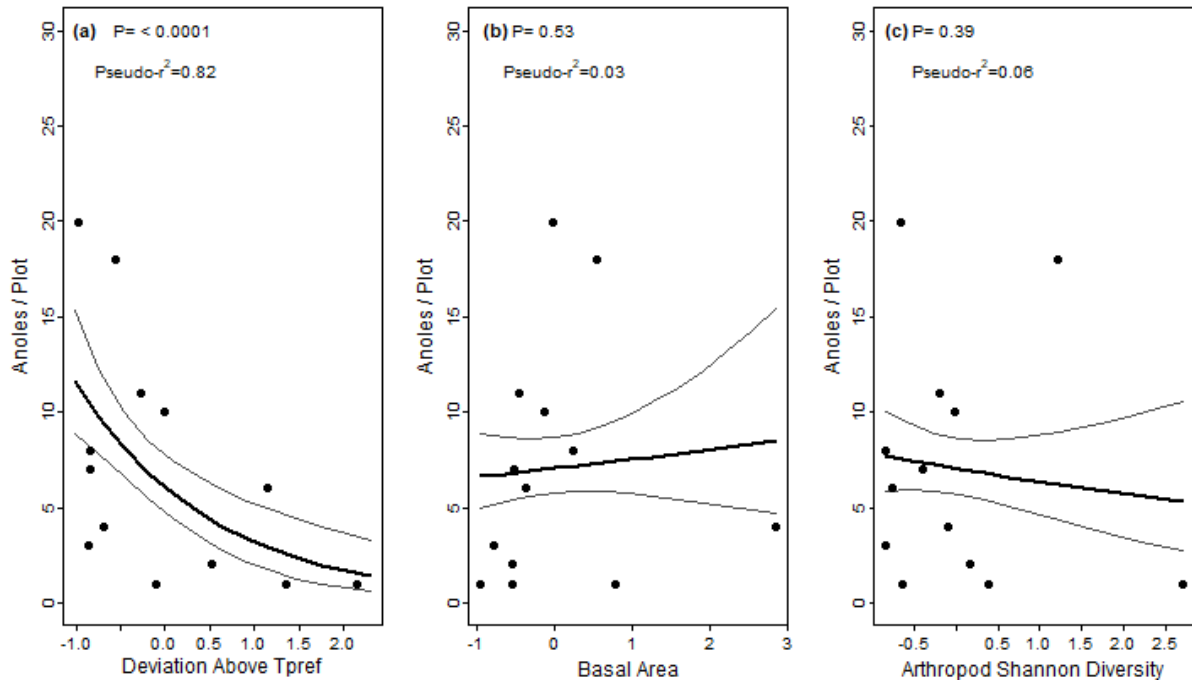
RESULTS OF OVER-CORRECTED THERMAL MODEL DATA
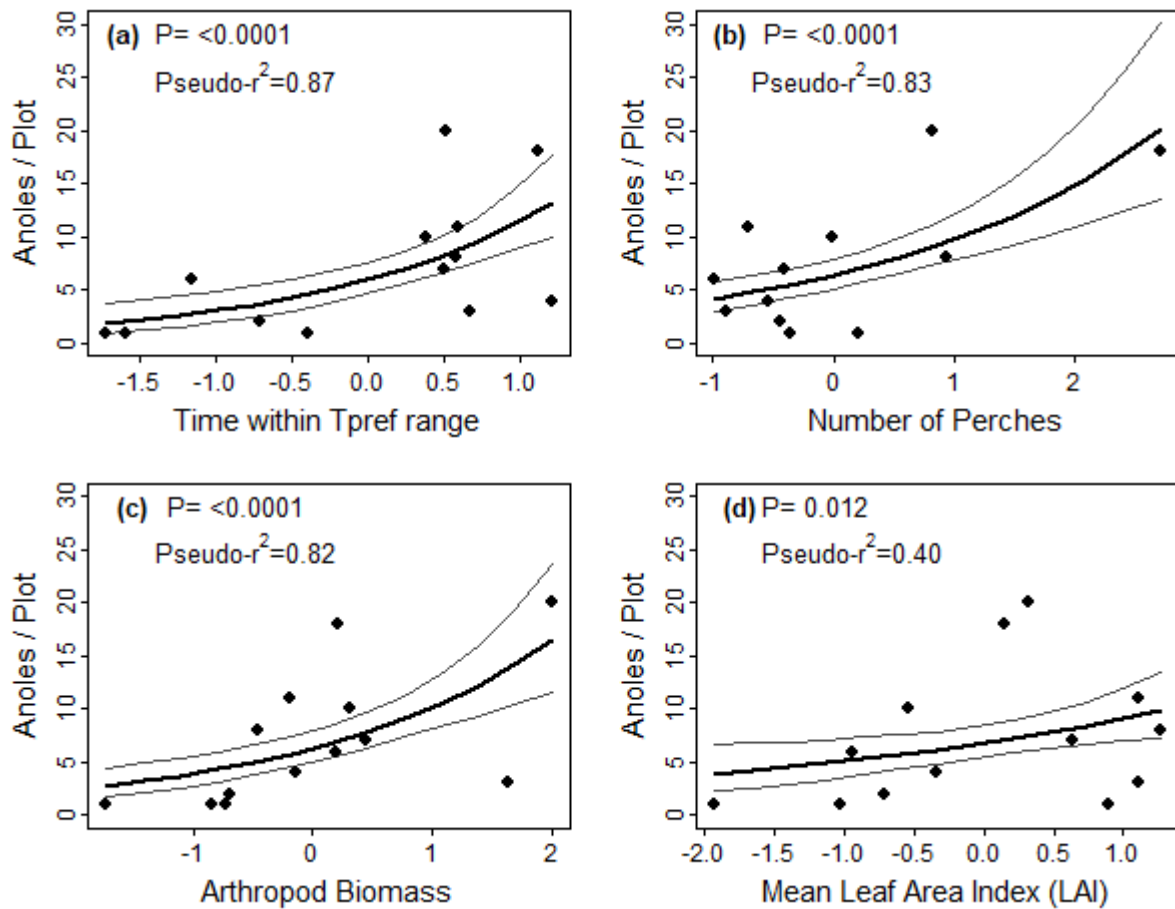
Figure A6.5: Relationships between *Anolis bicaorum* abundance and individual niche metrics in forest plots across Utila, Honduras for the over-corrected thermal model data. Relationships were estimated using multinomial Poisson mixture models with a constant detection rate across plots. All variables are scaled to a mean of zero and unit variance; (a) reflects thermal habitat quality, (b) reflects structural habitat quality, (c) reflects prey availability and (d) reflects canopy cover.
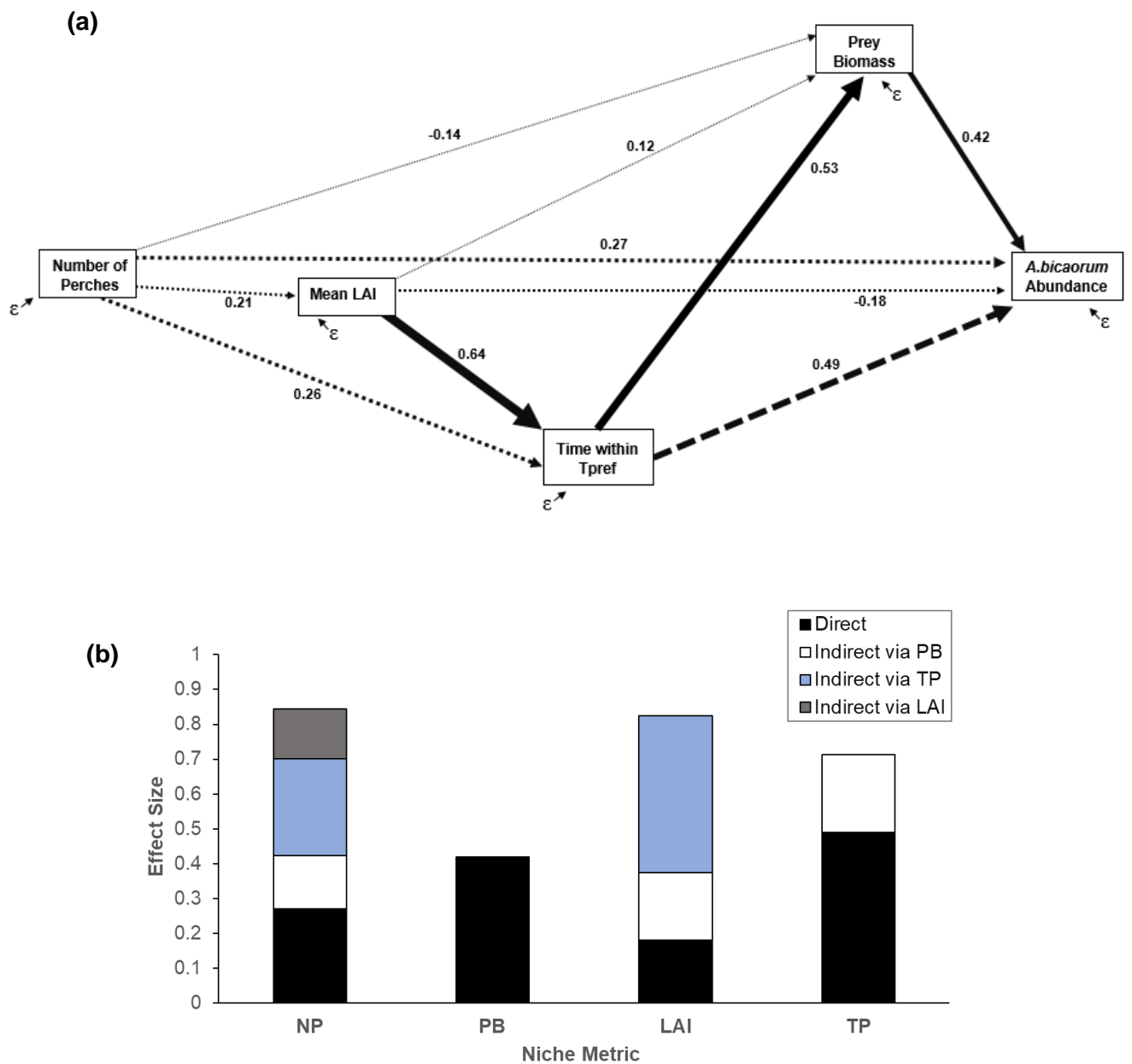
Figure A6.6: Direct and indirect effects of niche axes on *A. bicaorum* abundance for the over-corrected thermal model data. (a) Values are standardized path coefficients; line width is proportional to the strength of the effect, solid lines indicate P<0.05, dashed lines 0.05≥P<0.10, and dotted lines P≥0.10, and ε is unexplained variation. (b) The total effects of covariates on abundance. NP: number of perches; PB: prey biomass; LAI: mean leaf area index; TP: time within Tpref range.

Table A6.2: Results of the path analysis on the over-corrected thermal model data looking at indirect and direct effects, and relationships between, multiple niche axes on *A. bicaorum* abundance, in 13 forest plots on Utila, Honduras. Std.all, Standardised Coefficients.

Pathway	Estimate (± S.E)	*Z*	*P*-Value	Std.all
A. bicaorum **Abundance ~**				
Number of Perches	0.29 ± 0.19	1.51	0.132	0.27
Prey Biomass	0.45 ± 0.21	-0.78	0.035	0.42
Time within T_{pref}	0.58 ± 0.28	1.90	0.058	0.49
Mean LAI	-0.19 ± 0.24	-0.78	0.434	-0.18
Time within T_{pref} ~				
Mean LAI	0.64 ± 0.19	3.31	0.001	0.64
Number of Perches	0.26 ± 0.19	1.34	0.184	0.26
Mean LAI ~				
Number of Perches	0.21 ± 0.27	0.76	0.449	0.21
Prey Biomass ~				
Time within T_{pref}	0.53 ± 0.33	1.60	0.110	0.53
Number of Perches	-0.14 ± 0.25	-0.55	0.583	-0.14
Mean LAI	0.12 ± 0.31	0.38	0.703	0.12

Figure A6.7: Relationships between *Anolis bicaorum* abundance and individual niche metrics excluded from the final analysis, using the over-corrected thermal model data. Relationships were estimated using multinomial Poisson mixture models with a constant detection rate across plots. All variables were scaled to a mean of zero and unit variance, (a) deviation from T$_{pref}$ range, (b) basal area, (c) prey diversity.
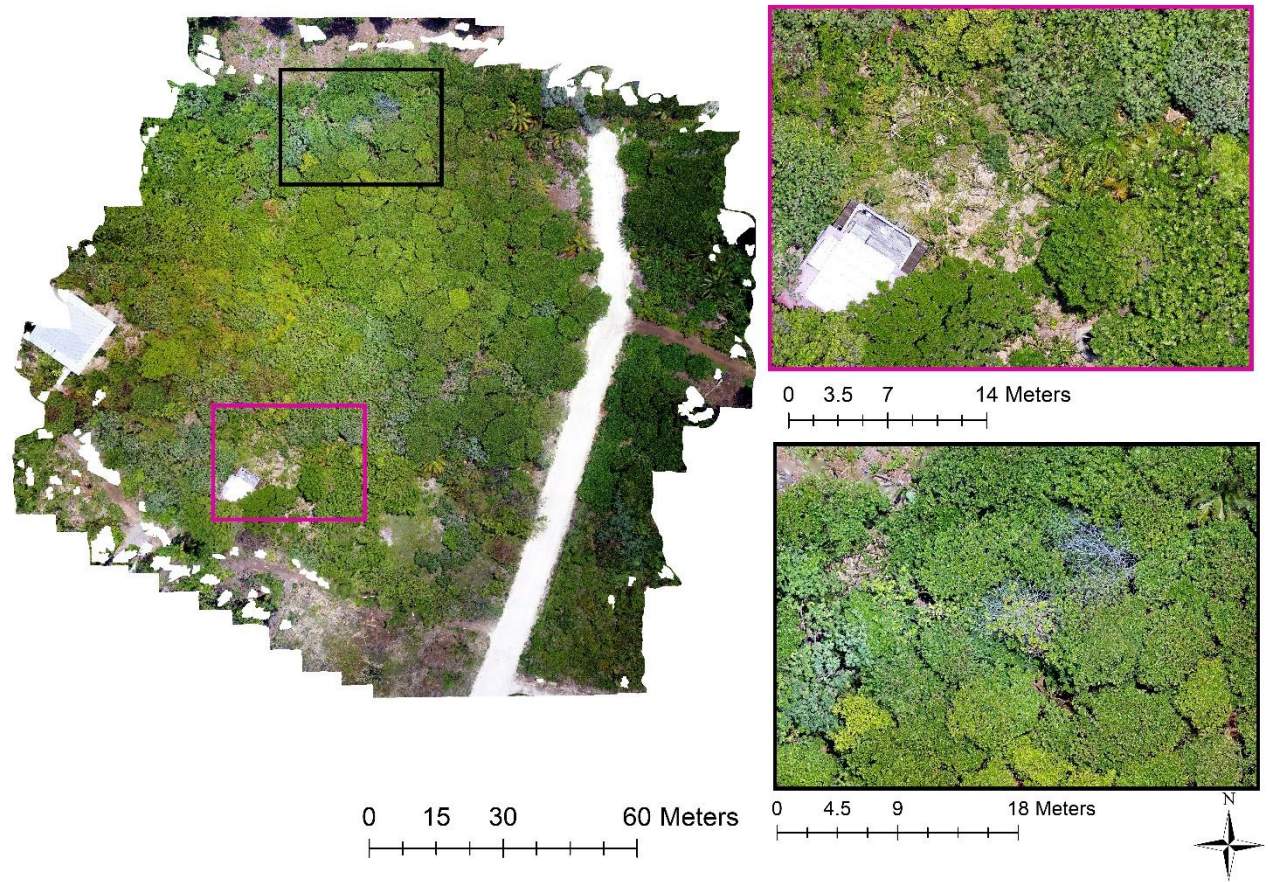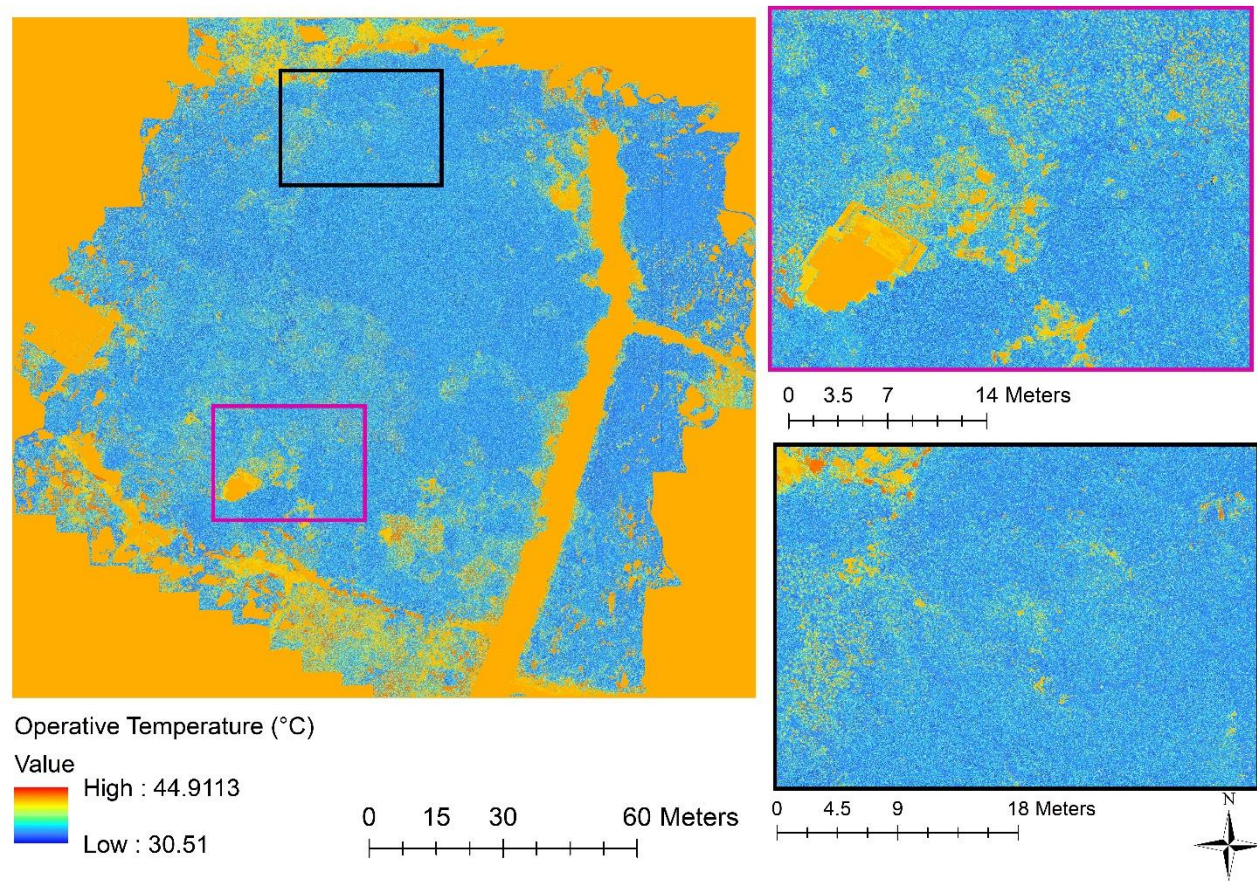
Appendix 7 – RGB and Operative Temperature Maps
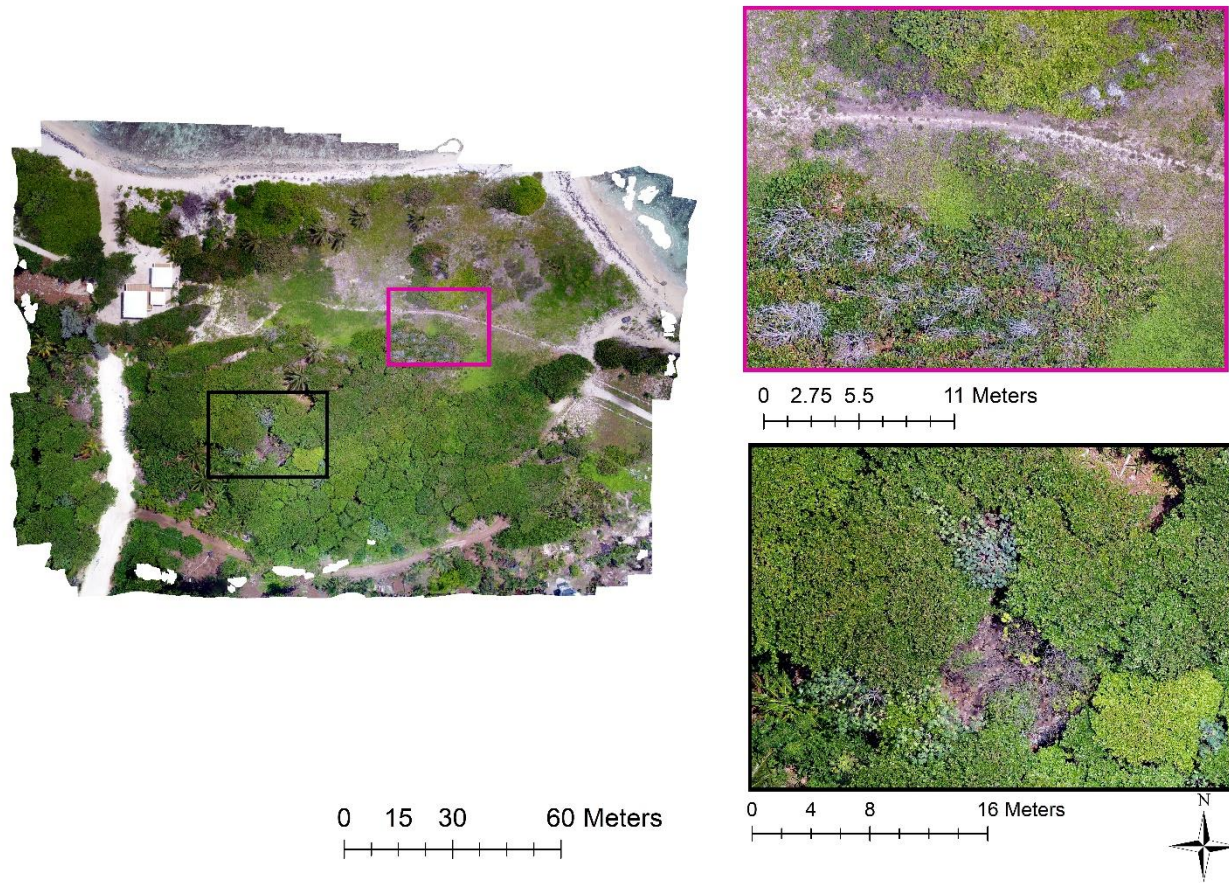
Figure A7.1: RGB raster layer of area surrounding Plot 2 with zoomed in and highlighted areas of interest (magenta and black insets)
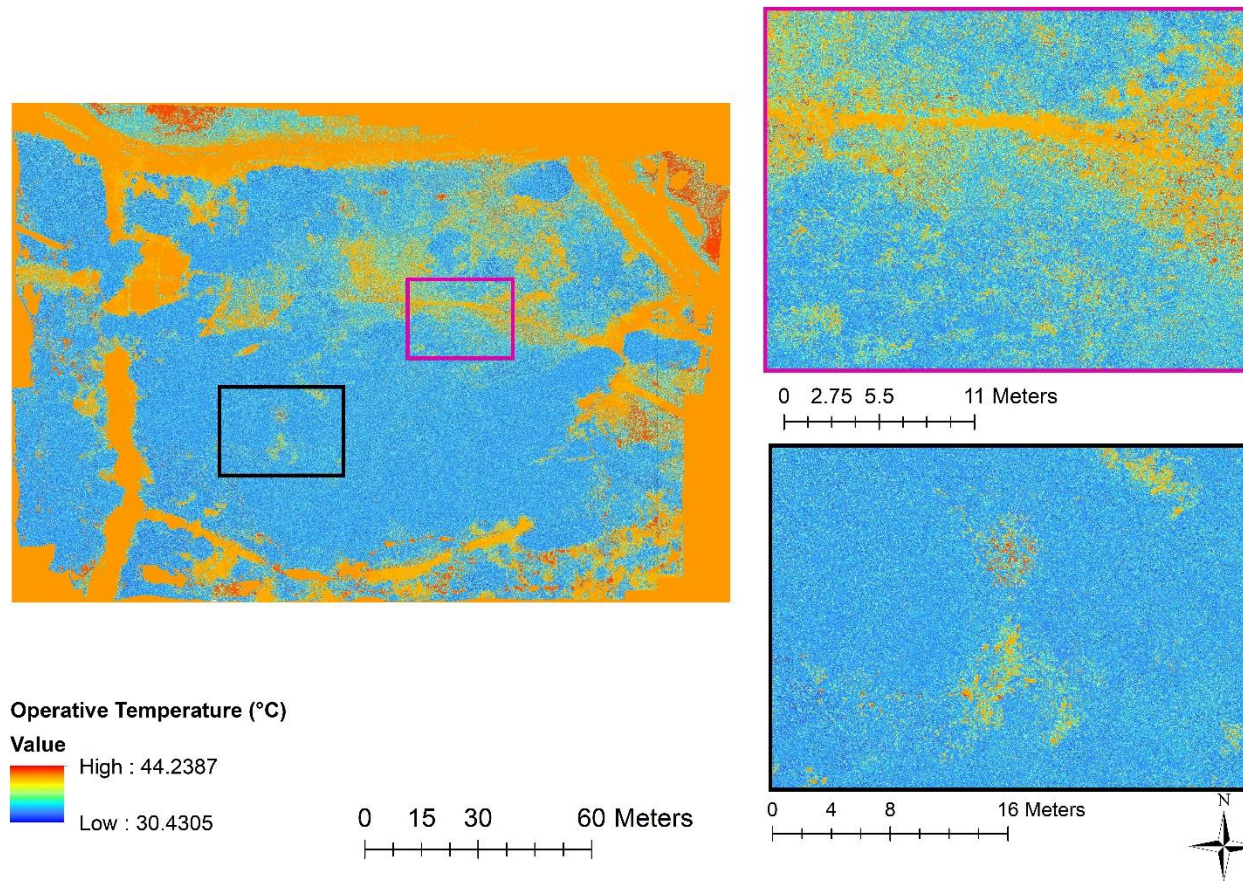
Figure A7.2: Operative Temperature (T$_e$) raster layer derived from predictions of Te.Air.UAV random forest model of area surrounding Plot 2 with zoomed in and highlighted areas of interest (magenta and black insets)
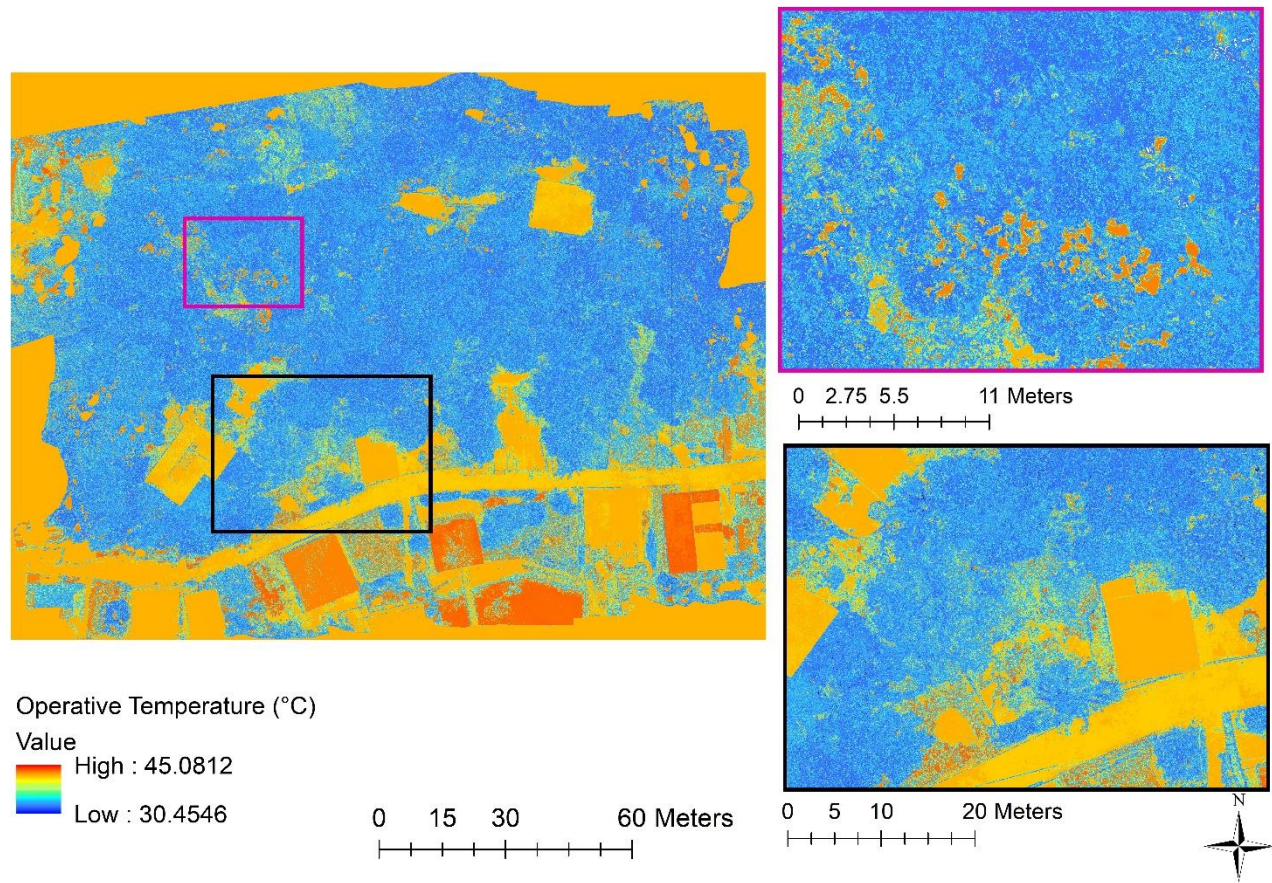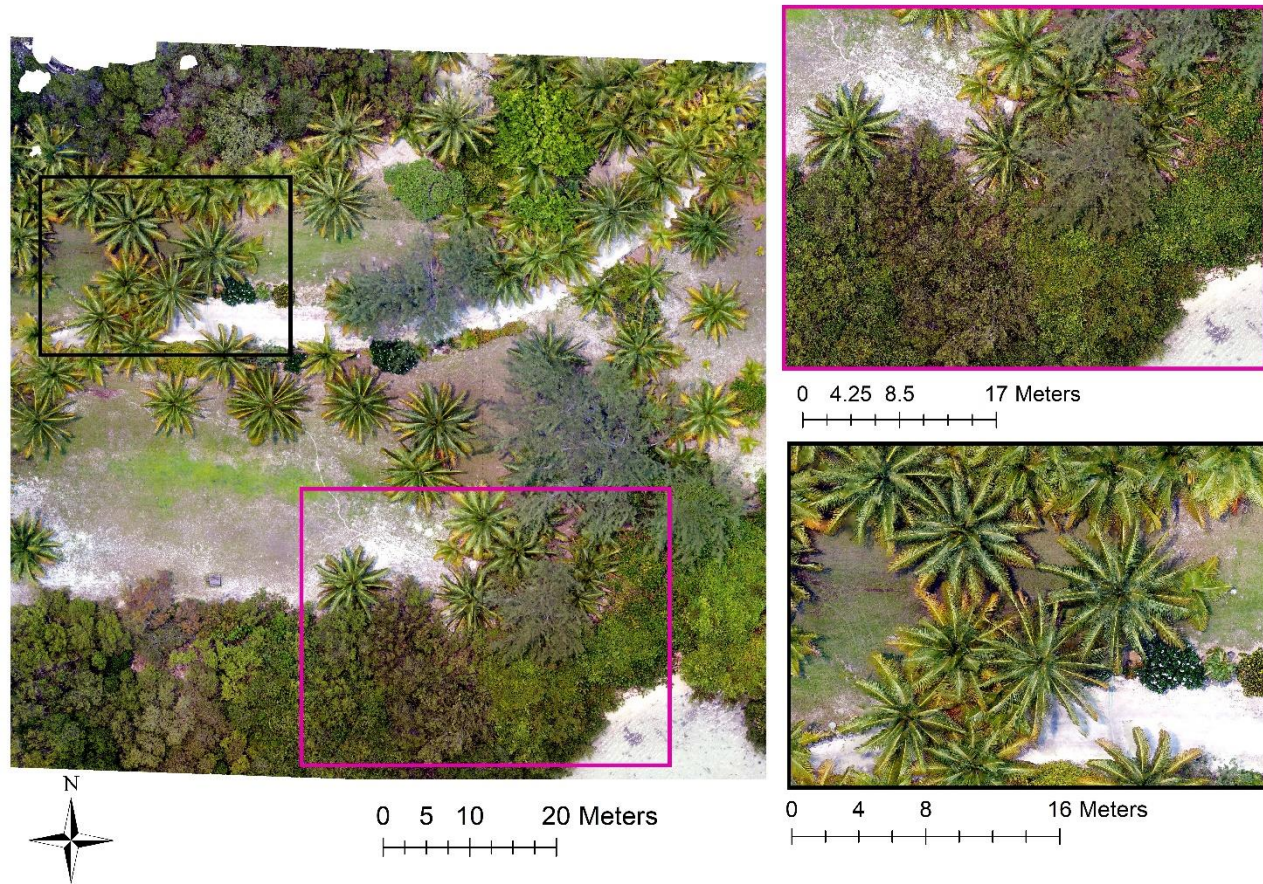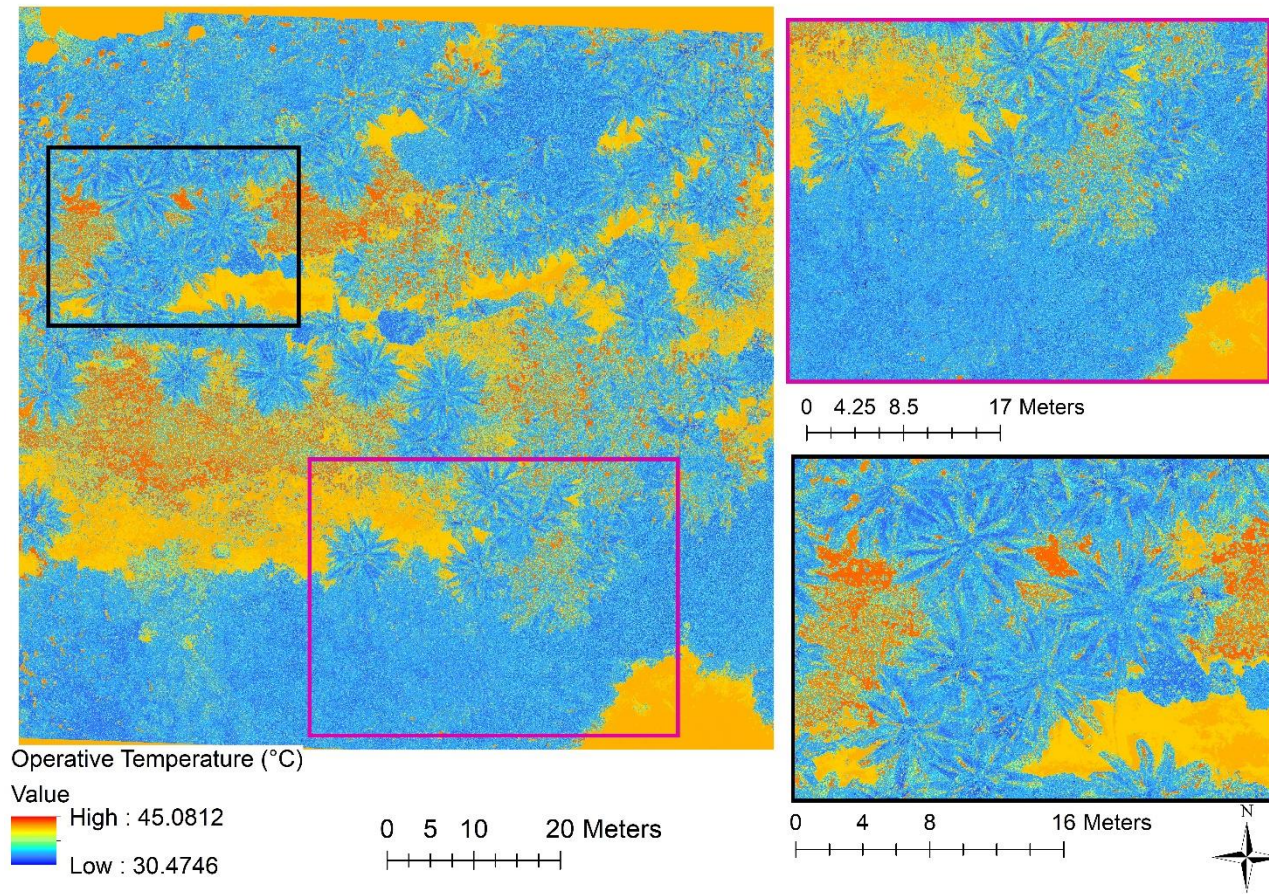
Figure A7.3: RGB raster layer of area surrounding Plot 3 with zoomed in and highlighted areas of interest (magenta and black insets)
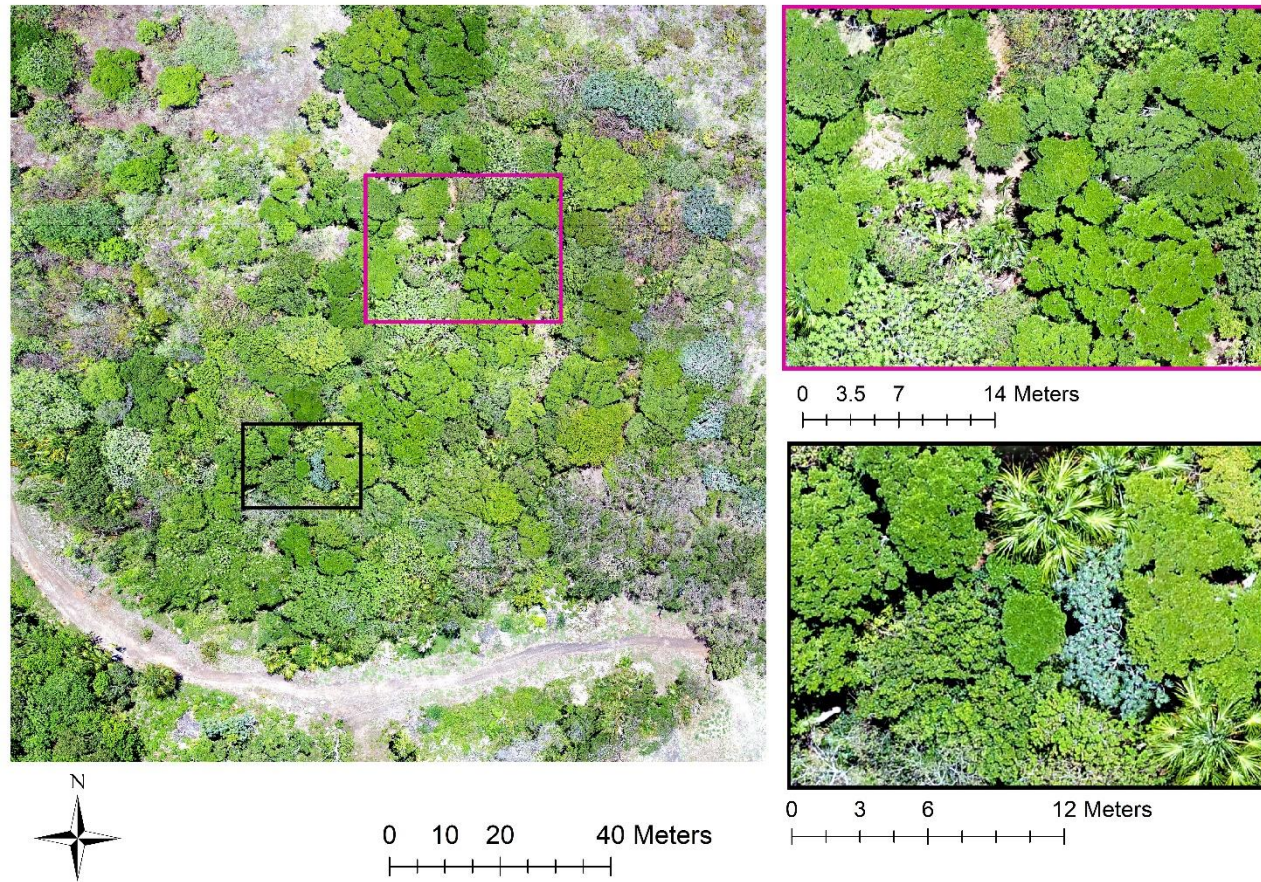
Figure A7.4: Operative Temperature (T_e) raster layer derived from predictions of Te.Air.UAV random forest model of area surrounding Plot 3 with zoomed in and highlighted areas of interest (magenta and black insets)
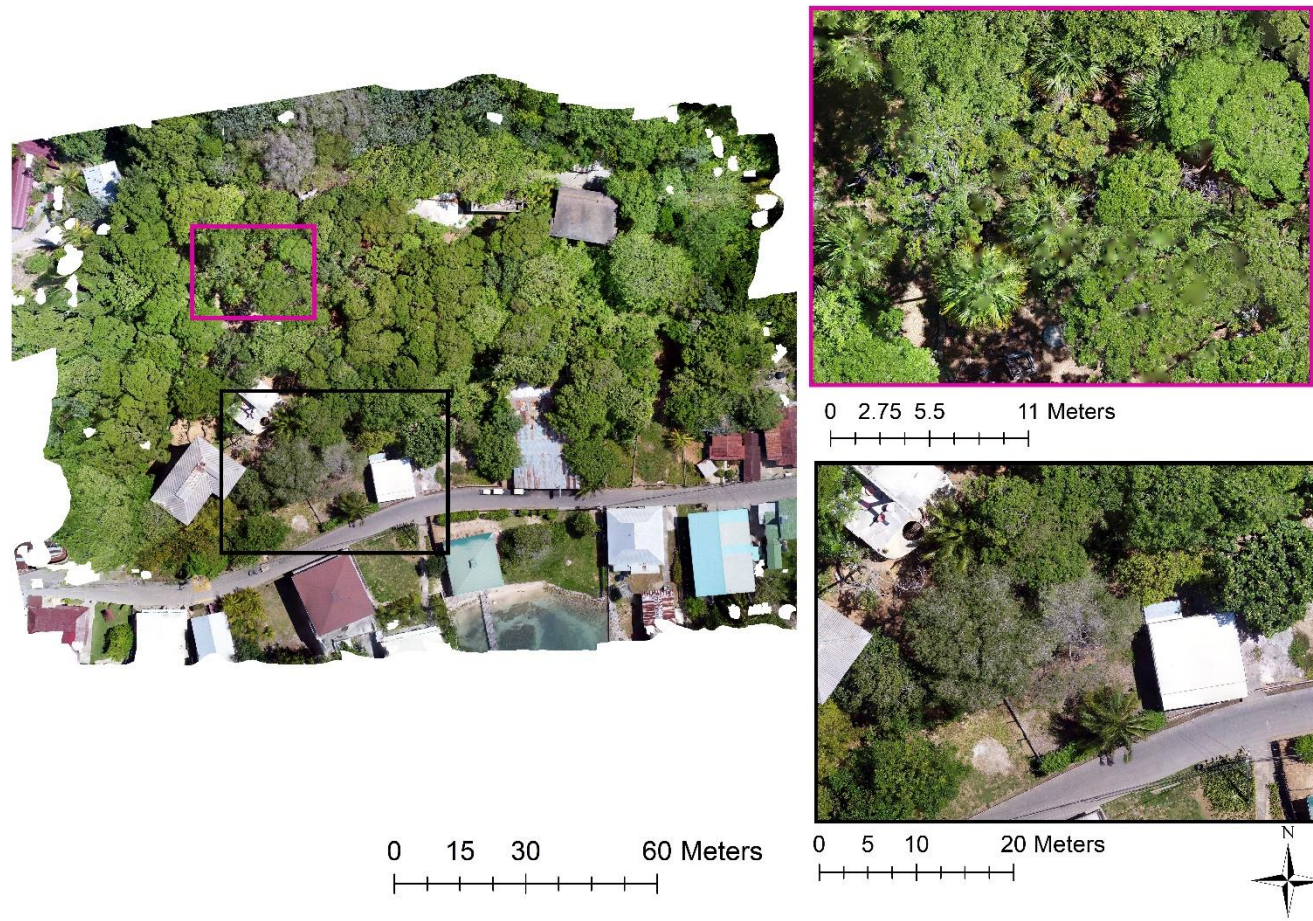
Figure A7.5: RGB raster layer of area surrounding Plot 5 with zoomed in and highlighted areas of interest (magenta and black insets)

Figure A7.5: Operative Temperature (T$_e$) raster layer derived from predictions of Te.Air.UAV random forest model of area surrounding Plot 5 with zoomed in and highlighted areas of interest (magenta and black insets)
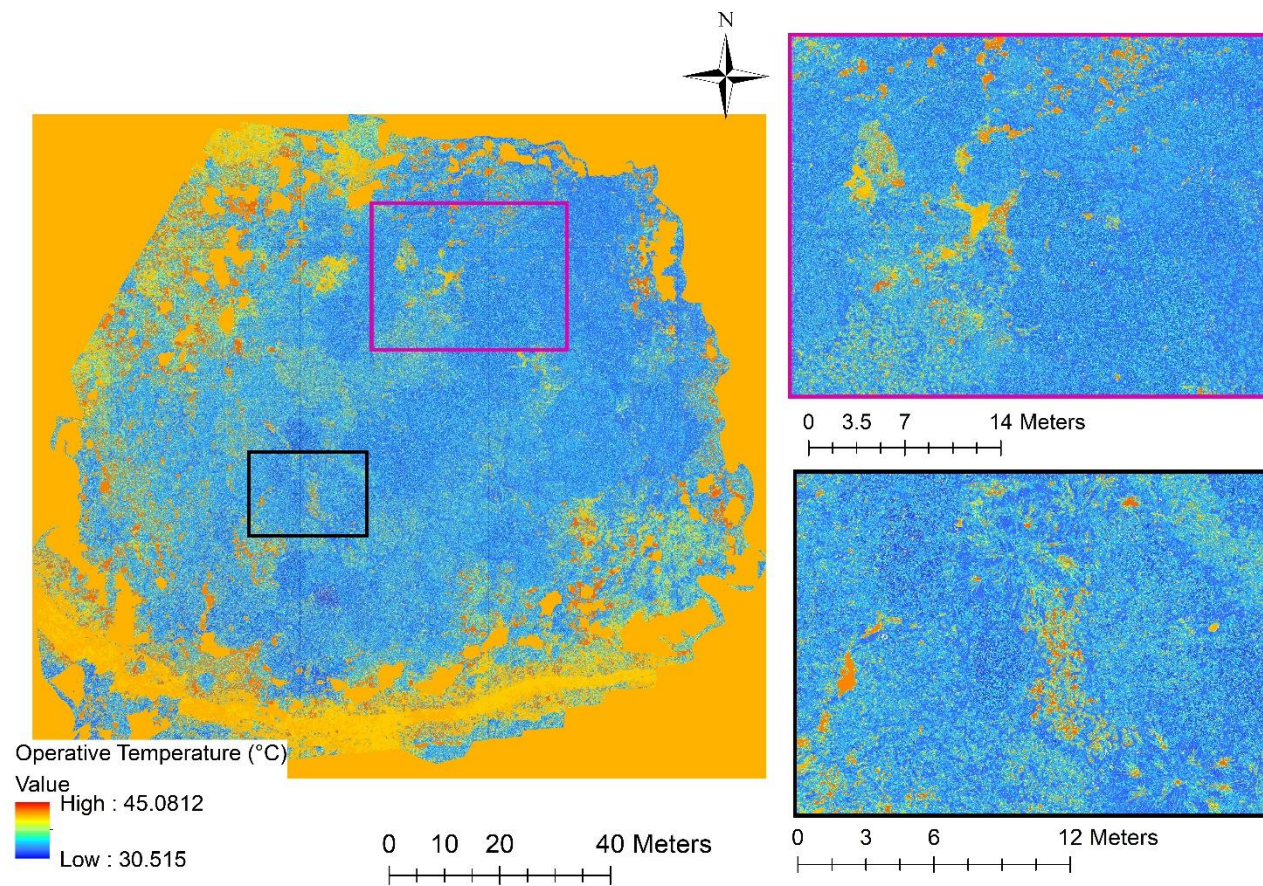
Figure A7.6: RGB raster layer of area surrounding Plot 8 with zoomed in and highlighted areas of interest (magenta and black insets)
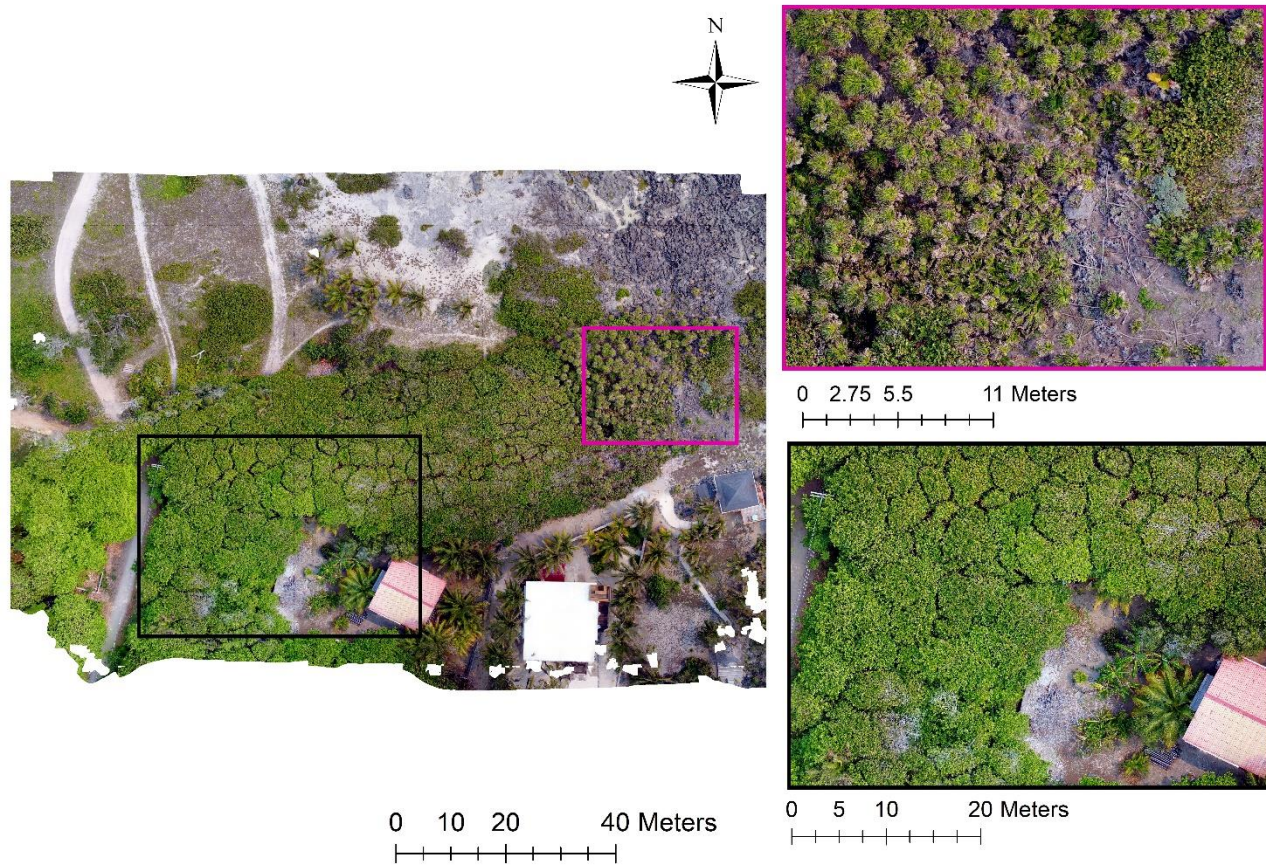
Figure A7.7: Operative Temperature (T$_e$) raster layer derived from predictions of Te.Air.UAV random forest model of area surrounding Plot 8 with zoomed in and highlighted areas of interest (magenta and black insets)
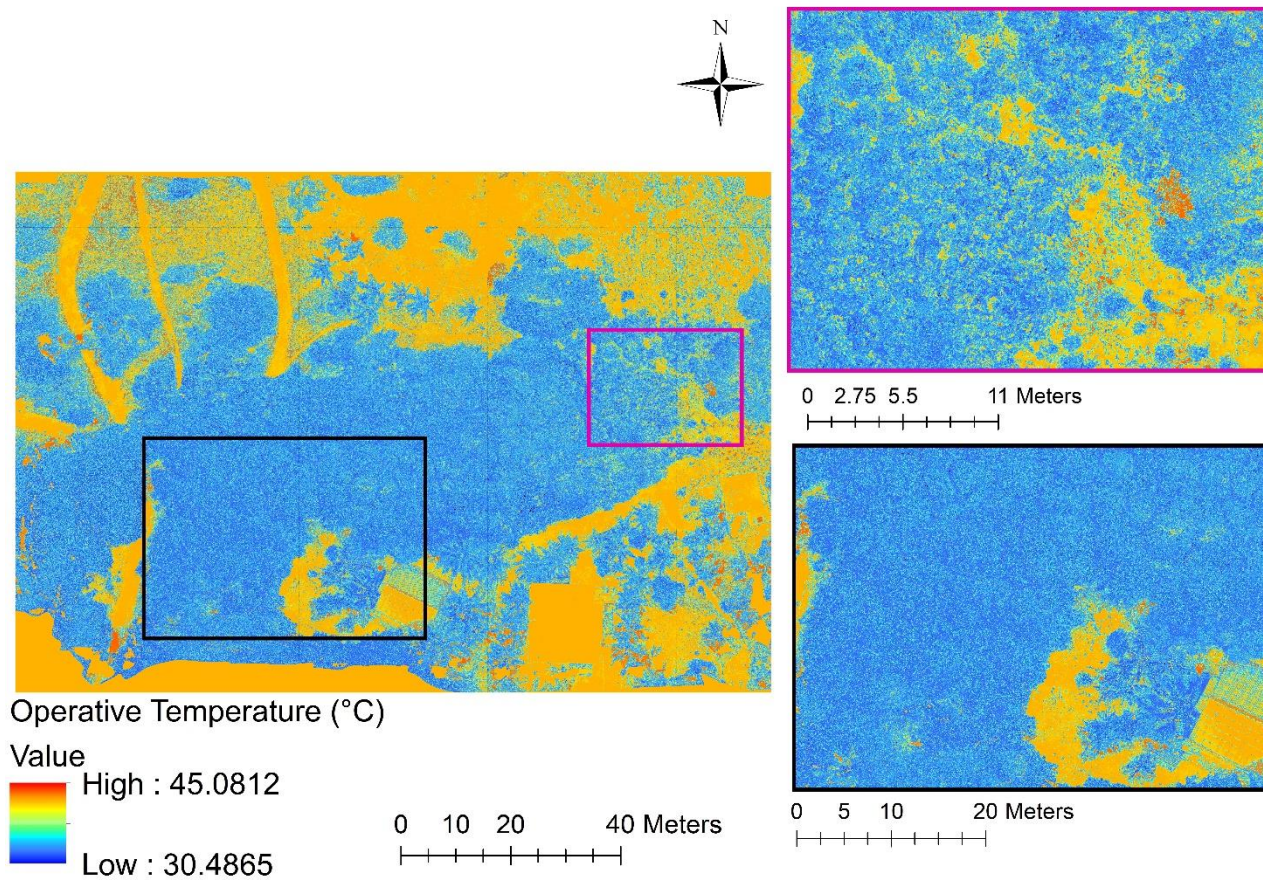
Figure A7.8: RGB raster layer of area surrounding Plots 9 and 10 with zoomed in and highlighted areas of interest (magenta and black insets)
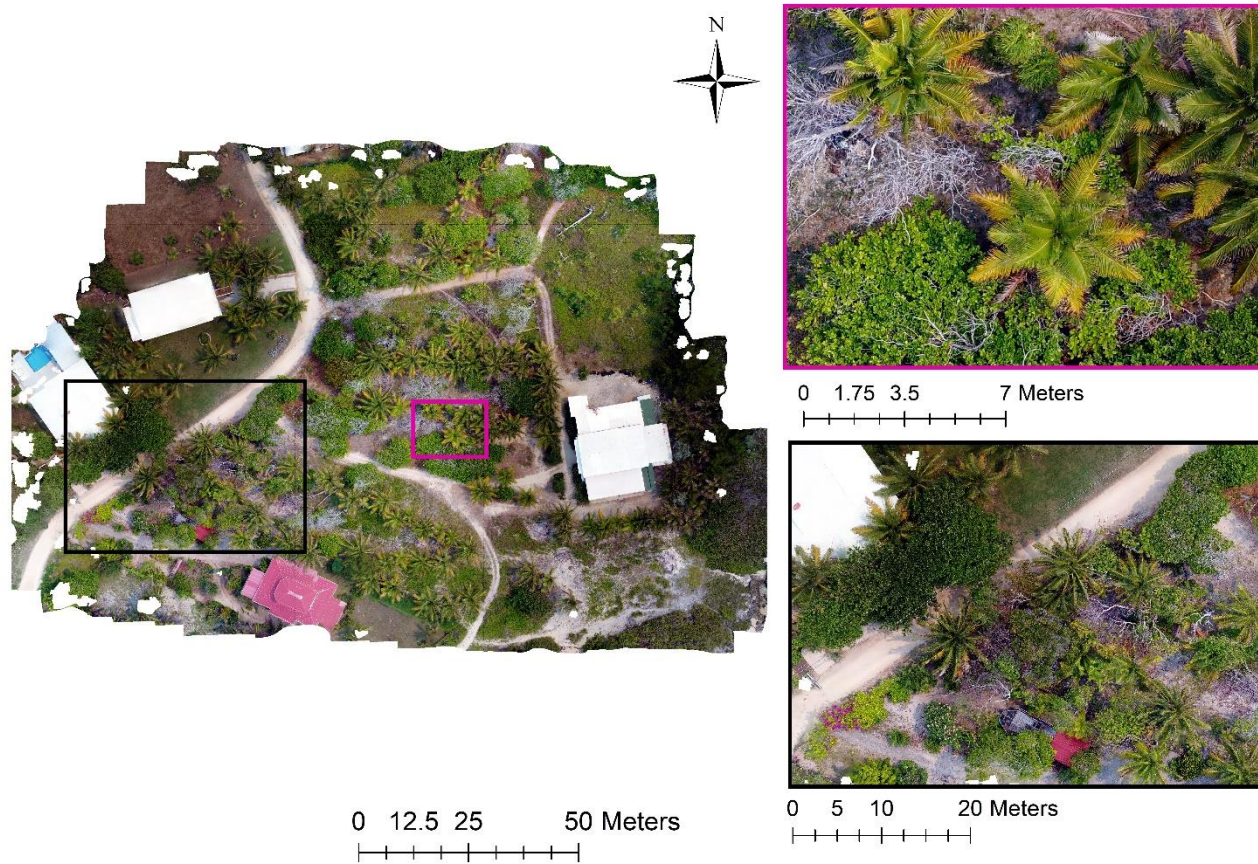
Figure A7.9: Operative Temperature (T_e) raster layer derived from predictions of Te.Air.UAV random forest model of area surrounding Plots 9 and 10 with zoomed in and highlighted areas of interest (magenta and black insets)

Figure A7.10: RGB raster layer of area surrounding Plot 11 with zoomed in and highlighted areas of interest (magenta and black insets)

Figure A7.11: Operative Temperature (T$_e$) raster layer derived from predictions of Te.Air.UAV random forest model of area surrounding Plot 11 with zoomed in and highlighted areas of interest (magenta and black insets)
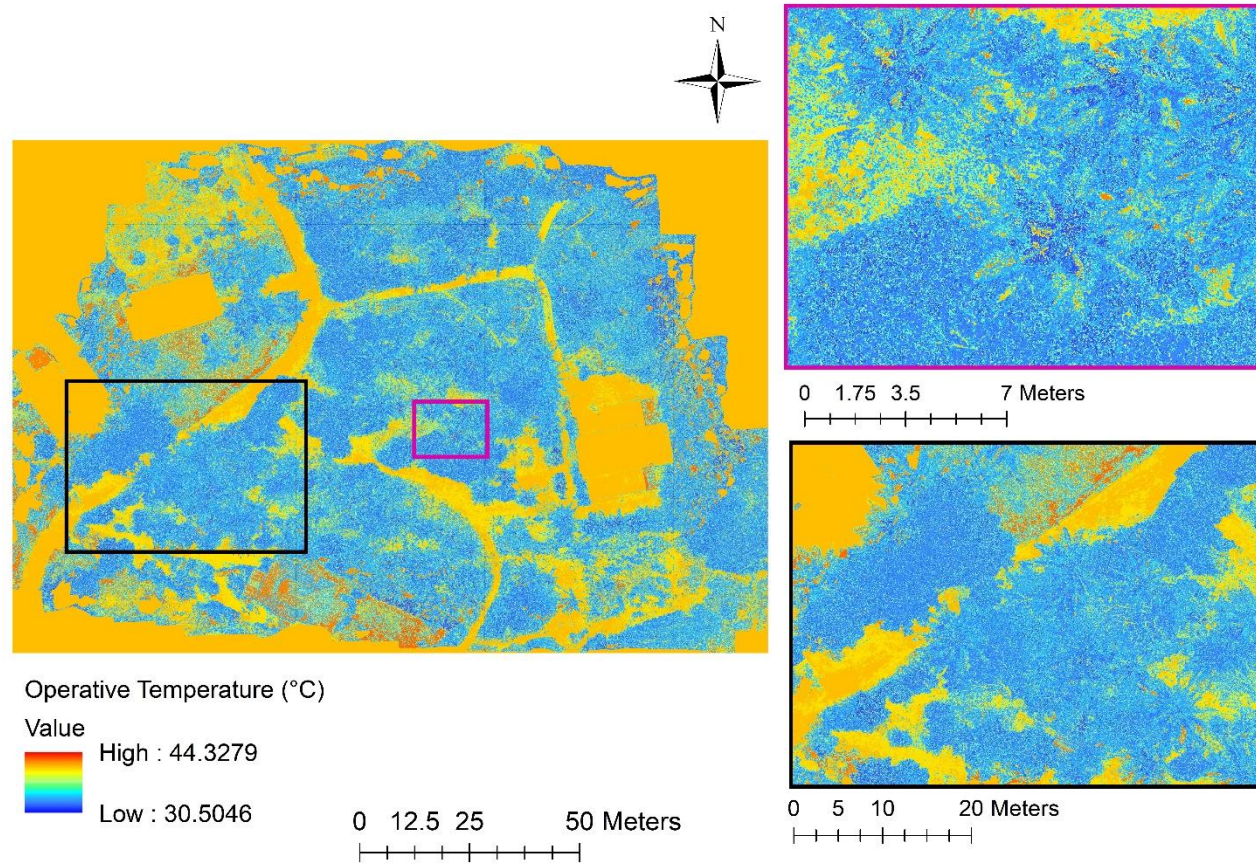
Figure A7.12: RGB raster layer of area surrounding Plot 12 with zoomed in and highlighted areas of interest (magenta and black insets)

Figure A7.13: Operative Temperature (T$_e$) raster layer derived from predictions of Te.Air.UAV random forest model of area surrounding Plot 12 with zoomed in and highlighted areas of interest (magenta and black insets)

Figure A7.14: RGB raster layer of area surrounding Plot 13 with zoomed in and highlighted areas of interest (magenta and black insets)
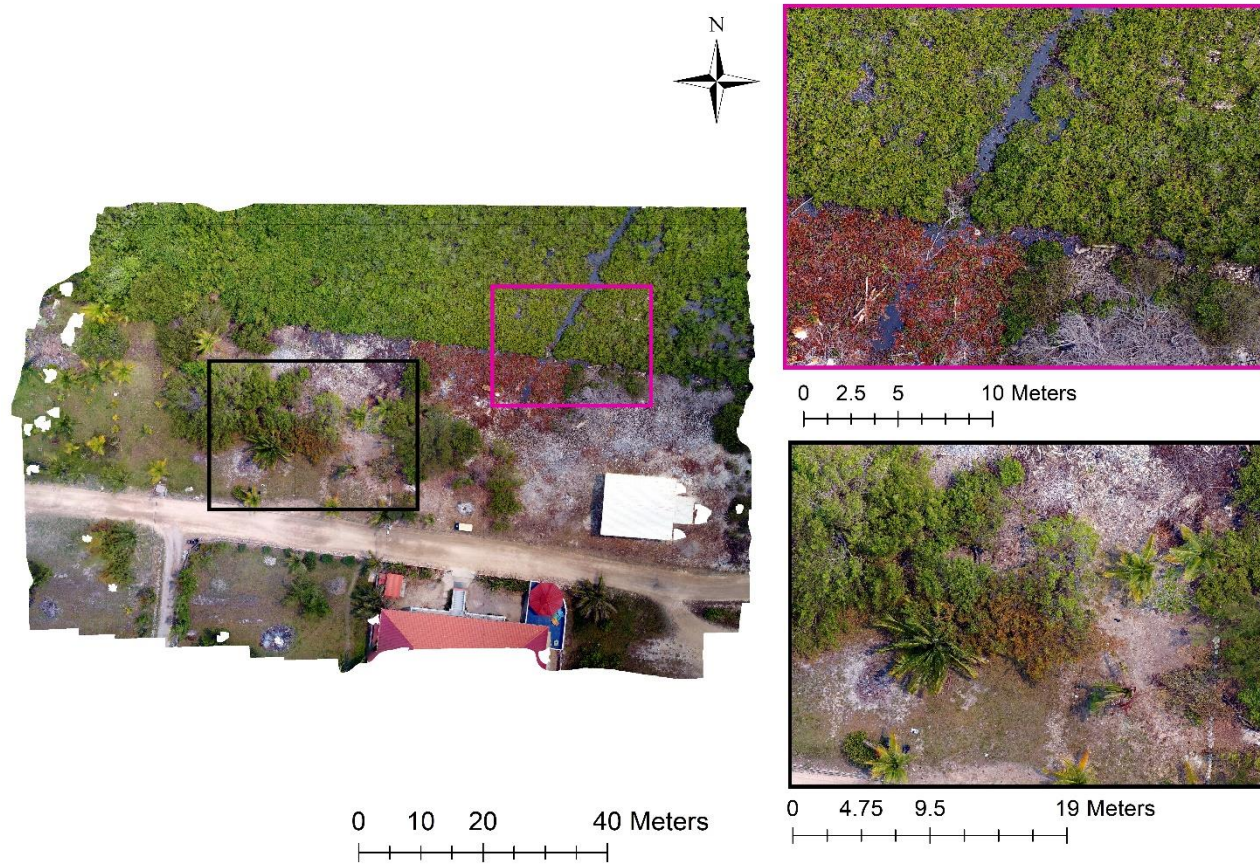
Figure A7.15: Operative Temperature (T$_e$) raster layer derived from predictions of Te.Air.UAV random forest model of area surrounding Plot 13 with zoomed in and highlighted areas of interest (magenta and black insets)
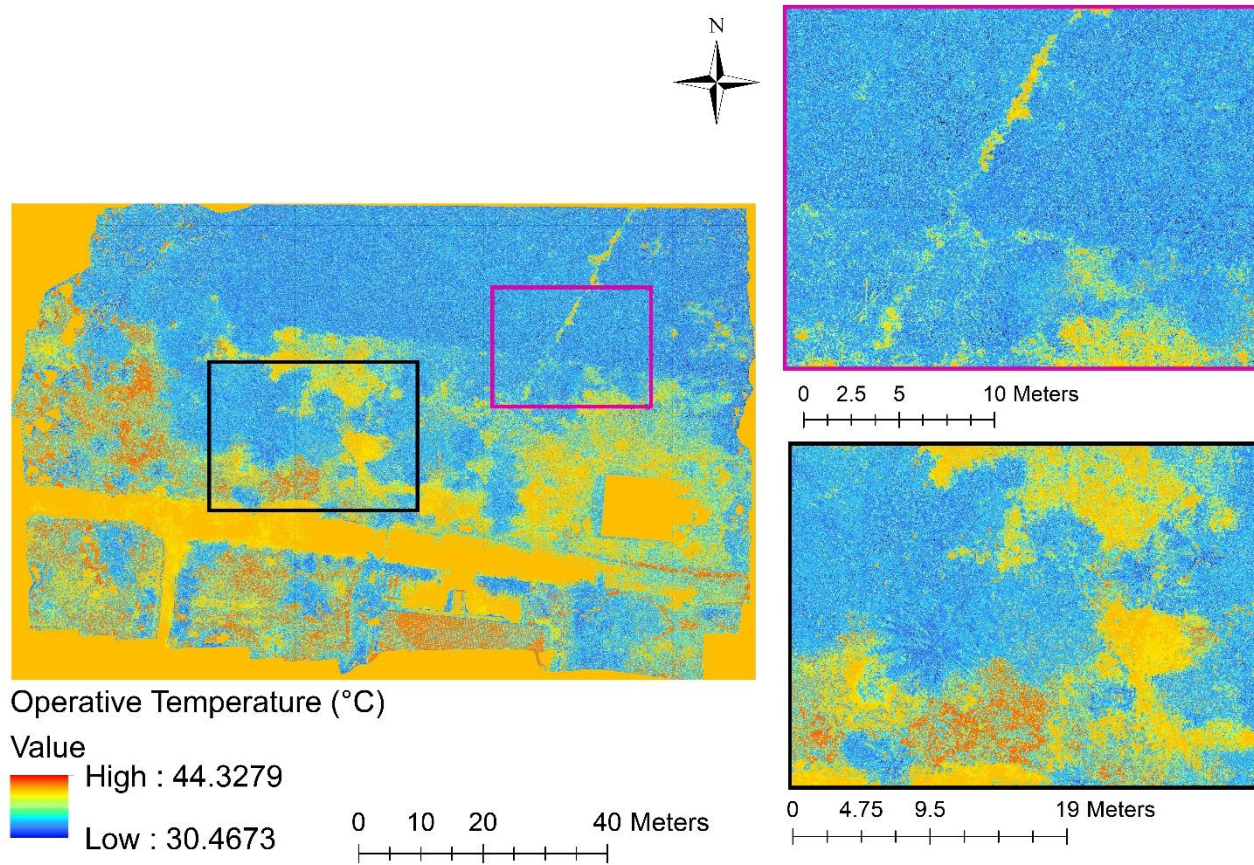
Figure A7.16: RGB raster layer of area surrounding Plot 14 with zoomed in and highlighted areas of interest (magenta and black insets)
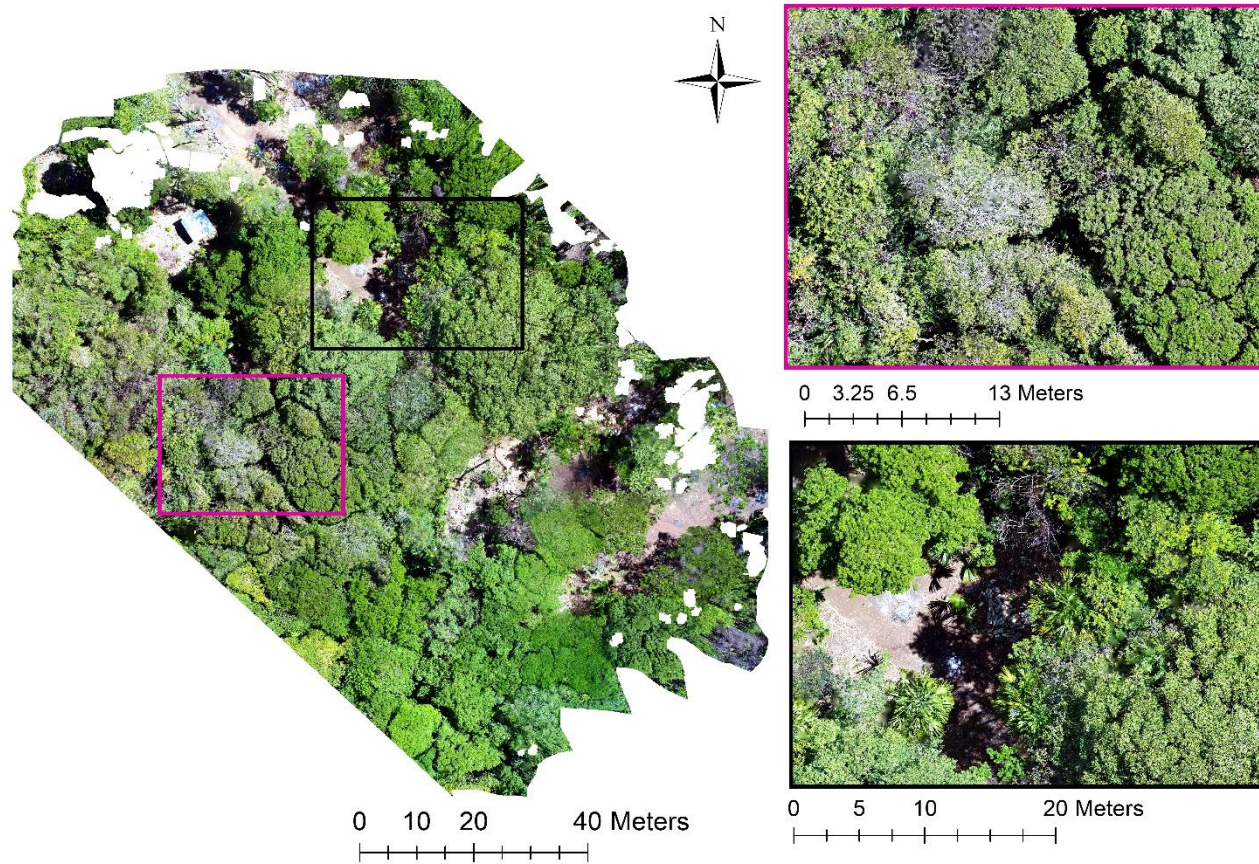
Figure A7.17: Operative Temperature (T_e) raster layer derived from predictions of Te.Air.UAV random forest model of area surrounding Plot 14 with zoomed in and highlighted areas of interest (magenta and black insets)

Figure A7.18: RGB raster layer of area surrounding Plot 15 with zoomed in and highlighted areas of interest (magenta and black insets)

Figure A7.19: Operative Temperature (T_e) raster layer derived from predictions of Te.Air.UAV random forest model of area surrounding Plot 15 with zoomed in and highlighted areas of interest (magenta and black insets)
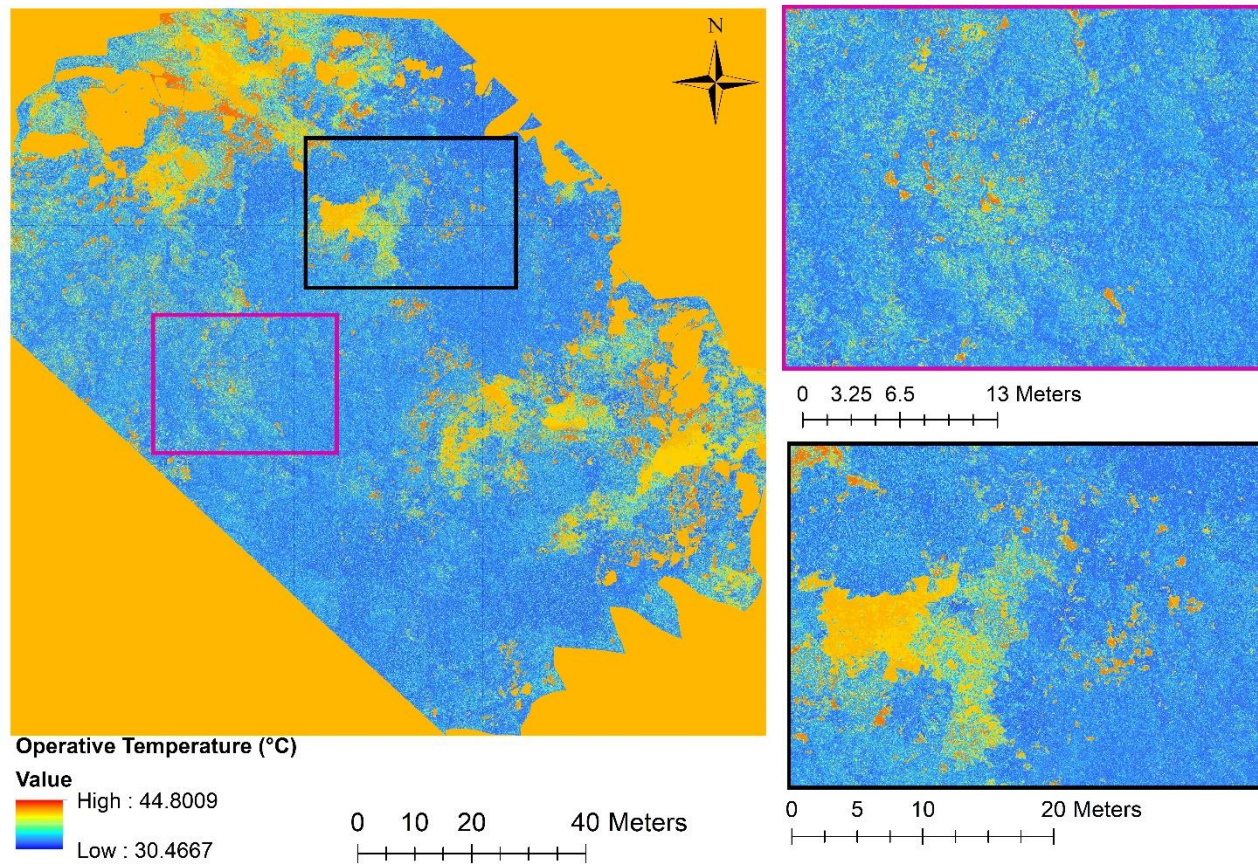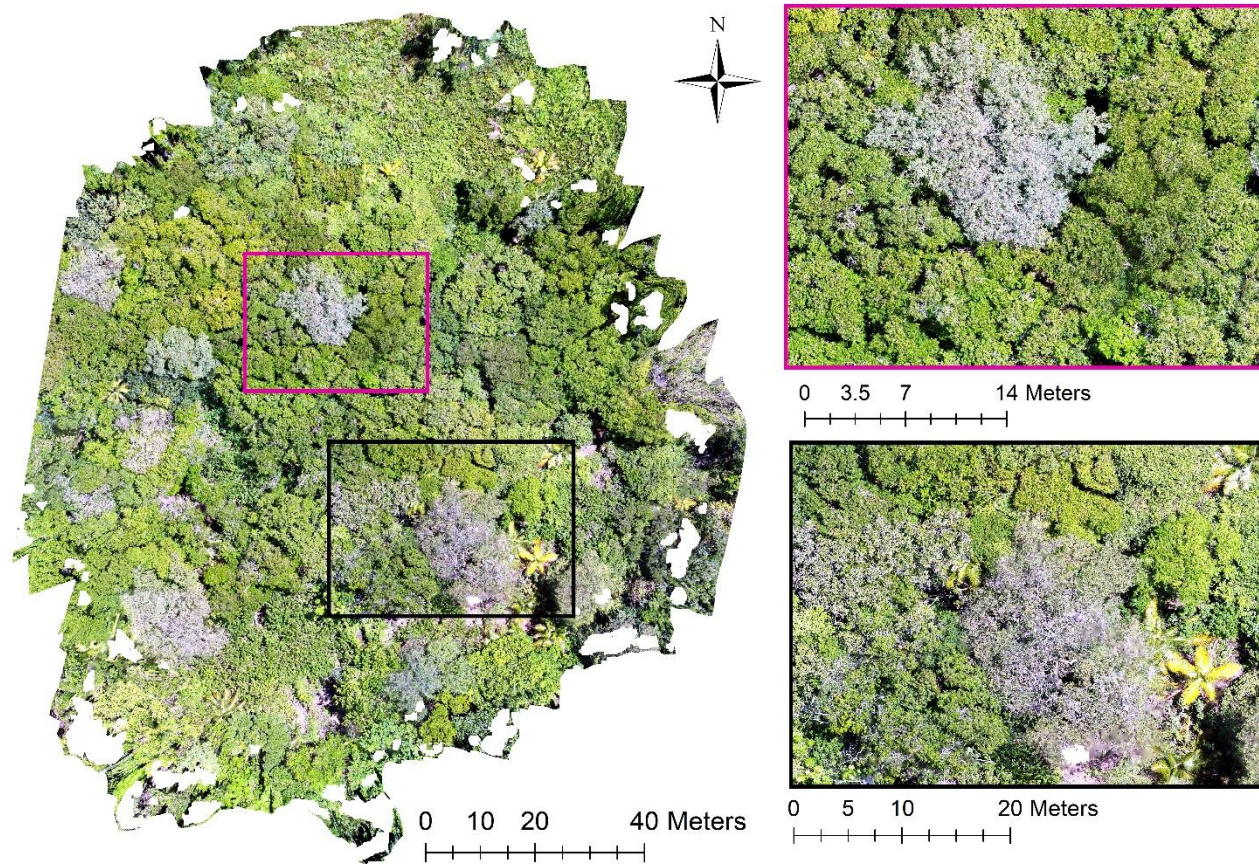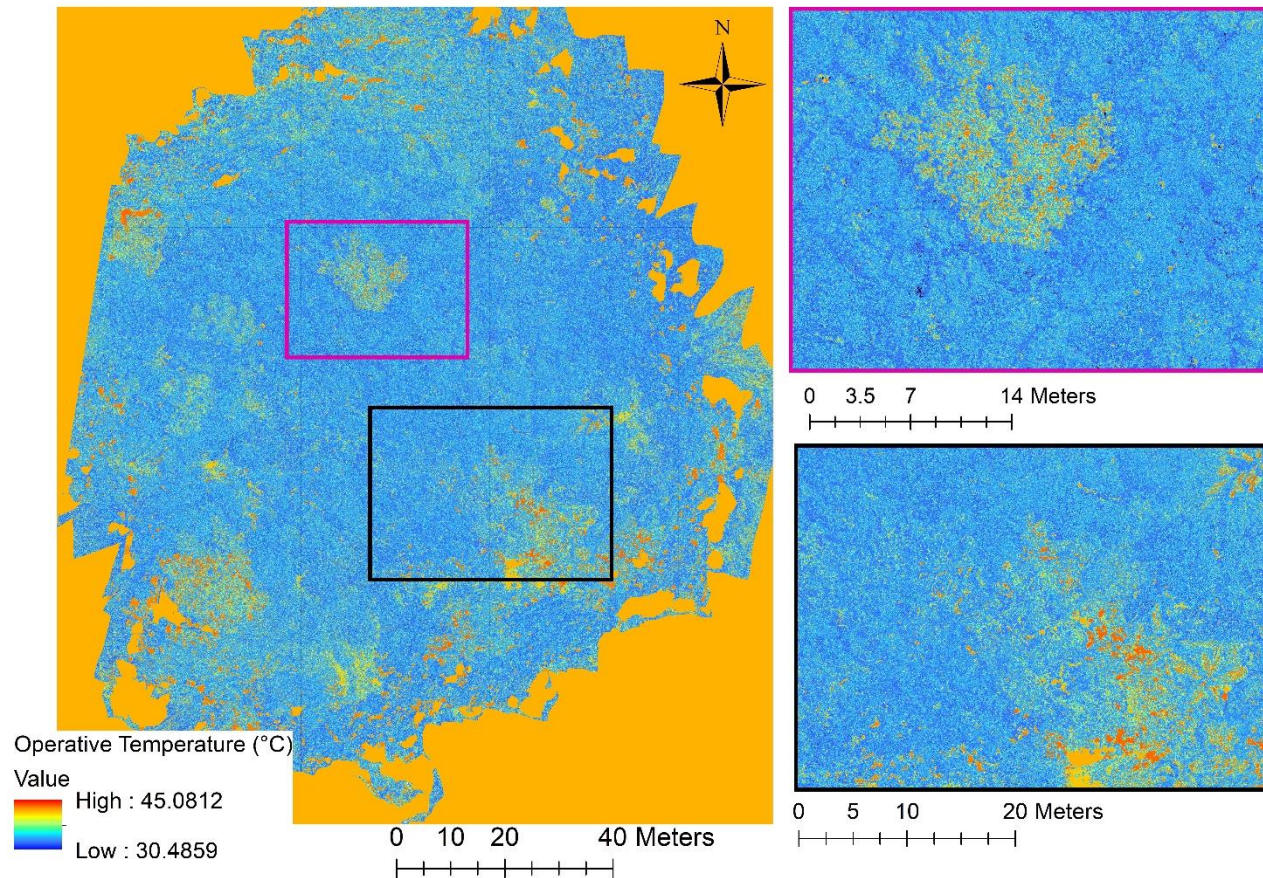
213

Appendix 8 – Confusion Matrices for WorldView-2 Land Cover Classifications (Chapter 5)

Table A8.1: Confusion Matrix for Random Forest Land Cover Classification on 2018 WorldView-2 Imagery (Chapter 5) based on Random Forest Out of Bag (OOB) estimate validation.

	Agricultural	Forest	Coastal	Dead Mangrove	Mangrove	Neotropical Savannah	Urban	Water	User's Accuracy (%)
Agricultural	54	10	0	0	3	4	2	0	73.97
Forest	5	95	0	0	16	1	2	0	79.83
Coastal	0	1	0	0	0	0	30	0	0
Dead Mangrove	0	0	0	0	1	7	0	0	0
Mangrove	4	15	0	0	55	5	2	0	67.9
Neotropical Savannah	4	1	0	1	0	110	0	0	94.83
Urban	6	4	2	0	2	0	102	1	87.18
Water	0	0	0	0	1	0	0	220	99.55
Producer's Accuracy (%)	73.97	75.4	0	0	70.51	86.61	73.91	99.55	

Table A8.2: Confusion Matrix for Random Forest Land Cover Classification on 2020 WorldView-2 Imagery (Chapter 5) based on Random Forest Out of Bag (OOB) estimate validation.

	Agricultural	Forest	Coastal	Dead Mangrove	Mangrove	Neotropical Savannah	Urban	Water	User's Accuracy (%)
Agricultural	56	10	1	0	0	6	5	0	71.80
Forest	5	109	0	0	6	7	2	0	84.50
Coastal	2	2	22	0	0	0	15	2	51.16
Dead Mangrove	0	0	0	3	0	2	2	1	37.5
Mangrove	3	7	0	0	43	6	2	0	70.49
Neotropical Savannah	7	3	0	0	3	85	1	1	85
Urban	11	5	2	0	0	2	97	2	81.51
Water	0	0	0	0	0	1	0	242	99.59
Producer's Accuracy (%)	66.67	80.15	88.00	100.00	82.69	77.98	78.22	97.58	

Table A8.3: Confusion Matrix for Random Forest Land Cover Classification on 2018 WorldView-2 Imagery (Chapter 5) based on independent test dataset validation.

	Agricultural	Forest	Coastal	Dead Mangrove	Mangrove	Neotropical Savannah	Urban	Water	User's Accuracy (%)
Agricultural	21	7	0	0	1	1	5	0	60
Forest	6	25	1	0	4	1	2	0	64.10
Coastal	0	0	0	0	0	0	0	0	No Data
Dead Mangrove	0	0	0	1	0	0	0	0	100
Mangrove	1	5	0	0	23	2	0	0	74.19
Neotropical Savannah	1	0	0	1	1	39	0	0	92.86
Urban	1	3	15	1	3	1	32	0	57.14
Water	0	0	0	0	0	0	2	69	97.18
Producer's Accuracy (%)	70	62.5	0	33.33	71.87	88.64	78.05	100	

Table A8.4: Confusion Matrix for Random Forest Land Cover Classification on 2020 WorldView-2 Imagery (Chapter 5) based on independent test dataset validation

	Agricultural	Forest	Coastal	Dead Mangrove	Mangrove	Neotropical Savannah	Urban	Water	User's Accuracy (%)
Agricultural	23	2	1	0	0	0	4	0	76.67
Forest	4	41	1	0	2	0	5	1	75.93
Coastal	0	1	6	0	0	0	1	0	75
Dead Mangrove	0	0	0	1	0	0	0	0	100
Mangrove	0	1	1	0	11	1	0	0	78.57
Neotropical Savannah	0	4	0	2	2	31	2	0	75.61
Urban	0	0	4	1	1	0	20	0	76.92
Water	0	0	0	1	0	0	0	81	98.78
Producer's Accuracy (%)	85.19	83.67	46.15	20	68.75	32	32	82	